AD NUMBER

ADB137279

NEW LIMITATION CHANGE

TO

Approved for public release, distribution unlimited

FROM

Distribution authorized to U.S. Gov't. agencies and their contractors; Critical Technology; May 87. Other requests shall be referred to WRDC/POSL, Wright-Patterson AFB, OH 45433-6563. This document contains export controlled technical data.

AUTHORITY

88 CG/SCCM [FOIA Office], 21 Aug 2004

AFWAL-TR-89-2012

IMPROVED FATIGUE LIFE BEARING DEVELOPMENT

E.N. Bamberger
B.L. Averbach
P.K. Pearson
S. VanPelt
M.J. Price

GE Aircraft Engines – Cincinnati, OH
Massachusetts Institute of Technology – Cambridge, MA
The Torrington Company – Torrington, CT

June 1989

Final Report for Period September 1984 – December 1988

AERO PROPULSION AND POWER LABORATORY
AIR FORCE WRIGHT RESEARCH AND DEVELOPMENT CENTER
AIR FORCE SYSTEMS COMMAND
WRIGHT-PATTERSON AIR FORCE BASE, OHIO 45433-6523

The following notice applies to any unclassified (including originally classified and now declassified) technical reports released to "qualified U.S. contractors" under the provisions of DoD Directive 5230.25, Withholding of Unclassified Technical Data From Public Disclosure.

NOTICE TO ACCOMPANY THE DISSEMINATION OF EXPORT-CONTROLLED TECHNICAL DATA

1. Export of information contained herein, which includes, in some circumstances, release to foreign nationals within the United States, without first obtaining approval or license from the Department of State for items controlled by the International Traffic in Arms Regulations (ITAR), or the Department of Commerce for items controlled by the Export Administration Regulations (EAR), may constitute a violation of law.

2. Under 22 U.S.C. 2778 the penalty for unlawful export of items or information controlled under the ITAR is up to two years imprisonment, or a fine of $100,000, or both. Under 50 U.S.C., Appendix 2410, the penalty for unlawful export of items or information controlled under the EAR is a fine of up to $1,000,000, or five times the value of the exports, whichever is greater; or for an individual, imprisonment of up to 10 years, or a fine of up to $250,000, or both.

3. In accordance with your certification that establishes you as a "qualified U.S. Contractor", unauthorized dissemination of this information is prohibited and may result in disqualification as a qualified U.S. contractor, and may be considered in determining your eligibility for future contracts with the Department of Defense.

4. The U.S. Government assumes no liability for direct patent infringement, or contributory patent infringement or misuse of technical data.

5. The U.S. Government does not warrant the adequacy, accuracy, currency, or completeness of the technical data.

6. The U.S. Government assumes no liability for loss, damage, or injury resulting from manufacture or use for any purpose of any product, article, system, or material involving reliance upon any or all technical data furnished in response to the request for technical data.

7. If the technical data furnished by the Government will be used for commercial manufacturing or other profit potential, a license for such use may be necessary. Any payments made in support of the request for data do not include or involve any license rights.

8. A copy of this notice shall be provided with any partial or complete reproduction of these data that are provided to qualified U.S. contractors.

D E S T R U C T I O N N O T I C E

For classified documents, follow the procedures in DoD 5200.22-M, Industrial Security Manual, Section II-19 or DoD 5200.1-R, Information Security Program Regulation, Chapter IX. For unclassified, limited documents, destroy by any method that will prevent disclosure of contents or reconstruction of the document.

REPORT DOCUMENTATION PAGE

1. REPORT SECURITY CLASSIFICATION Unclassified	1b. RESTRICTIVE MARKINGS
2a. SECURITY CLASSIFICATION AUTHORITY	3. DISTRIBUTION/AVAILABILITY OF REPORT Distribution authorized to U.S. Government agencies and their contractors. Critical technology, May 1987. Other requests for this document shall be referred to WRDC/POSL, WPAFB, OH 45433-6563.
2b. DECLASSIFICATION/DOWNGRADING SCHEDULE	
4. PERFORMING ORGANIZATION REPORT NUMBER(S) R89AEB259	5. MONITORING ORGANIZATION REPORT NUMBER(S) AFWAL-TR-89-2012
6a. NAME OF PERFORMING ORGANIZATION GE Aircraft Engines 6b. OFFICE SYMBOL (if applicable)	7a. NAME OF MONITORING ORGANIZATION Air Force Wright Aeronautical Laboratories Aero Propulsion and Power Laboratory (AFWAL/POSL)
6c. ADDRESS (City, State, and Zip Code) Cincinnati, Ohio 45215	7c. ADDRESS (City, State, and Zip Code) Wright-Patterson Air Force Base Ohio 45433-6563
8a. NAME OF FUNDING/SPONSORING ORGANIZATION Aero Propulsion and Power Laboratory 8b. OFFICE SYMBOL (if applicable) WRDC/POSL	9. PROCUREMENT INSTRUMENT IDENTIFICATION NUMBER F33615-84-C-2430
8c. ADDRESS (City, State, and Zip Code) Wright Research and Development Center Air Force Systems Command Wright-Patterson AFB, OH 45433-6523	10. SOURCE OF FUNDING NUMBERS PROGRAM ELEMENT NO. 62203F; PROJECT NO. 3048; TASK NO. 06; WORK UNIT NO. 37

11. Title (Include Security Classification)
Improved Fatigue Life Bearing Development

12. PERSONAL AUTHOR(S)
Bamberger, E.N., Price, M.J. (GEAE); Averbach, B.L. (MIT); Pearson, P.K., and VanPelt, S. (Torrington-Fafnir)

13a. TYPE OF REPORT	13b. TIME COVERED	14. DATE OF REPORT (Yr., Mo., Day)	15. PAGE COUNT
Final	FROM 9-84 TO 12-88	June 1989	172

16. SUPPLEMENTARY NOTATION
Subject to Export Control Laws

17. COSATI CODES			18. SUBJECT TERMS (Continue on reverse if necessary and identify by block number)
FIELD	GROUP	SUB. GR.	Bearings, Rolling Element, Life, Fatigue, Wear, Carburizing, Coating, Debris, Surface Effect
13	09	--	
21	05		

19. ABSTRACT (Continue on reverse if necessary by block number)
This report describes a program to develop/evaluate a rolling-element bearing material that has a fatigue life of three-to-five times that of VIM-VAR M50, the current standard aircraft gas turbine engine bearing material. Because the application of any such extended-life material will be primarily in advanced, high-speed engines, it was also essential to demonstrate adequate fracture toughness to preclude race fracture at the high expected DN levels. Improved corrosion resistance (relative to M50) was another desirable feature of this advanced bearing material.

The program consisted of three phases. Phase I was a basic technology study. In Phase II, full-scale bearing component testing and evaluation were carried out. Phase III, a mid-contract amendment, was designed to evaluate the fracture toughness (K_{Ic}) of several advanced, high-performance, high-temperature bearing steels over a temperature range of -65° to 400°F.

20. DISTRIBUTION/AVAILABILITY OF ABSTRACT	21. ABSTRACT SECURITY CLASSIFICATION
UNCLASSIFIED/UNLIMITED ☐ SAME AS RPT. ☐ DTIC USERS ☒	Unclassified

22a. NAME OF RESPONSIBLE INDIVIDUAL	22b. TELEPHONE NUMBER (Include Area Code)	22c. OFFICE SYMBOL
Nelson H. Forster	(513) 255-4347	WRDC/POSL

DD Form 1473, JUN 86

Block 19 Continued

The program was completed successfully; all three goals were met. It was shown by component and full-scale bearing tests that a thin dense chrome (TDC) coated M50NiL bearing material can improve life to over 5 times that of M50 in a contaminated-oil environment. The M50NiL per se has K_{Ic} more than double that of standard through-hardened M50, and the TDC coating provides excellent long-term corrosion protection to both M50 and M50NiL components.

The Phase I effort included a study to achieve better understanding of the material characteristics necessary to meet the program objectives. This included review of surface/subsurface failure mechanisms in current high-performance, high-speed, mainshaft bearings for turbine engines. This study confirmed that the majority of rolling element bearing failures (95%) are the result of surface distress caused by a number of disparate events. Because of this, it was concluded that increasing the tolerance of the bearing surface to distress could improve overall bearing life to the levels required by the contract objectives.

Based on an extensive material/process evaluation in Phase I, the M50NiL-TDC combination was selected for full-scale bearing testing in Phase II. Phase II involved testing of 40-mm bore ball bearings in a contaminated-oil environment produced by adding 2.5 ppm of 20-μm size Al_2O_3 to the lubricant. Two test series were performed. The first consisted of 10 tests on VIM-VAR M50 bearings, the second of 11 tests on M50NiL TDC coated bearings.

The B_{10} life of the M50 bearings in the contaminated-oil environment was 87 hours; the M50NiL-TDC coated bearings had a B_{10} life of 480 hours under the same test conditions. Prior to and during these tests, measurements were made to document the propagation rate of Al_2O_3 induced surface damage. It was observed that the initial flaws (dents, surface distress) propagated by a micropeeling mechanism which ultimately developed into a macroscopic spall. The data show that the overall "peeling rate" of M50NiL was about one-sixth that of M50. Because in these tests all of the bearing lifetimes were spent in peeling (the test was stopped when a spall was generated), it is apparent that the two independent observations – rolling-contact fatigue life and peeling rate of the two materials (M50, M50NiL) – are consistent.

Corrosion tests performed on tested bearings confirmed that the TDC coating continued to provide corrosion protection even after hundreds of hours under severe test conditions and on all bearing surfaces.

A M50NiL-TDC coated mainshaft ball bearing (133-mm bore) was also evaluated in a rigorous test cycle with excellent results.

The Phase III effort generated a comprehensive data base of the fracture toughness and Charpy impact (C_V) characteristics of six advanced bearing and gear steels. A nominal correlation between K_{Ic} and C_V has been demonstrated.

Preface

This final report describes the work performed by GE Aircraft Engines, Cincinnati, Ohio, under U.S. Air Force Contract F33615-84-C-2430. The report covers the period September 1984 to December 1988.

The program was aimed at developing an extended-life material, for rolling-element bearings, possessing adequate fracture toughness for high-DN (>2.4 million) operation as well as improved corrosion resistance. The program was sponsored by the Aero Propulsion and Power Laboratory, Wright Research and Development Center (WRDC/POSL), Air Force Systems Command, Wright-Patterson Air Force Base, Ohio. The Air Force Project Engineer was Mr. N. Forster. The GEAE Technical Program Manager was Mr. E.N. Bamberger. Funding for Phase III of the technical effort was provided by Mr. C. Ames, U.S. Army AATD, Ft. Eustis, Virginia and Mr. D. Popgoshev, USN, NAPC, Trenton, New Jersy.

In the performance of this program, GEAE used a team approach; The Torrington Company Advanced Development Center – Fafnir Bearing Division, Massachusetts Institute of Technology, and Spire Corporation were key members. Mr. P.K. Pearson, Dr. B.L. Averbach, and Dr. P. Sioshansi were the principal investigators respectively for these organizations.

Special acknowledgments are also due to the following individuals for their substantial contributions to the technical effort: Mr. Michael Price of GEAE for assessing fracture toughness of various bearing and gear steels and for authoring Appendix A of this final report; Mr. Dave Kroeger of GEAE for assisting Mr. Price in this endeavor, including managing the sizeable logistics considerations; and Mr. Steve Van Pelt of Torrington/Fafnir under whose direction the full-scale bearing test program was performed and who personally did much of the painstaking work in mapping and detailing the propagation of surface defects in these bearings. Others contributing significantly to the overall program effort were: Mr. K. Asher and Mr. W. Crecelius, GEAE; Mr. T. Dickinson and Mr. H. DaVerio, Torrington/Fafnir; and Dr. J. Hirvonen, Spire Corporation.

Table of Contents

Table of Contents (Concluded)

List of Illustrations

List of Illustrations (Continued)

List of Illustrations (Continued)

List of Illustrations (Continued)

List of Illustrations (Continued)

List of Illustrations (Concluded)

List of Tables

1.0 Summary

This final report covers a four-year, three-phase effort to evaluate and define an alternate material fabrication technique and/or a material process for use in turbine engine mainshaft rolling-element bearings capable of operating at 3 million DN (DN = bearing bore diameter in mm × rpm) and displaying an RCF (rolling contact fatigue) life three to five times better than that of the current-state-of-the-art bearing material VIM-VAR (vacuum induction melted – vacuum arc remelted) M50. A secondary objective was to define an extended-life, fracture-tough, bearing material having improved corrosion resistance (equivalent to a 14-Cr steel). A final consideration was that any material/material combination selected should be at a stage of development where production introduction was feasible within 3 to 5 years after completion of the development effort.

In addition to the primary effort, a second task (Phase III) was added during midprogram. This consisted of evaluating the fracture toughness (K_{Ic}) and Charpy impact (C_V) characteristics of several advanced, high-performance, high-temperature bearing and gear steels over the temperature range of -65° to 400°F. This effort is discussed in Appendix A of this report.

To achieve the program objective, a comprehensive evaluation of potential materials and processes was made. From this, a number of candidate materials/processes were selected, and these were evaluated in various laboratory tests including RCF, corrosion, and rolling-element behavior in hard-particle-contaminated environments.

To develop better understanding of the material property improvements necessary for extended RCF life, the program included investigation of surface/subsurface failure mechanisms in current high-performance, high-speed mainshaft bearings of turbine engines. This investigation confirms (and documents) what has been recognized for some time: the majority of rolling-element bearing failures (>95%) are the result of surface distress from a broad range of causes including but not limited to oil contamination, processing-induced damage, corrosion-induced micropitting, metal-to-metal contact due to mixed or boundary lubrication modes, etc.

Based on these data and failure statistics, the development program (Phase I) was oriented toward improving the ability of the bearing surface to resist damage, or to sustain it in a manner that would not result in spalling fatigue failures. This approach was deemed more efficacious than attempting to improve the bulk fatigue properties of the material. It was concluded that by increasing the tolerance of the surface to distress, overall bearing life could be improved to the levels required by the contract objective.

Consequently, the major thrust of the experimental work was centered on means to improve surface characteristics. These included application of coatings and implementation of surface modifications.

Because surface distress became the focus of investigation, the more standard RCF life tests were not adequate by themselves. A test method was developed that permitted quantitative analysis of the effect of oil-entrained contamination (considered one of the major causes of bearing distress). This procedure, using a small, controlled amount (2.5 ppm) of hard-particle contaminants mixed into the lubricating oil, proved successful in laboratory element tests and subsequently in full-scale bearing tests. An additional feature of the controlled-contamination baseline testing was the ability to establish surface distress initiation and propagation rates.

Based on all of the preliminary test results, coupled with other relevant data, a carburized material (M50NiL) was selected as the prime structural substance for the Phase II testing. A thin dense chrome coating (TDC) was chosen to provide overall corrosion resistance as well as enhance the ability of the functional bearing surfaces to tolerate oil-entrained contaminants.

Full-scale bearing tests demonstrated that M50NiL bearings with TDC coatings have about 6 times the lives of standard M50 bearings. Failures were induced at the raceway surfaces of these rings, and the primary mechanism of failure was a peeling action at the surface. When the peels reached a critical size, spalling occurred.

The M50NiL, TDC rings were more resistant to peeling, probably because of residual compressive stresses in regions just below the race surfaces, and this translated into extended life. In service, the combination of peeling resistance and the excellent corrosion resistance provided by the TDC coating should provide bearings with very long life.

An engine-size ball bearing (133-mm bore) having M50NiL inner and outer rings TDC coated was also appraised in a severe component test. No indications of distress were noted.

Finally, the Phase III effort has generated a large data base on the toughness characteristics of a number of advanced bearing and gear materials.

2.0 Introduction

GE Aircraft Engines performed this research and development program under Contract F33615-84-C-2430. The objective was to develop and evaluate a rolling-element bearing material having fatigue-life capability three to five times that of VIM-VAR M50, the current standard aircraft gas turbine engine bearing material. Because application of any such extended life material will be primarily in advanced, high-speed engines, it was necessary that the selected material also have the fracture toughness required to prevent race fracture at the expected high-DN levels. In addition, improved corrosion resistance (relative to M50) was a goal. Achieving the latter would significantly reduce the high costs and logistics problems currently encountered by DoD as a result of bearing corrosion.

The program consisted of three phases. Phase I was a basic technology study, and Phase II covered full-scale component testing and evaluation. In Phase I, candidate materials were evaluated using experimental data and subjective analysis. A series of screening tests included rolling-contact fatigue, fracture toughness, and corrosion resistance; the candidate materials were evaluated, and one candidate material/process was selected for the Phase II component evaluation. In this second phase, full-scale bearing performance and life tests demonstrated that the overall goal of the program had been met.

Phase III, a midcontract amendment, evaluated the fracture toughness (K_{Ic}) of several advanced, high-performance, high-temperature bearing and gear steels over a temperature range of -65° to 400°F.

This final report describes the work performed and discusses the results. It deals primarily with the Phase II and Phase III results, the work in Phase I having been detailed in an interim report (Reference 1). However, portions of the interim report are reprised herein in order to present a total and integrated summary of the overall effort in one volume.

3.0 Background

The objective of the program discussed in this report was to develop a rolling-element bearing material having a significantly improved fatigue life relative to VIM-VAR M50, the current standard bearing material. Coupled to this primary objective were two secondary goals: (1) fracture toughness adequate to sustain 3-MDN (3 million DN) operation safely and reliably and (2) corrosion resistance equivalent to that of 14-Cr steel. The following is a discussion of the approach and general technical philosophy GEAE and the associated team members brought to this complex assignment.

The current standard bearing material, a Cr-Mo-V high speed tool steel known as M50, has been used since about 1957 and has logged millions of flight hours in U.S. commercial and military aircraft gas turbine engines. In over three decades of evolutionary improvements, illustrated in Figure 1, it has remained the superior bearing alloy.

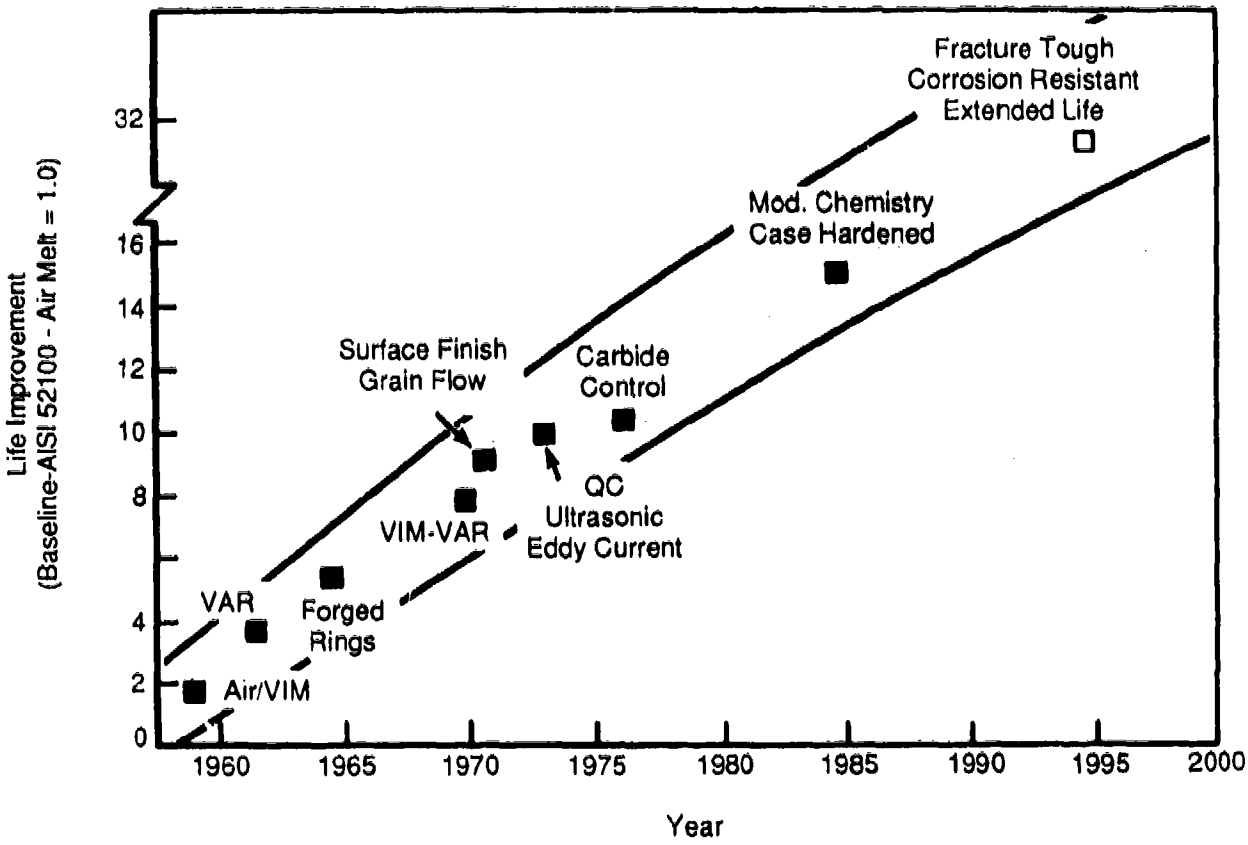

Figure 1. Evolution of M50 Bearing Steel.

The low failure rate of current-generation bearings can be ascribed to continuing improvement in M50 subsurface fatigue resistance as well as, of course, improved design and analytical capabilities. For example, the widely used ASME Design Guide for bearings (Reference 2) projects a combined material and lubricant factor of 12 for M50. In actual practice, this has proved to be a conservative number. Operationally verified material life factors of 20 to 40 are the rule rather than the exception. Admittedly, since the issuance of the ASME document, further and significant improvements were made in the M50 processing (VIM-VAR melting) as well as in bearing manufacturing techniques (controlled grain-flow, hardness, and surface refinements).

Over the past 25 years GEAE, other aircraft engine manufacturers, bearing companies, Government agencies, and organizations such as steel companies have developed, investigated, and evaluated literally dozens of "improved" bearing materials. Despite these extensive efforts, a satisfactory replacement for M50 was not identified.

In the late 1970's, it was recognized that because of increasing inner ring hoop stresses due to higher DN bearing operation, M50 was reaching a life-limiting condition. GEAE, with USAF support, developed a carburizing grade of M50 known as M50NiL (the Ni standing for the addition of nickel to the basic alloy; the L signifying reduced carbon content to permit carburizing).

M50NiL was extensively evaluated and, as reported in Reference 3, has the required fracture toughness for 3 MDN operation. RCF testing also indicated that M50NiL offers a potentially significant improvement in bulk RCF life compared to through-hardened VIM-VAR M50. As a result of the development efforts, M50NiL is now bill of materials on several GEAE mainshaft bearings (CF6-80C, CFM56-5, and T700) and is being development tested for a number of other applications in GEAE advanced engines.

One of the earliest and basic considerations in shaping the Improved Fatigue Life Bearing Development program was the concurrent need for a longer life and fracture-tough (resistant) material. It was considered that any significant rolling-element life improvement (3 to 5 times VIM-VAR M50) would lose much value unless considered in the light of high speed-operation where adequate fracture toughness becomes an equally important concern. GEAE felt strongly that it was absolutely essential that any life improvement be accompanied by a commensurate improvement in the fracture toughness of the material. Any technical effort not meeting this guideline would find limited application in advanced propulsion systems.

Lastly, the desired improved corrosion resistance added yet another difficult requirement. High-chrome alloys such as AMS 5741, CRB-7, and TRW 2001 exhibit better corrosion resistance than steels such as M50, M50NiL, etc. However, the high-Cr materials are all through-hardened and thus do not possess the needed fracture toughness. GEAE has, in the past, performed some work for NASA on modifying a 14-Cr steel to a lower carbon, carburizing grade (Reference 4). The initial experimental work using a straight 14-Cr steel (AMS 5749) was, however, unsuccessful.

To improve corrosion resistance of a bearing material, there are essentially two options. The first, as described above, is the use of a high-Cr, inherently corrosion-resistant material. The second is to use protective coatings or surface-modification techniques. Based on the results of attempts to improve the life and fracture resistance of high-Cr steels, GEAE chose to concentrate on the coating or surface-modification approach.

Corrosion is an important issue because corrosion is the major cause of bearing rejection at overhaul. It has been established that over 30% of bearing rejections made at overhaul are because of corrosion. Data supporting this situation are shown in Table 1 (from Reference 5). The influence of corrosion on bearing failures, per se, is not as well documented; however, there is little doubt that corrosion on critical surfaces, such as raceways, causes pitting that can precipitate spalling fatigue. In the case of high-DN bearings, more severe damage, such as fracture, is likely to occur.

Table 1. Aircraft Bearing Rejections at Overhaul by Cause.

	Percent of Total		
Category	1969	1971	1977
Dimensional Discrepancies	15	10	18
Corrosion/Pitting	32	30	29
Improper Installation, Damaged During Removal or Handling	7	5	6
Wear, Excessive Internal Clearances	-	15	8
Fatigue, Surface or Subsurface Initiated	2	3	1
Cage Wear	2	3	-
Indentations/Contaminants (Nicks, Scratches, Dents)	14	19	20
Other - Change in Directives, Specs, Time Compliance, etc.	28	15	18

The effect of corrosion on bearing life will assume greater importance as condition monitoring becomes an established practice in Air Force and Navy aircraft engines. Condition monitoring is expected to reduce and possibly eliminate scheduled overhaul cycles. Since cosmetic or even mild pitting corrosion alone will probably not trigger a warning, the threat of a corrosion pit resulting in more severe bearing distress and/or failure becomes considerably greater.

Bearing corrosion is, therefore, a serious drain on Department of Defense resources as well as a potential starting point for bearing failure. While corrosion is not the direct, critical, technical barrier to advanced bearing technology that low fracture toughness or limited fatigue life are, it is important, in view of the widespread occurrence, and carries extensive economic and strategic implications. The most recent available data show that the cost of bearing corrosion at one Air Force overhaul center alone was $4 million per year.

Other recent data for commercial engines, which are less susceptible to corrosion problems because of different usage factors, indicated a cost of close to $800,000 on one engine model over about a 2-year period. These are bearing replacement costs only and do not include associated teardown and overhaul expenses which far exceed the hardware cost.

While work has been conducted in the past on developing corrosion-resistant bearing alloys, the conventional approach has been to improve the bearing lubricant by the addition of corrosion-resistant additives. This approach has had a degree of success as evidenced by the data reported in Reference 5. However, to achieve a truly significant reduction in bearing losses due to corrosion, it is essential to make the bearing material as impervious to corrosion as possible with current materials technology.

Returning to the prime objective, that of increasing bearing fatigue life, the traditional goal has been to improve the bulk fatigue characteristics of the structural material. This has, as shown in Figure 1, proved to be a viable approach for the past two to three decades. However, based on a vast body of evidence gathered from actual engine bearing failures or bearings rejected for some form of distress, the failure mode which has been addressed by improving bulk RCF, and which is evidenced by subsurface-initiated fatigue, is rarely identified as the primary failure mode in modern, high-performance, aircraft engine bearings. Surface distress followed by surface destruction and subsequent surface/subsurface fatigue propagation is by far the predominant failure mode. This issue was addressed in detail in Reference 6.

Consequently, the GEAE team, with Air Force Project Management concurrence, reached the decision that "Life Improvement" would become a dual objective consisting of improving the bulk fatigue properties of the selected material coupled with enhancing the ability of the bearing surface to survive in increasingly hostile environments.

Because the latter consideration became the major driving force for the technical effort, the following considerations had to be addressed.

The combinations of loads, temperatures, rotational speeds, and lubricants being proposed for rolling-element mainshaft gas turbine bearings operating up to 3 MDN suggest that these bearings will be functioning in the boundary lubrication regime. Values of the lubricant film thickness, h, may be as low as 2 μin, and the specific film thickness could be less than unity. Under these conditions, surface distress occurs at the raceway and rolling-element surfaces rather than in the subsurface region. Having started at the surface, damage will either continue to propagate at the surface or, depending on a number of operational variables, generate a deep spall that can begin to have a serious effect on continued bearing operation. Preliminary bearing tests (performed prior to the initiation of the contract but reported herein) show that damage can be initiated at microstructural features such as carbides and at surface asperities that are well within the accepted tolerances for acceptable finishes. The microscopically damaged regions develop into microspalls, and these in turn evolve into the usual spalling failures.

These findings, coupled with engine experience, indicated the following approaches would be advantageous to extending bearing life under expected advanced-engine operating conditions:

- Reduce the size of microstructural features such as carbides.
- Introduce substantial compressive stresses, of the order of 30 ksi to a depth of about 0.03 inch, to inhibit the initiation of microcracks and to slow the subsequent propagation by fatigue.
- Improve corrosion resistance in order to avoid chemically induced failure-initiation sites.
- Exclude extraneous hard particles (that can dent, score, or pit the rolling-element surfaces) and/or provide a bearing surface capable of sustained life in the presence of such particles.

These considerations led to the logical conclusion that a major improvement in bearing life could be achieved by improving the integrity of the bearing surface and rendering this surface more tolerant to air- or oil-entrained debris or contaminants; that essentially summarizes the technical rationale for the work reported in this document.

4.0 Phase I – Evaluation of Materials, Fabrication Techniques, and Processes

Phase I comprised a basic technology study. Candidate materials and processes were evaluated using newly generated experimental data, information previously obtained, and subjective analyses. A number of basic tests were dictated by the overall program goals:

- Rolling-Contact Fatigue
- Corrosion
- Contamination (Measurement of the ability of the bearing surface to withstand oil-entrained contamination.)

Other pertinent material properties such as fracture toughness, hardness, hot hardness, and wear resistance were considered (based on available data) in overall assessment of material/process candidates.

Lastly, more subjective considerations such as near-term producibility/availability, repairability, potential cost impact, etc., were factored into the overall material/process assessment and selection.

Phase I consisted of the following tasks:

- Review of Surface/Subsurface Initiated Failure Mechanisms
- Material and Process Candidate Selection
- RCF Testing
- Corrosion Testing
- Contamination Testing
- Assessment of Other Properties and Characteristics
- Selection of Prime Candidate Material and Process
- Baseline Full-Scale Bearing Testing

4.1 Review of Surface/Subsurface-Initiated Failure Mechanisms

As discussed in the Introduction and Background, the selected technical approach was to extend rolling-element bearing life through a combination of improving the bulk fatigue characteristics of the bearing material coupled with enhancing the ability of the bearing surface to survive in hostile environments including air or oil-entrained contamination, corrosive media, and minimal oil films (boundary lubrication). Of the two considerations, the attainment of damage-tolerant surfaces was considered by far the more important because of the preponderance of surface-initiated bearing failures.

This portion of the report is intended to support the above decision by:

1. Briefly reexamining the conditions leading to boundary lubrication.
2. Commenting on recent bearing test results performed under boundary lubrication conditions.
3. Reviewing the results of some precontract Torrington-Fafnir bearing tests where identification of failure initiation was the prime objective.
4. Presenting a compendium of photographs illustrating the range of surface-initiated failures in aircraft engine mainshaft bearings.

Lastly, some major technical issues in extending bearing life at high DN's will be addressed.

Ball and roller bearings made of VIM-VAR M50 steel have operated successfully up to 2.3 MDN. However, at higher speeds and temperatures several of the operating parameters reach critical values and combine to exceed the limits at which M50 can operate safely. These critical factors include high hoop stresses, Hertzian stresses, thin elasto-hydrodynamic (EHD) lubricating film, and the physical and chemical characteristics of the bearing surfaces. High-speed operation markedly increases the frequency of stress cycling, and even a seemingly low rate of crack propagation can lead to a major crack in a few hours. Test data presented later in this section indicate that failures start at the surface with the thin EHD films typical of mainshaft gas turbine bearings. This focuses attention on the physical characteristics of the surface, the microstructure, sensitivity to corrosion, and on the use of techniques for surface modification. It is apparent that surface distress will be a major problem at any speed, and the photographs of bearing failures observed in current engines (shown later) confirm that surface, rather than subsurface, initiation is the predominant mechanism even under present-day operating conditions.

4.1.1 Rolling-Element Lubrication

Theoretical treatment of the lubrication of ng-element surfaces involves consideration of the properties of thin films of polymer liquids at high pressures and shear rates along with evaluation of the physical and chemical interactions between the lubricant and the surfaces. In practice, adjustments to the expected lifetimes of ball and roller bearings are made by introducing a lubricating factor, F, as a multiplier of the AFBMA (Anti-Friction Bearing Manufacturers Association) fatigue life. These multipliers are listed in the ASME (American Society of Mechanical Engineers) Design Guide (Reference 2) and in the catalogs of bearing manufacturers. In mainshaft gas turbine bearings, however, film thickness is reduced to the point where surface damage becomes an important consideration in the bearing life; therefore, it is worthwhile to review briefly the factors that influence the lubricant film.

The Mobil EHL Guidebook, Third Edition (Reference 7), is a convenient reference; it summarizes the procedures for calculating film thickness (h) and provides a convenient compilation of the relevant equations.

1. Viscosity, speed, and the pressure viscosity coefficient have the greatest effect on film thickness, and they all have about equal weight. A 20% increase in any of these variables will increase the film thickness by about 14%.

2. The effects of temperature are incorporated by the temperature dependence of the viscosity. In a typical case, viscosity can decrease by a factor of 30 as the temperature rises from 68° to 212°F.

3. Materials for the rolling elements do not affect the film thickness. Surface tension effects are neglected.

At a sufficiently high temperature, all lubricants reach a critical state where the lubricating film collapses. This is the critical scuffing temperature, about 3000° to 3950°F for mineral oils and somewhat higher (3950° to 4800°F) for diphenyl lubricants.

Surface roughness has been designated in rms (root mean square) values, and a specific film thickness, λ, is defined as:

$$\lambda = h(\sigma^2_1 + \sigma^2_2)^{-1/2} \qquad \text{(Equation 1)}$$

where: h = film thickness

σ_1 = rms roughness of Body 1

σ_2 = rms roughness of Body 2

With values of $\lambda < 1$, boundary lubrication prevails, and this condition occurs with typical film thickness in the 1 to 4 μin range. Elasto-hydrodynamic lubrication is considered to occur at $\lambda > 2$, usually with film thickness greater than 10 μin. The intermediate region is one of marginal or mixed lubrication.

4.1.2 Bearing Tests Under Boundary Lubrication

Preliminary calculations for a prototype mainshaft bearing running in synthetic oils (Mil-L-7808 or Mil-L-23699) at 300°F indicate that film thickness could be as low as 2 to 4 μin. Normal asperities, with the most favorable finishing methods, will result in a net roughness of at least 5 μin; thus, it is evident the specific film thickness could be less than unity and that boundary lubrication will prevail.

Bearing test data on M50 and 18-4-1 bearings run under boundary lubrication are scarce; therefore, the recent investigation reported in Reference 8 is of particular interest. The test bearings had a 40-mm bore and carried a radial load, $F_1 = 1980$ lbf, corresponding to a mean contact pressure of $P = 421$ ksi. These were run at 420°F at 3000 rpm in Shell Turbo T32 oil. The film thickness, calculated by the Cheng equation, was $h = 0.8$ μin. The normal calculated fatigue life without a material factor, L_{10}, for these bearings was 272 hours. Three bearing materials were evaluated: M50, 18-4-1, and 52100.

The tests were run under three different lubricating conditions: (1) oil sump, with the bottom rolling element half submerged in oil; (2) oil vapor, with the bearings bathed in oil vapor rising from the sump at 420°F; and (3) exhausted oil vapor, with the oil vapors from the sump exhausted by a fan. Final failure occurred by spalling fatigue. With bearings of 18-4-1, a B_{10} life of about 7 times the nominal rating was obtained with sump lubrication. With oil-vapor lubrication, the B_{10} life was equal to the nominal rating, and with the exhausted oil vapor, the B_{10} life was only 3.5% of the nominal life; M50 behaved similarly to 18-4-1; 52100, as expected at this temperature, was markedly inferior. The ratio 7:1:0.034 for the B_{10} lifetimes illustrates the deleterious effects of starved lubrication. The materials factor for 18-4-1 and M50 was, reportedly, 7 under these conditions.

The nature of the fatigue damage followed a pattern consistent with surface-initiation mechanisms. Under the best condition, oil sump lubrication, the initial damage consisted of micropitting – minute, shallow cavities. After prolonged running, the micropits developed into spalls of the usual size. With oil vapor lubrication, the initial damage, slightly roughened races, was observed long before the first signs of fatigue were detected. With the exhausted oil vapor lubrication, the bearing races exhibited pronounced kinematic sliding and wear marks. After longer times, numerous small pits occurred, followed eventually by fatigue spalls. It is apparent that the damage was initiated with a shallow peeling at the surface, and that these peeling defects eventually generated the more generally observed deep fatigue spalls.

4.1.3 Preliminary Bearing Tests (Torrington-Fafnir)

Evaluation of the fatigue life of bearings by means of simulated tests are successful only in limited areas. Realistic lifetimes of mainshaft bearings are most reliably obtained from full-scale bearings tests. However, bearing tests at 3 MDN require specialized facilities; therefore, an attempt was made to arrive at a simpler test procedure which would evaluate the critical factors expected to influence the life at 3 MDN. The ultimate test would still require bearings to be run at 3 MDN, but it was felt that procedures for an initial screening of materials, processing methods, and surface modifications should be devised.

The testing problem becomes evident in a consideration of the lifetime data presented in the previous section on 40-mm bearings of M50. The nominal B_{10} life was calculated to be 272 hours. Even with a conservative materials factor of 7, the B_{10} rises to 1900 hours, almost 3 months, and it is evident that at least a year would be required to generate a significant life curve. Considering the program objective of achieving an even longer extended life, the running times become very long indeed.

It is anticipated that 3 MDN bearings may operate at or near 300°F with one of the established synthetic lubricants such as Mil-L-7808 or Mil-L-23699. The film thickness is expected to be of the order of 2 to 4 μin. Since the normal ground and honed surfaces have roughness values of the order of 6 μin, the specific film thickness will be less than unity, and boundary lubrication conditions are expected to prevail.

Because preliminary test data indicated that failures under these conditions of boundary lubrication would start at the surface, it appeared appropriate to study the initiation of fatigue damage in a thrust bearing operating with the appropriate film thickness and the appropriate lubricant. Most of the bearing lifetime is spent in the initiation stage, and data on initiation phenomena would thus be useful in developing new processing procedures for extending the life of bearings operating at speeds up to 3 MDN. A 40-mm thrust bearing (Fafnir 2AAM 208WO MBR) was selected for the preliminary tests. Bearings were run at 10,000 rpm at a thrust load of 2450 lbf, corresponding to a maximum compressive stress of 380 ksi, using a 7808 type lubricant at 300°F. These bearings were the same bore size as those described in Reference 8 but were subjected to thrust loading. Film thickness values calculated with the Cheng equation are shown in Figure 2 along with the corresponding values for a Mil-L-23699 lubricant. The film thickness values at 10,000 rpm are of the order of 3 to 4 μin, and are in the boundary lubrication range. Film thicknesses calculated with the Archard-Cowking equation using the TRESCAP computer program are slightly thinner. These thrust bearings simulate Hertzian loading and lubrication conditions typical for a gas turbine mainshaft bearing. Missing are the hoop stresses, dynamic loads, and speeds expected at 3 MDN; these can only be achieved in special test facilities.

Since lifetimes of nearly 3000 hours were expected, and because the primary concern was initiation of fatigue damage at the surface, a procedure was adopted whereby the bearings were run for a predetermined time then dismounted for microscopic examination of the running surfaces to identify the likely failure-initiation mechanism for bearings run under the test conditions. The first tests were run on bearings made of VIM-VAR M50.

Figure 3 illustrates a typical area of microscopic surface failure observed on the inner ring surface of a test bearing after 147 hours of operation. Figure 3a, a photomicrograph at 100×, shows a grinding groove surrounded by a white region and a series of small micropits. Figure 3b, a SEM (scanning electron microscope) picture at 1000×, shows that these micropits are usually associated with large carbides. Figure 4a, a SEM photograph at 3000×, shows a cracked carbide in the same area, along with other pits probably initiating at carbides. Figure 4b, a SEM photograph at 1000×, shows other examples of pitting at carbides.

A similar sequence of damage sites was observed in another area of the same inner ring. A grinding groove is shown at 100× in an optical photomicrograph in Figure 5a; this exhibits the same type of pitting and microcracking seen in Figure 3. Microscopic damage associated with carbides is illustrated in Figure 5b, a SEM photograph at 1000×.

Similar observations were made after only one hour of operation in a larger diameter (120-mm bore) thrust bearing (also VIM-VAR M50) operating under similar conditions. Figure 6 shows localized damage at 1000× (SEM); here also it is evident that the microcracks are

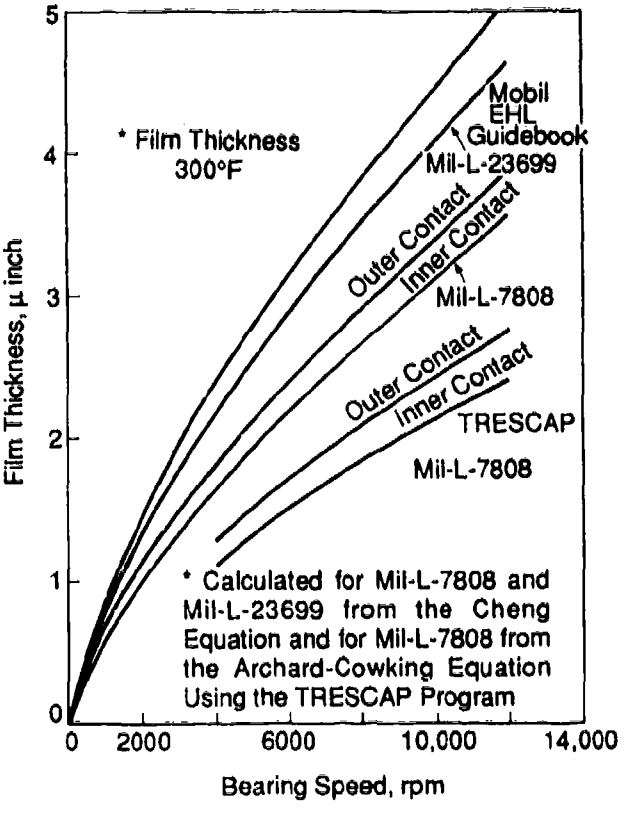

Figure 2. Lubrication Film Thickness at 300°F.

(a) Grinding Groove at 100×, Optical

(b) Micropits at 1000×, SEM

Figure 3. Microscopic Surface Failures on Inner Ring of Thrust Bearing After 147 Hours of Operation.

(a) Cracked Carbide at 3000 ×, SEM

(b) Pitting at Carbides, 1000 ×, SEM

Figure 4. Microscopic Damage of Carbides at Bearing Ring Surface.

(a) Pitting Associated with Groove, 100 ×, Optical

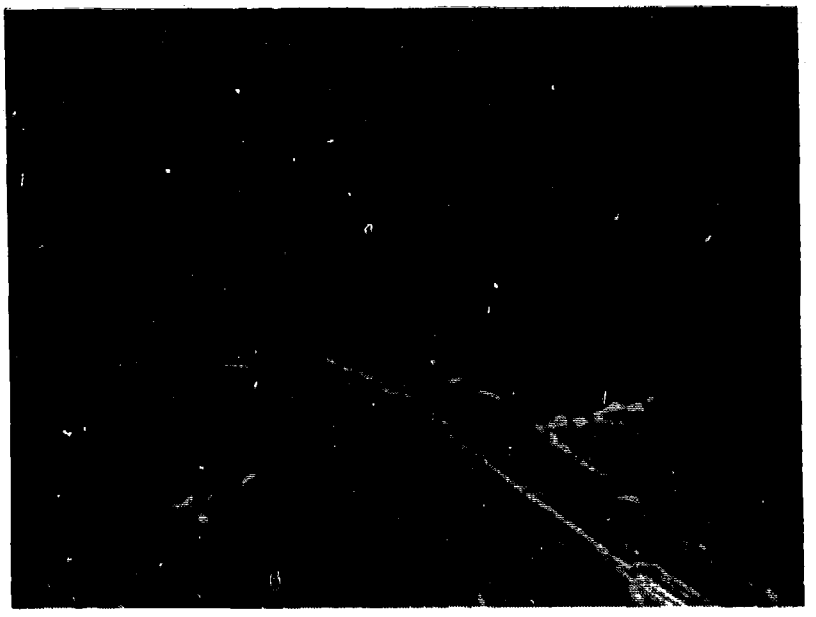

(b) Microscopic Damage Associated with Carbides, 1000 ×, SEM

Figure 5. Microscopic Damage at Grinding Groove.

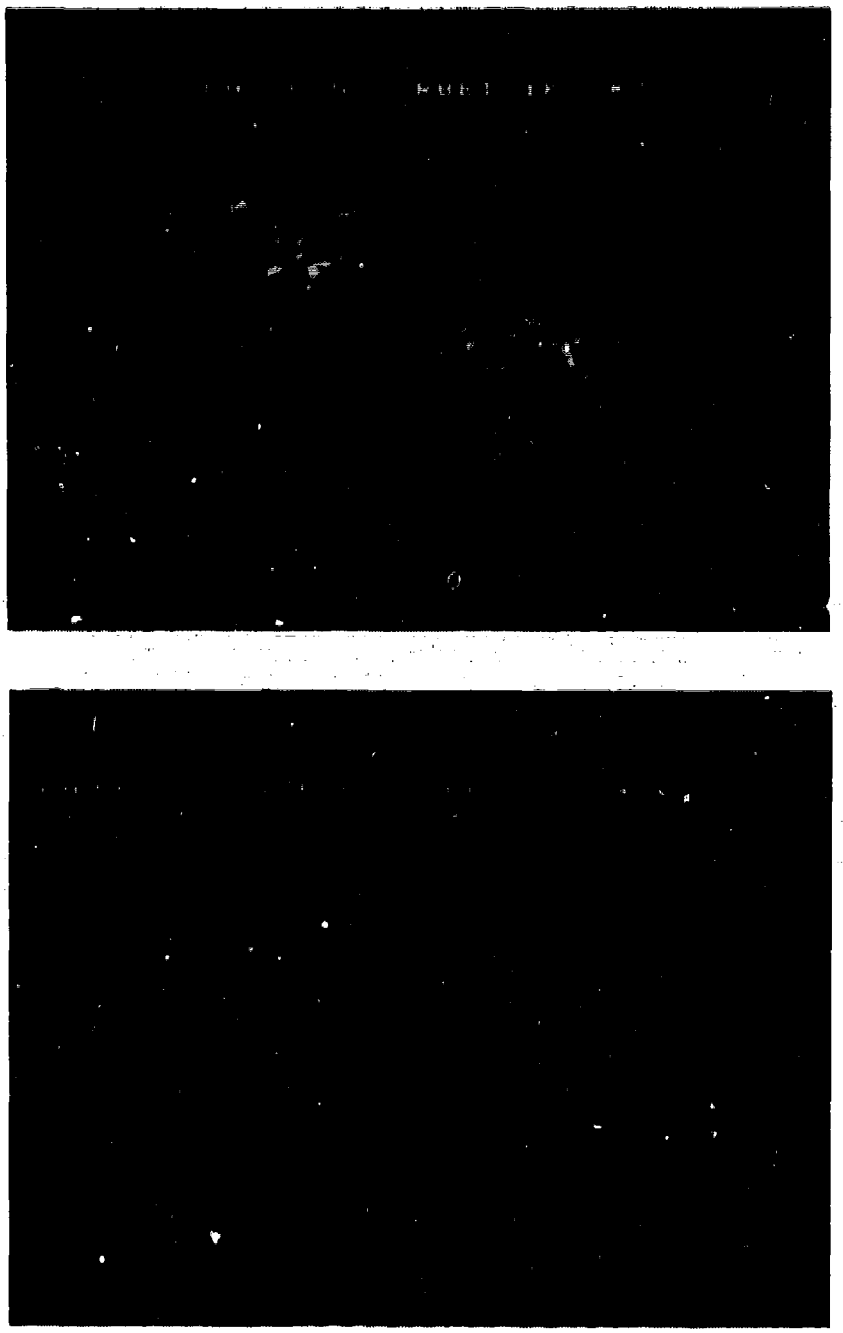

Figure 6. Microscopic Damage in 120-mm Bore Thrust Bearing After 1 Hour of Operation (1000 × SEM).

associated with carbides and appear to have initiated with plastic flow that sheared the matrix material at the carbide interface. It must be emphasized that these bearings have not failed in the conventional sense, rather the initiation of damage is being observed before any distress on a macroscopic scale is evident. It should also be emphasized that the grooves, around which some of the microcracks were initiated, are not abnormal but considered to be part of an acceptable surface finish. Several regions of microfailure were observed in these test bearings, and it was concluded that microscopic failures start at the surface, probably in Mode II shear in the vicinity of carbides, and that the microfissures grow into the shallow spalls characteristic of surface failures.

The surfaces are vulnerable because of the thin EHD films and the presence of topographical initiation sites such as grooves and carbides. The surface spalls have been observed to grow into deep spalls in some instances, and on occasion, particularly in thin-walled rings, the crack will propagate radially and grow into a Mode I crack. In most instances, however, these surface cracks become a series of shallow spalls that cause failure by a peeling mechanism.

From these data, it was concluded that failure resulting from low EHD film thickness will initiate as microcracks at the surface. Since EHD characteristics are not easily modified, it appears that bearing life under these conditions will be improved by reducing the size of potential initiation sites, such as the carbides, and by modifying the surface characteristics to minimize the propensity for damage.

This mechanism also strongly suggests that external sources of surface distress, such as pits introduced by corrosion and fretting or by abrasive debris, will have deleterious effects. Such exogenous pits are probably larger than those associated with the carbides and would thus accelerate the initiation of spalling.

These observations of surface distress and the mechanisms by which peeling and spalling are initiated under boundary lubrication conditions suggest that the lifetime of 3 MDN bearings will be determined largely by the time for the initiation of micropitting, peeling, and other surface phenomena. Surface modification and bearing processing techniques that impart resistance to surface damage can be evaluated by frequent observations of the initiation mechanism on a microscopic scale in bearing tests similar to those described here. As will be seen later, this test procedure, somewhat modified, was successfully adopted in the baseline testing.

A series of preliminary experiments were also run at a lower speed, 5600 rpm, with all other conditions remaining the same. In accordance with Equation 1, the film thickness was thus reduced to about 2 μin. The damage mechanisms were similar to those observed after 24 hours of operation, rather than after about 150 hours at the higher speed. Excursions in engine speeds are common in a normal flight profile, and these data focus attention on potential problems associated with lower speed (lower λ) operation.

4.1.4 Typical Surface-Initiated Failures in Mainshaft Bearings

Jet engine mainshaft bearings operate at about 2.3 MDN or less, but even under these conditions most failures are surface initiated. In this section, optical and SEM photographs of typical failures, or incipient failures, found in field operation are presented. The illustrations in this section are typical of surface distress observed in jet-engine mainshaft bearings. The time to reach these conditions varied from a few hours to several thousand hours, depending on the operational environment. These photographs are representative of the various types of surface distress caused by marginal EHD conditions, by oil-entrained contaminants, by corrosion, by skidding, and by other aberrations in the operating conditions.

These field data support the basic premise of the program objective in that the great majority of failures, even in current engines, are initiated at the surface rather than by the classical subsurface mechanism. This point has been emphasized in Reference 6. The photographs also provide a good tie-in to the failures induced in the subsequent baseline tests discussed in a later section of this report.

Figure 7 shows typical surface distress observed as a consequence of skidding. The surface appears frosty at low magnifications, but micropitting is evident at higher magnifications. This type of surface distress is typical of

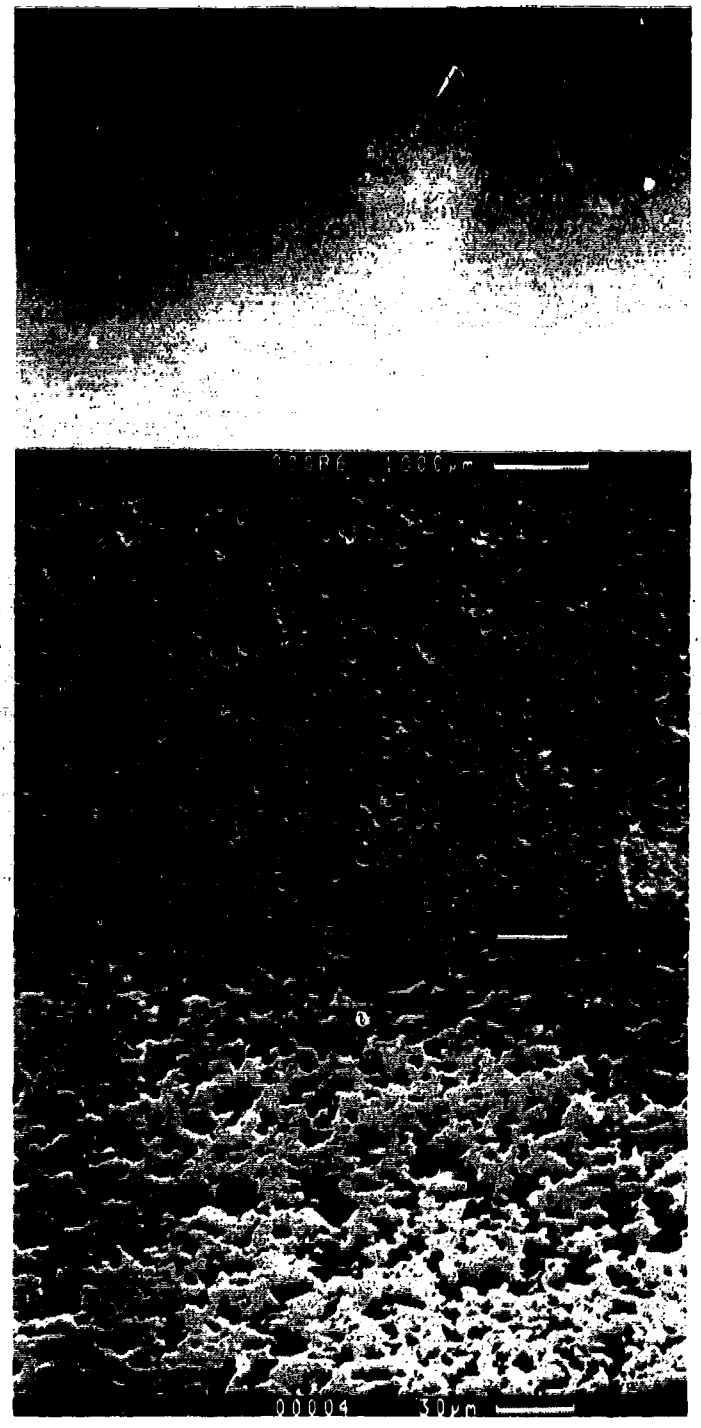

Figure 7. Surface Damage Resulting from Ball Skidding. *This is a typical "orange peel" appearance and will usually propage to more extensive micropitting and spalling.*

situations where local metal-to-metal contact (adhesive wear) has occurred. A related type of surface damage (Figure 8) was induced by the presence of an abrasive contaminant such as Al_2O_3. This type of damage can be localized or widespread, as in Figure 9 where the oil was apparently contaminated with hard abrasive particles.

Corrosion can also be an important contributor to surface fatigue. Figure 10 shows an example of a massive surface fatigue failure caused by corrosion pitting.

Figure 11 illustrates typical corrosion pits in M50, with the usual "mud-cracking" appearance indicated in the lowest photo. Figure 12 shows incipient surface fatigue spalling that initiated at corrosion pits.

Figure 8. Surface Damage Caused by Hard Contaminant Such as Al_2O_3.

Micropitting associated with marginal EHD lubrication is shown in Figures 13 and 14. The score mark was caused by a hard contaminant, and the failure occurred as a result of plastic deformation on the raised shoulders immediately next to the score. This type of failure is very similar to that shown in Figure 5, which illustrates the same type of damage at a grinding groove. Another example of surface fatigue resulting from marginal EHD lubrication, Figure 15, illustrates the microscopic damage associated with heavy score marks caused by contamination in the lubricant.

Nonabrasive debris can cause denting, and Figure 16 illustrates the micropitting and local damage caused by this type of contaminant. Figure 17 shows a more severe case of micropitting and denting caused by debris, and Figure 18 shows debris damage and denting that developed into shallow surface spalls. Denting is a common mechanism for the initiation of spalling.

Figure 19 shows microspalls that developed at grinding grooves under conditions of marginal lubrication, and Figure 20 illustrates extended pitting at the grinding grooves under conditions where the EHD film was too thin to prevent metal-to-metal contact.

Figure 21 illustrates another instance of micropitting associated with skidding. The microscopic scale of this initial damage should be noted. A more macroscopic example of pitting is shown in Figure 22, at 6× and 32×, in a ball bearing race. Figure 23 is an example of micropitting that has propagated into a large spall.

Figure 24 illustrates the role of large undissolved carbides in the initiation of microspalling. Damage can also be associated with excessive use of nital etch during inspection. Microspalling associated with this type of chemical attack is shown in Figures 25 and 26, and the results of severe debris damage are illustrated in Figure 27.

These examples of surface distress in mainshaft bearings support the view that, under marginal EHD lubrication, damage will start at the surface. The initial event is development of a region of localized plastic flow severe enough to result in microspalling. This local flow can be caused by denting associated with debris particles, by scoring associated with the presence of abrasive particles, or by metal-to-metal contact at the shoulders of grinding grooves.

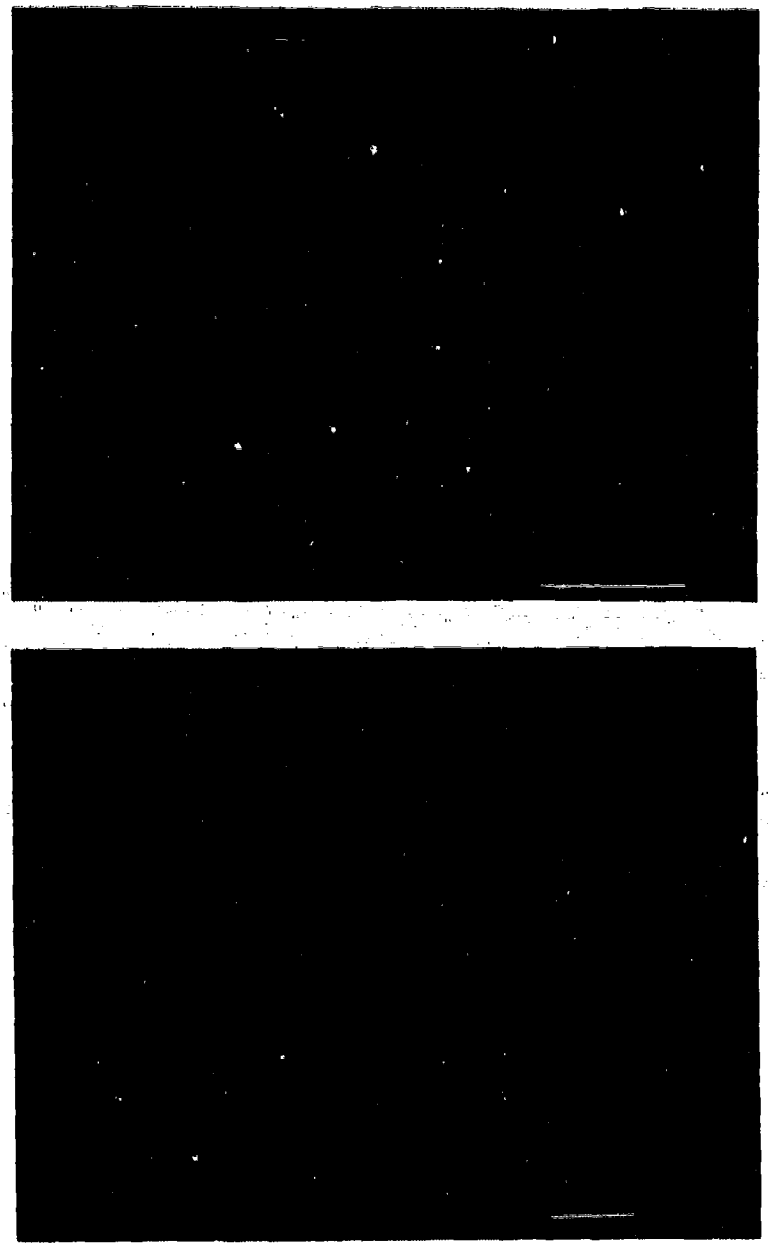

Figure 9. Kinematic Wear Damage on Ball Surface Caused by Oil Contamination with Hard Abrasive Particles.

In addition, micropits may be produced chemically, by corrosion or infrequently by the overextended application of the nital etchant used during inspection for grinding damage. However they are formed, these pits become potential sites of deeper spalls which lead to failure. Most of the bearing life is apparently spent in this initiation stage where microspalls form and develop into macrospalls.

4.1.5 Critical Parameters for Extended Life at 3 MDN

Operating Stresses – A typical ball bearing at 3 MDN can operate at a maximum compressive Hertzian stress as high as 350 ksi. For a 120-mm bore at 25,000 rpm and with 12 rolling elements, this represents 1.8×10^7 cycles per hour. The usual limits for HCF (high-cycle fatigue), 10^9 cycles, are achieved within 6 hours. This illustrates the difficulty of using any test piece other than a bearing to assess the behavior of materials at 3 MDN.

Hoop stress is one of the critical operating parameters, and this has been calculated in Reference 9. For a 120-mm bore bearing, the free-ring tangential stress at the inner race surface was estimated to be 35 ksi. With fit-up stresses, these hoop stresses could reach as high as 50 ksi. The operating stress cycle thus ranges from 300 ksi compressive under the rolling element to +50 ksi tensile between elements.

Fracture Toughness – Hoop stresses are tensile and can lead to Mode I tensile fractures. For M50, with a K_{Ic} value of 20 ksi·in$^{1/2}$ the critical crack size at 2 MDN with a hoop stress of 25 ksi is 0.25 inch and this is considered adequate. At 3 MDN and 50-ksi hoop stress, the critical crack size becomes 0.06 inch, and this is considered unacceptably small. Consequently, in order to be equivalent at 3 MDN to the value at 2 MDN with M50, the fracture toughness should be about 45 ksi·in$^{1/2}$. This level of fracture toughness has been achieved in M50NiL, and the successful operation of this material in bearings run at high hoop stresses has been reported in References 10, 11, and 12.

Thus, one criteria for extended lifetime at 3 MDN is a fracture toughness in the ring material of at least 45 ksi·in$^{1/2}$ to preclude serious Mode I tensile failures.

Fatigue Crack Initiation and Propagation at 3 MDN – Fracture toughness alone does not ensure extended lifetimes. At 3 MDN, failures will probably start at the surface, at a microstructural feature such as a carbide or a surface asperity, or as the result of hard particle damage. All of these are considered normal but are of the order of the EHD film thickness. Assuming that a defect forms by Mode II shear and develops into an initial crack about 0.005-inch long, then for a hoop stress of 50 ksi the Mode I stress intensity is K ≈ 6 ksi·in$^{1/2}$ since the maximum normal stress in the y-direction (along the rolling direction) is of the order of 200 ksi, ΔK becomes 206 ksi, with the R factor, $\theta_{min}/\theta_{max}$, becoming -29. Crack-propagation rates, da/dN, have not been measured for R factors in this range. Typical values (Reference 11) are shown in Figure 28 for M50 and M50NiL for R = 0.1. The values of da/dN at R = -30 are probably lower than those shown in Figure 28, but the magnitude of da/dN, even in the vicinity of the apparent threshold values, is still high enough that a macroscopic crack will develop within a few hours at the cycling rate applied in a 3-MDN bearing.

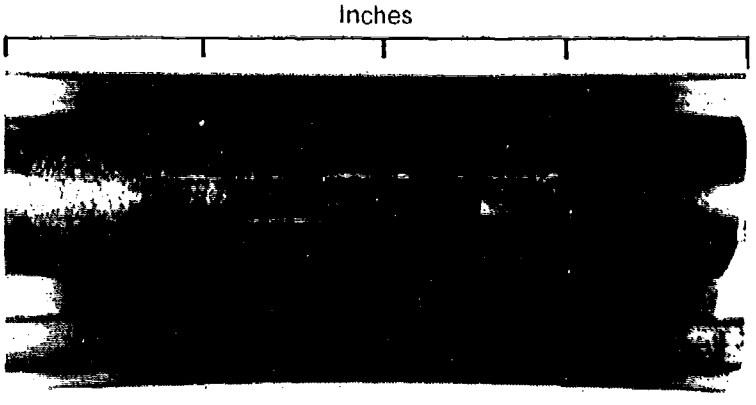

Figure 10. Massive Surface Fatigue Failure Caused by Corrosion Pitting.

This calculation emphasizes the assumption that lifetimes at high DN can only be extended by minimizing the opportunities for surface damage, thus lengthening the initiation time. In a

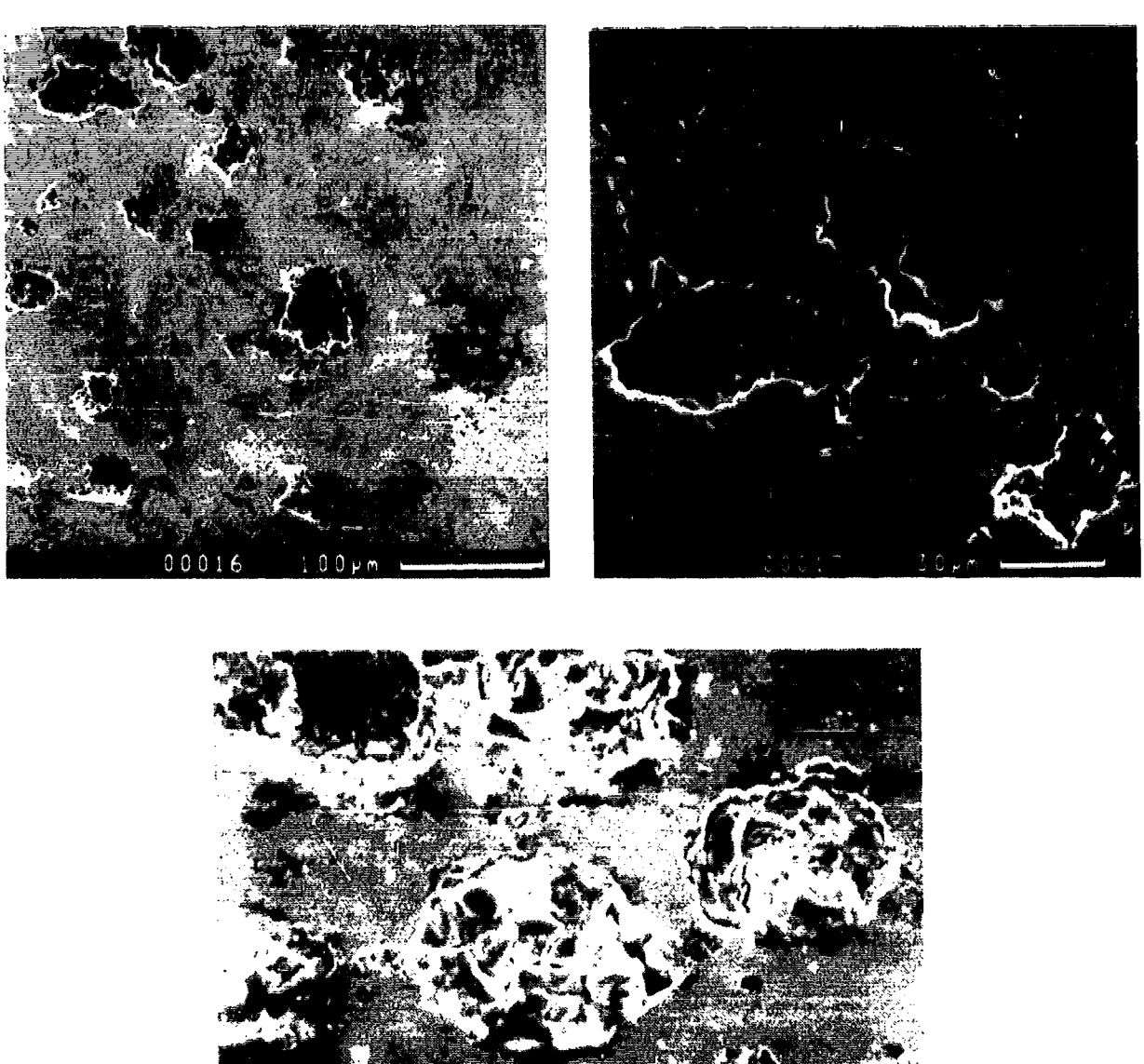

Figure 11. Corrosion Pits in M50 Bearing Steel. *Notice typical "mudcracking" apperance.*

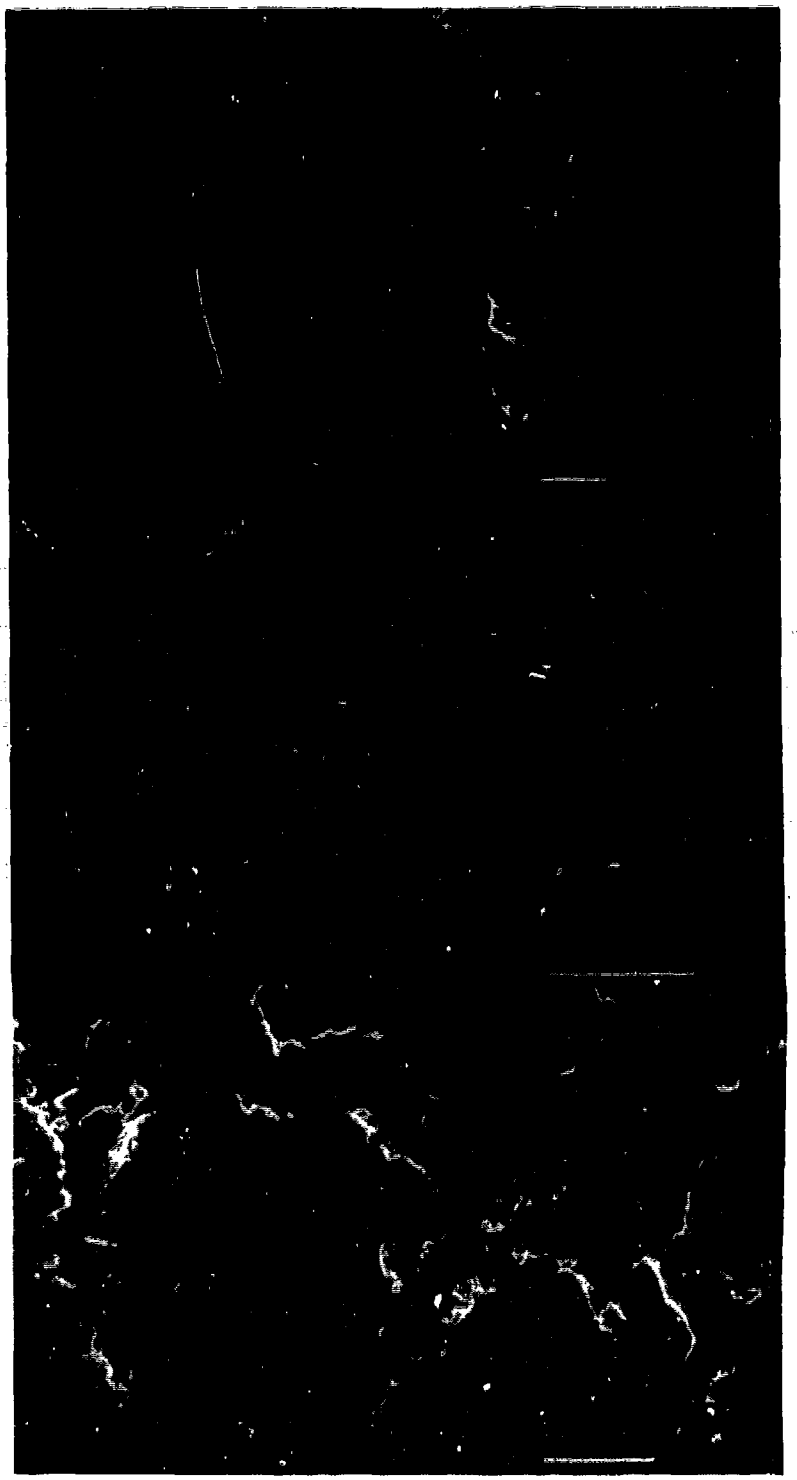

Figure 12. Incipient Surface Fatigue Spalling Resulting from Corrosion Pitting.

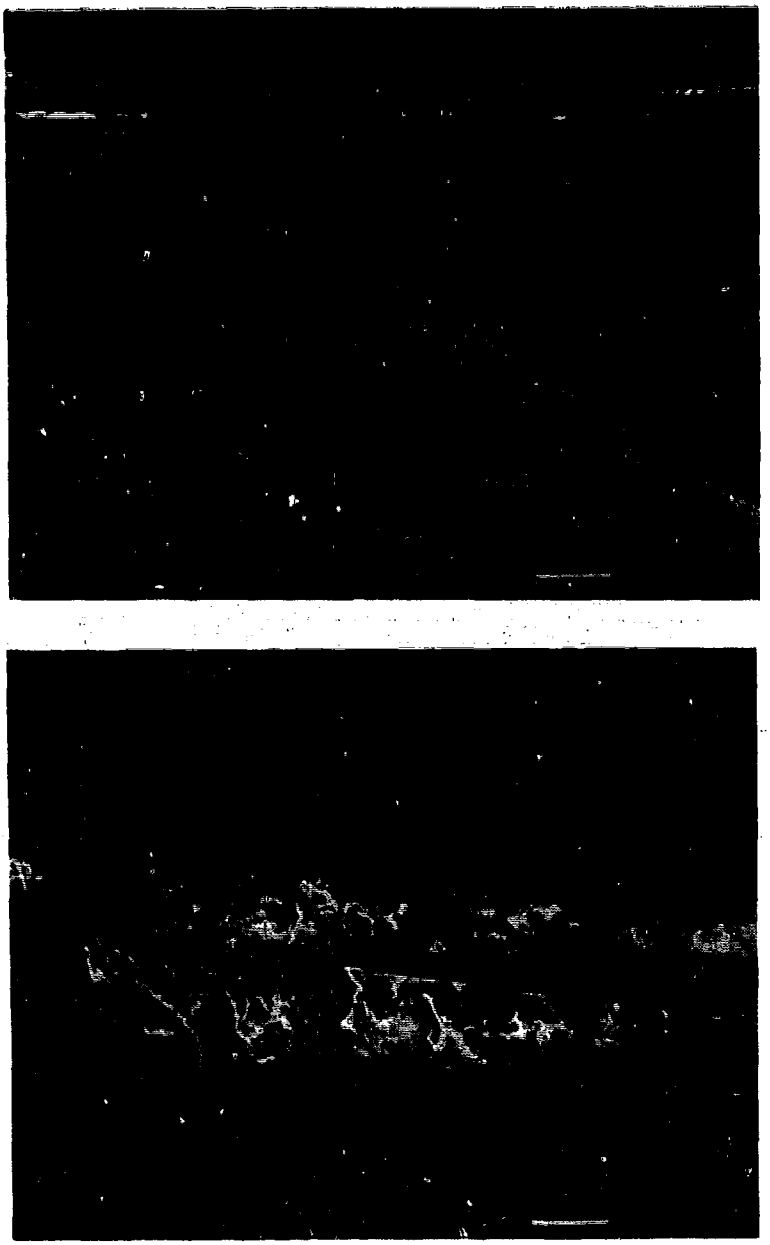

Figure 13. Micropitting Resulting from Marginal EHD Lubrication Associated with Score Mark Caused by a Hard Contaminant. *Failure occured on the "shoulders" of the score where some material has been plastically deformed.*

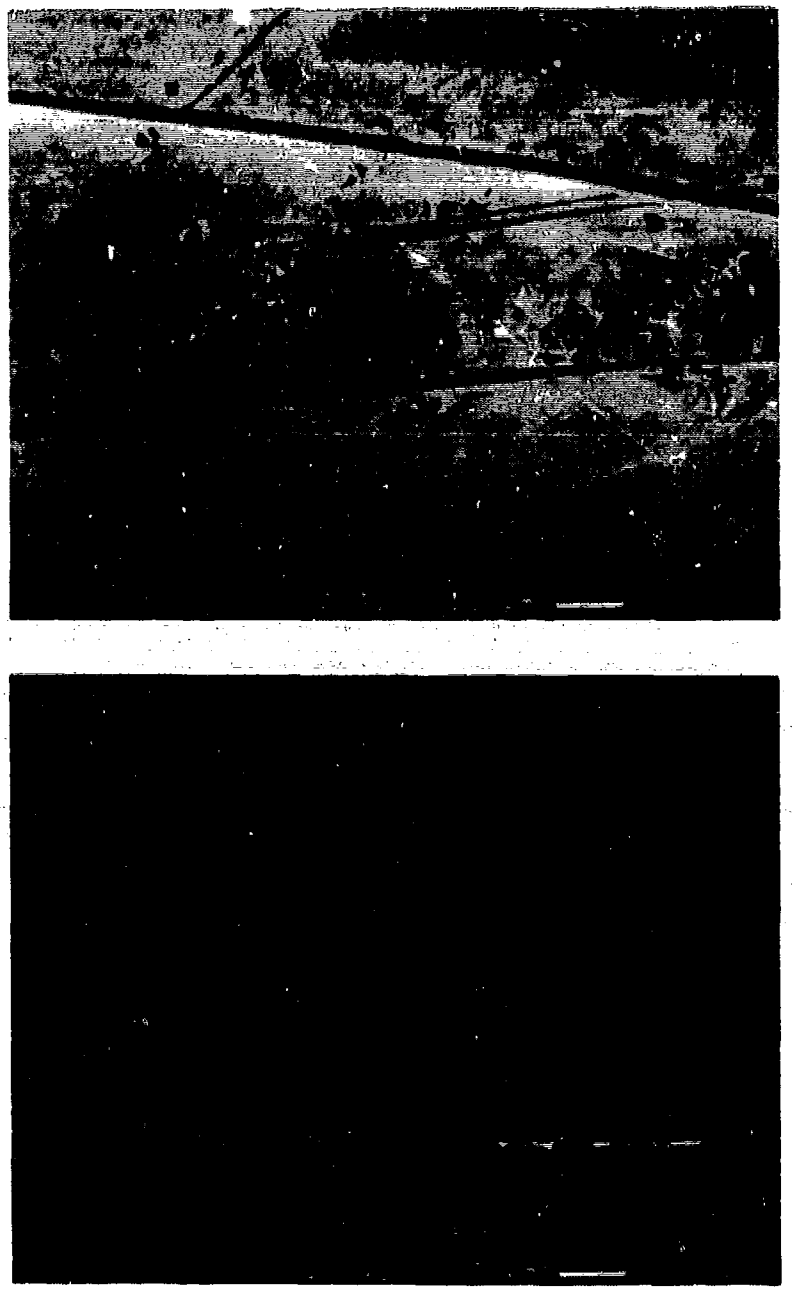

Figure 14. Micropitting Resulting from Marginal EHD Lubrication. *Extensive surface damage occured near score marks (top); surface fatigue is in a much earlier stage in nonscored area (bottom).*

Figure 15. Surface Fatigue Resulting from Marginal EHD Film Associated with Heavy Score Marks Caused by Contamination in Lubricant.

material such as M50, once a crack has reached a barely macroscopic size (for example 0.005 inch) the driving force is sufficient to generate failure within a short time.

It is apparent that surface characteristics will become a very important factor in determining the life of a high-speed bearing. Preliminary work indicated that several parameters should be considered.

Surface Finish – Microspalling may be accentuated in the vicinity of the deepest grinding grooves. It may be impractical to eliminate these grooves, but it should be possible to develop finishing methods that tend to minimize the groove depths. A more stringent specification on maximum groove size or one that addresses surface topography may be necessary.

Carbide Size – It is evident that surface pitting can start at large carbides. The sizes of the carbides observed to be the sites of micropits were not considered excessive by current specifications. It is possible to change the materials processing to produce smaller carbides; this has been achieved in M50NiL. Materials and processing procedures that introduce large carbides should evidently be avoided.

Contamination – Contamination of the oil system can introduce abrasive particles that damage bearing surfaces, and the damaged regions become nucleation sites for microspalling. It may be difficult to control contamination below the size of a practical filter, but the entire lubrication system, seals, filters, and sumps should be reviewed to eliminate sources of abrasive contaminants. The damage need only be on a microscopic scale to act as an initiation site.

Interruptions in the oil supply are also critical; metal-to-metal contacts are accentuated, and the resultant surface damage can lead to early failure even after normal flow is restored.

Residual Stresses – Residual stresses in the rolling-elements may be the most important characteristic in controlling the initiation of microspalls. References 10, 1[illegible], and 12 show that residual compressive stress in the range of 20 to 40 ksi for a depth equivalent to the depth of maximum shear stress is very effective in suppressing spalling in full-scale test bearings. Almost all ground surfaces have a thin layer of very high compressive stress, 150 ksi, for a depth of about 0.0001 inch, induced by the grinding. This stress layer is too shallow to be effective in suppressing fatigue initiation since many of the macrostructural features, such as the carbides, are larger. Compressive stresses for a significant depth, 0.020 to 0.040 inch, are required to be effective.

The effectiveness of a pattern of deep compressive residual stresses in arresting a propagating crack is illustrated in Figure 29, where the crack propagation rate at a cyclic peak load through a carburized case in M50NiL is shown (Reference 10). The crack stopped in the region where the residual compressive stress was about 20 ksi, and it was reinitiated by momentarily increasing the load. The arrest occurred at an applied value of $\Delta K = 12$ ksi·in$^{1/2}$. Subsequent experiments have demonstrated that residual compressive stresses of the order of 30 to 40 ksi are also

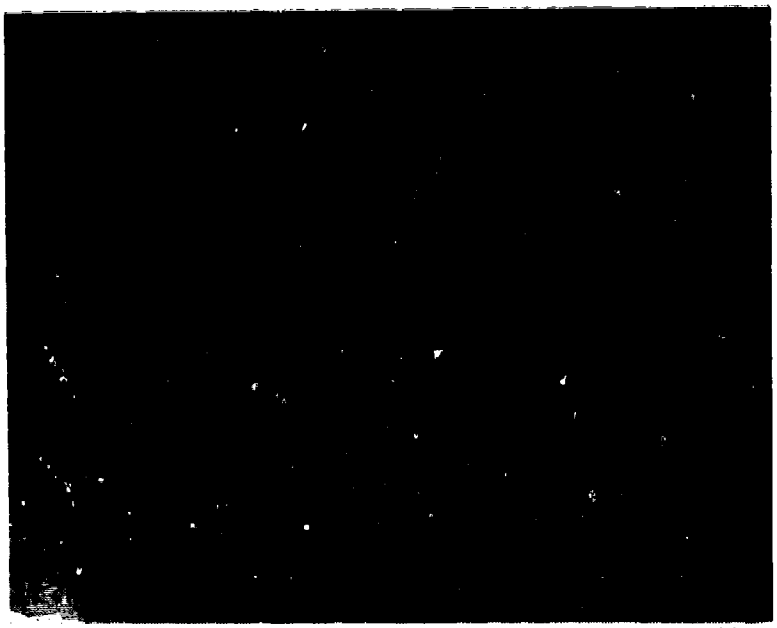

10×

32×

Figure 16. Micropitting and Debris Denting in Raceway Surface.

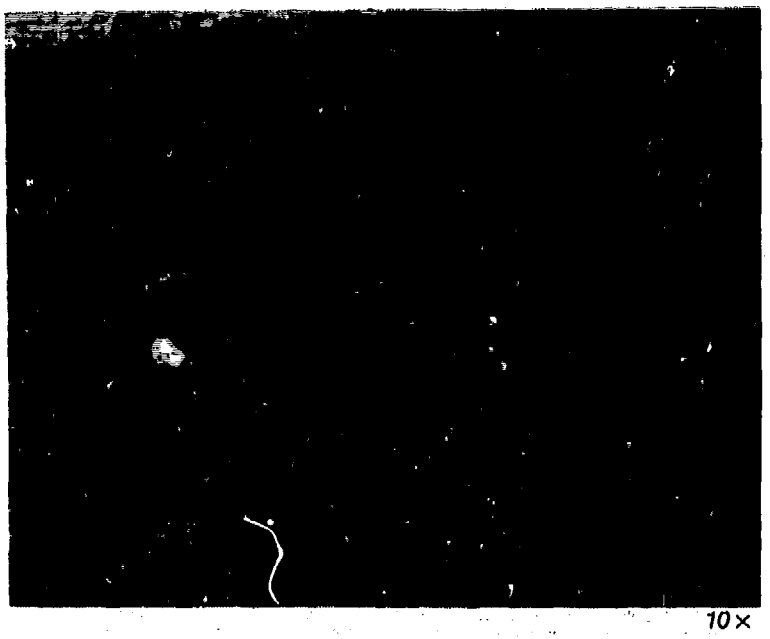

10×

32×

Figure 17. Excessive Debris Damage (Denting).

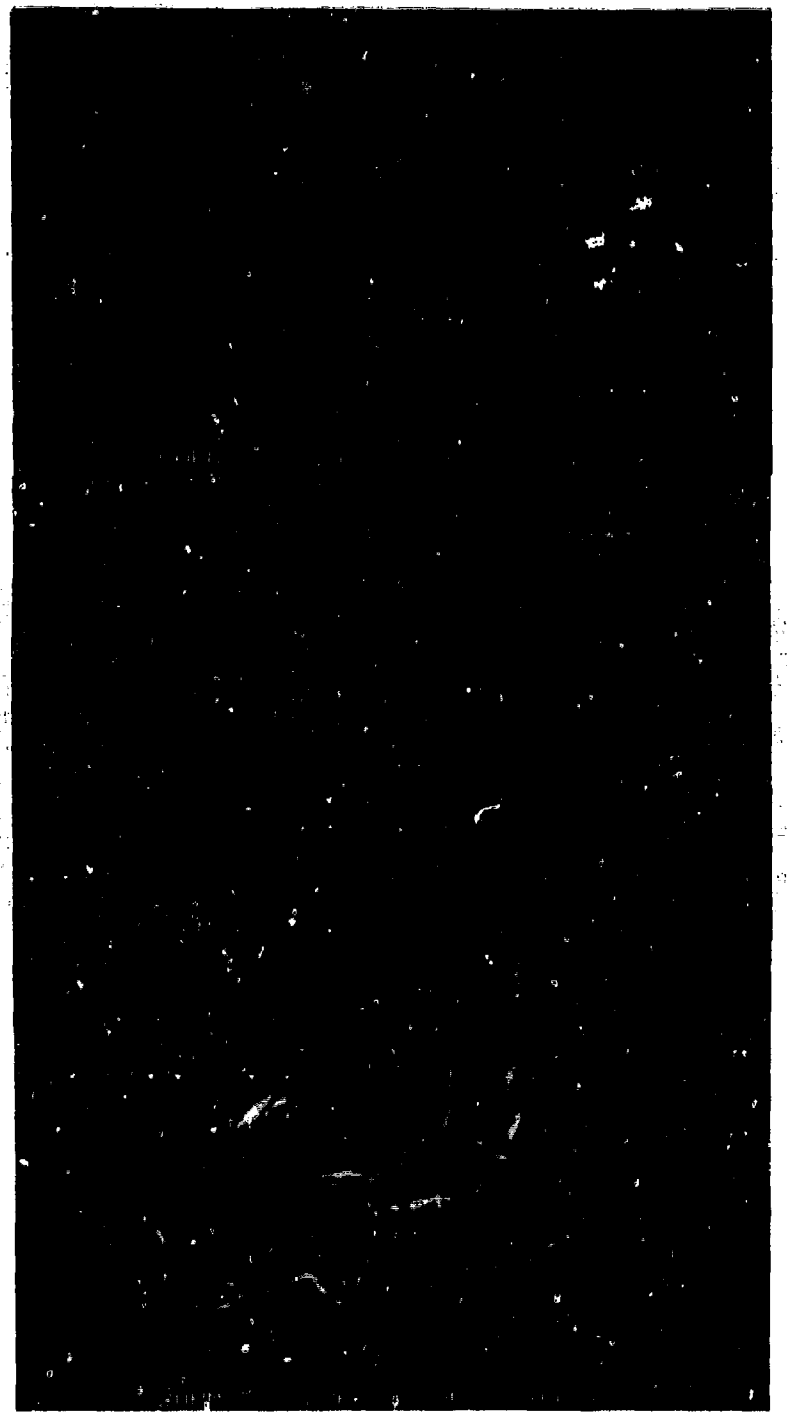

Figure 18. Debris Damage (Denting) Propagating into Surface Fatigue.

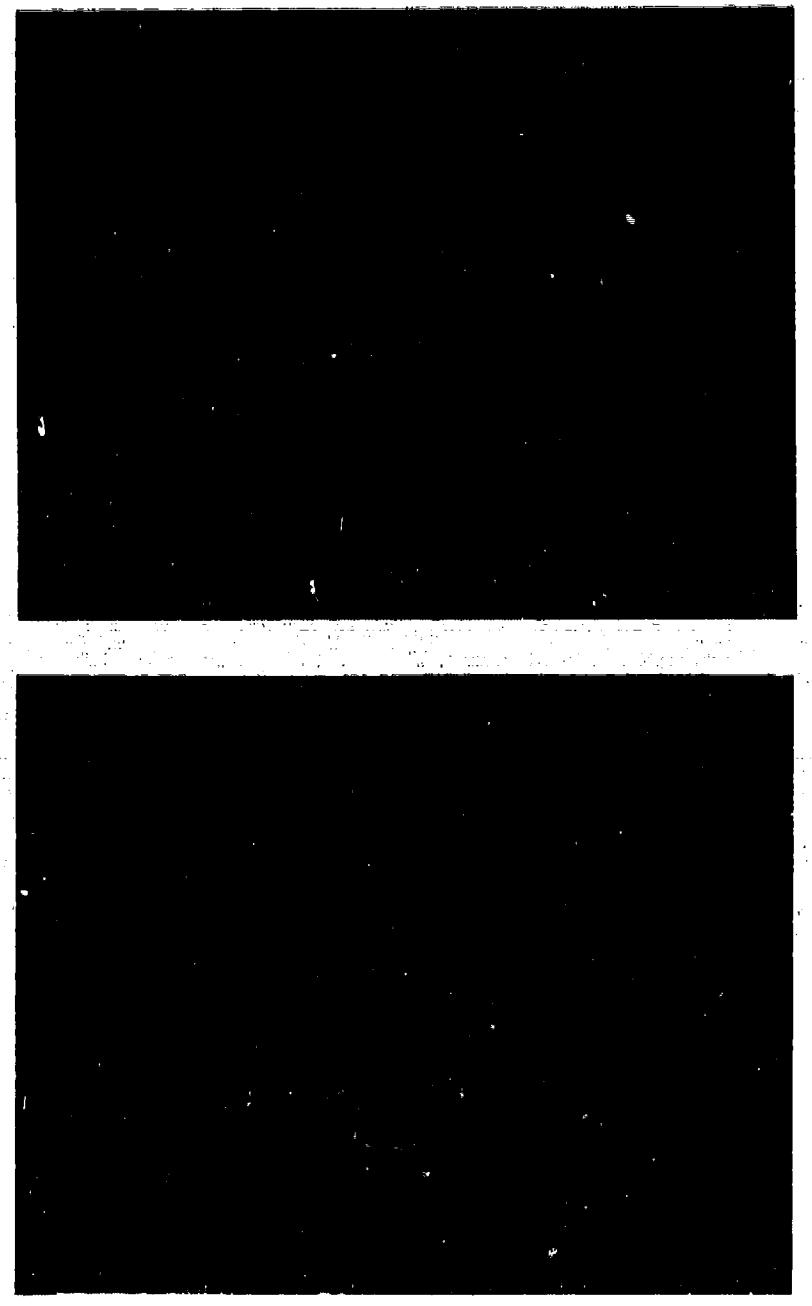

Figure 19. Microspalls Resulting from Marginal EHD Film and High Load. *Note partial destruction/deformation of grinding grooves.*

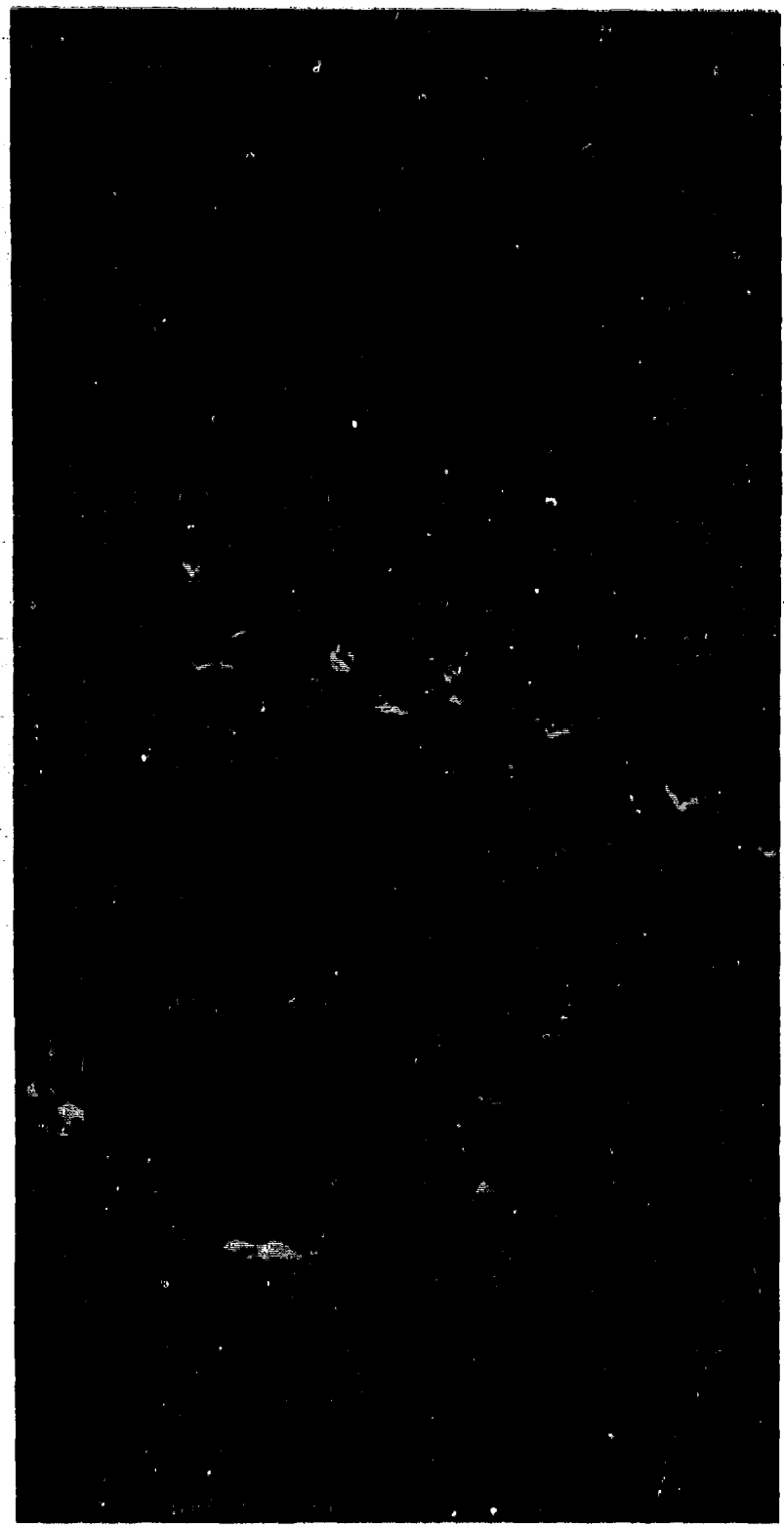

Figure 20. Micropitting Resulting from Marginal EHD Lubricant Film.

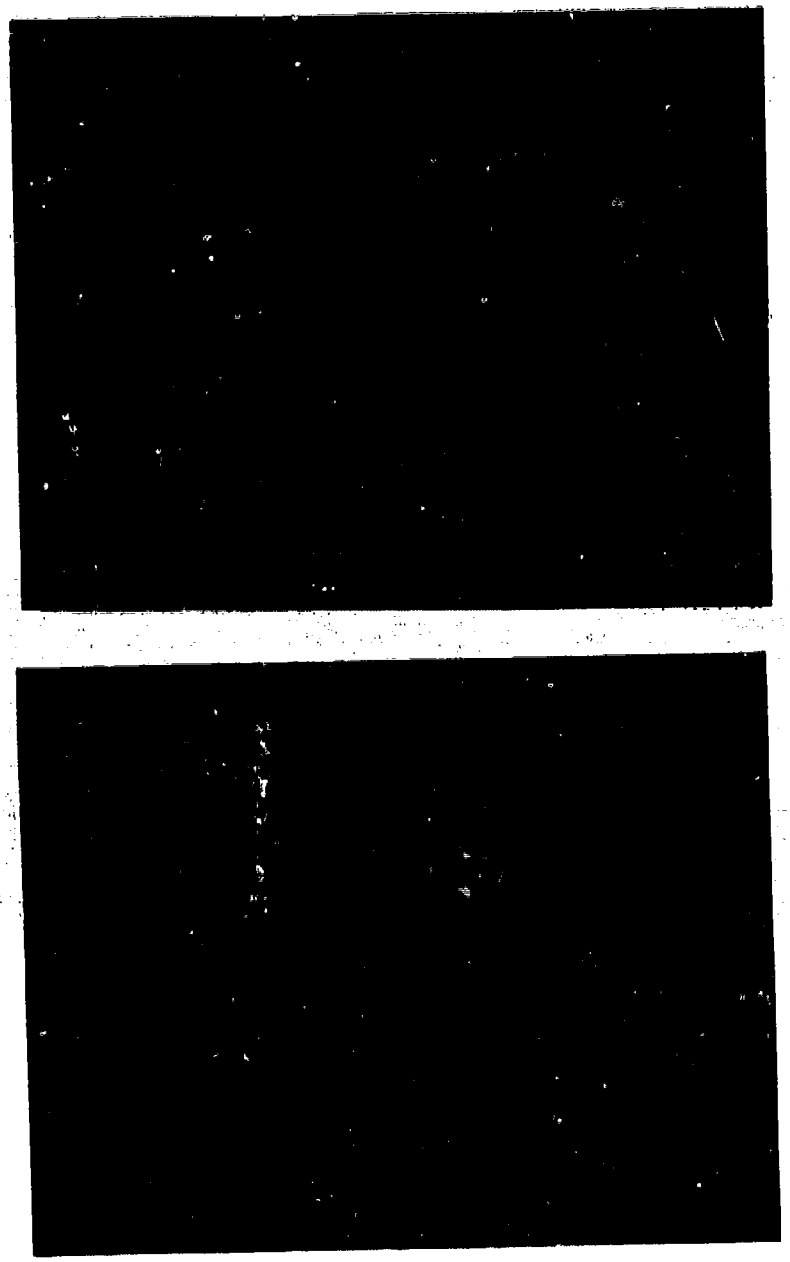

Figure 21. Micropitting on Ball Surface Caused by Skidding.

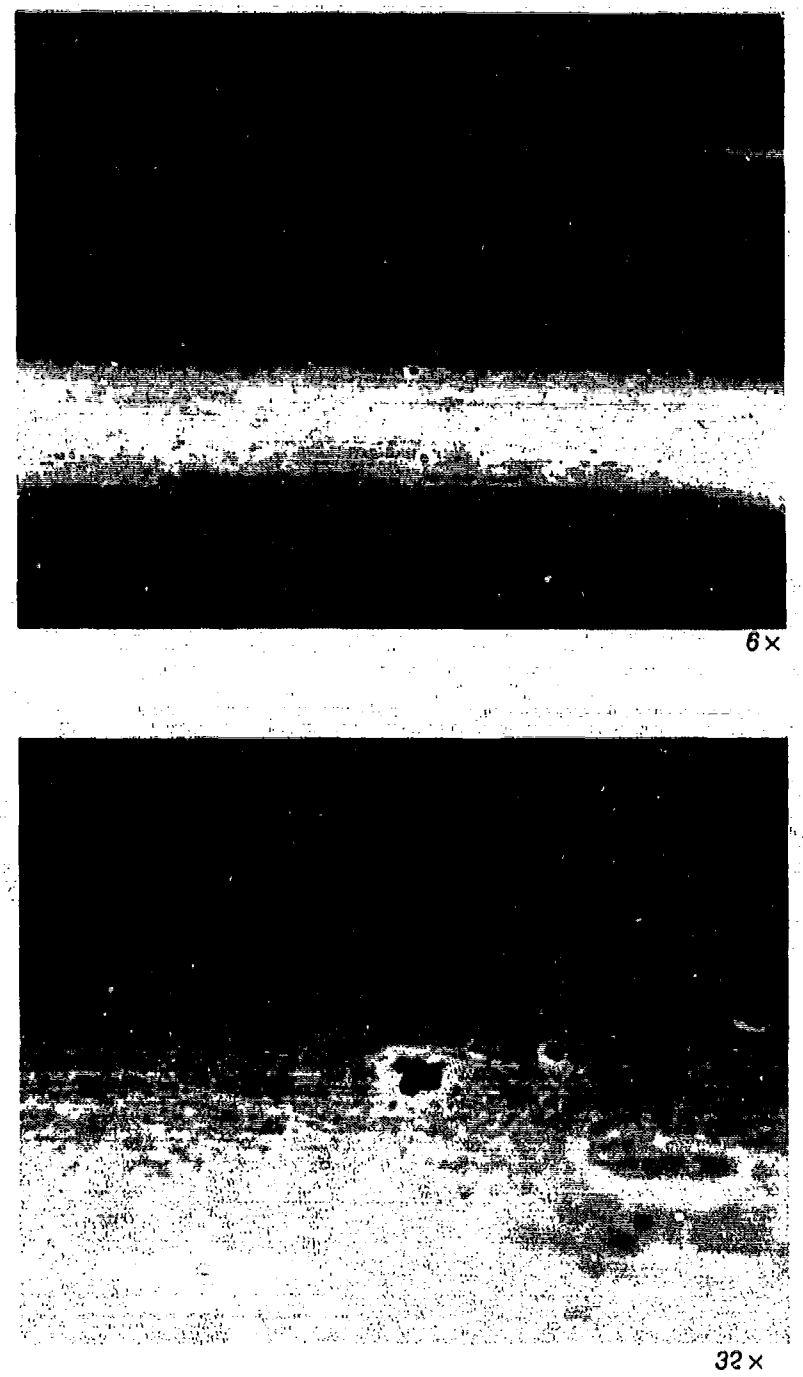

Figure 22. Micropitting on Ball Bearing Raceway.

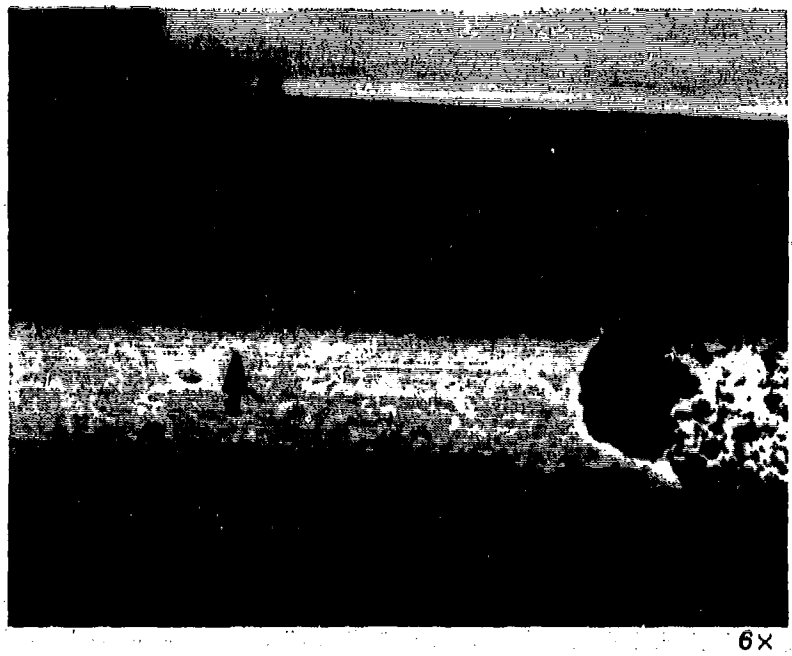

6×

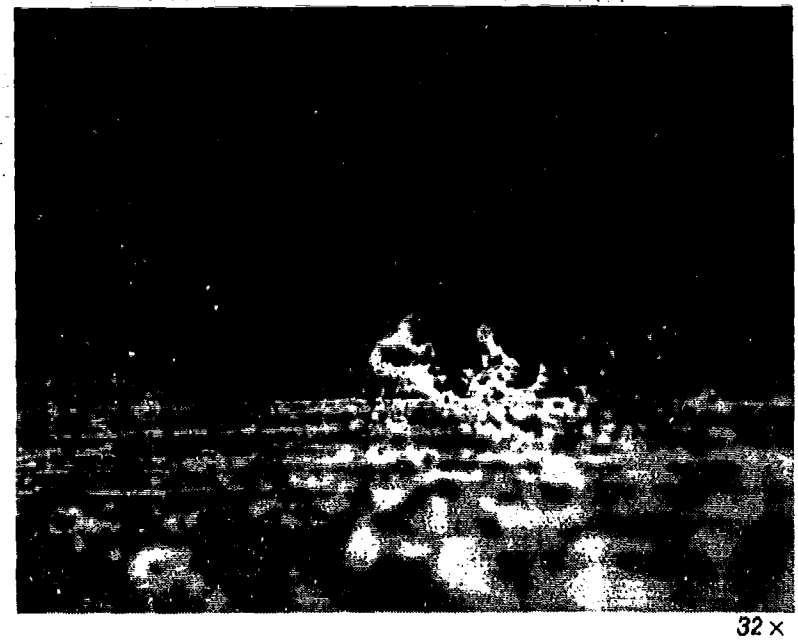

32×

Figure 23. Micropitting on Ball Bearing Raceway, Propagating into Spall. *The spalling is visible at the right-hand side of the upper photo.*

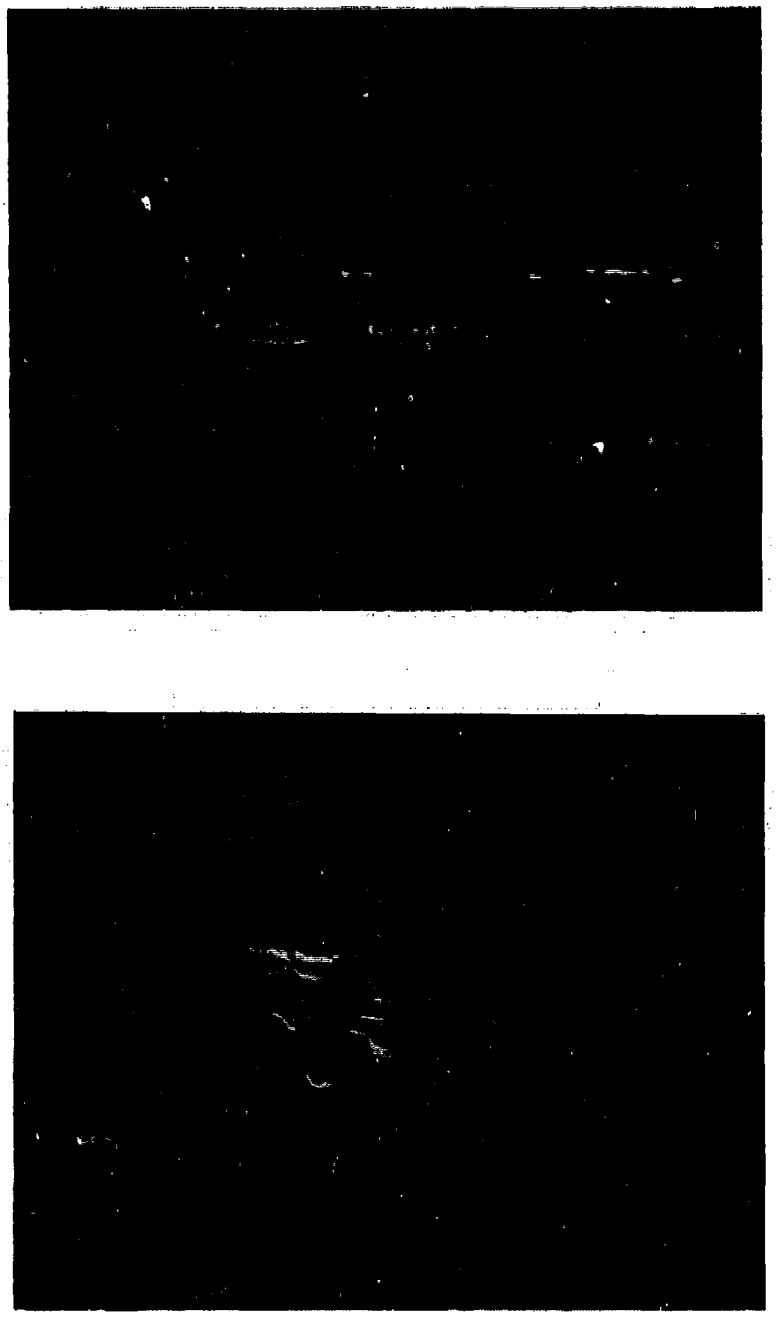

Figure 24. Carbide Banding Across Raceway. *Incipient microspalling is noticeable in the top photo, and damage due to heavy Nital etch is evident in the bottom photo.*

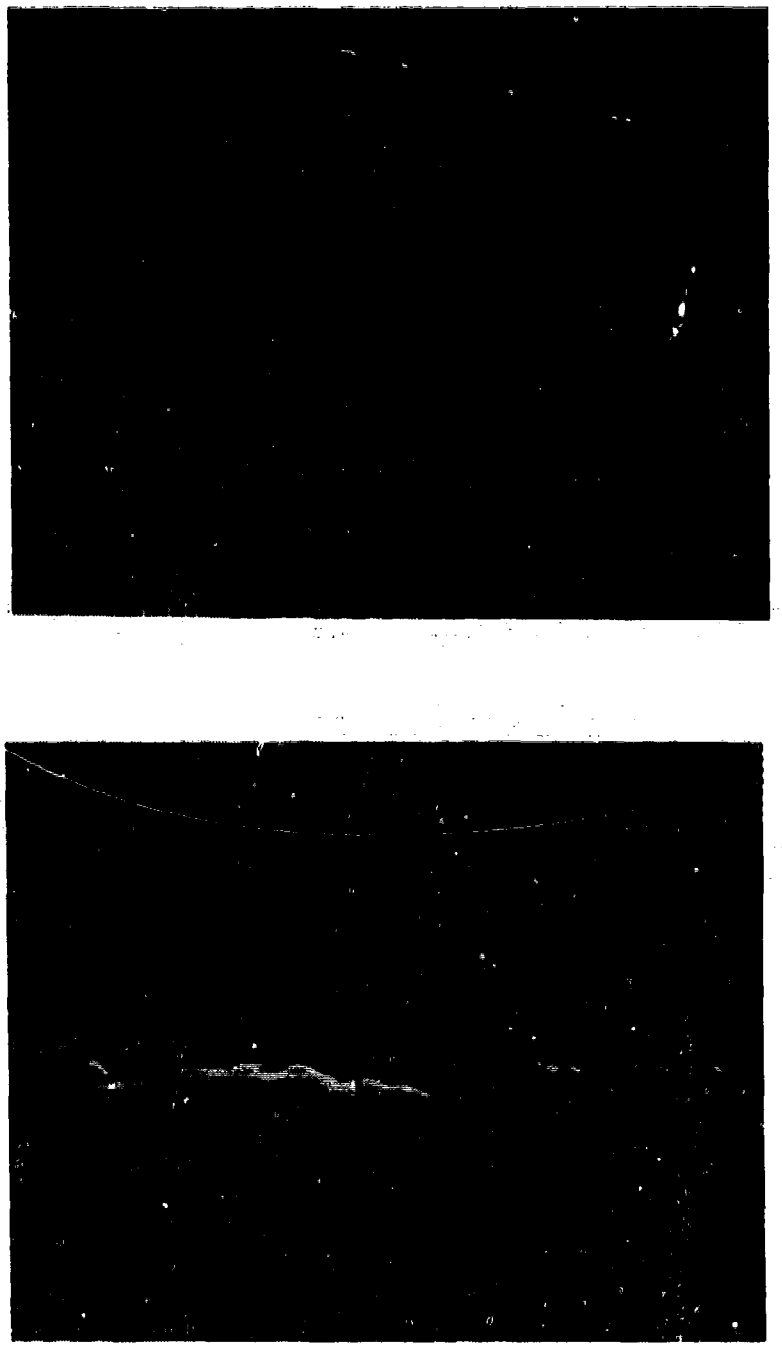

Figure 25. Microspalling Resulting from Heavy-Nital-Etch Damage.

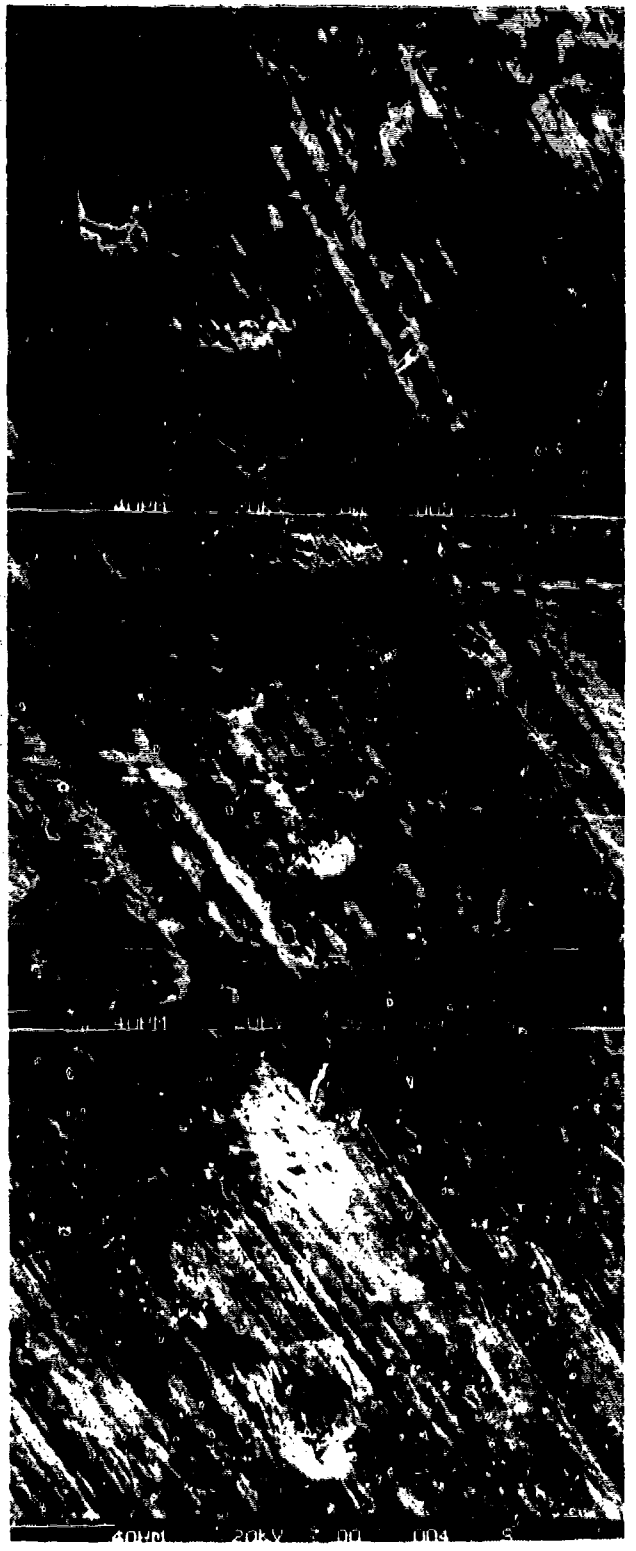

Figure 26. Skid Marks on Ball Bearing Showing Incipient Melting.

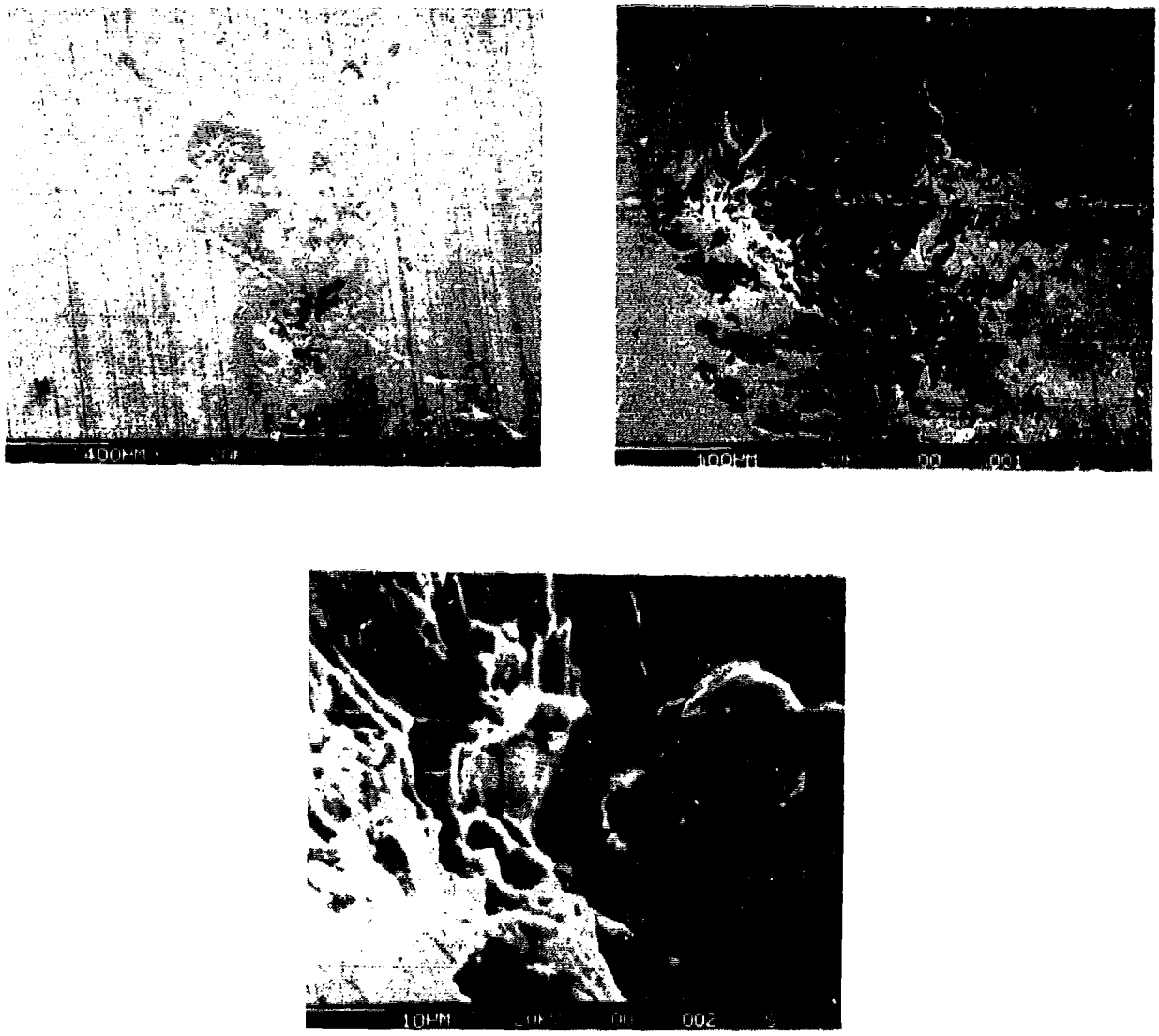

Figure 27. Microspalling Resulting from Debris Denting. *Note burnished layer surrounding spalled area (top photo) indicating deformation caused by dent.*

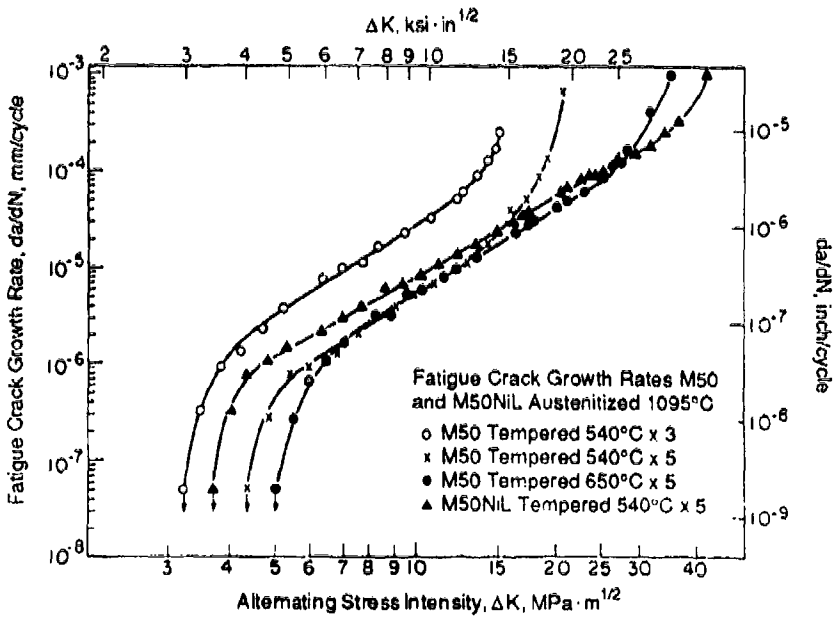

Figure 28. Crack Propagation Rates in M50 and M50NiL at R = 0.1.

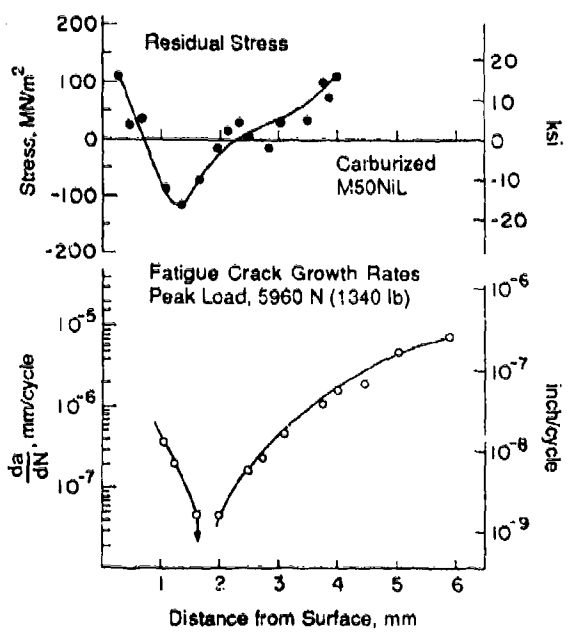

Figure 29. Effect of Residual Compressive Stresses on the Crack Propagation Rates in Carburized M50NiL.

very effective in suppressing the initiation of a fatigue crack. The control of residual stresses may thus become an important means of extending lifetimes in bearings, especially those operating in the high-DN regimes.

4.1.6 Surface Modification

Since spalling appears to start with surface distress, it may be possible to modify the running surfaces to resist the initial mechanisms that produce micropitting. In addition to reducing the sizes of the carbides which appear at the surface, it may be possible to change the chemistry of the surface. The damage is probably caused by plastic flow which arises from the metal-to-metal contacts inherent in boundary lubrication. It may be possible to reduce the extent of the localized flow by modifying the surface.

Surface modification by ion implantation has shown considerable promise for imparting corrosion resistance in various bearing materials (References 13 through 15). M50 rolling elements have been implanted with Cr, Cr + P, and Cr + Mo and run successfully in test bearings. RCF specimens of 440C stainless steel with Ti and N show an apparent increase in fatigue life over untreated specimens. Sliding wear tests on 52100 with Ti and C implanted have shown improved performance. Ion implantation of rolling-element surfaces is technically feasible, but whether the technique could increase resistance to surface distress was an issue for consideration in this investigation.

Coatings can also be used to modify the surfaces. Thin, dense, hard Cr plating has been used with some success by Torrington-Fafnir in a variety of applications. Titanium nitride and titanium carbide coatings have also been applied to bearings in a few instances. The resistance to surface flow should be very good, but the coatings may be too thin to afford protection for large carbides, and the resistance to peeling may not be improved.

4.1.7 Corrosion Resistance

Corrosion resistance will become an even more important factor in the life of bearings operating at high DN. Since failures start at the surface, corrosion pits or fretting corrosion will introduce initiation sites even before a bearing is run. This problem will become acute as the bearing operating time increases.

Several approaches have been considered. The surface chemistry can be modified by ion implantation to improve the corrosion resistance. Plating with Cr and TiN also improves corrosion resistance. It is also possible to use a stainless steel bearing material, that is, one that contains more than 13% Cr. The usual stainless bearing alloy, 440C, and modifications such as AMS 5749 have adequate corrosion resistance, but the bearing properties are not as good as those of M50, probably because of the presence of large carbides. The fracture toughness of 440C and AMS 5749 is also low. Attempts to improve the fracture toughness of these materials have not met with much success to date.

4.1.8 Summary

In considering the features that become important in extended-life mainshaft bearings to operate at speeds up to 3 MDN, a few significant factors are evident:

1. High-DN bearings will operate at a high cyclic rate; it is thus necessary to suppress initiation of fatigue cracks. Once started, a crack will grow to critical size very rapidly.

2. The lubrication film thickness may be as low as 2 to 4 μin, and boundary lubrication is probable.

3. Failures will probably start at the surface, and particular attention to surface phenomena will be required to extend initiation time.

To minimize surface distress at the bearing surfaces, the following approaches may be considered:

1. Introduction of residual compressive stresses for a significant depth in order to inhibit fatigue crack initiation.

2. Reduction in size of excess carbides in the microstructure to minimize the sizes of the initial pits and microcracks.

3. Achievement of corrosion resistance by surface modification, coating, or alloy additions to the matrix to prevent surface distress by corrosion or pitting.

4. Use of a material with a fracture toughness of at least 45 ksi·in$^{1/2}$ to prevent massive failure even if localized spalling occurs.

4.2 Materials and Process Selection

Several families of materials as well as a number of processes were considered viable candidates for this program. Each was considered in depth; in the early portion of the program, no reasonable material and/or fabrication technique was ruled out, although some guidelines were established for the selection criteria. The three which were held to be basic by GEAE are as follows.

1. **The material/fabrication technique selected must be at a stage of development (or being) where it is reasonable to expect production within the next 3 to 5 years.** *Essentially this ruled out any materials and/or fabrication techniques which needed to be developed from "scratch."*

2. **The most likely material will be a composite or bihardness structure.** *The simple fact that high hardness and good fracture toughness are mutually exclusive, coupled with the fact that high hardness is essential to adequate RCF life, made this guideline obvious. It was recognized, however, that several approaches were available to achieve the composite structure. Again, only those material and/or fabrication techniques having a realistic chance of meeting the proposed time frame were considered.*

3. **Corrosion resistance is a highly desirable feature.** *However, since corrosion resistance, per se, does not functionally affect the design or operational capability of the material (whereas limited life and poor fracture toughness do), the achievement of this goal was considered vital but not necessarily critical to the general success of the program. On the other hand, it was recognized that corrosion can have a derating effect on bearing life if the corrosion pitting occurs in the raceway areas or on rolling elements.*

For the past decade, GEAE has been engaged in development to improve fracture toughness and extend rolling-element fatigue life. The alloy M50NiL (0.13 C, 4 Mo, 4 Cr, 3.5 Ni, 1.2 V), developed as a result of part of this effort under Air Force Contract F33615-80-C-2018, generally meets these requirements. Fracture toughness is high, on the order of 45 ksi·in$^{1/2}$, and fatigue life based on RCF tests is better than that of M50. One of the prime thrusts of the GEAE approach in the proposed program was, therefore, to consider whether this material (or a derivative) could be improved with respect to corrosion resistance and further extended life.

4.2.1 Candidate Material and Process Survey

The initial selection process was most important in that it determined the scope, extent, and general direction of the program. Care was taken to assess all factors relative to the materials/processes being evaluated and to ensure an objective assessment. Several sets of guidelines were set up; the three basic ones are described above. Other peripheral guidelines such as those shown in Table 2 were also reviewed to evaluate various material factors.

Table 2. Material Characteristics/Properties Effect on RCF Life.

Characteristic	Beneficial	Not Beneficial	Not Established	Comments
Hardness	X			Increasing hardness reduces fracture toughness.
Subsurface Compressive Residual Stress	X			
Grain Flow Conformity	X			
Grain Size			X	Existing data on grain size may be misleading.
Small, Uniformly Dispersed Carbides	X			Contrary to traditional dispersed carbides.
Powder Metallurgy			X	Powder preparation and cleanliness are problems.
Surface Finish	X			Up to a Point; also need fine carbides to achieve high finish.
Cleaner Steel	X			
Coatings to Increase Hardness		X		Generally too thin to be effective.
Coatings to Increase Corrosion Resistance	X			If corrosion-pitting resistance becomes source of failure initiation.
Increased Wear Resistance, Abrasive-Contamination Tolerance			X	

Certain preliminary requirements were weighted in screening the most promising materials. In those cases where it was difficult to find relevant data (such as fracture toughness or RCF resistance) for the materials/processes being considered, general correlations were made (such as fracture toughness with impact data or ductility, or RCF with hardness). Corrosion resistance is generally directly related to Cr content, although in the case of coatings (even Cr coatings) allowances must be made for coating quality and integrity.

Based on the above considerations, a first list of candidate materials and processes was drawn up. The listing is shown in Table 3.

4.2.2 Selection of Specific Materials

From the listing in Table 3, M50NiL was deemed to have the best chance for near-term payoff based on the extensive data developed under AF direct contract work and internal GEAE testing. M50NiL was developed and extensively

Table 3. Candidate Materials and Processes.

Materials	• M50NiL • Pyrowear 53 • CBS 1000M • Vasco X2M • 12 or 14 Cr Steels (Such as TRW 2001, CRB-7, AMS 5749) • AMS 5749 Mod.
Processes	• Carburizing • Carbonitriding • Nitriding • Electron Beam Renardening • Powder Metallurgy
Surface Modifications	• Cr-Ion Implantation
Coatings	• Thin Dense Chrome • TIN, CVD (Chemical Vapor Deposited) or Ion Plasma Deposited • TIC • Electroless Nickel

evaluated under Air Force Contract F33615-84-C-2018. Production has been implemented for critical bearings in military and commercial engines, and it is currently flying in several GEAE advanced commercial engines.

As shown in Figure 30, M50NiL possesses about twice the RCF life of M50 at 700 ksi maximum stress, as measured by the GEAE RCF test rig. The fracture toughness of the core material, as shown in Figure 31, is approximately 45 ksi·in$^{1/2}$ – double that of normally through-hardened M50. High-cycle fatigue resistance (both case and core) is excellent (> AISI 4340), and extensive process evaluation has shown the material to be less sensitive than most carburizing materials to normal processing variabilities.

Additional details on M50NiL as well as several of the other carburizing grades of bearing steels shown in Table 3 are reported in Reference 13. A second class of potentially viable candidate materials were the 14-18% chrome "corrosion resistant" steels.

While these materials possess good corrosion and fatigue resistance, the fracture toughness characteristics are inadequate (in the same range as M50 and 52100, about 16 to 20 ksi·in$^{1/2}$).

For several years, GEAE had been working to achieve a carburizing grade 14-Cr steel in order to improve the fracture toughness. These efforts were only partly successful, the primary problem being difficulty in achieving the needed combination of case hardness, minimum case carbide formation, and a low-ferrite core. Efforts were also made at reduced Cr levels (9 to 12%) to find out whether a more effective carburizing treatment could be achieved while maintaining acceptable corrosion resistance. While the attempts to carburize this lower Cr material were somewhat more successful, process repeatability and reliability were judged too variable to consider this material for incorporation into the current study (considering the production-introduction time constraints).

Consequently, the M50NiL was selected as the candidate material for this program.

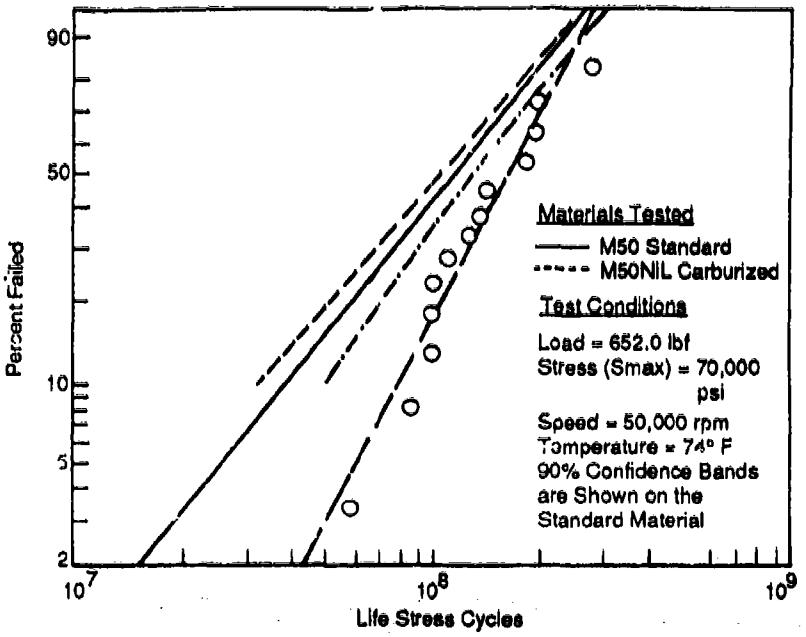

Figure 30. RCF Lives: M50 Versus M50NiL.

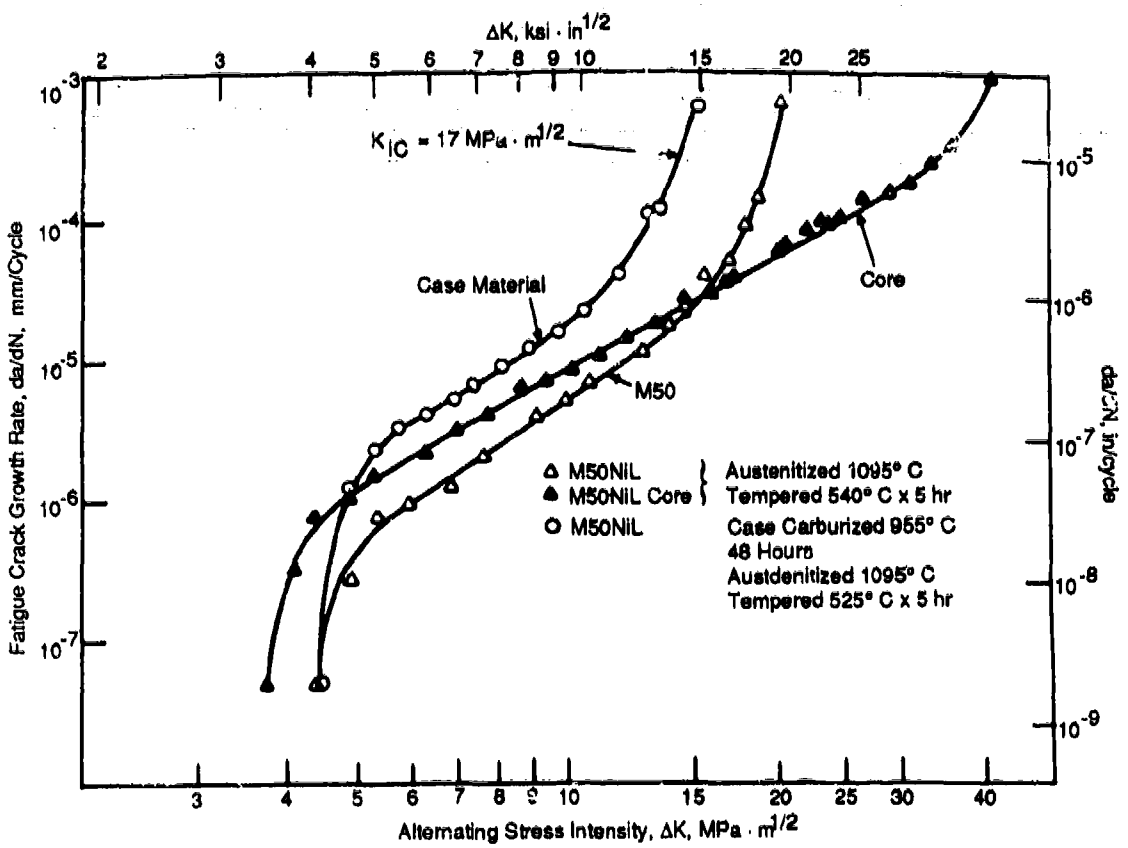

Figure 31. Fracture Toughness: M50 Versus M50NiL.

4.2.3 Selection of Processes

The goal of all the surface treatments, whether they produce a monolithic material (such as carburizing, nitriding, or ion-implantation) or an overlay (such as chromium plating or TiN coating), was as follows:

1. A corrosion-resistant surface with an increase in wear resistance.

2. Subsurface residual compressive stresses of 30 ksi or greater to increase time to crack initiation, reduce crack propagation rates, and increase bearing fatigue life.

Considerations were given to all of the surface-hardening techniques shown under "Processes" in Table 3. Based on the choice of M50NiL as the prime candidate material, carburizing was a natural choice for process selection.

Carburizing is an established production process for selective hardening of steels. It is used successfully in the processing of M50NiL. However, alloys containing chromium, such as M50NiL, usually require special carburizing procedures. With the higher chromium contents, an oxide structure (spinel) is assumed to form at the surface, and this interferes with the uniform diffusion of carbon. To counteract this, the material is oxidized before carburizing (preoxidation), and the subsequent carburization process proceeds more uniformly, presumably because of a depletion of chromium at the very surface. In practice, this method has proved quite successful with M50NiL.

4.2.4 Surface Modifications and Coatings

A number of surface modification techniques were considered for inclusion in this program. Ion implantation was of specific interest because it is reported to produce an excellent corrosion-resistant surface on any material.

Ion implantation is basically a surface-alteration technique and consists of injecting elemental ion species into the surface of a material by use of a high-energy ion beam from a high-frequency accelerator. Because the surface is metallurgically altered *in situ*, an enriched layer (Cr, Ta, etc.) is generated integral to the original surface, with no sharp metal-coating interface. This process has been developed by the United States Navy (NRL and NAPC) and represents one approach to achieving a corrosion-resistant bearing material.

The advantages of ion implantation over conventional coatings or other surface treatment are:

- No change in dimensions or surface character; existing bearings can be implanted without further processing.

- None of the interface bonding problems associated with coatings.

- Material bulk properties remain the same.

- Choice of alloying element is not limited by solid solubility or diffusion parameters.

Cr-ion implantation has been successfully applied to materials such as M50 (Reference 13), and the process was considered of sufficient technical importance to be included as part of this program. GEAE selected the Spire Corporation of Bedford, Massachusetts, to carry out the ion-implantation studies.

Recent advances in chromium plating involve application of thin dense chromium (TDC) with controlled residual stresses. Torrington-Fafnir Bearing Company, using their process called Fafcote TDC, has shown that these platings can survive on the working surfaces of rolling element bearings, and bearing operation may be improved, particularly under marginal lubrication. The plating process must, however, be carefully controlled, especially with respect to surface preparation and residual stress patterns, in order to achieve consistently good results. Appendix B details a recommended procedure for TDC application.

Hard, thin coatings for the wear protection of surfaces have been used for many years, particularly for cutting tools; however, only recently a specific effort was made to understand the role of these hard, thin coatings for rolling-element bearings (References 16 and 17).

Chemical vapor deposited (CVD) CrC-TiC, TiN, and "hard" Mo coatings as well as others were evaluated by the Air Force (Reference 18) under high Hertzian stresses (600 to 700 ksi). Based on limited test results, the above three coatings showed good adherence under these ultrahigh-stress conditions. The coatings were tested on a number of substrates including CRB-7, T-15, and M50. Since the CVD temperatures exceeded the tempering temperatures of these materials, the test bars had to be rehardened after coating. This technique is acceptable for experimental work but would be impractical on a production part, primarily because of potential distortion.

GEAE also investigated physical vapor deposited (PVD) TiN and "hard" Mo coatings. Early results, such as adherence tests, were encouraging. Corrosion tests using the USN test protocol described later have been performed on PVD TiN with good results.

A hard coating was selected for evaluation as an option for corrosion and wear resistance improvement. It was recognized that this family of hard coats consists of ceramics that are very hard and brittle. Therefore, there was the underlying concern that, if adherence was not absolute, debris particles generated could be damaging to other unprotected bearing and drive system components. Adhesion, therefore, became a critical requirement in the evaluation and development of this family of coatings.

In summary, the following materials and processes were selected as potentially capable of meeting the requirements set forth in the contract Statement of Work:

Material:	M50NiL
Process:	Carburizing
Surface Treatments:	Ion Implantation Thin Dense Chrome PVD - TiN

4.3 Mechanical and Physical Property Testing

The primary testing performed as part of this program consisted of: (1) rolling contact fatigue, (2) corrosion, and (3) contamination (effect on RCF behavior). The results of each are described in detail in Reference 1 (the program Interim Report) and briefly summarized in the following subsections.

4.3.1 Materials and Processes

VIM-VAR M50 (AMS 6491) – This material was used as the baseline for all testing. It (as well as the M50NiL) was the substrate for all coatings and surface modifications investigated in this program. Latrobe Heat E3410 M50 was used; the chemistry is listed in Table 4. It was heat-treated using standard practice for M50. Test bar hardness

Table 4. Chemical Analysis of M50 and M50NiL.

	C	Si	Mn	S	P	W	Cr	V	Ni	Mo	Co	Cu	Fe
M50	0.83	0.22	0.29	0.001	0.012	0.02	4.13	1.02	0.06	4.26	0.01	0.04	Balance
M50NiL	0.14	0.24	0.20	0.002	0.006	0.02	4.04	1.19	3.47	4.25	0.02	0.04	Balance

was RC 62 ± 0.5, ASTM grain size was 8, and RC rig bar surface finish was 6 to 8 Ra (arithmetic average roughness height).

VIM-VAR M50NiL (AMS 6278) – Latrobe Heat E3389 M50NiL was used. Chemical analysis of the heat is shown in Table 4. Core fracture toughness of this heat (a GEAE specification) was reported by Latrobe to range between 47.3 and 53.9 ksi·in$^{1/2}$ (ASTM E-399). The material was carburized to a case hardness of RC 62 (surface), an effective case depth (hardness to RC 58) of 0.020 to 0.25 inch, and a core hardness of RC44 ± 1. Case grain size was ASTM 7 to 8; core grain size was ASTM 5 to 7. RC bars were ground to a surface finish of 6 to 8 Ra.

Thin Dense Chrome – Torrington-Fafnir Bearing Company's "Fafcote" TDC was used for these studies. Coating thickness was approximately 0.00007 in. The surface had the "pebbly" appearance characteristic of this coating process. SEM photos of typical TDC coated surfaces are shown in Figure 32.

Ion Implantation – Three elemental species were implanted into M50 and M50NiL: (1) Cr, (2) Cr + P, and (3) Ta. The implantation was done by Spire Corporation of Bedford, Massachusetts. A brief description of the process reported by Spire follows.

1. Cr — 2×10^{17} Cr^+/cm^2 at 15 keV
2. Cr + P — 2×10^{17} Cr^+/cm^2 at 15 keV followed by 1×10^{17} P^+/cm^2 at 40 keV
3. Ta — 1×10^{17} Ta^+/cm^2 at 15 keV

Specimens were implanted on a rotational jig (Figure 33). During implantation, the RCF rods were exposed to the beam through slots in a surrounding tantalum shield that ensured the implantation beam was within ±30° of normal to the surface. Although temperature could not be measured directly, it was estimated to be less than 300°F.

TiN - PVD Coating –TiN was applied to the M50 and M50NiL substrates using the low-temperature PVD process. Two sources of TiN were evaluated. American Plasma Technology of Piqua, Ohio, furnished several sets of bars with PVD TiN; Spire Corporation supplied one set.

Note that the American Plasma coated bars were produced and evaluated under a separate but complementary GEAE IR&D (Independent Research and Development) project. However, since the work has relevance to the overall effort discussed herein, evaluation of the American Plasma coated specimens is discussed as part of this narrative. Also note that these TiN specimens were aimed at a somewhat different end application than the one addressed in this report.

4.3.2 Rolling-Contact Fatigue Testing

All RCF testing was performed on the GE developed rigs shown in Figure 34. These machines have been used for a number of years, and detailed descriptions of the machines and the operational characteristics are presented in Reference 19. Test conditions were as follows:

Load	652 lbf
Max Hertzian Stress	700 ksi
Speed	50,000 rpm
Temperature	RT/ambient
Lubrication	Wick (about 20 drops/minute) nonrecoverable
Lubricant	Mil-L-23699

Table 5 is a summary of all of the RCF testing performed as part of the reported program. A total of 196 tests were completed (excluding the 100 baseline tests that were also part of this program).

200×

500×

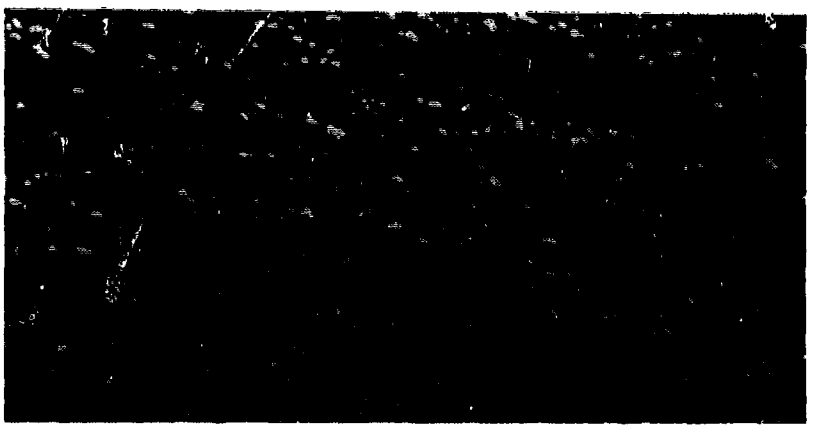

1000×

Figure 32. SEM Photographs of Falcote TDC Coating.

Figure 33. Fixture for Ion Implantation of RCF Bars (Spire Corporation).

Table 5. Summary of RCF Tests.

Material/Process	Life (10^6 Cycles) B_{10}	B_{50}	Slope	Failure Index
M50NiL Baseline	53	167	1.7	49/80
M50 TDC	69	203	1.7	9/20
M50 Cr^+ Implant	99	173	3.4	5/20
M50 Ta^+ Implant	130	502	1.3	5/20
M50 Cr^+ + P Implant	145	244	3.6	11/16
M50 TiN No. 3	142	286	2.7	4/10
M50 TiN No. 4	144	259	3.2	6/10
M50 TiN No. 5	71	98	6.0	3/10
M50 TiN No. 6	117	297	2.0	5/10
M50NiL Baseline	97	217	2.3	13/20
M50NiL TDC	109	331	1.7	8/20
M50NiL Cr^+ Implant	148	490	1.6	5/20
M50NiL Ta^+ Implant	150	262	3.4	4/20
M50NiL Cr^+ + P Implant	147	344	2.2	6/20

Test Conditions

Max Hertzian Stress: 700 ksi
Speed: 50,000 rpm
Lubricant: MiL-L-23699
Temperature: RT/Ambient

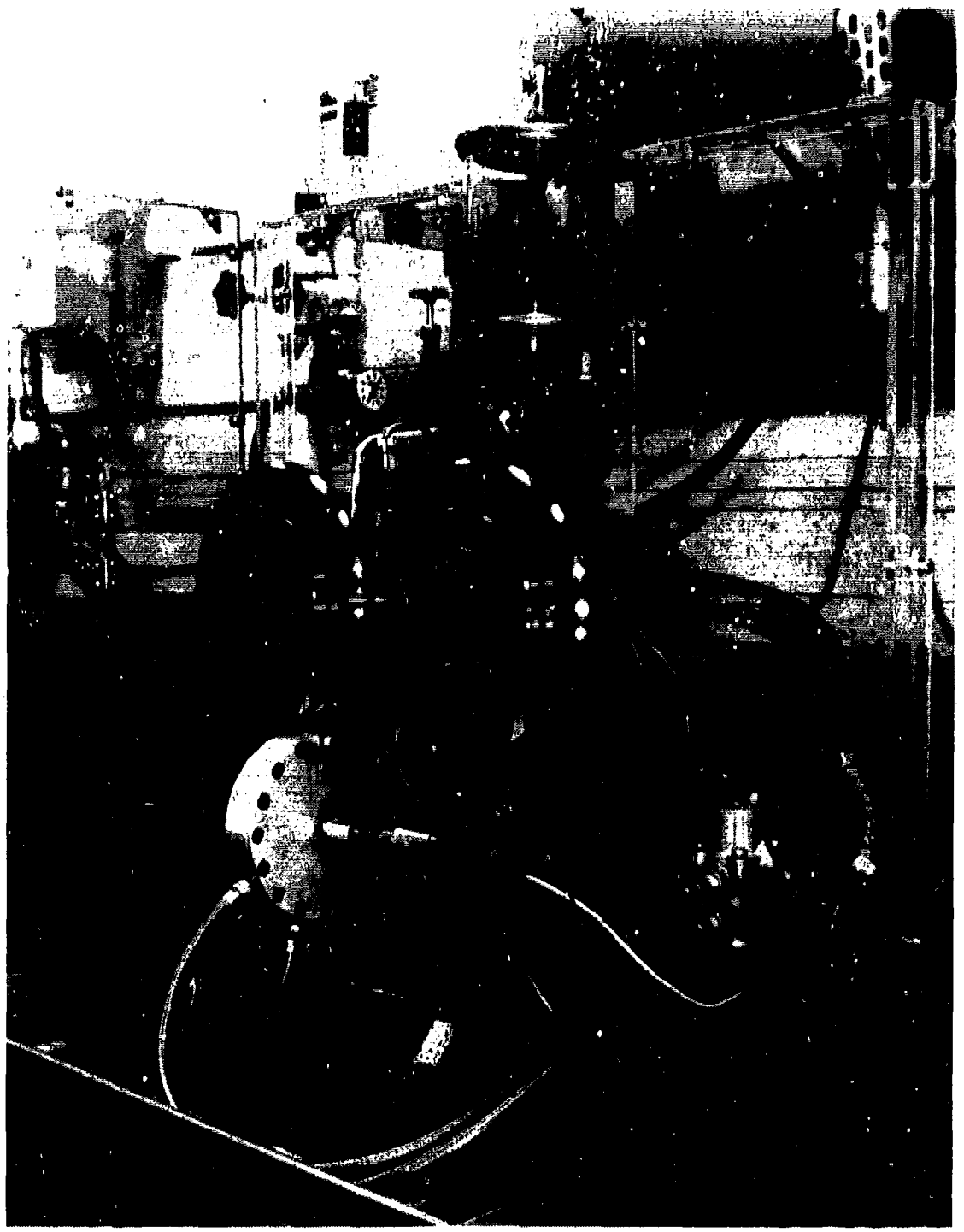

Figure 34. Closeup of GEAE High-Speed RCF Rig.

The first test series evaluated the Fafcote-TDC coating on both M50 and M50NiL. The results showed a directional but not statistically significant improvement in RCF life.

The second series of RCF rig tests was performed on M50 and M50NiL ion implanted test specimens. Three species were tested: (1) Cr^+, (2) $Cr^+ + P$, and (3) Ta^+.

The summary data in Table 5 show that this process improved RCF life for both M50 and M50NiL. However, in reviewing the surface profile traces made across the running tracks, some deformation (25 to 50 μin) was observed on all bars. This raised a question as to whether shallow surface tempering had taken place during implantation and whether this could have influenced life in terms of allowing an increase in the roller-bar contact zone, thereby reducing the contact stress. The tempering could not be confirmed by hardness measurements, although the tempered zone, if real, would be so shallow that microhardness measurements might not accurately locate it. In addition, the deformation was not uniform or consistent when comparing different test bars or even upon comparing running tracks on the same bar.

The final series of RCF tests was performed on PVD TiN on M50 substrate. From the results shown in Table 5, the TiN did offer RCF life improvements, although the degree of improvement varied considerably from batch to batch. The tests series identification in Table 5 (M50TiN No. 3 and No. 4) refers to different process batches evaluated. A number of problems were encountered with this coating process, the two major ones being adhesion and nonhomogeneity. In the early phases of testing, adhesion was a serious concern due to flaking and peeling of the coating. This was somewhat alleviated by working with the vendor and incorporating a number of process improvements.

The nonhomogeneity problem (that is, a totally impervious surface) was also improved but not to the point where, at least at this stage, it could be expected to provide absolute corrosion protection. There is no doubt that the high hardness of the TiN coating (2500 VHN, Reference 20) had a beneficial effect in the RCF life improvement achieved in these tests. By the same token, the brittleness associated with high hardness is a problem in rolling-contact bearings because of the high-frequency cyclic stressing of the surface. Thus, while TiN is probably an excellent surface-protective coating for more static or area-contact wear situations, application to highly loaded, high-speed, rolling-element bearings is more problematical.

4.3.3 Corrosion Testing

Corrosion is a destructive chemical or electrochemical reaction of a material with the environment. Corrosive action is commonly associated with metals in contact with liquids, as differentiated from destruction by gaseous chemical reactions such as oxidation or mechanical mechanisms such as erosion and abrasion (although corrosion and mechanical action often operate together, exacerbating each other).

Because improved corrosion resistance was one of the desired characteristics, a number of corrosion tests were conducted on the RCF rig test bars both prior to and after testing to ascertain the integrity of any protective coating. Similarly, during the course of the full-scale bearing tests (Phase II), corrosion tests were performed to evaluate the effect of the operating environment on the coatings. The full-scale bearing corrosion tests will be discussed in a later section.

The U.S. Navy has developed an effective method of corrosion testing, utilizing an oil/artificial-salt-water mixture, which has proven to be quite acceptable in simulating turbine engine environments and generating realistic and repeatable data. GEAE has successfully used this procedure for a number of years. The procedure is described in detail in Reference 5 and is summarized briefly in the following paragraphs.

Test specimens (either RCF bars or actual bearings) are cleaned by successively washing in separate baths of toluene, ethanol, hexane, and acetone. Cleaned test specimens are handled only by rubber-gloved hands and are air-dried at room temperature.

The specimens are then immersed for 1 hour in a specially prepared lubricant/chloride solution. The lubricant solution consists of a Mil-L-23699 type oil to which three parts per million (ppm) by weight of chlorides (ASTM D665, synthetic sea water) are added. The water content of the lubricant solution is adjusted to 600 ppm (weight) by the addition of distilled water.

After immersing in the lubricant solution, the specimens are removed and drained for 30 minutes at room temperature. If RCF bars are used, they are then placed into an all polyethylene fixture. Actual bearings are simply suspended from a plastic cord. The fixtured bars (or bearings) are then suspended in a large beaker with a small amount of water at the bottom (not in contact with the test specimens). The top of the beaker is covered with aluminum foil. The beaker and contents are then cycled alternately between a 150°F oven and a 37°F refrigerator. Total exposure consists of 14 cycles; each cycle comprising 8 hours at 150°F and 16 hours at 37°F. Upon completing 14 cycles, the test bars or bearings are removed and examined for evidence of corrosive attack.

Corrosion tests were performed on RCF bars to assess the following surface protective coatings or surface alternations:

- TDC
- Cr^+ Implanted
- Cr^+ + P Implanted
- Ta^+ Implanted
- PVD TiN

Tests were performed on new, as-processed bars as well as on several bars of each type that had completed (suspended test) RCF testing.

4.3.4 Corrosion Test Results

TDC M50 and M50NiL – After the 14-cycle exposure, visual examination showed no indications of corrosion on any of the TDC bars exposed to the corrosive environment. Control bars (bare M50) exhibited the expected corrosion damage.

Several M50 and M50NiL TDC coated bars were recycled through the corrosion test after completion of RCF testing. The areas evaluated were running tracks that had not failed (spalled) and had survived the full time to suspension (48 hours or 288 $\times$ 10^6 test cycles). Again, no evidence of corrosion was noted.

Ion-Implanted M50 and M50NiL – The results of corrosion testing on M50 and M50NiL bars having Cr^+, Cr^+ + P, and Ta^+ implantation were similar to those with the TDC coating. No visual evidence of corrosion was observed prior to or after testing selected specimens.

PVD-TiN on M50 – Corrosion testing was performed on several iterations of TiN coatings on M50. All tests were conducted in the as-received condition and, because of the results, invalidated any need to corrosion test a tested RCF specimen.

Corrosion pitting (resulting from "pinhole" breaks in the surface) was observed in the early TiN coatings. In the later, iterative coatings, a significant improvement in the surface homogeneity reduced the incidence of corrosion pitting. However, even with the best coating available (at that time) some corrosion pitting was evident. It may well be possible that a PVD TiN process can be developed that will provide 100% protection against corrosion. However, within the framework and time available in this contract, failure to achieve total corrosion protection,

coupled with the potential for serious subsurface corrosion (subsequent pitting/spalling failures), eliminated PVD TiN from further consideration.

4.3.5 Contamination Tests and Results

A major cause of bearing surface distress is oil-entrained contamination, particularly hard particles such as Al_2O_3, silicates, etc. Figures 8, 9, and 13 through 15 in Section 4.1 illustrated the damage caused by hard-particle contamination. While extensive attempts have been made to clean-up bearings and sump systems, it is unrealistic to expect that system contamination can be totally eliminated. Consequently, it is necessary to improve the damage tolerance of bearing surfaces. There are several possible approaches to this, some seemingly at odds with each other. They include the following:

1. Provide a surface-protective coating
2. Increase the surface residual compressive stress
3. Reduce the material/surface hardness
4. Increase the material/surface hardness

In this study, GEAE chose to evaluate all but Item 3. Item 1 was investigated by the use of TDC. Item 2 by evaluating M50NiL as well as ion implantation. Lastly, the PVD TiN coating meets the requirement of Item 4, but relatively poor performance effectively eliminated it from further serious consideration for this program.

To establish the effect of hard contaminants in the lubricant on bearing performance, GEAE used a procedure developed earlier for an in-house study of the effects of Al_2O_3 contamination on the RCF life of M50 bearing steel.

To accomplish this, a test protocol was developed that could reliably and repeatedly provide a controlled contamination environment. A ball/rod tester (Reference 21) was judged to be a good test vehicle since it can be operated in the fully flooded condition; also, the rotation of the ball/rod test assembly acts as a pump and thus provides a recirculation mode.

After extensive experimentation, and based on engine-oil sampling data, a "standard" contamination fluid was defined consisting of 2.5 ppm of 20-μm Al_2O_3. Initial testing indicated this mixture would reproduce the ball scoring observed in some engine bearings in the presence of Al_2O_3. To ensure that the Al_2O_3 particles were thoroughly distributed, each contaminated batch of oil per test (2 liters) is stirred with a magnetic stirrer for 24 hours prior to the test. In addition, oil samples taken during and after the tests are analyzed to ensure that the desired level of contamination is being maintained.

Test conditions were as follows:

Max. Hertzian Stress:	786 ksi
Speed:	3600 rpm
Temperature:	RT/Ambient

The tests are suspended at 48 hours or failure, whichever occurs first. Table 6 summarizes the results of these tests. It should be noted that the fatigue lives in this table are not directly comparable to those established using the RCF rig. The ball/rod tests are performed at a higher Hertzian stress level (768 versus 700 ksi) and slower speed (3,600 versus 50,000 rpm) than the RCF rig. Both variables have a significant effect on RCF life. However, the general

Table 6. Summary of Ball/Rod Contamination Tests.

Material/Process	Life (10^6 Cycles) B_{10}	B_{50}	Slope	Failure Index
M50Baseline	3.76	13.67	1.5	6/7
M50 TDC	8.11	18.71	2.3	4/5
M50 Cr^+ Implant	4.32	16.50	1.4	4/5
M50 Ta^+ Implant	3.31	19.25	1.1	4/6
M50 Cr^+ + P Implant	3.23	16.59	1.2	2/5
M50 TiN No. 3	14.27	35.55	2.1	2/5
M50 TiN No. 4	14.47	17.42	10.1	3/5
M50 TiN No. 5	7.18	34.05	1.2	3/5
M50 TiN No. 6	7.06	15.35	2.4	4/5
M50NiL Baseline	5.73	14.73	2.1	7/9
M50NiL TDC	4.97	11.02	2.0	4/6
M50NiL Cr^+ Implant	4.01	12.99	1.6	4/5
M50NiL Ta^+ Implant	8.64	17.39	2.7	3/5
M50NiL Cr^+ + P Implant	4.33	15.67	1.5	4/5

Test Conditions

Max Hertzian Stress: 768 ksi
Speed, rpm: 3,600
Lubricant: Mil-L-23699 + 2.5 ppm 20-μm Al_2O_3
Temperature: RT/Ambient

trends noted in the previously discussed RCF tests carry over in most cases, as can be seen in the M50 and M50NiL baseline tests where the two materials were ranked in the same order.

The TDC coating plated on an M50 substrate showed a rather significant improvement in fatigue life. However, when tested on an M50NiL substrate, no statistical difference was seen between bare and coated specimens. This behavior is anomalous and not fully understood. The ion-implanted M50 and M50NiL specimens showed no significant differences in life compared to the baseline data. The only exception was the M50NiL-Ta^+ test result which showed some improvement.

In the majority of the ion-implanted specimen tests, the inability of that process to protect against oil-entrained contamination was not surprising considering the size of the Al_2O_3 contamination (20 μm) and depth of the ion-implanted layer (0.1 μm).

The TiN was evaluated on the M50 substrate only. As the data show, all of the TiN processes provided a good measure of surface protection, and two sets of TiN coated M50 (Nos. 3 and 4) provided almost fourfold improvement in life. Because of the high hardness of the PVD TiN, this was anticipated.

The following tabulation summarizes the results of the various protective coating evaluations. Ranking is relative to the baseline M50.

Process	RCF	Contaminated-Oil RCF	Full-Scale Bearings Posttest Corrosion
TDC	+	+ +	+ +
Ta^+	+ +	≈	− −
Cr^+	+ +	+	Not Tested
Cr^+ + P	+ +	≈	Not Tested
TiN	+ +	+ +	Not Tested

+ + = Substantially Better
+ = Better
≈ = Equivalent
− = Worse
− − = Substantially Worse

4.4 Baseline Testing – Full-Scale Bearings

Phase II of this program was concerned with full-scale bearing testing of the selected materials/process(es) combination in order to demonstrate (1) life improvement over VIM-VAR M50, (2) adequate fracture toughness, and (3) improved corrosion resistance.

To demonstrate the above characteristics, full-scale bearing testing was required. It was recognized early that this could evolve into an extremely time-consuming and expensive effort, especially that portion designed to demonstrate extended life. Based on full-scale bearing test experience with VIM-VAR M50 bearings in environments where bulk-fatigue properties were dominant, which means testing at a controlled temperature, consistent speed and load, with clean oil, and under full EHD lubrication condition, life factors ranging up to 100 had been demonstrated. A three- to fivefold improvement over these test results could literally mean years of bearing tests, which was obviously unreasonable. However, once the decision was made to concentrate on improving the initiation time for surface-induced distress (and subsequent spalling), the test and demonstration phase of this program became a much more realistic endeavor. This decision, coupled with successful development of the contamination test cycle, led both the GEAE team and the Air Force to conclude that a viable and potentially important approach to demonstrating improved life had been developed.

Concurrently, the two other characteristics – fracture toughness and corrosion resistance – were considered demonstrable by available data and test experience in the case of fracture toughness and by static tests for corrosion resistance. The task therefore was to develop and run a baseline test that could be used subsequently in Phase II to evaluate the effect of the selected material/process combination on improving surface-initiated failures. The bearing selected for this purpose was a 40-mm-bore ball bearing, shown in Figures 35 and 36, used by Torrington-Fafnir as a "standard" bearing test. Under the planned test load, the calculated AFBMA B_{10} life is 24 hours. With a relatively conservative materials factor of 12 for VIM-VAR M50, the B_{10} life should be on the order of 288 hours.

The test rig is shown in cross section in Figure 37 and photographically in Figure 38. In this bearing test rig, two opposed thrust bearings are evaluated on a single spindle. Eight spindle positions are available arranged in sets of two each on four tables. Each table has a separate lubrication system serving two spindles. Each spindle is V-belt driven by a 3450-rpm, 3-hp ac motor. Bearing lubrication and hydraulic-loading-piston lubricant are supplied at temperatures to 300°F by a gear pump and a 10-gallon stainless steel oil reservoir. Each test bearing is lubricated by two 1/16-inch jets, 180° apart, at the bearing inboard face. Separate pressure regulators are used for loading and lubrication.

Temperature readings of the bearings during test are made with a potentiometer monitoring a bayonet-type thermocouple that contacts the housing near the bearing outer diameter. The temperature of the oil going into and out of the test spindle is measured.

Drive motor rotation to each test spindle is stopped by an accelerometer if excessive vibration (due to surface distress or spalling) occurs. In practice, it was found that this vibration pickup could be tuned to sense very minimal, almost incipient, surface distress.

Test conditions were as follows:

Load	2700 lbf
Stress	380 ksi (Max)
Speed	10,000 rpm
Temperature	300°F
Lubricant	Mil-L-7808 (Exxon 2389)

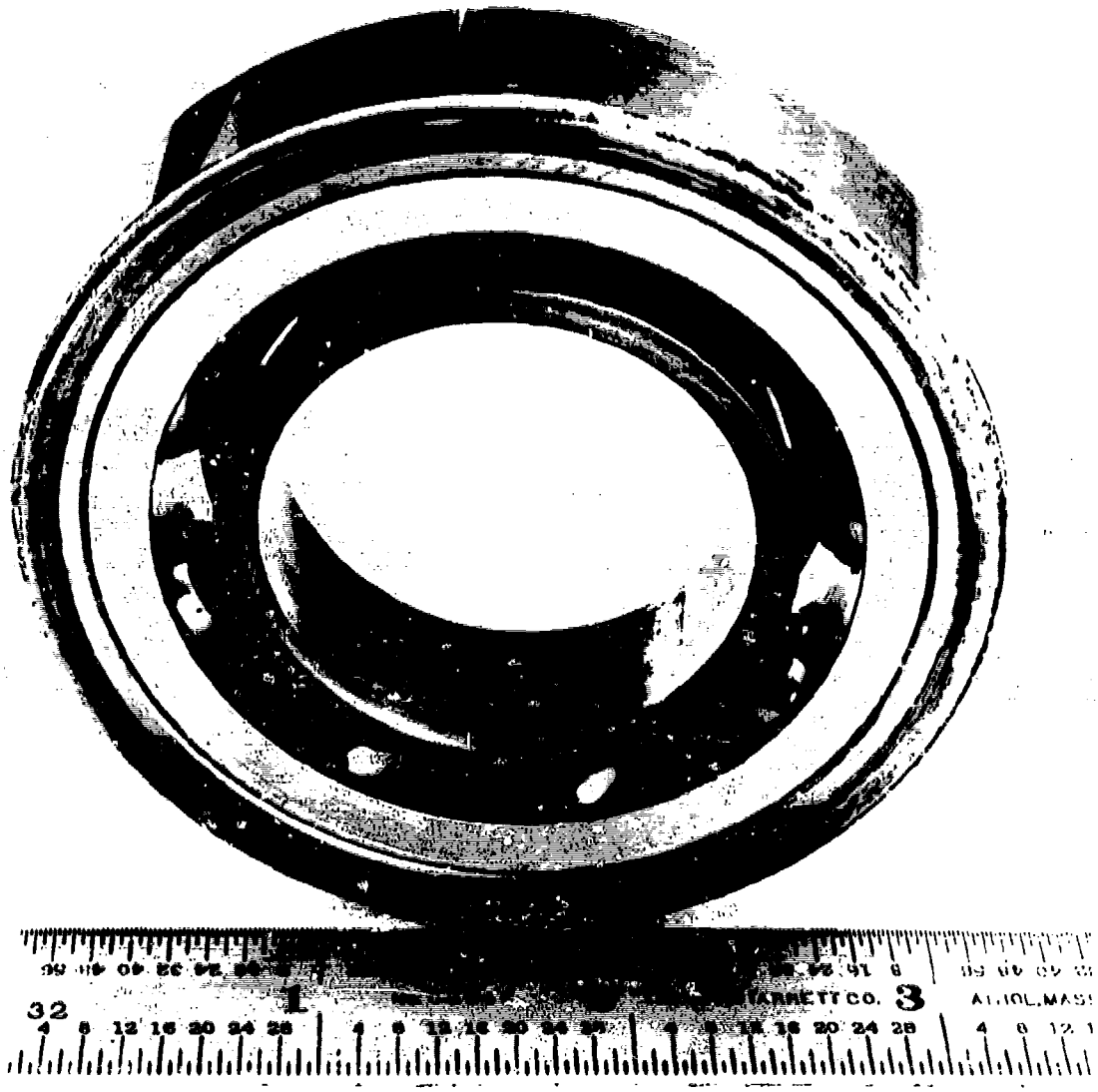

Figure 35. Assembled View of 40-mm Bore Ball Bearing.

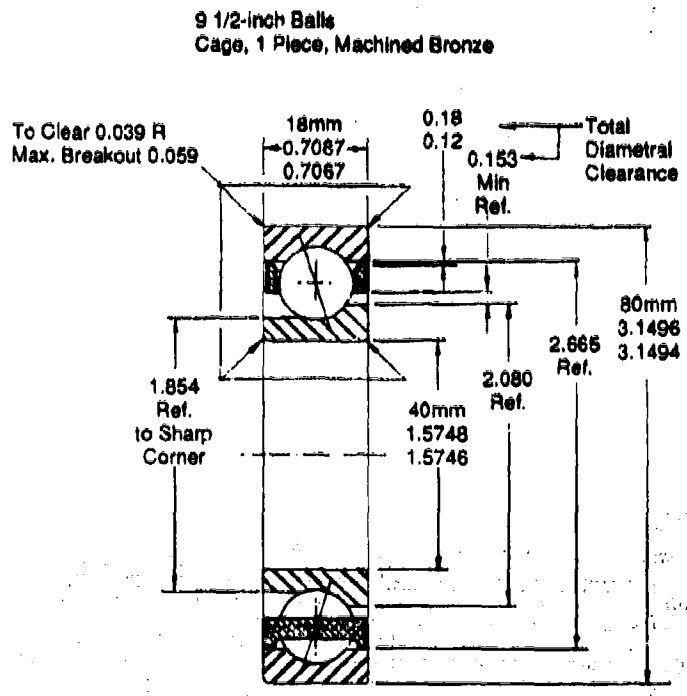

Figure 36. Engineering Drawing of 40-mm-Bore Ball Bearing.

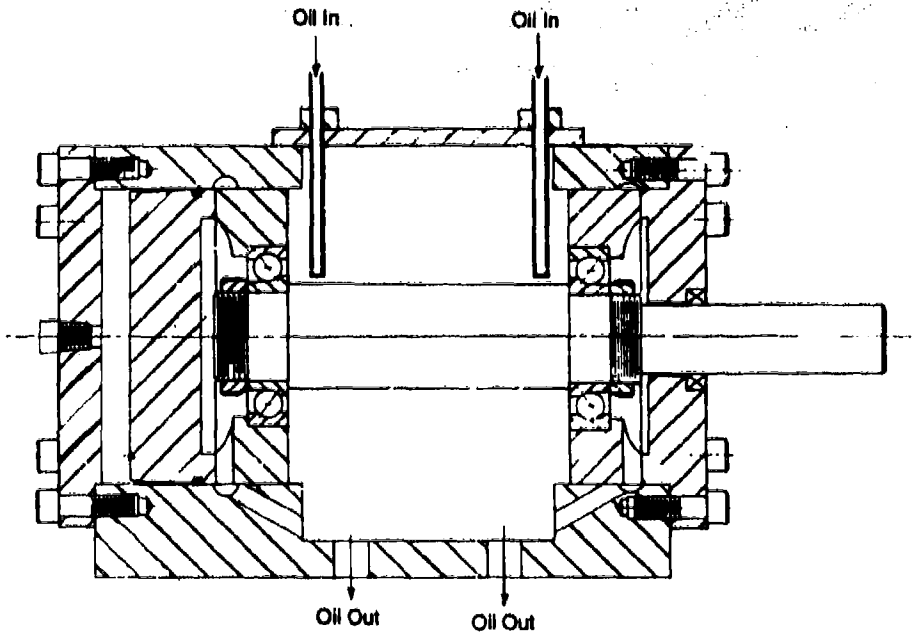

Figure 37. Cross Section of 40-mm-Bore Ball Bearing Test Rig.

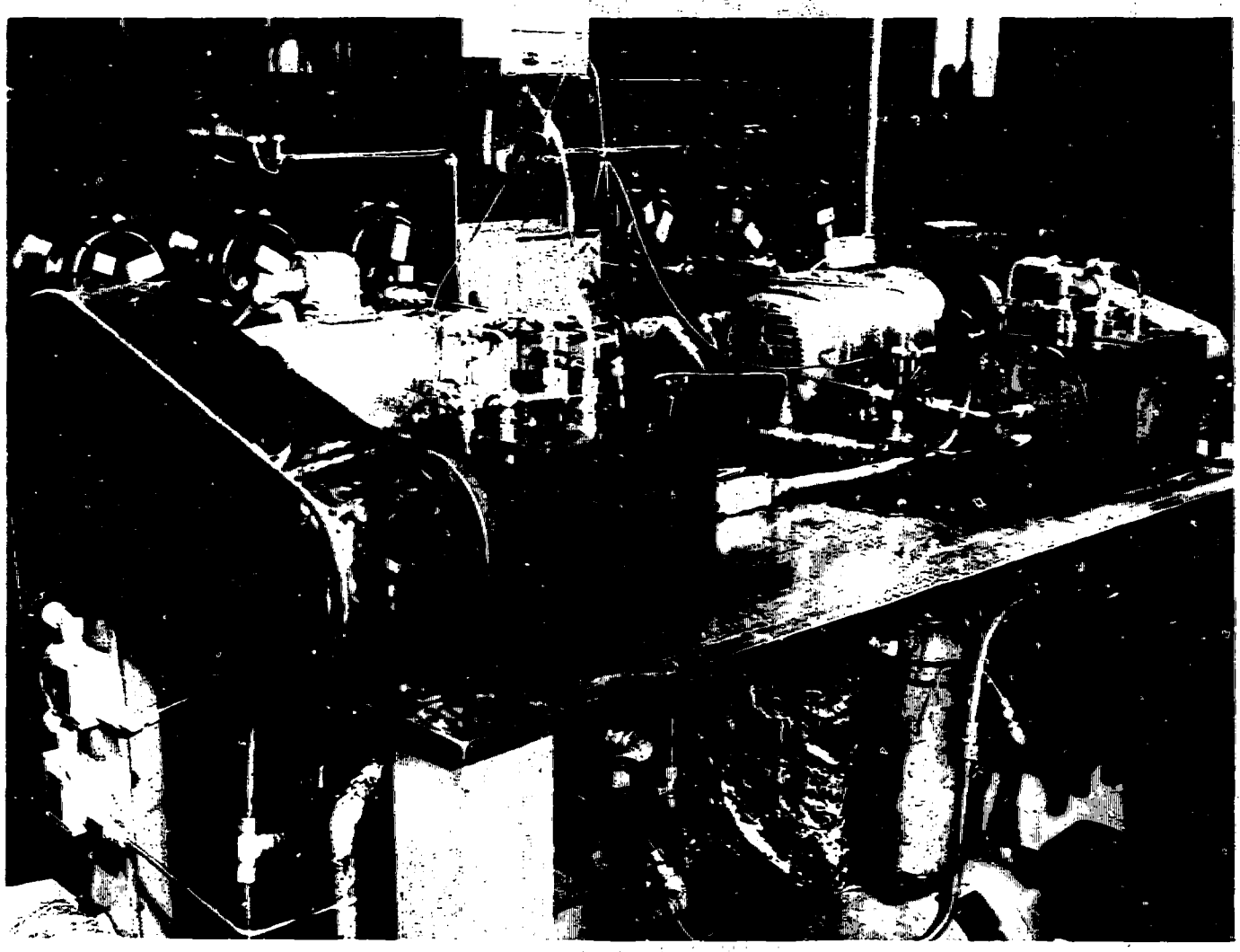

Figure 38. Closeup of 40-mm-Bore Ball Bearing Tester.

The test bearings (Fafnir 2AAM 208W0 MBR) were manufactured out of VIM-VAR M50. Initial testing was performed in uncontaminated oil. Bearings were dismounted after about 50 hours of running and the surfaces examined at 100× and occasionally in a SEM at 3000×. The sites of surface-damage initiation were evident. Grinding grooves developed burnished white regions alongside, and micropits developed in the white regions. Microcracks developed at the large carbides, and in some instances the carbides themselves cracked. In other instances, small regions of the surface were removed by a shallow peeling mechanism that had the appearance of interconnected microspalls. All of the damage was on a microscopic scale; the bearings were not failures by conventional definition since spalling in the usual sense had not developed. It appeared, however, that the initial peeling and microcracking mechanisms provided sites for the initiation of spalls. While this initial testing was demonstrating the feasibility of the proposed approach (tracking propagation of surface-initiated failures), the ball/rod controlled-contamination testing was reaching successful conclusion, so the concept of controlled contamination was then directly applied to the full-scale bearing tests.

The only change in the procedure was that the test bearings were prerun in contaminated fluid prior to being installed for actual testing. A separate test head was used for this purpose. The primary reason for this procedure was to ensure that any surface damage would be limited to permit tracking and documentation of individual surface defects.

Consequently, the bearings were first run in a rig in which the oil had been contaminated by the addition of 2.5 ppm of 20-μm size aluminum oxide. The contamination run lasted 15 minutes. The bearings were disassembled, washed, and examined for surface damage at 100×. The damaged areas were photographed to provide a reference for subsequent examinations. The bearings were reassembled in rigs with clean oil and run. Some bearings were disassembled periodically, cleaned, and photographed to record the progress of surface damage. Final failure occurred by spalling, and a very sensitive vibration detector was used to stop the test at an early stage in the spalling. In many instances, the spall was observed with most of the metal remaining in the cavity.

The initial tests were run in a somewhat different fashion. The contamination run was carried out as indicated, but the bearings were reassembled with new, clean balls and retainers. These failures developed very slowly, and the bearings were reassembled subsequently with the original contaminated balls and retainers. These bearings failed more rapidly. The contaminated balls and retainers were, apparently, needed to accelerate the test. The original failures are reported with the standardized test bearings, with the deviation in procedure noted.

The bearing test results are summarized in Table 7, and Weibull distribution of lifetimes is shown in Figure 39. As mentioned previously, of the 10 failures, 3 rings (35, 91, and 60) were contaminated in a different procedure and were not included in the Weibull analysis although the data appear to fit well with the remaining failures. Failure was defined as the occurrence of a spall. In most instances, however, it was possible to identify the initial surface damage that subsequently initiated the spall. The earliest failure, at 68 hours, had one of the largest initial flaws, 0.007 inch, and the ring with the longest life had the smallest initial flaw, 0.0005 inch.

The Weibull distribution in Figure 39 indicates a B_{10} life of 88 hours in this test. The AFBMA life calculated for these operating conditions is 24 hours. This indicates that M50, even with induced surface defects, still has a substantial operating life, although significantly reduced from the 288-hour B_{10} life expected from VIM-VAR M50 running in uncontaminated oil and with a reasonable materials factor.

Propagation of the significant flaw was documented in each of the rings listed in Table 7. Figure 40, top left, shows the initial flaw in Ring 20, produced during the 15-minute run in contaminated oil. After 22 hours of running in clean oil, the flaw had grown by a microspalling or peeling process. The spall was detected at 68 hours and had started at the head of the peeled region. The rolling direction of the ball was right to left; it is interesting to note that peeling occurs in the direction opposite the rolling direction. This mechanism was observed in each of the failures. Peeling was extended by a "pothole" mechanism with the ball breaking off small segments as it rolled over the edge of the flow. The spall, however, propagated by means of a crack that tended to undermine the material ahead of the defect and create the spall.

Table 7. Failure of Bearing Rings.

Ring No.	Hours	Cycles (10^9)	Comments
20	68	0.37	Inner Ring Spall
54	147	0.79	Inner Ring Spall
29	310	1.68	Inner Ring Spall
92	317	1.70	Inner Ring Spall
102	335	1.80	Inner Ring Spall
35 (1)	346	1.87	Inner Ring Spall
91 (2)	615	3.32	Inner Ring Spall
60 (3)	730	3.94	Inner Ring Spall
17	746	4.02	Inner Ring Spall
10	1127	6.09	Inner Ring Spall
62	1500	8.10	Retired
97	1500	8.10	Retired
24	1500	8.10	Retired

1. Ring 35 – Contaminated balls added at 250 hours.
2. Ring 91 – Contaminated balls added at 250 hours, contaminated retainer added at 311 hours.
3. Ring 60 – Contaminated balls added at 250 hours, contaminated retainer added at 311 hours.

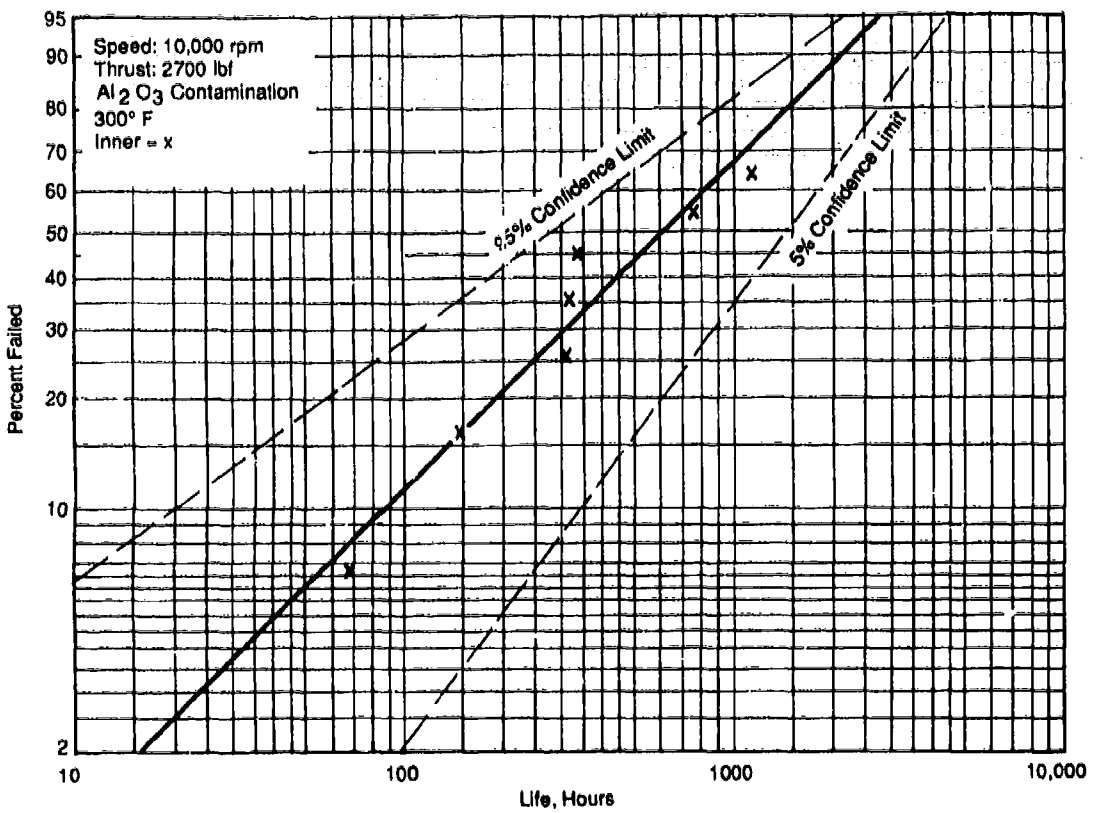

Figure 39. M50 Life Test Results.

(a) Initial failure after 15 minutes

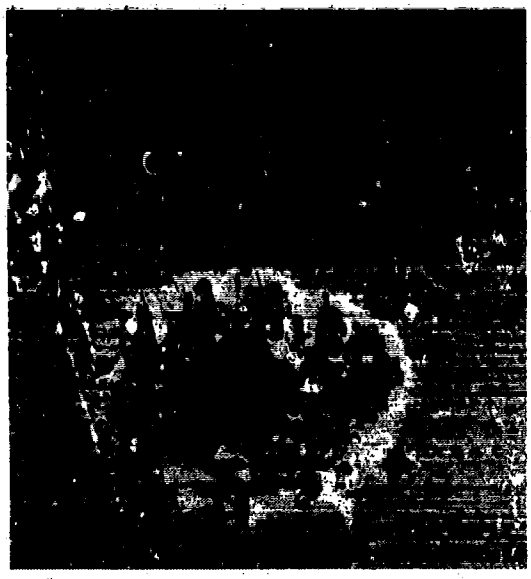

(b) After 22 hours of running

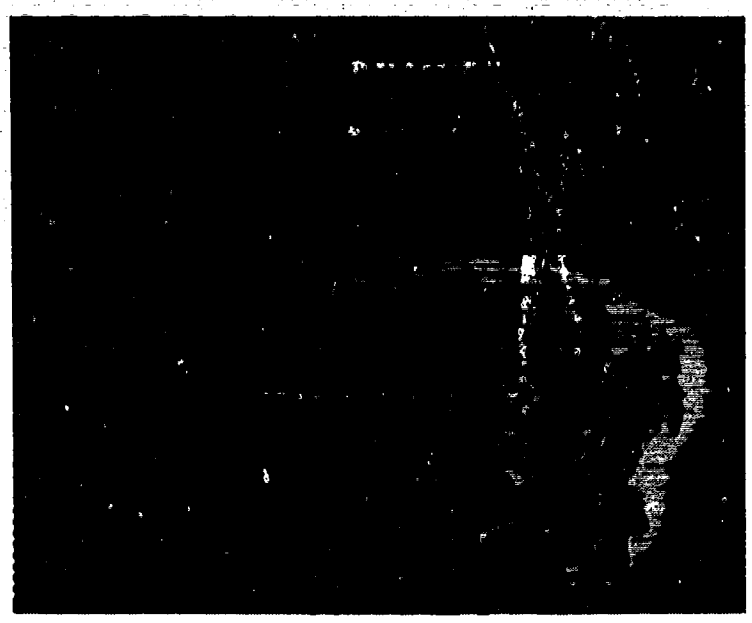

(c) After 68 hours; notice spall

Figure 40. Failure in Ring 20 After Contamination Run (100×).

Figure 41 shows a similar sequence for Ring 54. The initial flaw is shown at top left. The propagation by peeling is shown in the subsequent photomicrographs, with the final spall in the last panel. Figure 42 shows the initial flaw and the final spall in Ring 29. Figures 43, 44, and 45 show the propagation of peeling and the final flaws in Rings 35, 91, and 60. Although these rings were not tested with the exact same procedure as the rings mentioned previously, the mechanisms were similar, and the failures fit well within the Weibull distribution. The failure in Ring 10, Figure 46, is somewhat unusual in that the initial damage formed in the scuffed region surrounding a small dent. The flaw propagated by peeling, and then terminated in a spall.

Figures 47 through 49 are additional illustrations of failure progressions arising from small regions of surface distress. Figure 48 illustrates the initiation of micropitting from a surface tear caused by either grinding or hard-particle contaminant damage. Finally, Figure 49 is an eight-picture sequence over a period of 317 hours showing the growth of a surface-initiated spall.

4.5 Prime Candidate Selection

Follwing completion of the RCF, corrosion, and contamination-effects testing, a matrix of potential candidate materials was formulated. A rating system was set up based on (1) the data generated as part of the program effort; (2) prior data such as fracture toughness, hot hardness, etc. from various references; (3) other pertinent industry data; and (4) perceived or subjective data which included other guidelines such as time to introduction, temperature capability, etc. The matrix is presented in Table 8.

Based on this matrix, an overall assessment was made regarding the most promising overall candidate for an extended-life, fracture-tough, corrosion-resistant material. The assessment was subdivided into several considerations:

Structural Materials
Structural Materials Processing
Corrosion Resistant Coatings or Surface Modifications

- Extent of Corrosion Protection
- Effect on RCF
- Effect on Surface-Damage Protection

4.5.1 Structural Materials

M50NiL, CBS 1000M, and X2M are potential candidates for extended-life bearings. Based on prior work and extensive production testing/experience, M50NiL was the favored material. Pyrowear 53, a fourth extended-life material, did not meet the 6000°F operating temperature requirement.

Monolithic corrosion-resistant materials such as CRB 7, TRW 2001, AMS 5749, RSR 113, and RSR 565 do not meet minimum life extension or fracture-toughness requirements.

4.5.2 Structural Materials Processing

Gas carburizing is currently the most cost-effective process for achieving the bihardness material essential for extended life and fracture toughness. Existing (gas) carburizing procedures can be improved by vacuum carburizing techniques, but that will require additional process/equipment development.

State-of-the-art powder metallurgy offers no help in life or toughness improvement. Composite metal powders offer long-range potential, but a lengthy (5 to 10 years) development effort will be required. Electron Beam (EB) or laser hardening have long-term potential (especially EB) but also require considerable additional development.

(a) After 15 minutes

(b) After 27 hours

(c) After 75 hours

(d) After 147 hours

Figure 41. Ring 54 After Contamination Run (100×).

(a) After 303 hours

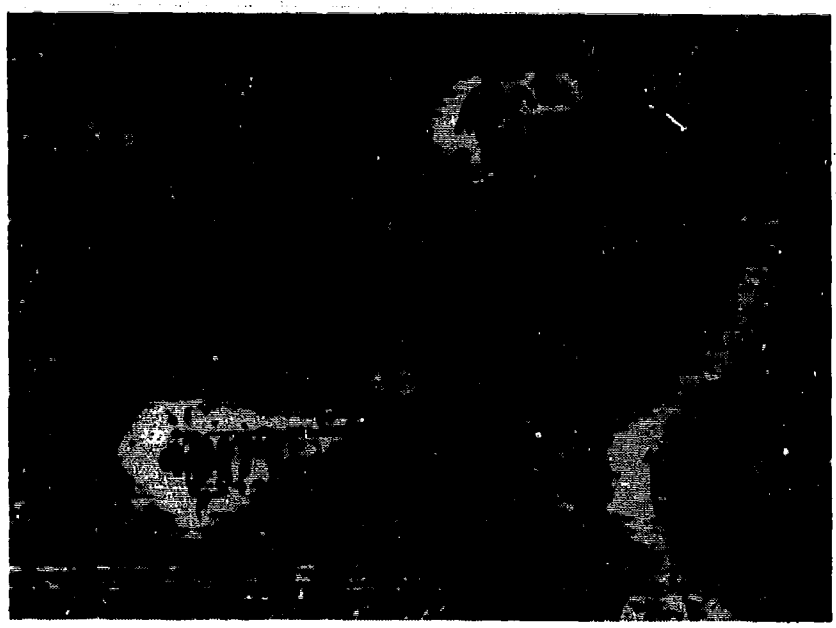

(b) After 310 hours

Figure 42. Ring 29 Failure (100×).

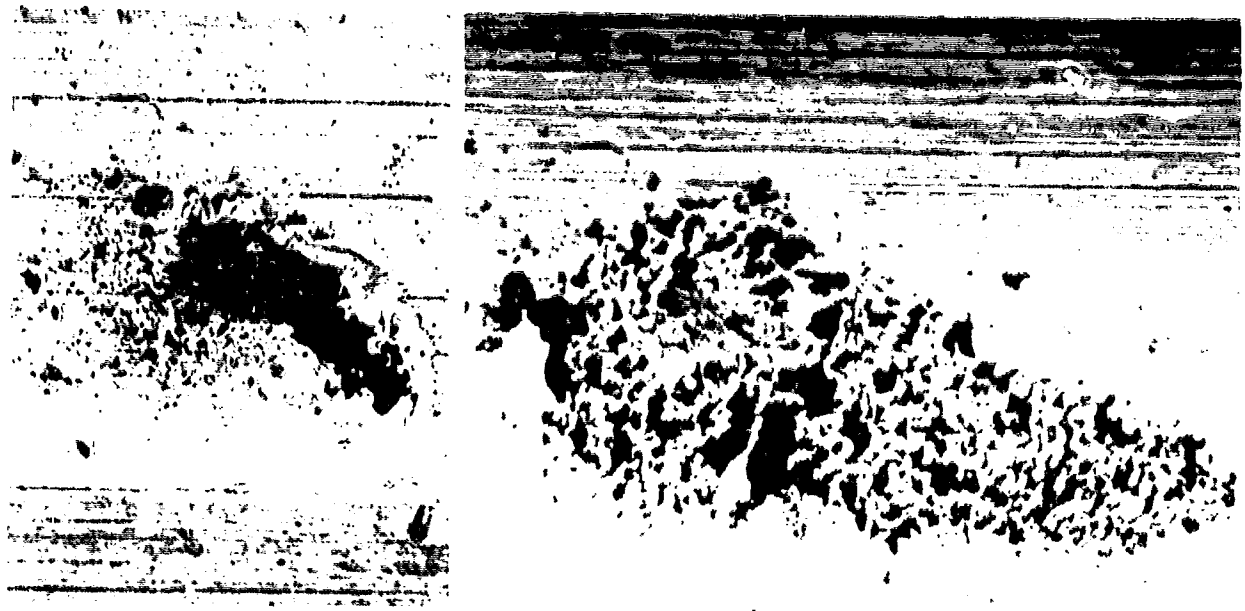

(a) After 275 hours

(b) After 325 hours

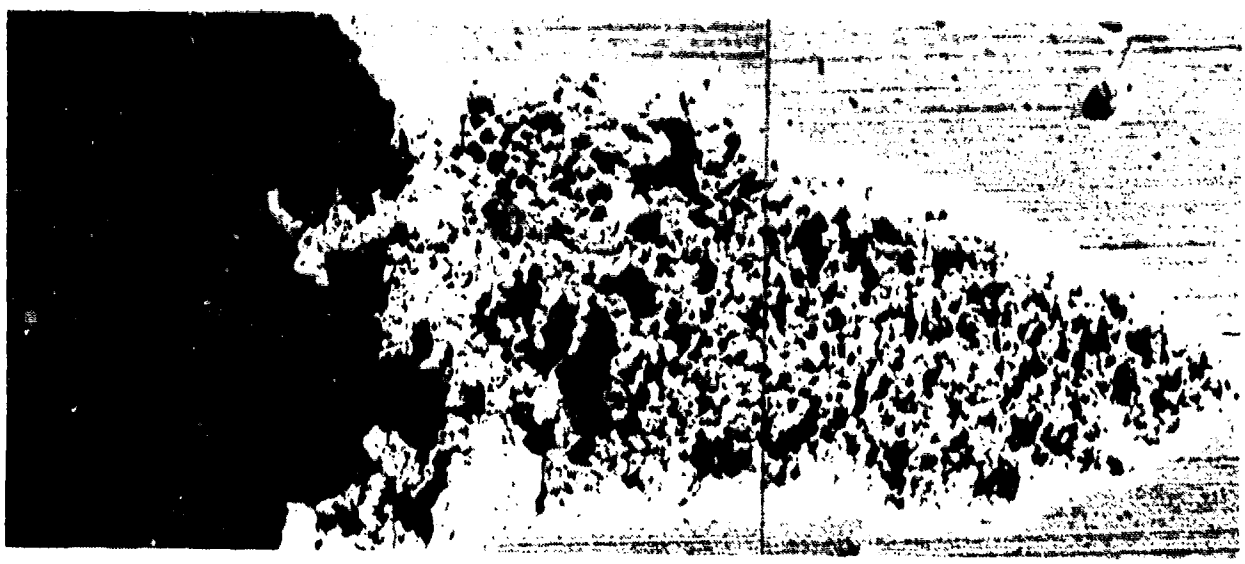

(c) After 346 hours

Figure 43. Ring 35 Nonstandard Run (100 ×). *Contaminated balls were added after 25 hours.*

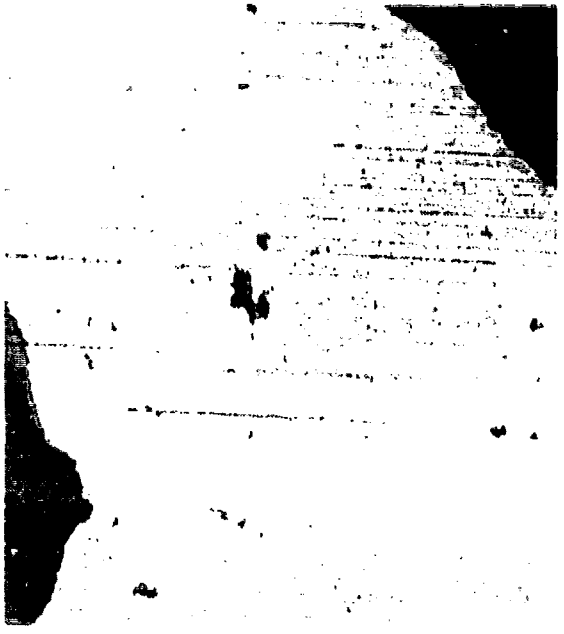

(a) After 300 hours

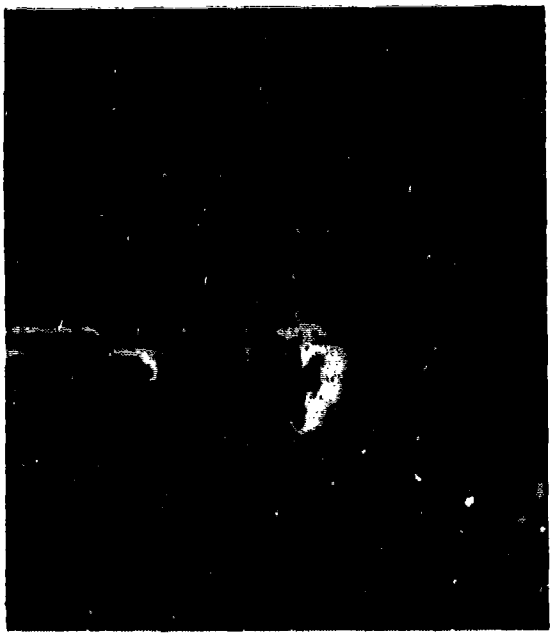

(b) After 363 hours

(c) After 615 hours

Figure 44. Ring 91 Nonstandard Run (100×). *Contaminated balls were added after 250 hours; contaminated retainer was added after 311 hours.*

(a) After 250 hours *50 ×*

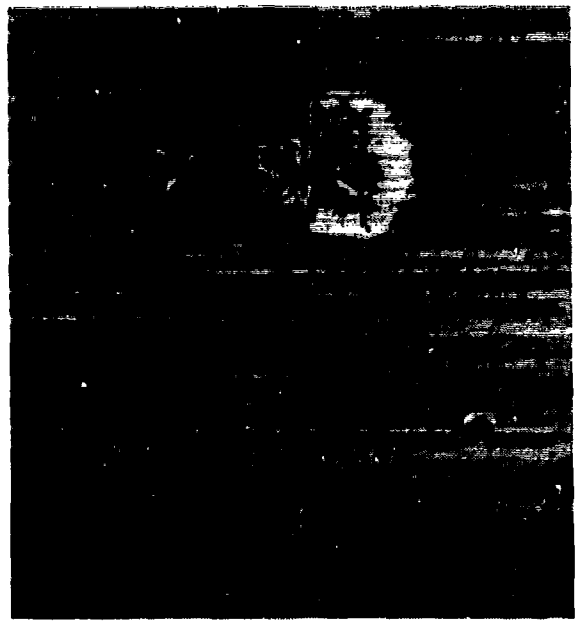

(b) After 363 hours *50 ×*

(c) After 615 hours *50 ×*

Figure 45. Ring 60 Nonstandard Run. *Contaminated balls were added after 300 hours; contaminated retainer was added after 311 hours.*

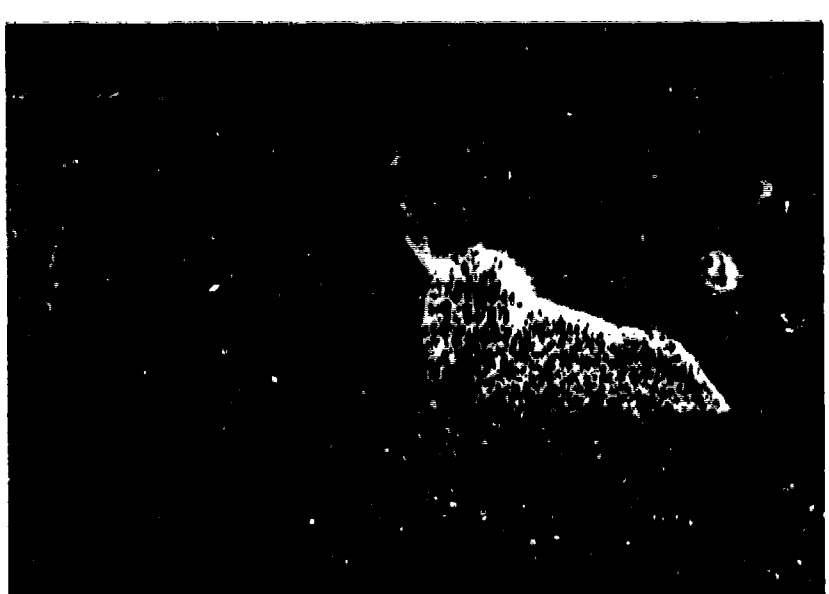

(d) After 730 hours *50×*

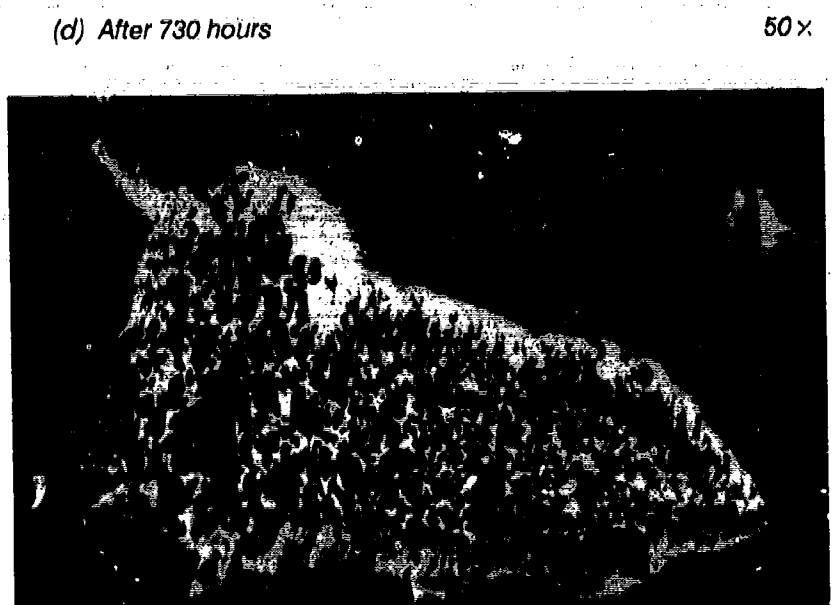

(e) After 730 hours *100×*

Figure 45. Ring 60 Nonstandard Run (Concluded).

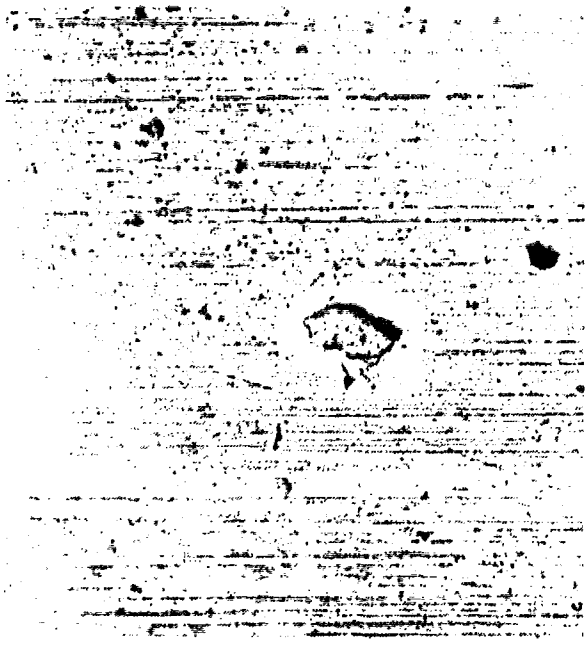

(a) After 33 hours

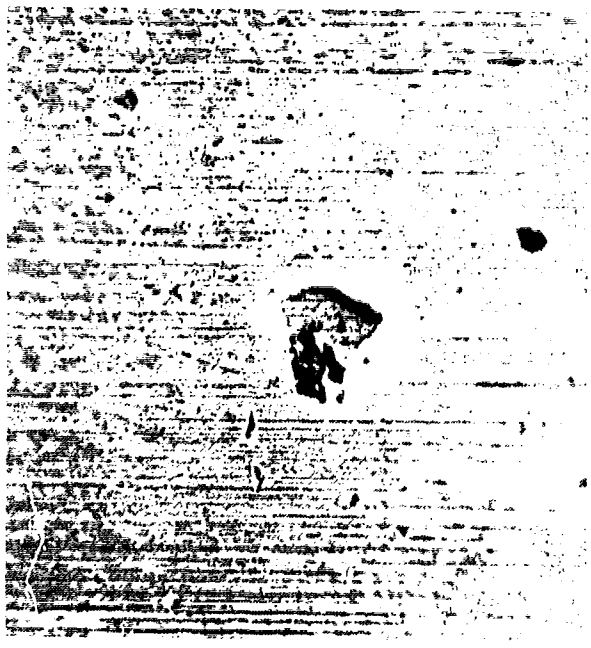

(b) After 444 hours

(c) After 1127 hours

Figure 46. Ring 10 (100×).

(a) After 15 minutes

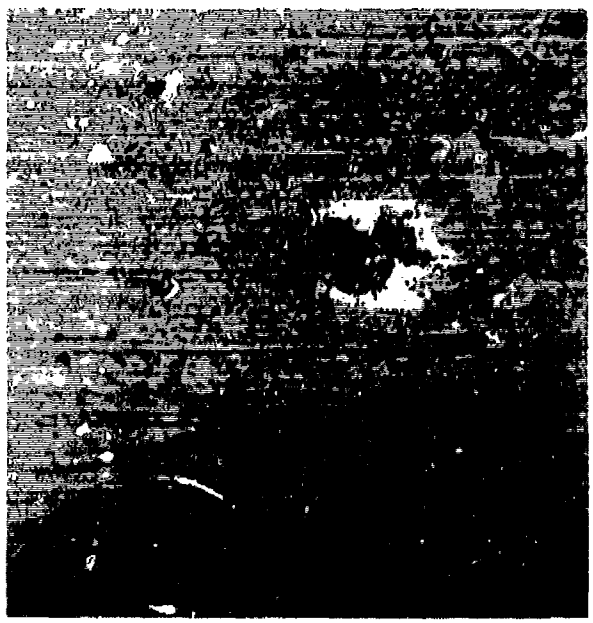

(b) After 15.4 hours

(c) After 30.0 hours

(d) After 33.4 6 hours

Figure 17 Ring 102 Failure Progression (100)

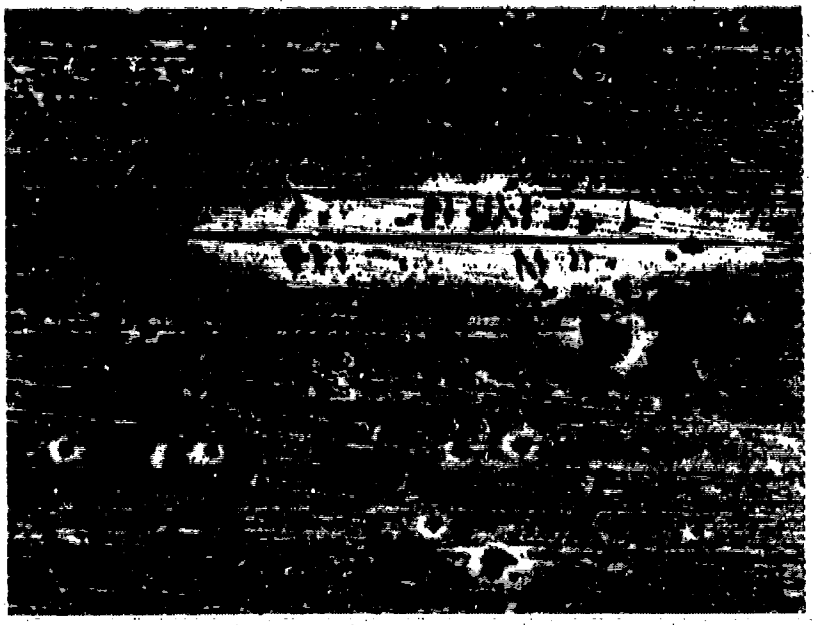

(a) After 347 hours *100×*

(b) After 746.5 hours *100×*

Figure 48. Ring 17 Showing Failure Initiation from Grinding Furrow or Al_2O_3 Groove. *Note the similarity of this pattern to that on the engine bearing shown in Figure 3.*

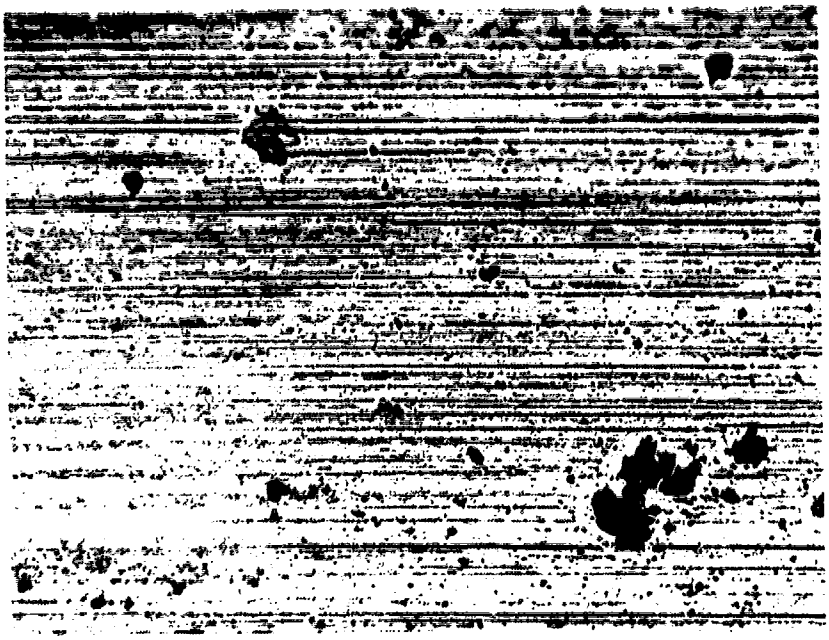

(a) After 15 minutes 100×

(b) After 15.4 hours 100×

Figure 49. Failure Progression in Ring 92. *Page 1 of 4.*

(c) After 30.5 minutes *100 ×*

(d) After 115 hours *100 ×*

Figure 49. Failure Progression in Ring 92. *Page 2 of 4.*

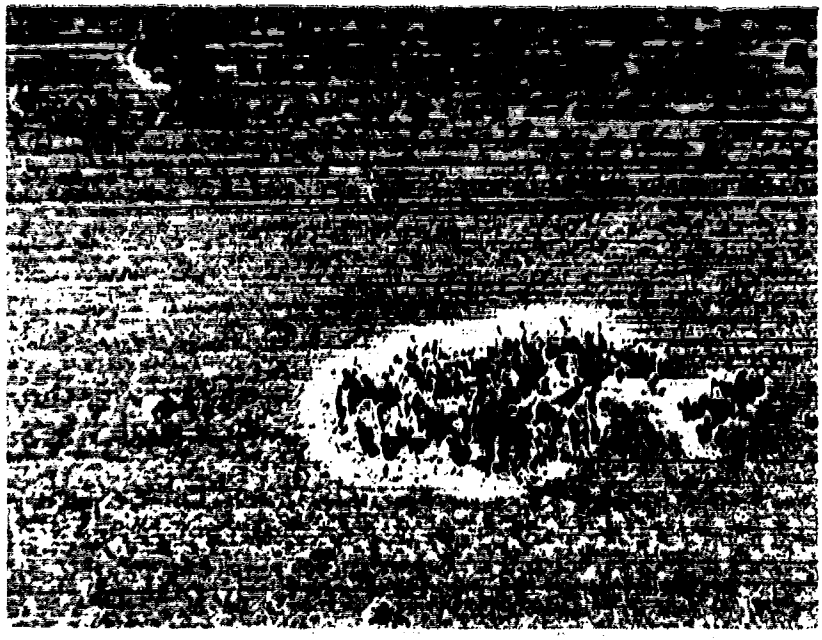

(e) After 132 hours *100×*

(f) After 150.6 hours *100×*

Figure 49. Failure Progression in Ring 92. *Page 3 of 4.*

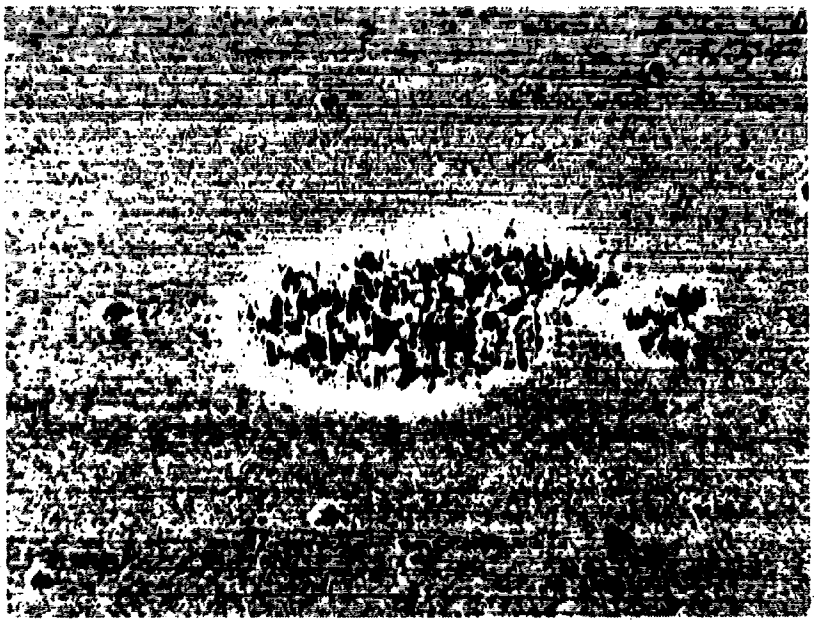

(g) After 153.3 hours *100 ×*

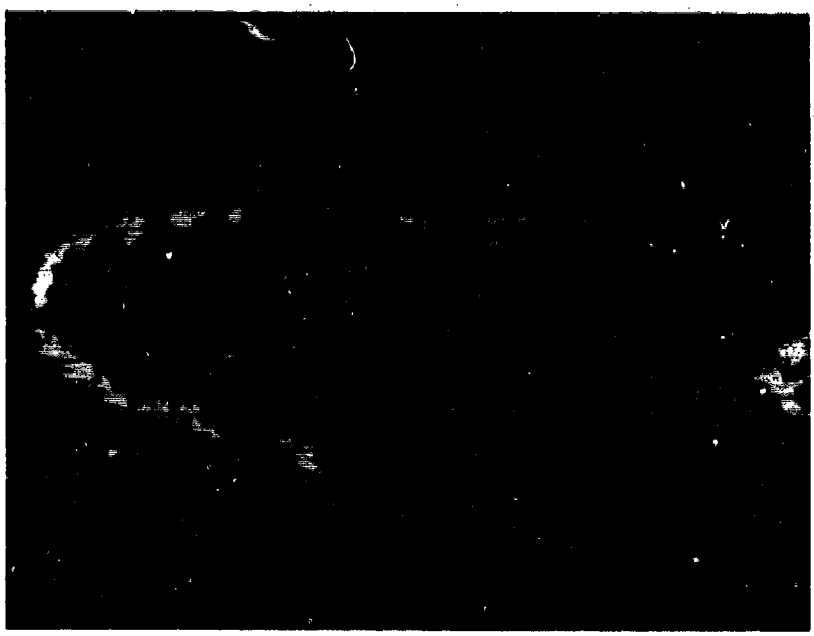

(h) After 316.6 hours *100 ×*

Figure 49. Failure Progression in Ring 92. *Page 4 of 4.*

Table 8. Candidate Materials/Processes for Extended-Life, Corrosion-Resistant Bearings.

Rating System: Numerical rankings are (except for Cost Impact) in ascending order of relative goodness; the base material/process rank is 1.

Column 1. Rolling Contact Fatigue – Numerical ranking as determined on GE RCF rig; VIM-VAR M50 is base.

Column 2. Fracture Toughness – K_{Ic} (ksi·in$^{1/2}$) as determined by compact tension test (ASTM E-399) or short-rod fracture (SAE ARP 1704); 40 ksi·in$^{1/2}$ is minimum requirement.

Column 3. Residual Stress Control – Numerical ranking of ability to achieve deep compressive residual stress consistently and predictably.

Column 4. Corrosion Resistance – Numerical ranking as determined by USN corrosion test; AMS 5749 (14-Cr steel) is considered base.

Column 5. Hot Hardness – Rockwell hardness; requirement is RC 58 at 600°F.

Column 6. Wear Resistance – Numerical ranking as determined by ball/rod contamination test, 2.5 ppm of 20 μm size Al_2O_3 in Mil-L-7808 or Mil-L-23699.

Column 7. Surface Quality – Numerical ranking of ability to achieve high surface finish and topography; M50 is base.

Column 8. Maximum Operating Temperature – Based on tempering temperature, °F.

Column 9. Near-Term Production – Numerical ranking: 3 is immediate, 2 is three to five years, 1 is more than 5 years.

Column 10. Cost Impact – Numerical ranking; VIM-VAR M50 is base.

Materials	**1** RCF	**2** K_{Ic}	**3** R.S.C.	**4** C.R.	**5** RC	**6** W.R.	**7** S.Q.	**8** °F	**9** N.T.P.	**10** C.I.	**Comments**
M50	1	20	N/A/	1	58	1	1	600	3	1	
M50NiL	3	47	3	1	58	1	3	600	3	1.3	Carburizing grade
X53	2.5	90	?	1	58	1	3	450	2	1.3	Carburizing grade
CBS 1000M	2.5	44	1	1	58	1	3	600	3	1.3	Carburizing grade
X2M	2.5	44	2	1	58	1	3	600	3	1.3	Carburizing grade
AMS 5749	1	18	N/A	3	58	1	---	600	3	1.1	
AMS 5749 Mod	N/A	N/A	---	3	N/A	1		600	1	N/A	Note A
CRB-7	0.8	18	N/A	3	58	1	0	600	2	1.3	
TRW 2001	1	18	N/A	3	58	1	0	600	2	2	
422	---	---	2	---	---	---	2	---	1	1.3	Carburizing grade
Processes											
TDC	1.2	N/A	N/A	3	N/A	2-3	N/A	Substrate	3	1.1	Note B
Cr Ion Implant	1	N/A	N/A	3	N/A	2	N/A	Substrate	3-2	3+(?)	Note C
Cr + P Ion Implant	1	N/A	N/A	3	N/A	2	N/A	Substrate	3-2	3+(?)	Note C
Ta Ion Implant	1	N/A	N/A	3	N/A	2	N/A	Substrate	3-2	3+(?)	Note C
TiN	3	N/A	N/A	Note D	N/A	5	N/A	Substrate	2	3+(?)	Note D

Note A: Ni mod, low-carbon carburizing grade
Note B: No derating effect on RCF or hot hardness
Note C: M50 substrate. No derating effect on RCF or hot hardness
Note D: Process control must be absolute to preclude pinholes that can result in severe cell corrosion

4.5.3 Corrosion-Resistant Coatings or Surface Modifications

Corrosion Protection – TDC was excellent on M50 and M50NiL. The protective layer was still intact after RCF rig testing at 700-ksi maximum stress.

Cr^+, Cr^+ + P, and Ta^+ implants were also excellent on M50 and M50NiL. Although the protective layer was generally compromised after 700-ksi stress RCF testing, that is not an overriding concern because normal service would not induce extremely high contact stress. Spot tests at 350-ksi showed no obvious loss in surface integrity.

TiN provided variable protection on M50 and M50NiL; it is very process (and control) dependent. In addition, it is subject to pinholes that result in deep localized corrosive pitting – creating a serious life-influencing problem. Spalling or flaking of TiN coating would introduce hard particles into the oil/sump system, an undesirable event.

RCF – TDC improved directional RCF resistance for M50 and M50NiL. In general, test results were in agreement with industry data on full-scale bearing tests. Disagreement with Reference 19 could be due to test procedures and generic Armoloy versus Fafcote TDC process differences. (TDC M50NiL RCF versus bare M50 is 2× + improvement – quite conservative.)

Cr^+, Cr^+ + P, Ta^+ implants provided directional improvement in RCF for both M50 and M50NiL.

TiN improved M50 (not evaluated on M50NiL), but results were inconsistent and process-control linked.

Surface-Damage Protection –TDC enhanced M50. No statistical improvement was noted on M50NiL.

Cr^+, Cr^+ + P, Ta^+ implants provided no significant improvement in resistance to contaminated-oil environment. This result was anticipated, considering the shallow layer of implanted material.

TiN offers significant improvement in contamination resistance on M50 and presumably on M50NiL, although the latter was not evaluated.

4.5.4 Summary and Recommendations

Summarizing the above, the following overall assessment was made:

- M50NiL offers potential 3 to 5× RCF life improvement over VIM-VAR M50.
- TDC, ion implantation, and TiN can provide some additional life extension.
- TDC and ion implantation provide adequate corrosion protection.
- TiN provides excellent resistance to contamination.
- TDC offers some degree of improved protection against contamination.

Based on the foregoing and considering subjective factors such as cost, producibility, repairability, timing, etc., the material/process selection for Phase II of this program was as follows:

Material: M50NiL
Process: Carburizing
Coating: TDC on Rings and (1) None on Rolling Elements or (2) Ta^+ Implantation on Rolling Elements

The decision regarding protection of the rolling elements is discussed in Section 5 of this report.

5.0 Phase II – Full-Scale Bearing Tests

The primary material and process candidates selected in Phase I were evaluated by full-scale bearing testing in Phase II.

Two sets of bearings were manufactured: the 40-mm-bore ball bearing configuration (FAF 2AAM 208WO) used in the Phase I baseline testing and an advanced engine mainshaft bearing. The latter was the GEAE F101/F110/CFM56 No. 3 bearing (GEAE Drawing 9340M90P02). Two of the No. 3 bearings were manufactured, and 16 of the 40-mm bearings were made. For both designs, the rings were M50NiL, Fafcote TDC coated on all surfaces. For the 40-mm-bore ball bearings, both bare and Ta^+ implanted balls were prepared. The test sequence was as follows:

A. Test Series 1 (40-mm Bearings)

1. Test Two Bearings with Ta^+ M50 Balls
2. Test Two Bearings with Bare M50 Balls

B. Midtest Analysis

1. Analyze tEst Data
2. Corrosion-Test Ta^+ Balls and TDC Rings
3. Decide Between Bare or Ta^+ Balls

C. Test Series 2 (40-mm Bearings)

1. Complete Life Testing of Additional Bearings
2. Analyze Results

D. Engine Bearings

1. M50NiL Rings, TDC Coated
2. Balls - M50
3. Component Test

Because all of the 40-mm bore test bearings used in A and C (above) were subjected to a prerun cycle in a contaminated environment (2.5 ppm/20-μm Al_2O_3), Test Series 1 permitted assessment of the effect of the Ta^+ implantation on protecting the ball surface. It was decided that if posttest corrosion testing of the Ta^+ balls showed that corrosion protection was still adequate, then the remaining bearing tests would be performed with the implanted balls.

If, on the other hand, no significant advantage was noted between the bare and ion-implanted balls, then the remaining tests would be performed with bar M50 balls. In either case, a total of at least 10 bearings of one condition were to be evaluated which is considered sufficient to provide a valid statistical sample.

5.1 Evaluation of M50 and Ta^+ Implanted M50 Balls

At the outset of the Phase II bearing test program, it had not yet been established whether the test series would be run with bare M50 balls or with Ta^+ implanted M50 balls. Because of long-lead time procurement, it was considered more cost-effective to procure a sufficient number of balls (bare and Ta^+ implanted) to run a 10-bearing test series with either type. It was decided to start the test series with four bearings, two containing uncoated balls and two with Ta^+ implanted balls. These bearings were run for an extended time period or until

failure, whichever occurred first. Upon removal from the test, the bearings containing both types of balls were corrosion tested, the result of which determined whether to continue the test series with the Ta^+ implanted balls. Since all bearing rings were TDC coated, the corrosion test was also used to evaluate the ability of this coating to survive under rigorous rolling contact. In addition, a new bearing (uncoated) was included as a control test in the corrosion cycle.

Three bearings were selected for the corrosion test:

Bearing No. 6: TDC coated M50NiL rings
Ta^+ implanted M50 balls
Test time = 423.8 hours (suspended)

Bearing No. 9: TDC coated M50NiL rings
Ta^+ implanted M50 balls
Test time = 347.3 hours (suspended)

Bearing No. 12: TDC coated M50NiL rings
Uncoated M50 balls
Test time = 722 hours

Bearing 12 had an inner ring spall and is included in the test series discussed in Section 5.2.

These three bearings were run through the U.S. Navy corrosion test summarized earlier in this report. Following the 14 cycles prescribed by the Navy test, the bearings were examined using optical microscopy as well as SEM. The results are illustrated in Figures 50 through 64 and summarized below.

Bearing No. 6 – Overall photo, Figure 50.

Inner Ring (M50NiL) - Running track burnished but no corrosion evident. Some fretting on bore, but again no indication of any corrosive activity. TDC coating was intact on all surfaces (see Figure 51).

Outer Ring (M50NiL) - Running track burnished, no evidence of corrosion. Evidence of cage rub on shoulders. Some indication of outer-race movement on outer diameter. TDC coating intact on all surfaces. No evidence of corrosion (see Figure 52).

Balls (Ta^+ - M50) - Localized corrosion and pitting (see Figures 53 and 54).

Bearing No. 9

Inner Ring (M50NiL) - Running track burnished, slight fretting on bore. TDC coating intact on all surfaces. No evidence of corrosion.

Outer Ring (M50NiL) - Running track burnished, shiny bands on shoulders indicating cage rub. Some evidence of ring movement on outer diameter. TDC coating intact, no evidence of corrosion.

Balls (Ta^+ - M50) - Localized areas of corrosion and pitting (see Figures 55 and 56).

Bearing No. 12 – Overall photo, Figure 57.

Inner Ring (M50NiL) - Running track burnished, some fretting on bore. Fatigue spall. TDC coating intact on all surfaces, including the area immediately adjacent to the spall (Figures 58 and 59).

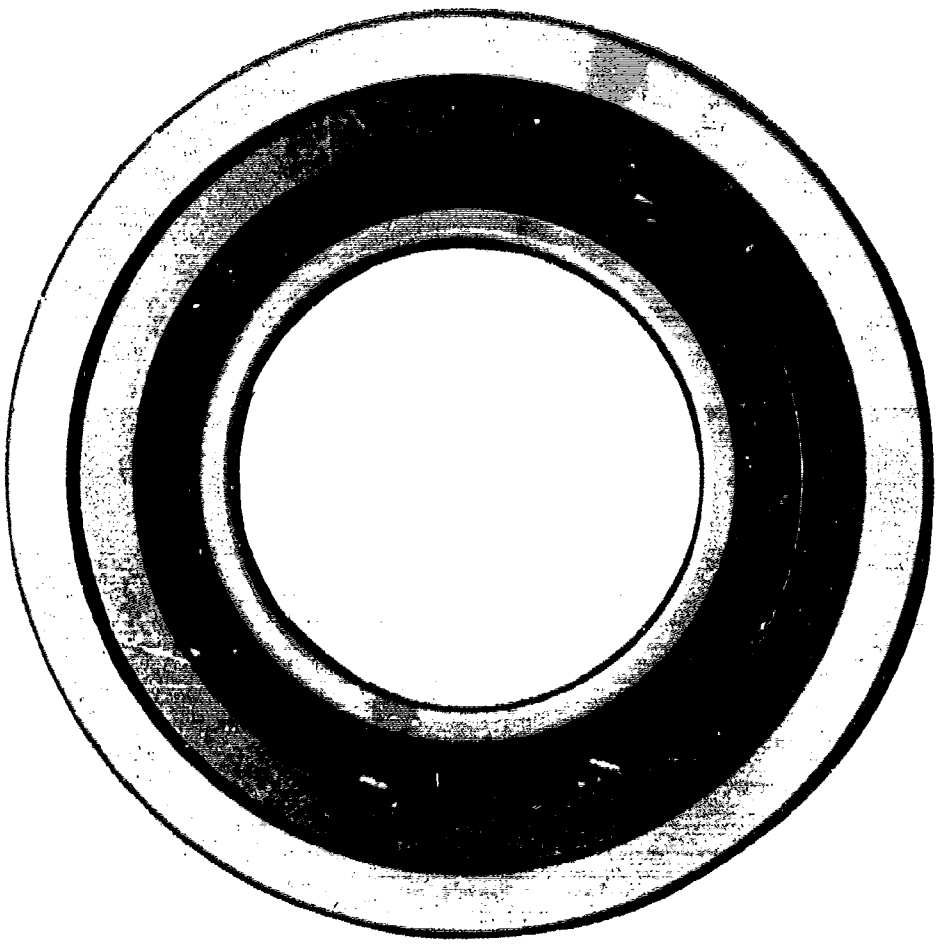

Figure 50. Bearing No. 6 After Corrosion Test.

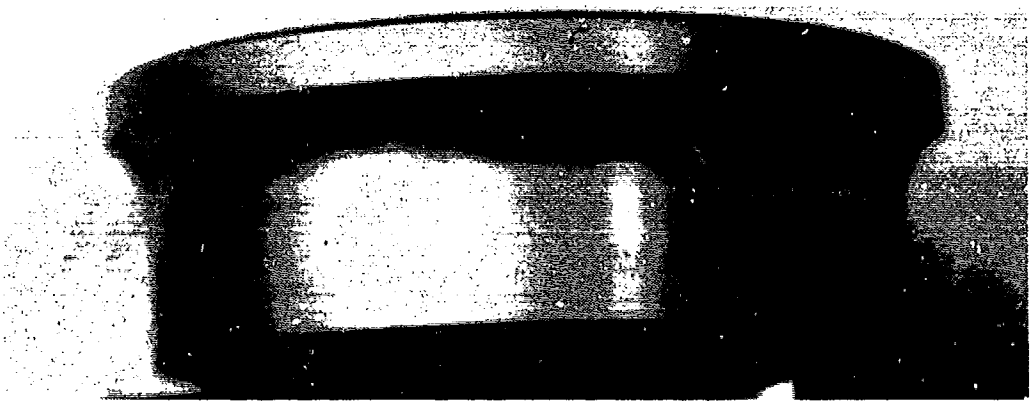

Figure 51. Bearing No. 6 Inner Ring After Corrosion Test.

Figure 52. Bearing No. 6 Outer Ring After Corrosion Test.

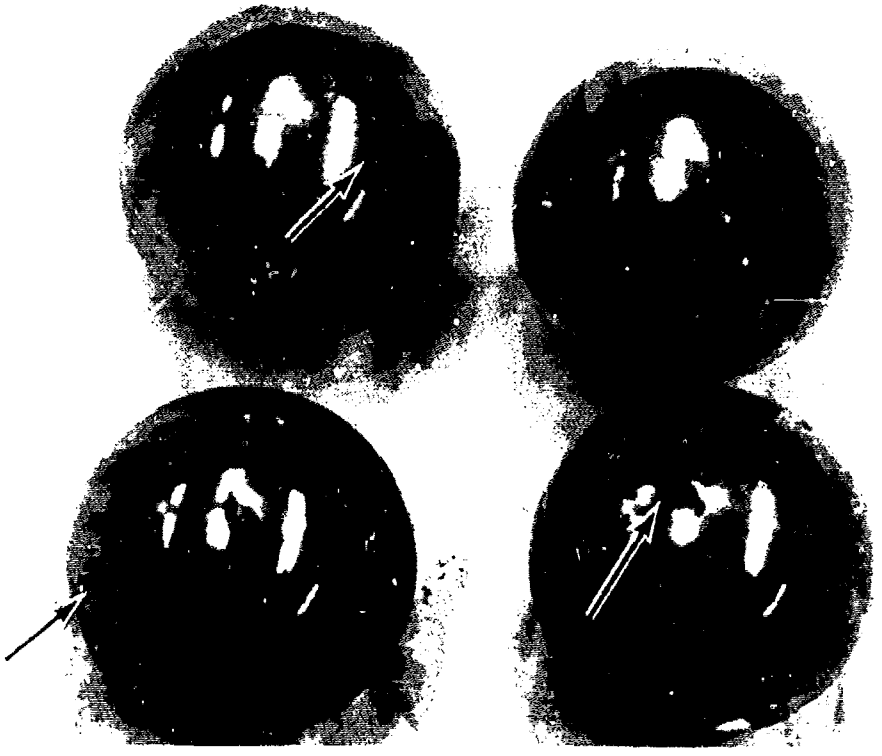

Figure 53. Balls from Bearing No. 6 After Corrosion Test.

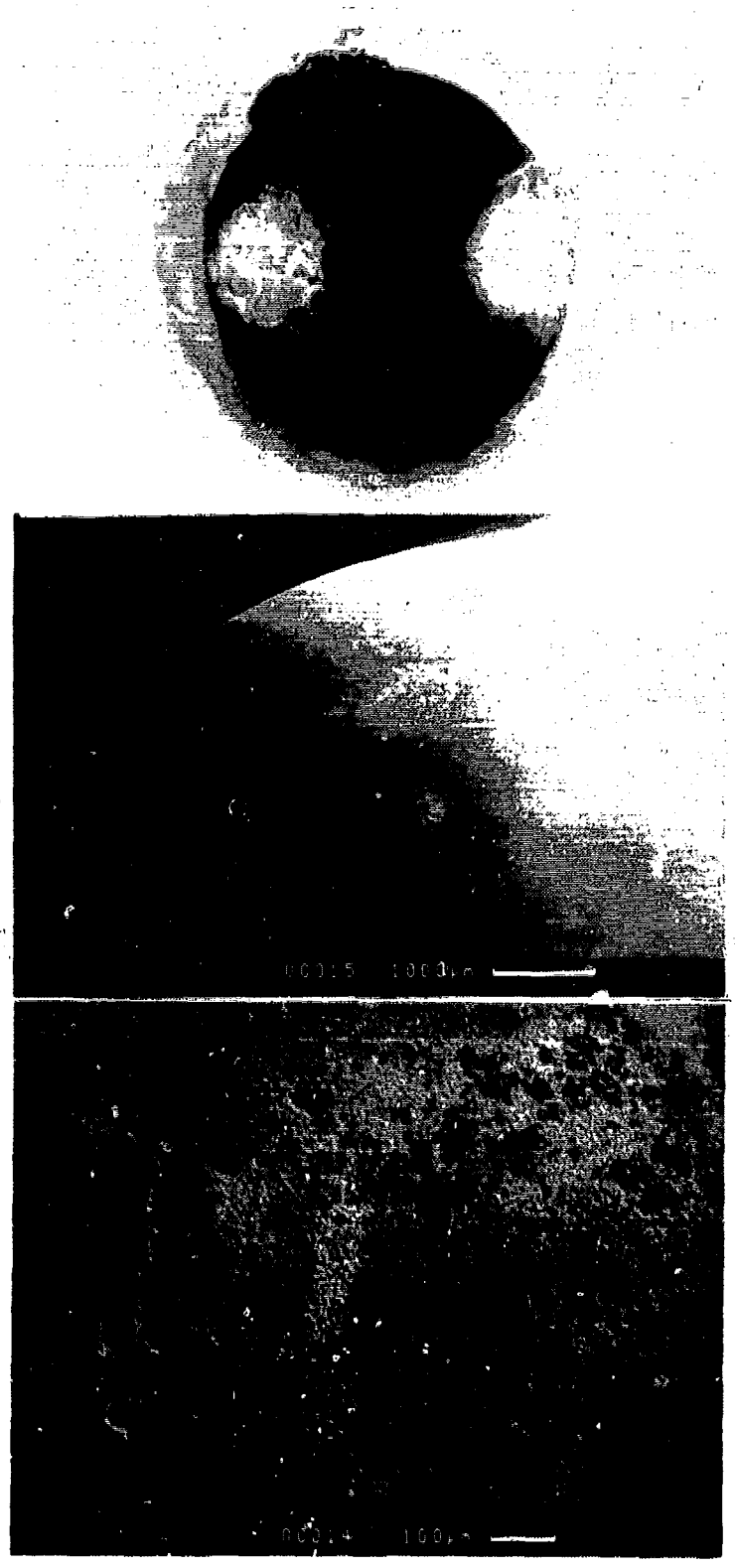

Figure 54. Typical Corrosion on Ta^{+} Implanted M50 Ball Bearing No. 6.

50×

500×

Figure 55. Corrosion Pitting on Ta^+ Implanted M50 Ball (Bearing No. 9 After 347 Hours). *Note typical "mudcracking" in lower photo.*

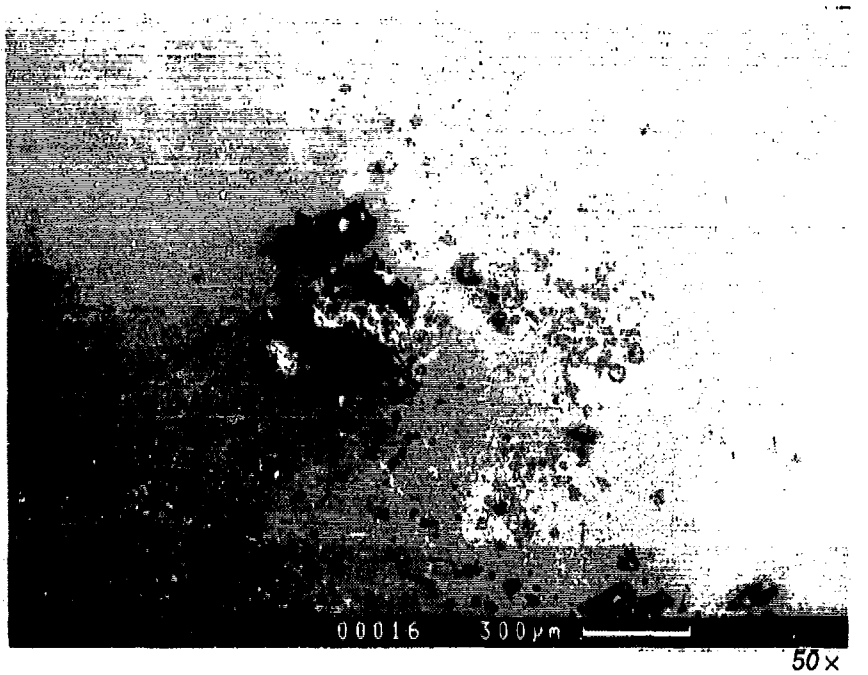

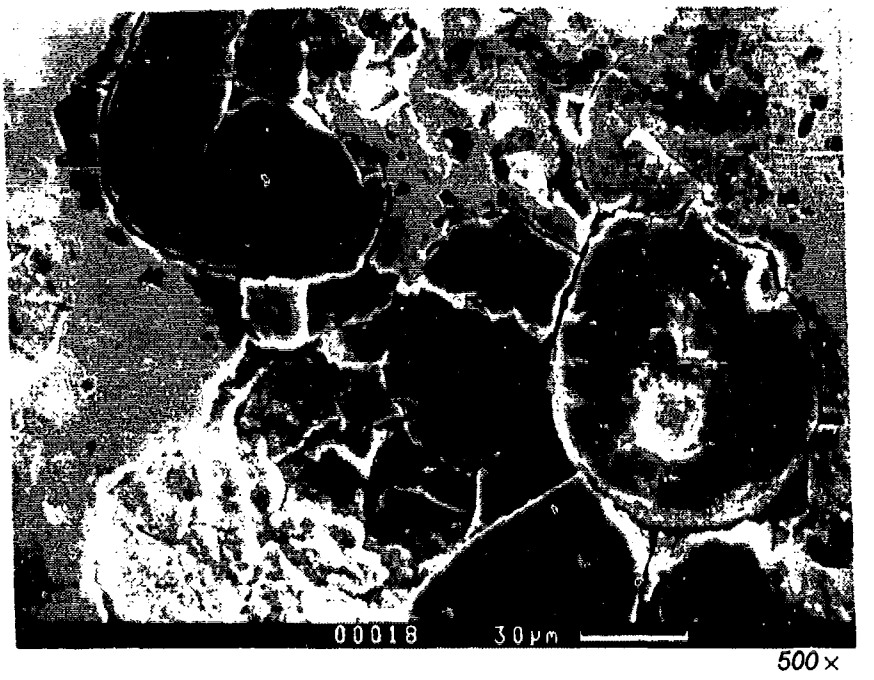

Figure 56. Typical Corrosion Pitting on Ta^+ Implanted Ball (Bearing No. 9 After 347 Hours).

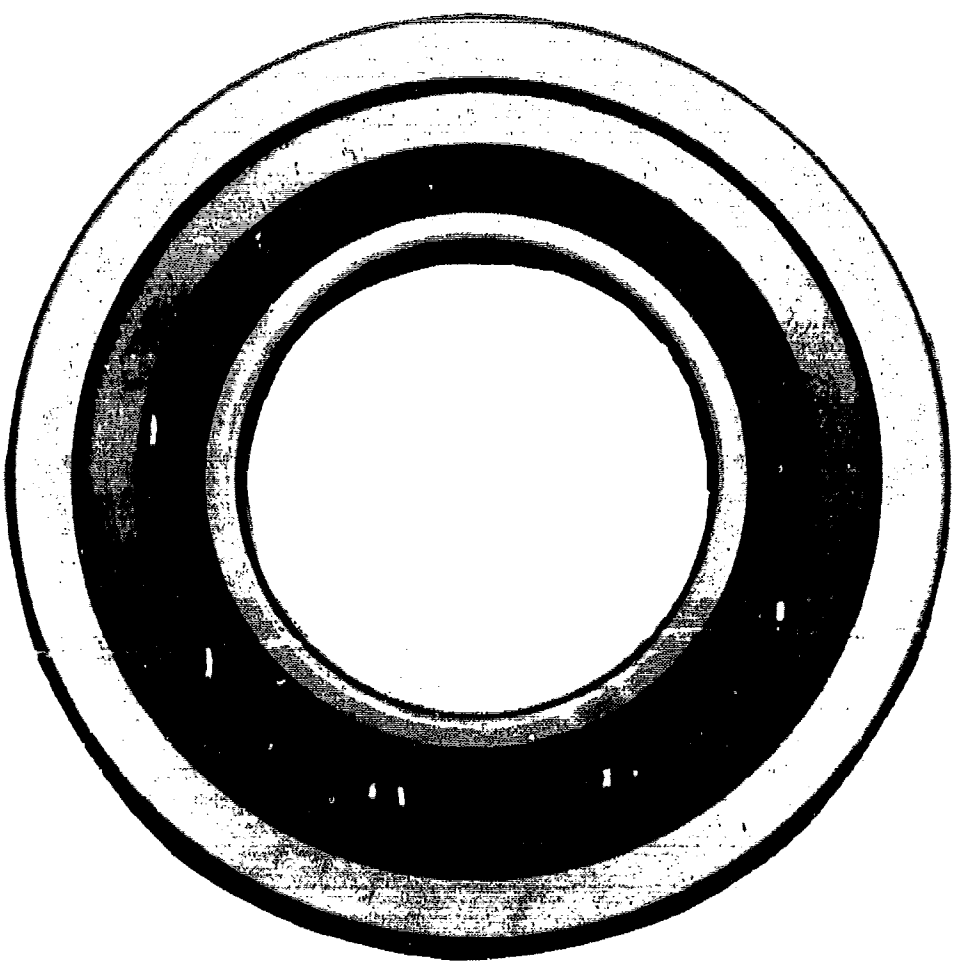

Figure 57. Bearing No. 12 After Corrosion Test.

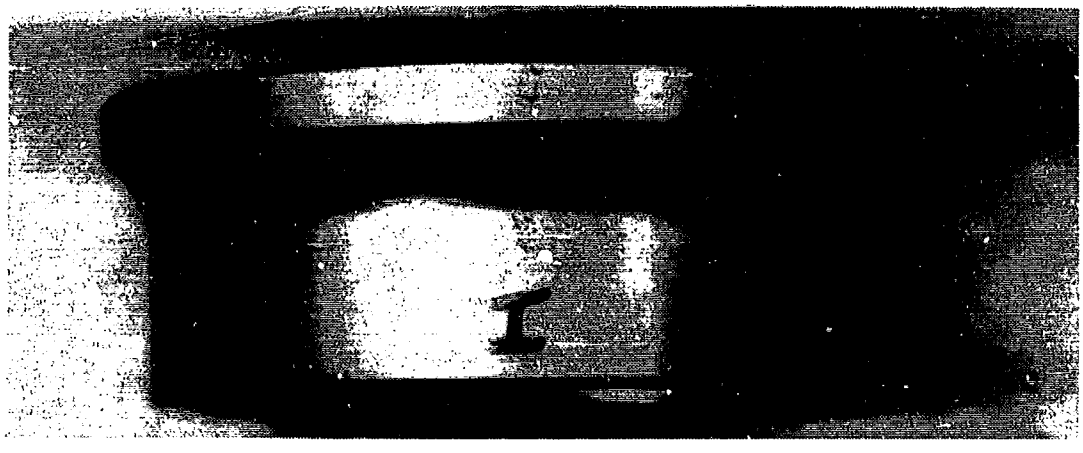

Figure 58. Bearing No. 12 Inner Ring After Corrosion Test.

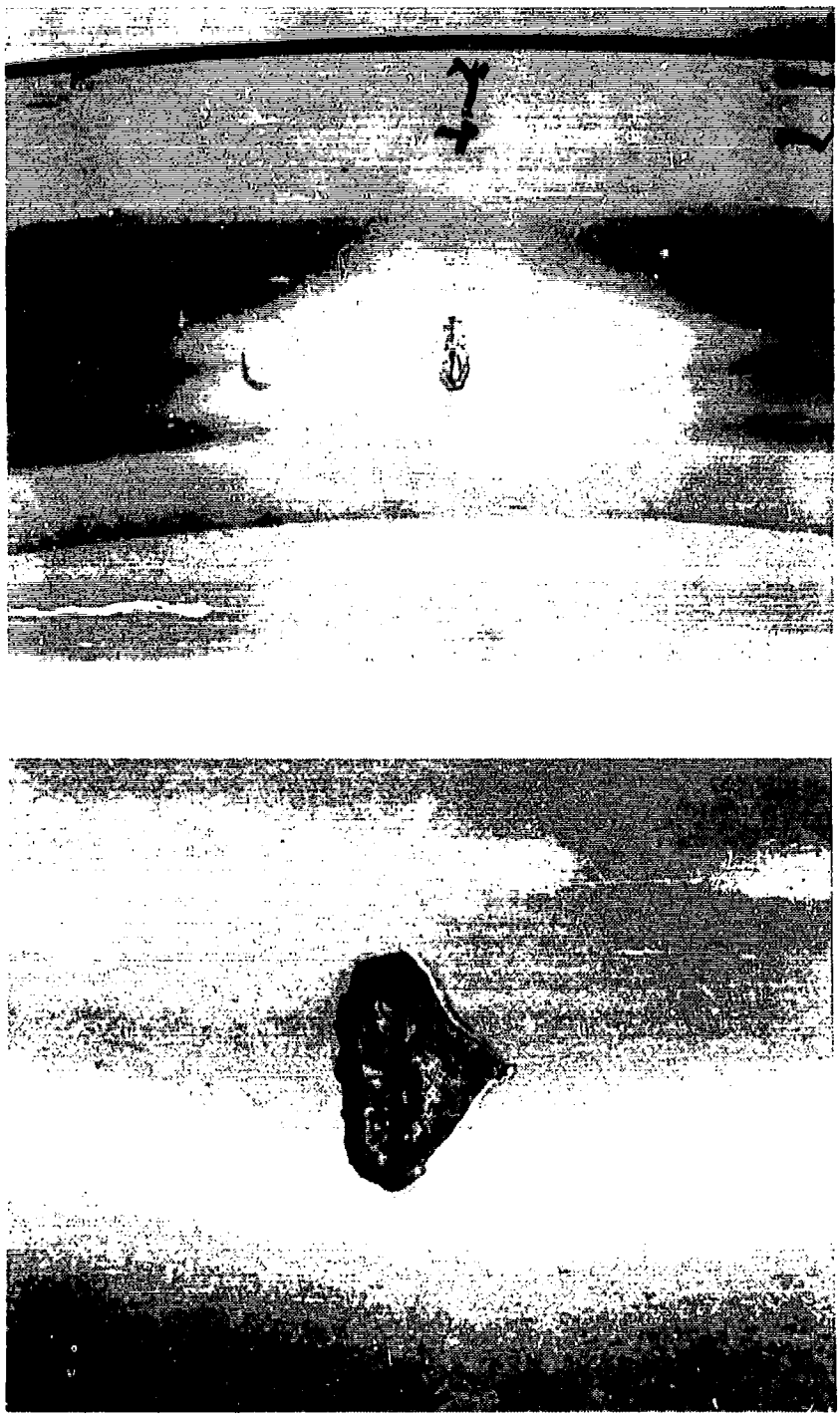

Figure 59. Spall on Inner Race of Bearing No. 12. *Note absence of corrosion even adjacent to spall.*

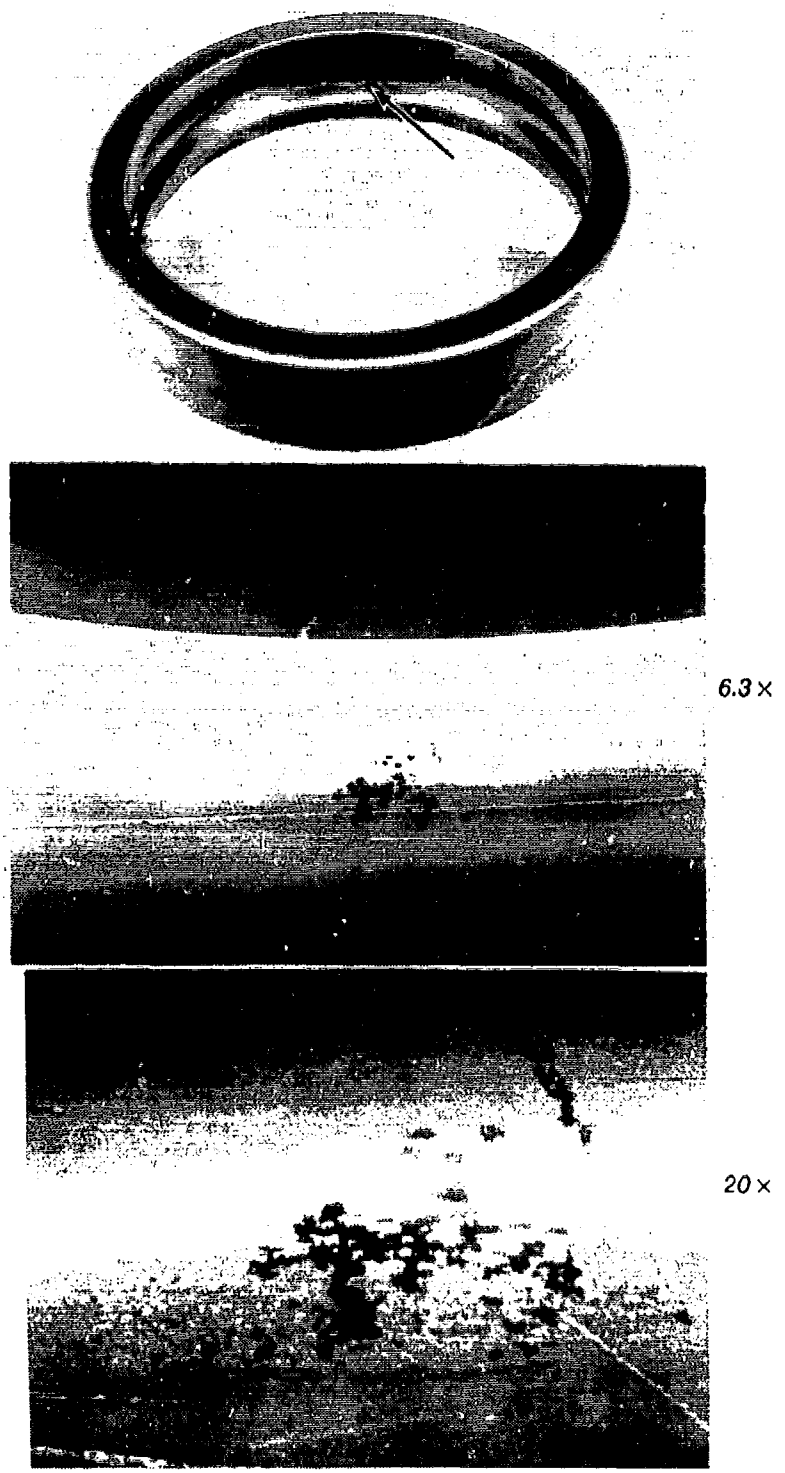

Figure 60. Localized Area of Corrosion Due to Lack of Coating.

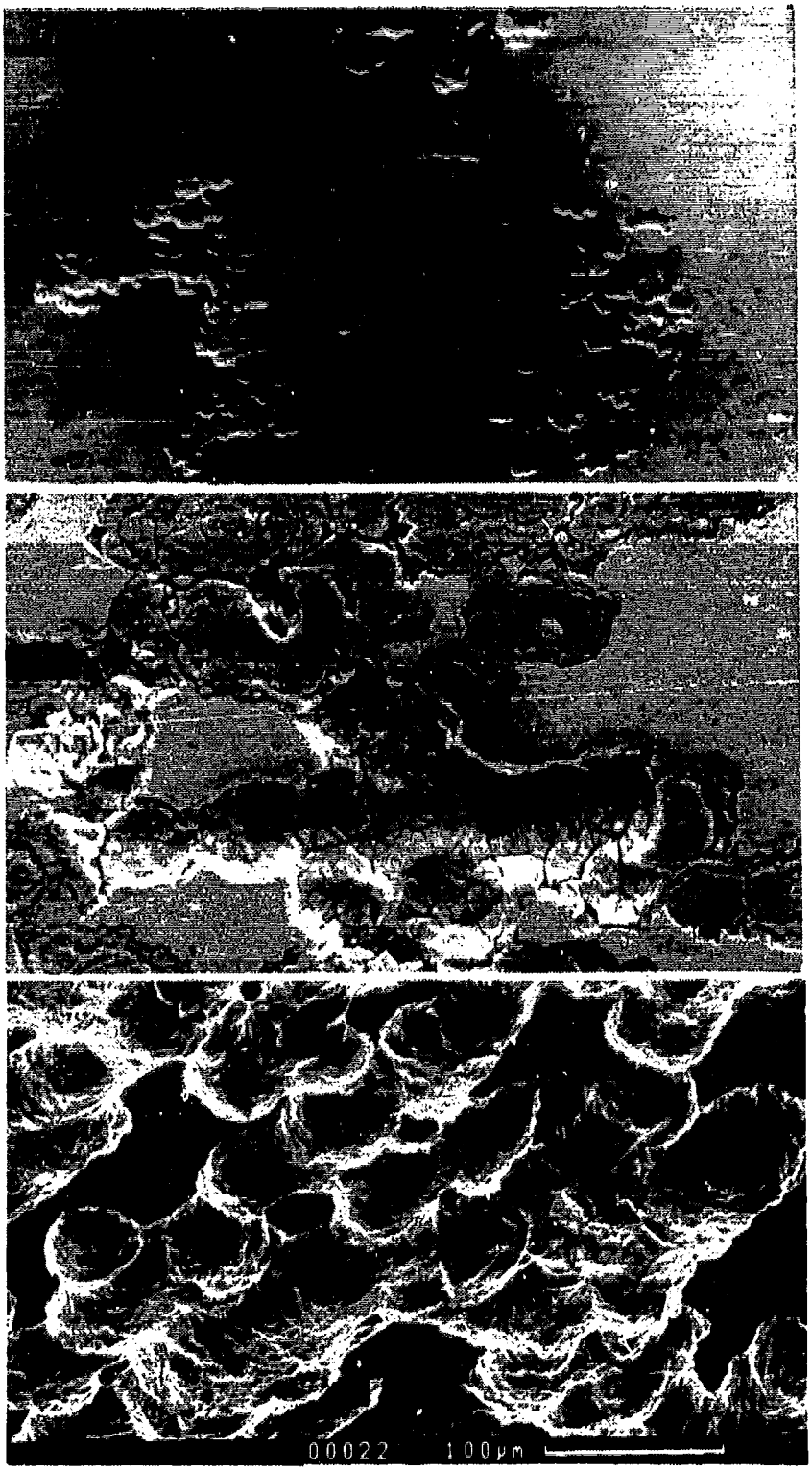

33 ×

Typical "mudcracking" corrosion pattern

33 ×

Corrosion pitting

33 ×

Figure 61. Bearing No. 12 Corroded Areas.

Outer Ring (M50NiL) - Running track burnished, slight evidence of ring rotation on outer diameter. Cage rub indications on shoulder. TDC coating intact on all areas except one patch (see Figures 60 and 61). SEM examination of this area indicated a coating problem (peeling) presumed due to a processing anomaly.

Balls (M50) - Evidence of corrosion and pitting. Balls were quite heavily varnished compared to the Ta^+ implanted balls in Bearing Nos. 6 and 9 (Figures 62 and 63).

Control Test Bearing – Heavily corroded, see Figure 64.

Based on these results, the remaining bearing tests were performed with uncoated M50 balls. Selected color photos corresponding to Figures 50 – 64 are presented as an addendum to this report.

The failure of the Ta^+ implantation to protect against corrosion was not unexpected. In prior testing (Reference 1) it was noted that under pure rolling conditions (RCF rig), the Ta^+ implanted test bar performed well and did not show any indication of coating breakdown after a similar corrosion test. However, in the tests performed in a contaminated environment in the ball-rod tester, the Ta^+ implanted test bars failed to protect against damage by the 20 μm Al_2O_3 particles in the oil.

In the test bearings, the Ta^+ implanted balls were not able to endure the minor scuffing and skidding action inherent in any full-scale test (and even more so in real-life engine operation). In fact, most of the corrosion pitting was observed in areas of the ball that also showed evidence of scuffing or skidding. It must be remembered that the test bearings were prerun (as were all test bearings) in contaminated oil (2.5 ppm of 20-μm Al_2O_3) for 15 minutes. Consequently, the bearing results are in good agreement with the ball-rod test data.

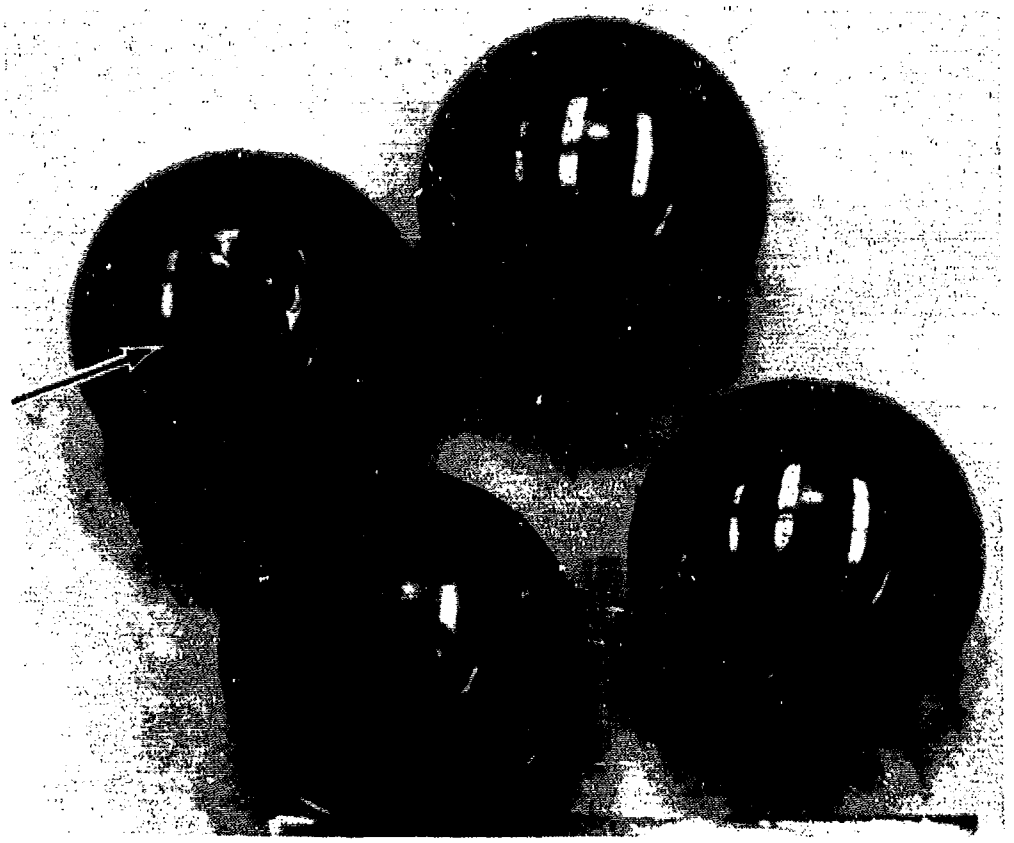

Figure 62. Balls from Bearing No. 12 After Corrosion Test.

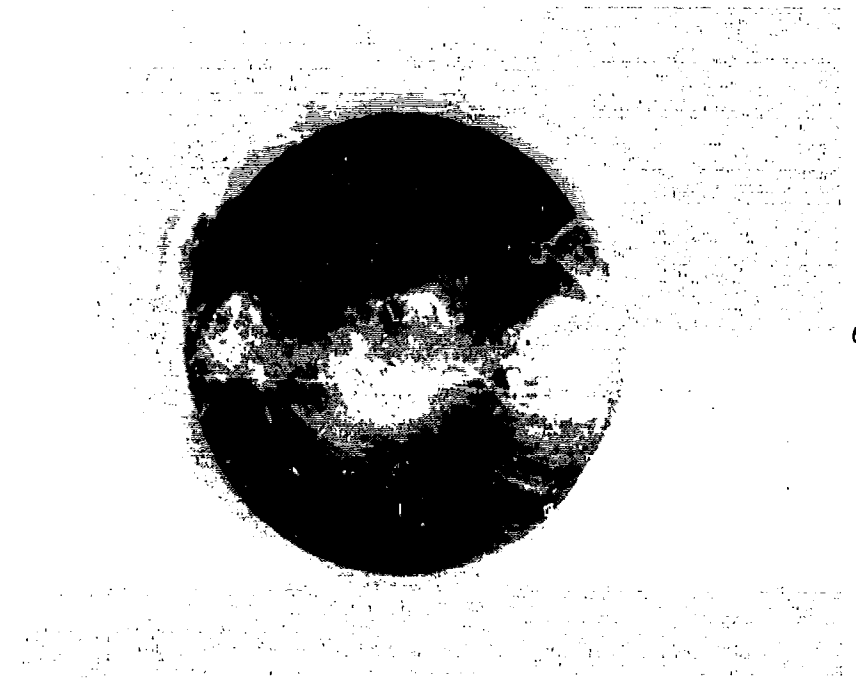

6.3×

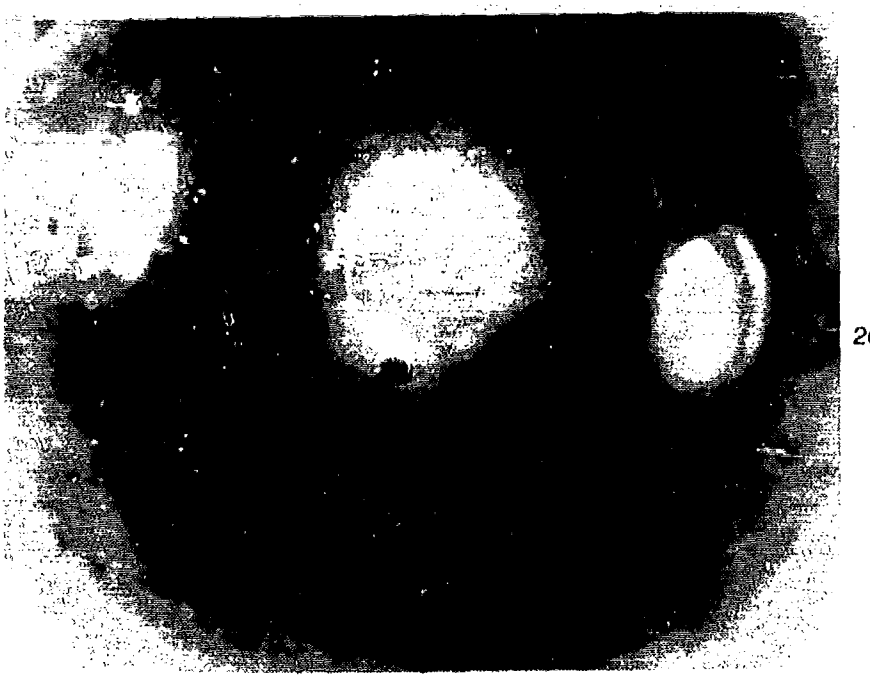

20×

Figure 63. Typical Corrosion on M50 Balls.

Figure 64. New, Uncoated Control Bearing After Corrosion Test.

5.2 M50NiL TDC Coated Bearing Tests and Results

Testing of the remaining M50NiL TDC coated bearings with bare M50 balls was resumed after the bearing corrosion test. The results of these tests are tabulated in Table 9 and the Weibull distribution is plotted in Figure 65. A total of 11 tests were performed. As can be seen from Table 9, only three inner-ring failures were experienced compared to the seven inner-ring failures noted in the M50 baseline tests (Table 7). Interestingly, two ball failures were encountered, indicative of the possibility that with M50NiL rings the rolling elements (ball or rollers) become a likely failure component. The three failures calculate a B_{10} life of 480 hours which is 5.5 times that for the M50 baseline bearings. The 480-hour B_{10} life is 20 times the calculated AFBMA life for this bearing. A comparison of these data is shown in Figure 66. Based on these results, coupled with the corrosion test results, it can be seen that the program goals (3 to 5 × life improvement with improved corrosion resistance) were met quite successfully.

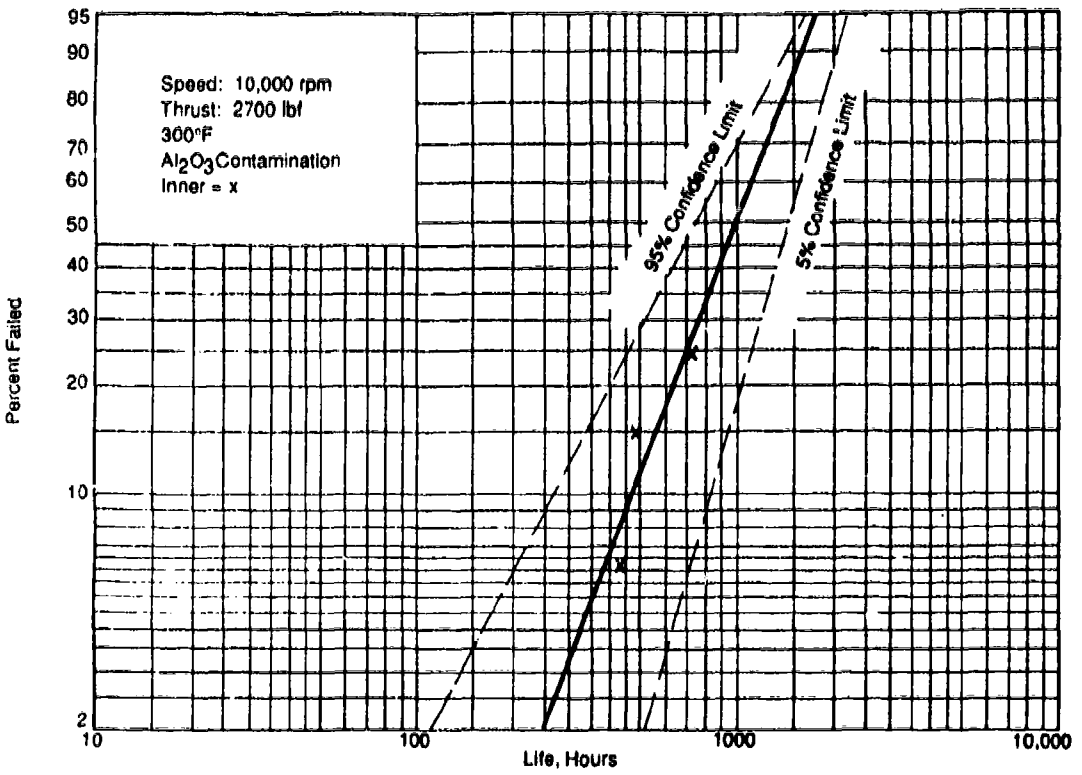

Figure 65. M50NiL TDC Life Test.

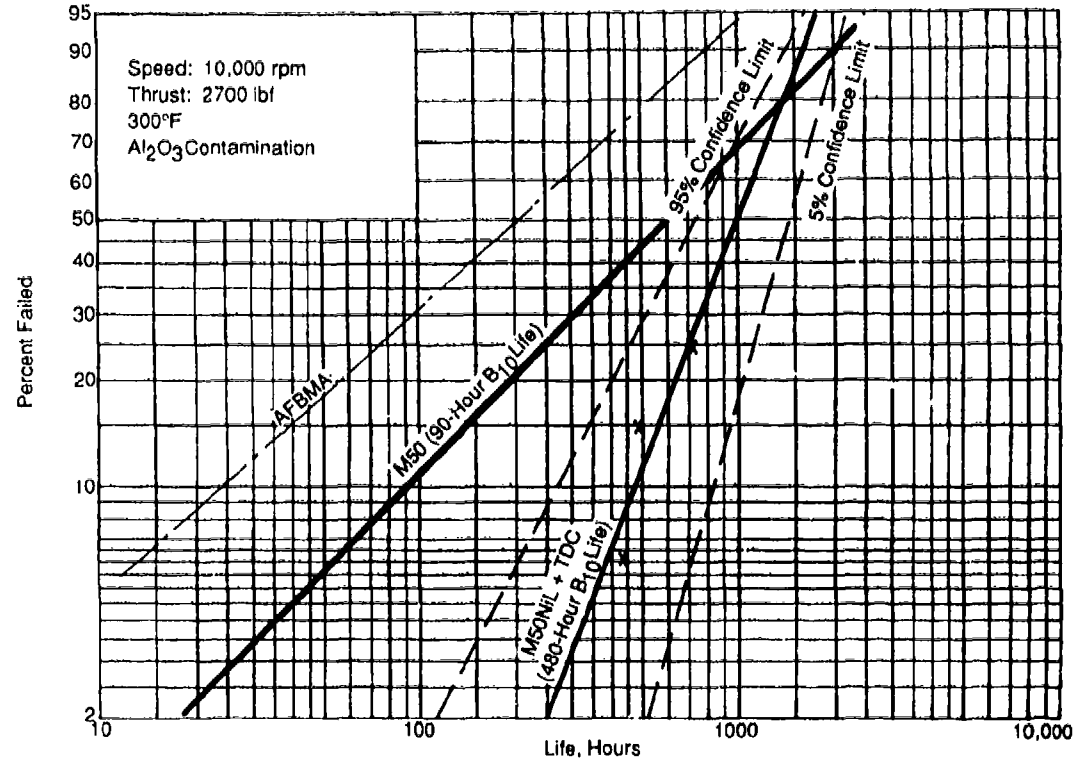

Figure 66. M50NiL TDC Life Test Data Compared with AFBMA Calculated Life.

Table 9. Test Results: M50NiL TDC Coated 208 Size Ball Bearings.

Outer Ring: M50NiL, TDC Coated
Inner Ring: M50NiL, TDC Coated
Balls: M50

Bearing	Life Hours	Life Cycles (10^9)	Comments
10	434	2.34	Inner ring spalled
15	486	2.62	Inner ring spalled
12	722	3.90	Inner ring spalled
24	695	3.75	Retired, ball failure
7	1100	5.94	Retired, ball failure
30	1504	8.12	Retired
14	1535	8.29	Retired
16	1535	8.29	Retired
5	1544	8.34	Retired
13	1587	8.57	Retired
20	1684	9.09	Retired

Perhaps even more important, it was desirable to observe and understand the surface-failure initiation/propagation process in the M50 and M50NiL-TDC coated bearings. As discussed earlier, an accurate photographic record (optical and SEM) was maintained on the base-line bearings. This same protocol was followed on the Phase II test bearings. The tests were stopped periodically; the bearings were disassembled and cleaned, and the rings were photographed to record the progress of surface damage. In the following discussion, the findings are analyzed and a comparison is made between the failure propagation rates of M50 relative to M50NiL.

The bearing was considered failed when a spall was generated which tripped a very sensitive vibration sensor. In each case, the spall in the ring was preceded by a peeled region. These peeled regions started at surface defects in the load path and grew in length as the test proceeded. The growth direction was generally opposite to the rolling direction. The progression of peeling is shown in ring 54 (M50) in Figure 67, which shows a series of photomicrographs of the same region at 100×. The peeled region grew in the direction opposite to rolling and finally developed a spall which then propagated in the direction of rolling. A similar sequence is shown for Ring 15 (M50NiL, TDC) in Figure 68. The initial defects are much smaller than in Figure 67, but the final size of the peel at spalling is about the same.

More common, however, in the M50NiL-TDC rings was that a surface defect did not propagate to a spall even after extended test times. Typical examples of this are shown in Figures 69 and 70.

The initial sizes of the significant flaws, that is, the ones which eventually developed into spalls, are liste in Table 10. The nominal size of the contaminating alumina particle was 0.0008 inches, and it is interesting to note that the sizes of the initial surface flaws were of the same order. The average initial flaw size was 0.004 inch, but the flaws ranged from 0.0004 to 0.008 inches in length. On the other hand, the initial flaws in the M50NiL-TDC rings were all small, averaging 0.0015 inch, but since only three failures were recorded the differences may not be significant.

The final length of the peel which led to a spall was 0.017 inch in M50 and 0.011 inch in M50NiL-TDC. Here also, the scatter in the data is such as to suggest that the final peel length was the same for both materials. Comparison of the sizes of the initial defects with the lifetimes suggests that short life occurs in bearings with the largest initial flaws, and this is consistent with the concept that the peel propagates to a given length at which a spall develops. This critical peel size appears to be about 0.016 inch for these bearings under these test conditions.

The peeling rates were established for each of the failed bearings by measuring the length of the peeled area at various stages in each test run. The overall peeling rate was computed from the final length of the peel, prior to the development of the spall, and the number of cycles that had been run. The overall peeling rates are listed in Table 11. There was considerable scatter in the data for both M50 and M50NiL-TDC, but the average values for each material are useful for comparison. The M50 peeled at an overall rate of about 1.1×10^{-11} in/cycle and the M50NiL TDC at a rate of 1.8×10^{-12} in/cycle. Thus, M50 peels about 6 times as fast as M50NiL-TDC. Interestingly, the B_{10} life of M50 was about one-sixth that of M50NiL-TDC. Since the entire life of these bearings was spent in peeling, it is evident that the two independent measurements of the behavior of these two materials are consistent.

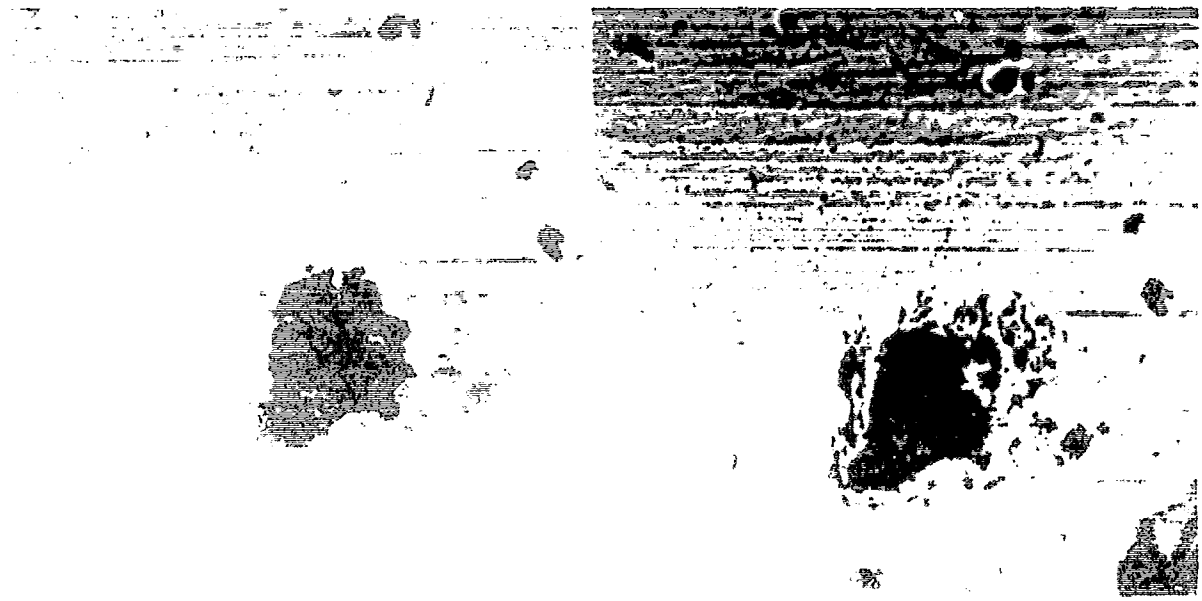

(a) After 5 minutes contamination time

(b) After 27 hours on test

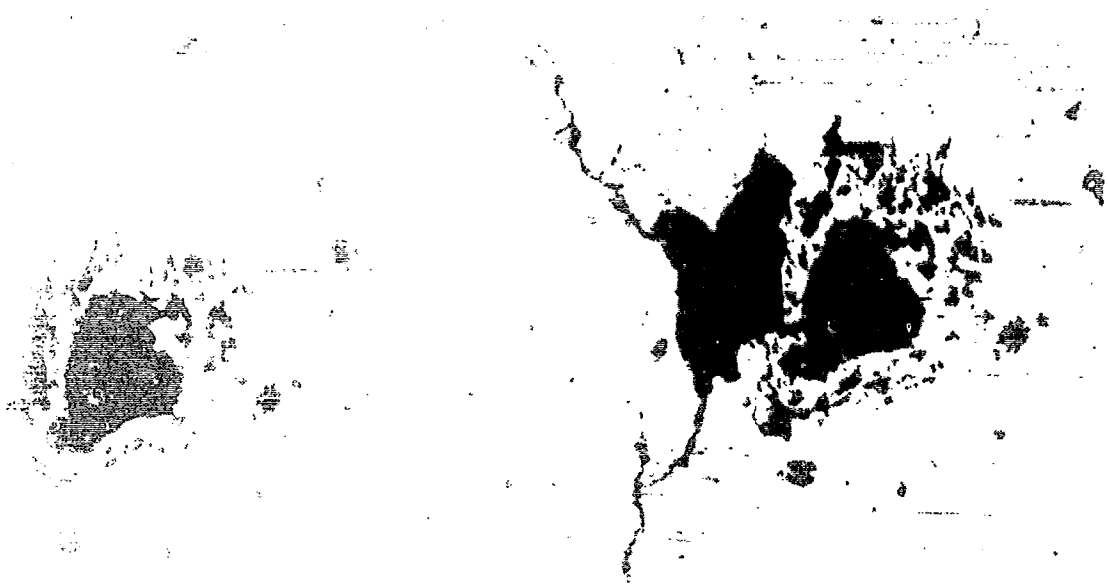

(a) After 5 minutes contamination time

(b) After 27 hours on test

Figure 67. Surface Damage in M50 Ring 5-1 (100 ×)

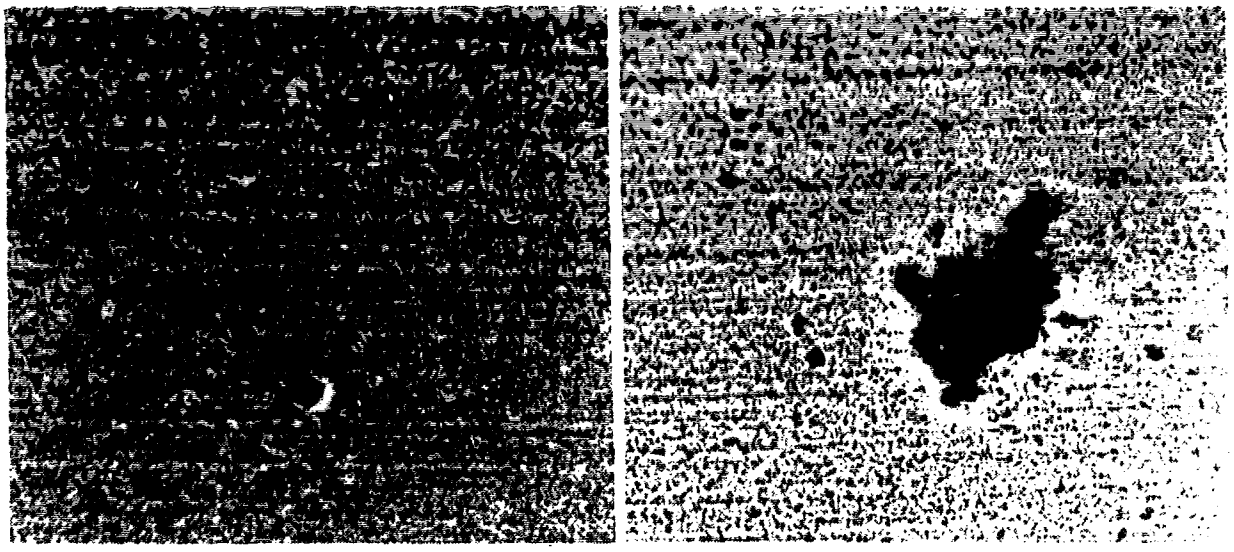

(a) After 15-minute contamination run

(b) After 24 hours on test

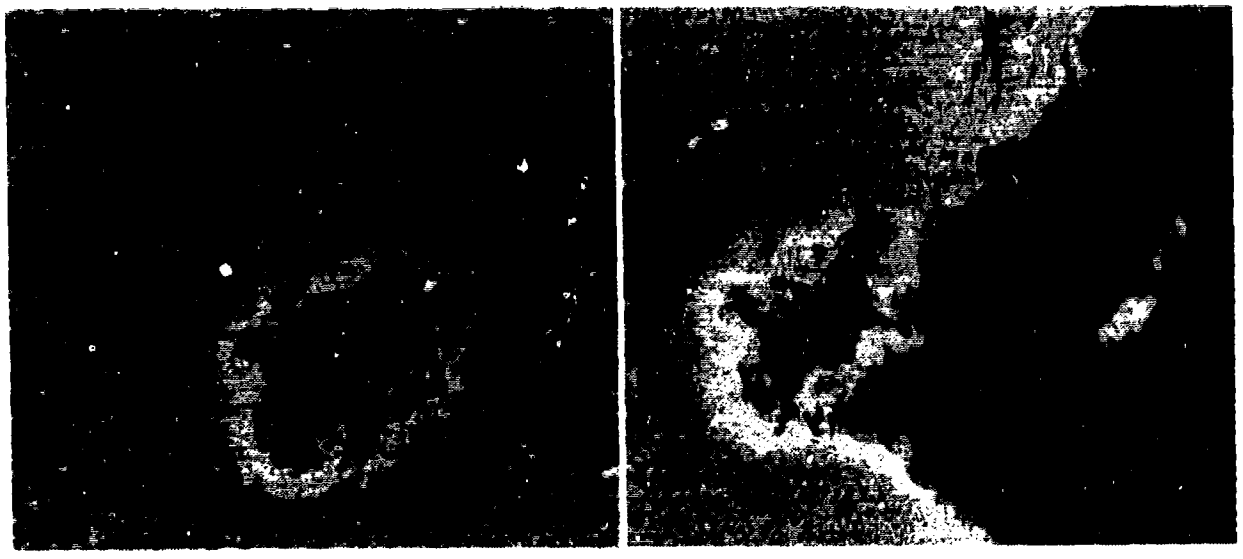

(c) After 392 hours on test

(d) After 485 hours on test

Figure 68. Surface Damage in M50 TDC Ring 15 (100×).

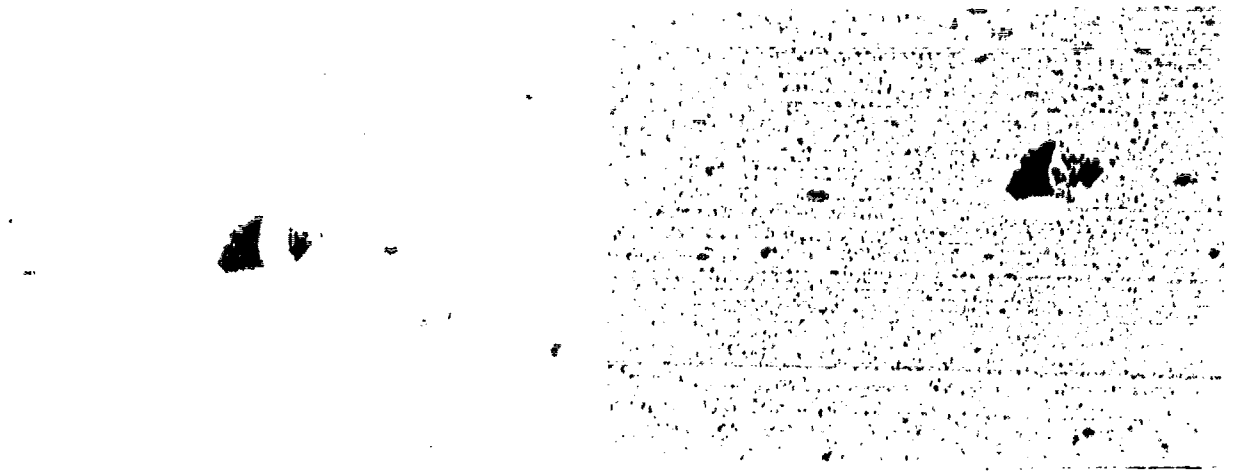

(a) After 15-minute contamination run

(b) After 24 hours on test

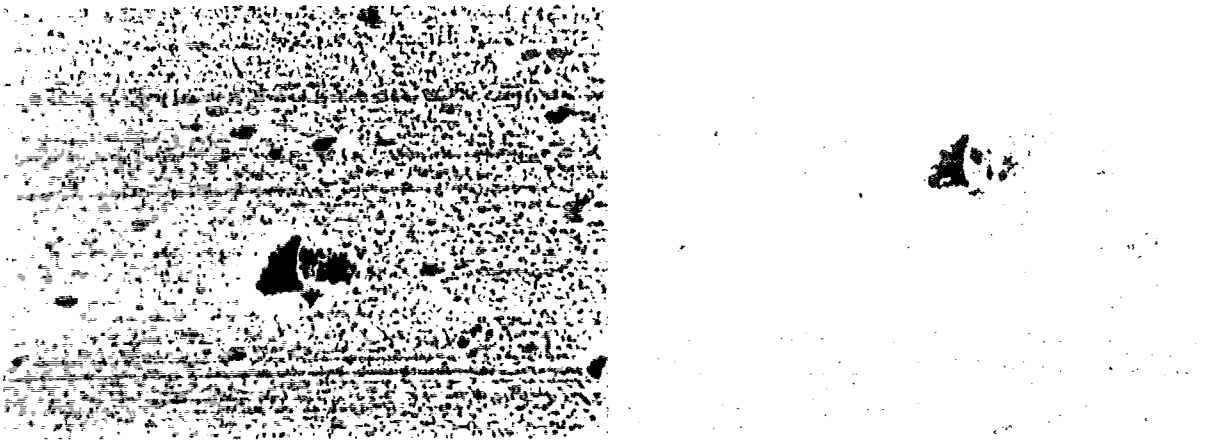

(c) After 177 hours on test

(d) After 608 hours on test

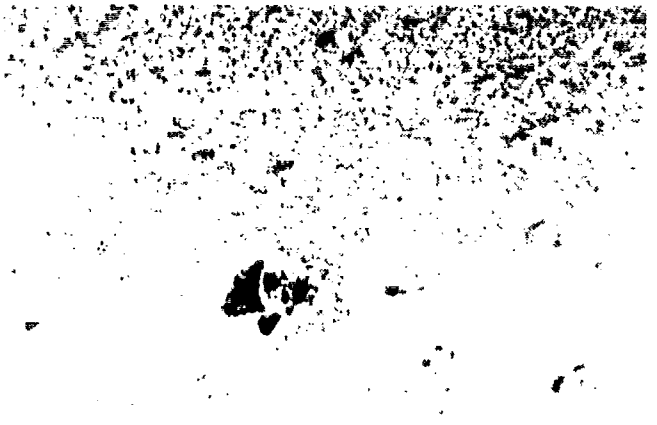

(d) After 1535 hours on test

Figure 69. Surface Damage in M50NiL TDC Ring 16 (100×).

(a) After 605 hours on test

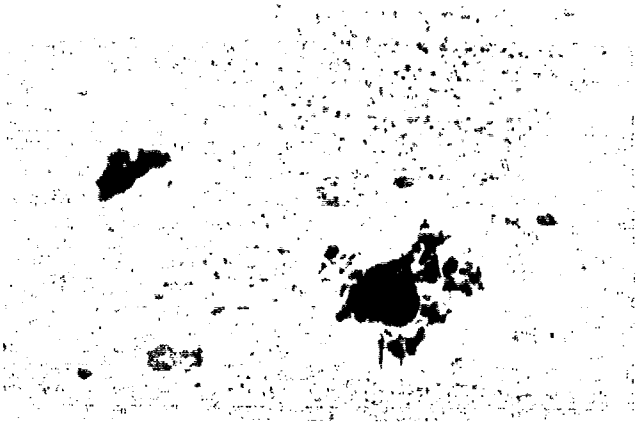

(d) After 839 hours on test

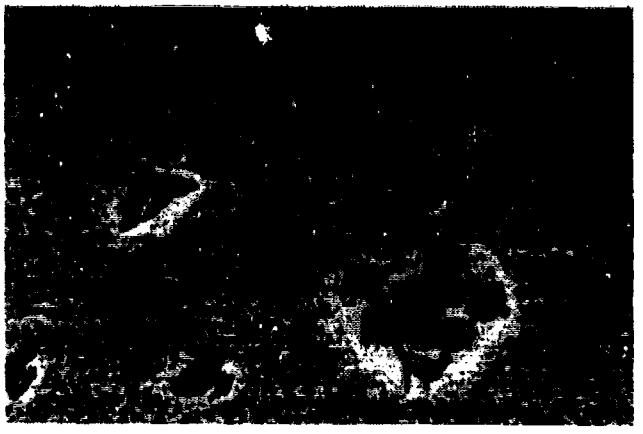

(d) After 1016 hours on test

Figure 70. Surface Damage in M50NiL TDC Ring 5 (100 ×).

Table 10. Length of Peeled Regions in Front of Spalls.

Ring	Material	Life, 10^9 Cycles	Initial Defect Length		Final Length	
			μin	mm	μin	mm
20	M50	0.37	7.087	0.18	23.228	0.59
54	M50	0.79	7.874	0.20	23.228	0.59
29	M50	1.68	2.362	0.06	5.512	0.14
92	M50	1.71	5.906	0.15	41.732	1.06
102	M50	1.80	4.331	0.11	8.267	0.21
17	M50	4.03	1.181	0.03	4.724	0.12
10	M50	6.09	0.394	0.01	14.567	0.37
Average	M50	--	4.331	0.11	17.323	0.44
10	M50NiL	2.34	0.787	0.02	16.525	0.42
15	M50NiL	2.62	0.196	0.05	11.811	0.30
12	M50NiL	3.90	0.157	0.04	4.725	0.12
Average	M50NiL	--	0.157	0.04	11.024	0.28

Table 11. Overall Propagation Rates of Spalling.

Ring	Material	Initial Defect Length		Overall da/dn	
		μin	mm	in./Cycle	mm/Cycle
20	M50	8.661	0.22	3.74×10^{-11}	9.5×10^{-10}
54	M50	7.874	0.20	1.26×10^{-11}	3.2×10^{-10}
29	M50	2.362	0.06	1.90×10^{-12}	0.5×10^{-10}
92	M50	5.905	0.15	2.09×10^{-11}	5.3×10^{-10}
102	M50	4.331	0.11	8.0×10^{-14}	0.022×10^{-10}
17	M50	1.181	0.03	8.6×10^{-13}	0.22×10^{-10}
10	M50	0.394	0.01	2.32×10^{-12}	0.59×10^{-10}
Average	M50	4.331	0.11	1.10×10^{-11}	2.8×10^{-10}
10	M50NiL	0.787	0.02	7.10×10^{-13}	0.18×15^{-10}
15	M50NiL	1.969	0.05	3.78×10^{-12}	0.96×10^{-10}
12	M50NiL	1.575	0.04	8.27×10^{-13}	0.21×10^{-10}
Average	M50NiL	1.575	0.04	1.77×10^{-12}	0.45×10^{-10}

Peeling rates during the test were, however, not constant. The rate at the beginning of the process was usually an order of magnitude higher than at the end. For example, in Table 12, the peeling rates at various stages in the test for M50 Rings 20 and 54 are listed. At the beginning, the peel rate in Ring 54 was 3.973×10^{-11} in/cycle; at the end the peel rate had fallen to 5.118×10^{-12} in/cycle. Similarly, the peel rates were high at the beginning for the M50NiL-TDC rings but fell to very low values at the end. Ring 16, of M50NiL-TDC, was retired without failure after 1535 hours. Peeling occurred at the initial defects, but the rate dropped to such a low value that even the largest peel did not reach the critical size for spalling. The high initial peeling rates and the subsequent fall-off are characteristic of short cracks (Reference 20), and the reduction in crack-growth rate is probably associated with the lack of complete closure as the small crack propagates during peeling.

Table 12. Peeling Rates During Growth of Peeled Area.

Ring	Material	Life, 10^9 Cycles	Initial Defect Length, µin	Initial Defect Length, mm	Overall da/dn, in./Cycle	Overall da/dn, mm/Cycle
10	M50	0	8.661	0.22	–	–
		0.12	15.748	0.40	5.905×10^{-11}	15.0×10^{-10}
		0.37	22.441	0.57	2.678×10^{-11}	6.8×10^{-10}
Overall					3.74×10^{-11}	9.5×10^{-10}
54	M50	0	7.874	0.20	–	–
		0.15	13.780	0.35	3.973×10^{-11}	10.0×10^{-10}
		0.41	15.748	0.40	7.480×10^{-12}	1.9×10^{-10}
		0.79	17.717	0.45	5.118×10^{-12}	1.3×10^{-10}
Overall					1.26×10^{-11}	3.2×10^{-10}
15	M50NiL	0	1.969	0.05	–	–
		0.13	8.661	0.22	5.315×10^{-11}	12.5×10^{-10}
		2.1	11.024	0.28	1.181×10^{-12}	0.30×10^{-10}
		2.6	11.811	0.30	1.575×10^{-13}	0.04×10^{-10}
Overall					3.779×10^{-12}	0.96×10^{-12}
16	M50NiL	0	2.756	0.07	–	–
		0.13	3.937	0.10	9.055×10^{-12}	2.3×10^{-10}
		0.96	5.315	0.135	1.575×10^{-13}	0.04×10^{-10}
		3.3	5.709	0.145	1.575×10^{-14}	0.04×10^{-11}
		8.3	5.906	0.150	3.937×10^{-15}	0.01×10^{-11}
Overall					3.937×10^{-13}	0.11×10^{-10}

Peeling and the subsequent spalling crack may be seen more clearly from the circumferential section shown in Figures 71 and 72. The depth of the peel is about 0.004 inch. This can be seen in Figure 71 from a section of the peel which is almost completely undermined but still in place. The peeling apparently proceeded by means of a sequence of small crack parallel to the surface at about this depth. A spalling crack formed at the end of the peel; typically, these cracks started at an angle of about 20° to the surface plane. The crack direction changed as it propagated to form the classic spalled flare. In Figure 72, a longitudinal section through the peeled region in Ring 35 shows the typical shallow scalloping mechanism of this mode of failure. The propagation of the peeling by the development of shallow subsurface cracks parallel to the surface is also evident (Figure 73).

This type of failure has been observed by others (Reference 22) and has been called pitting in some instances. A detailed analysis of this mode of failure is being made, but some of the principal features are evident. When the surface is damaged, the EHD layer is essentially removed at the initial damage site, producing a microregion with a high coefficient of friction. As the balls roll over this area, the depth of the maximum shear stress is closer to the

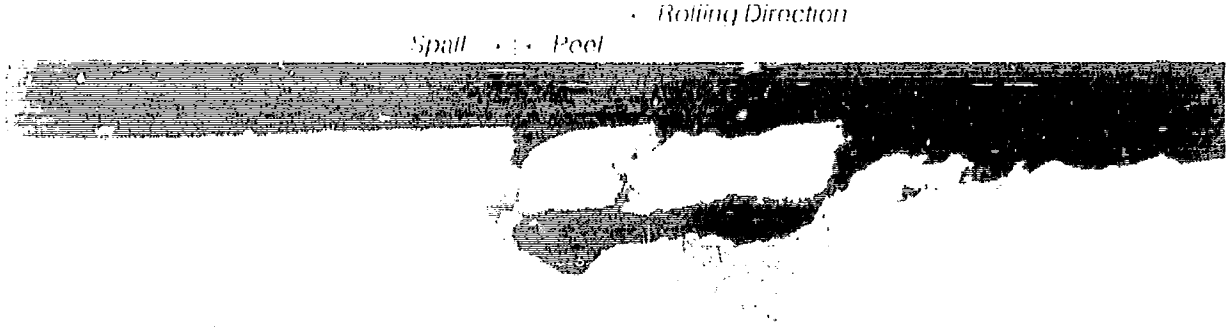

Figure 71. Longitudinal Section Through Peeled Region in M50 Ring 20 (400 ×).

Figure 72. Longitudinal Section Through Peeled Region in M50 Ring 35 (50 ·).

Figure 73. Longitudinal Section Through Peel and Initial Spalling in M50 Ring 35 (400 ·).

surface in the damaged region than in the surrounding areas, and the sense of the maximum shear stress at the tip of the defect is in the direction opposite the rolling direction. Microyielding is accentuated because of the breach in the EHD layer, and shakedown stresses are developed (Reference 23). Shakedown stresses appear when a material is loaded beyond the elastic limit and then unloaded. Residual stresses are developed, and these are of opposite sign to those induced by the load. Thus, in the damaged region in the test bearings, the cyclic shear stresses at the tip of the defects result in enhanced shakedown stresses that produce maximum residual stress at about 0.004 inch from the surface. The maximum compressive load is in the z direction, normal to the surface. The application of cyclic loadings thus results in a tensile stress, in the z direction, that has a maximum value at the depth of maximum shear stress.

Residual tensile stresses at this depth have been measured by Voskamp (Reference 24) in radial bearings that have been run for extended periods. It is postulated that these residual stresses in the near-subsurface region result in peeling which propagates as a mixed Type I and Type II fracture in the early stages. Small cracks are generated at the tips of the surface defects, and an example of this is shown in Figure 73. The general direction of the peeling is opposite to the rolling direction, and the peel propagates by succession of shallow microspalls that peel away a surface layer about 0.004 inch deep.

When the peel becomes large enough to destroy the EHD film in a macroscopic area, a spalling crack forms at the forward edge. This is also a mixed-mode fracture (Reference 25), but it is now dominated by stresses in deeper regions below the surface. In M50 there is a residual tensile stress, arising from the heat treatment, of the order of 10 ksi. The combination of this residual tensile stress, the Hertzian shear stress (120 ksi), and the stress concentration arising from the sharp crack at the head of the peel, as shown in Figure 71, results in a mixed-mode crack that starts at an angle of about 20° to the surface and progresses to form a spall on cyclic loading.

If it is assumed that the peel constitutes a crack culminating at the head, then the critical stress for the initiation of a spall can be calculated. The initial crack propagation is assumed to be in Mode I, and K_{Ic} for M50 may be taken as 20 ksi·$m^{1/2}$. Assuming the critical peel length to be 0.016 inch and using the relationship:

$$\sigma_c = K_{Ic}/(\pi a_c)^{1/2} \qquad \text{(Equation 2)}$$

where σ_c is the critical tensile stress and a_c is the critical crack length, the value, σ_c = 88 ksi is obtained. This value is of the order of the shakedown stress expected for M50 and is remarkably close to the residual stress values in the z direction measured by Voskamp (Reference 24). This critical stress for spall formation is only approximate but is consistent with the observations in the current bearing tests (Table 13).

Table 13. Effective Critical Stress for K Mode Failure.

Ring	Hours	Life, 10^9 Cycles	Flaw Size		Stress	
			in.	mm	ksi	MPa
20	68	0.37	0.020	0.51	81	
54	147	0.79	0.015	0.38	94	649
29	310	1.68	—	—	—	—
35*	346	1.87	0.045	1.1	54	373
91*	615	3.32	—	—	—	—
60*	730	3.94	0.035	0.89	60	414
10	1127	6.09	0.01	0.25		

* Rings 35, 91, and 60 were not tested with the standard procedure. The critical flaw size, a_c, could not be determined in Rings 29 and 91.

The peeling rates in M50NiL TDC are about one-sixth of those in M50. It is suggested that this difference is caused by the presence of residual compressive stresses in the M50NiL rings in regions below the surface (Reference 26). Typically, the residual stress at the peeling depth is -50 ksi (that is, in compression) in contrast to the + 10 ksi (in tension) in the M50. Compressive stresses retard peeling by opposing the crack opening and also retard the subsequent spalling crack by the same mechanism. The role of the TDC coating is not a factor in these tests since the original defects, introduced with 20-μm (0.0008-inch) alumina particles were deeper than the coating thickness. In operations where surface damage is minimized, the TDC could have a beneficial effect in reducing the onset of peeling by suppressing corrosion pits and damage by soft particles.

In summary, the bearing tests have demonstrated that M50NiL rings with TDC coatings run about 6 times as long as the standard M50 rings. Failures were induced at the surfaces of these rings, and the primary mechanism of failure was a peeling action at the surface; when the peels reached a critical size, spalling occurred.

The M50NiL TDC rings were more resistant to peeling, probably because of the residual compressive stresses in regions just below the race surfaces, and this translated into extended lifetimes. In service, the combination of peeling resistance and corrosion resistance should provide bearings with very long lifetimes.

The working model that emerges from these observations is one where initial damage grows by a mechanism of peeling until a critical size for spalling is reached. The peeling proceeds rapidly, so that even a microscopic flaw will grow to the critical size within a relatively short time. Emphasis must thus be put on either the total avoidance of scratches, grinding grooves, dents, and contaminant particles or developing materials that will resist the growth of these initial flaws.

The development of this type of test (that is, the precontamination cycle) is considered to be significant in that it provides valid evaluation of the resistance of a material to surface damage by micropeeling and also provides an important technique for the development of bearings with enhanced life.

5.3 M50NiL TDC Coated Bearing Engine Test

One of the contract requirements was to manufacture a current engine mainshaft bearing using the materials and processes selected. The bearing was then to be tested to demonstrate the scale-up capabilities of the material/process combination.

The bearing selected was a 133-mm bore mainshaft ball bearing common to the GEAE F101, F110, CFM56 family of engines. Two of these bearings were manufactured. The inner and outer rings were M50NiL, TDC coated; the balls were M50, and the cage was silver-plated 4340. To evaluate the bearing, it was run as a "slave bearing" on a two-bearing shaft component test. Initially it had only been the intention to run a continuous steady-state (constant load and speed) test for 150 hours. However, because the M50NiL bearing was "piggy backed" onto a special test cycle, the bearing actually saw a much more intensive duty cycle than had been planned. The actual test schedule is shown in Table 14. After 229.7 hours of testing, the bearing was disassembled and visually examined. As seen in Figures 74 and 75 no evidence of any distress was noted. Particularly encouraging was the fact that, similar to the 208 size bearings, no indication of coating damage was observed in the raceway, despite the fact that the bearing had experienced many shutdown and start-up cycles during the testing.

Table 14. M50NiL 3B Bearing Test Schedule.

Cycle	Load, lbf	Speed, rpm	Outer-Race Temperature, °F (Max. Temperature Run)	Time, Hours
1	10,000	14,709	380	6.7
2	10,000	14,709	317	6.2
3	10,000	14,709	323	4.6
4	5,000	14,709	257	0.5
5	5,000	14,700	340	3.9
6	10,000	14319	302	1.3
7	10,000	14,710	341	6.9
8	10,000	14,720	354	9.1
9	10,000	14,717	360	4.8
10	7,000	14,705	336	1.2
11	7,000	14,711	338	1.0
12	7,000	14,709	370	2.5
13	7,000	14,706	393	1.9
14	7,000	14,710	400	16.6
15	9,000	14,714	346	0.6
16	9,000	14699	413	2.6
17	11,000	14,700	410	2.1
18	13,000	14,702	415	2.1
19	15,000	14,710	404	2.5
20	12,000	14,707	416	2.6
21	10,000	14,700	350*	150.0
(Cycle 21 was endurance run.)			Total:	229.7

* Average over 150 hours.

Figure 74. Outer Raceway of 133-mm Bore Ball Bearing (TDC Coated) After Component Test.

Figure 75. Loaded Inner Ring (TDC Coated) of 133-mm Bore Bearing After Component Test.

THIS

PAGE

IS

MISSING

IN

ORIGINAL

DOCUMENT

Appendix A

Fracture Toughness and Charpy Impact Properties of Selected High-Temperature Bearing and Gear Steels

A.1 Summary

Fracture toughness (K_{Ic}) measurements were obtained for six advanced, high-performance bearing and gear steels. Data were generated at elevated (400°F), ambient, and cryogenic (-65°F) temperatures. In addition, the effect of long-term ageing at (450°F) on room temperature toughness was examined. A series of conventional impact tests was also completed in order to investigate the potential correlation between Charpy and compact tension toughness data.

All the materials were tested in the heat treated condition most appropriate to the intended use (bearing or gear) and in accordance with the strict requirements of ASTM E399-83, E813-81, and A-370 (E23).

The toughness results were used to construct temperature transition curves for each steel, and the effects of ageing as measured by both E399-83 K_{Ic} and E23 Charpy techniques were compared. A preliminary correlation between the K_{Ic} and Charpy (C_v) results was attempted using the room temperature data; as a result, a tentative numerical relationship was developed.

A.2 Introduction and Background

As an amendment to Air Force contract F33615-84-C-2430, this appendix describes a program of work designed to evaluate the fracture toughness of several high-performance bearing and gear steels. A number of these advanced, high-temperature steels have recently been proposed and introduced for use in elevated-temperature gear and bearing applications. Clearly, the integrity and performance of such steels must be precisely determined and understood in order to ensure that the correct design and application are achieved. Therefore, as part of the continuing effort to assess the suitability of materials, this program was initiated to determine the critical stress intensity factor (K_{Ic}) of six such steels at three different temperatures. In addition, conventional impact testing was included in the test schedule in an attempt to provide a direct comparison with the K_{Ic} results and perhaps generate a correlation, if possible, between the two test methods.

The six steels considered for evaluation in the program are listed below:

1. AISI 9310 (Baseline)
2. Pyrowear 53
3. CBS 600
4. CBS 1000
5. Vasco X-2M
6. M50NiL

A seventh material, Amax B, was originally included in the list of candidates but was not tested due to availability problems.

The materials outlined above are all carburizing steels containing varying degrees of alloying element additions. Generally, the more highly alloyed steels offer a much greater resistance to softening at elevated temperatures (see Figure A-1) coupled with a much greater probability of survival in severe environments; however, ductility and toughness are somewhat reduced compared to AISI 9310.

Currently, the gear industry standard material is still AISI 9310. Although this material has performed adequately at temperatures up to 300°F in the past, it has begun to be replaced systematically by the more highly alloyed steels for use in hostile conditions up to 450°F.

The requirement to measure the fracture toughness of these high-temperature steels has been driven by this selective replacement of AISI 9310 in certain key applications. During conventional operation, the fracture toughness of AISI 9310 and generic counterparts has not resulted in any design limitations. However, with the introduction of lower ductility materials capable of sustained operation in faster and more heavily loaded transmission systems, fracture toughness requires greater design consideration. Therefore, in order to establish future design guidelines for fracture toughness requirements, it has become necessary to obtain valid fracture toughness values for the materials considered over the pr ed operating temperature range (-65° to 400°F) and also to quantify the likely effect of long-term operation (ag ng) at high temperature (450°F) on the value of K_{Ic}.

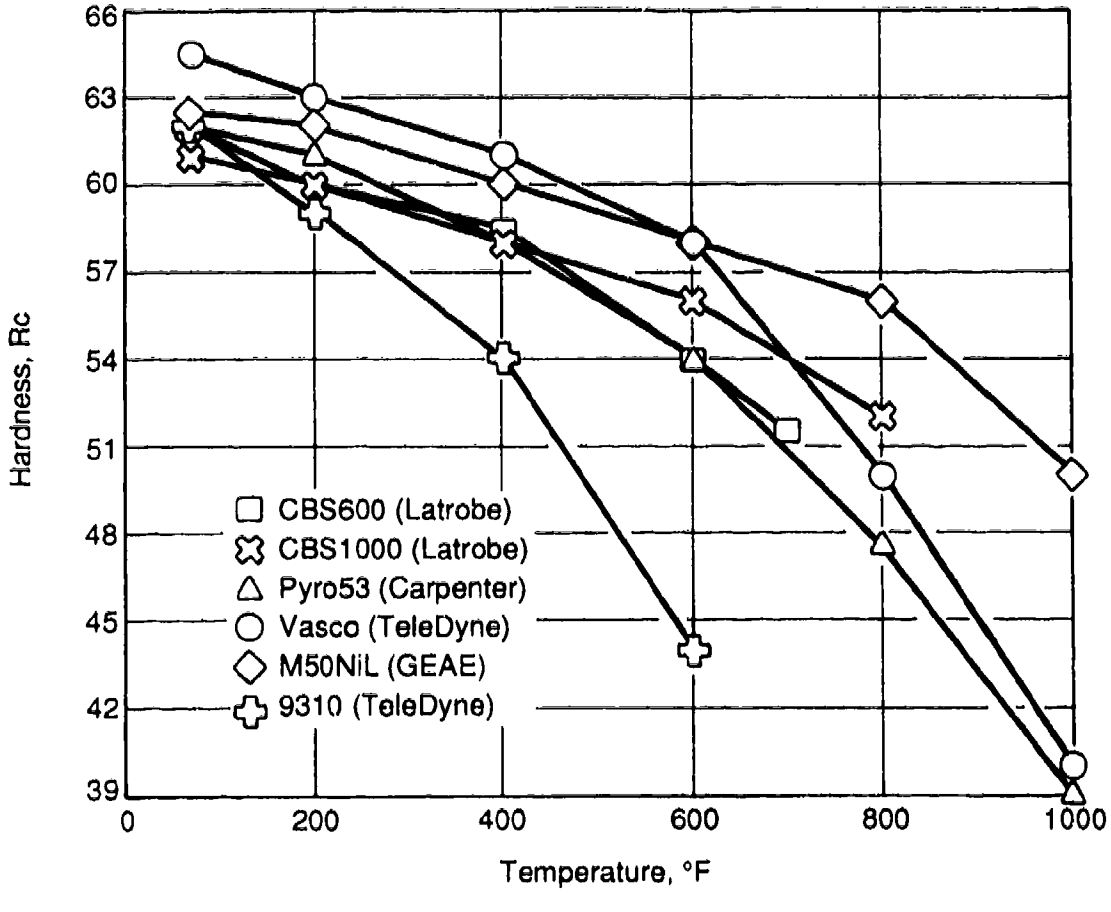

Figure A-1. Hot Hardness.

A.3 Procedure

A.3.1 Testing and Materials

The six materials evaluated in this test program are detailed in Table A-1 along with the respective chemistries. Each material was purchased in bar form and with the exception of AISI 9310 produced by double vacuum melting (VIM-VAR) technique. The AISI 9310 material was obtained in the single vacuum arc melted condition (VAR).

Table A-1. Material Chemistries.

Material	Producer	C	Mn	Si	Cr	V	W	Mo	Ni	Cu	Process
AISI 9310	Teledyne Vasco	0.11	0.58	0.32	1.18	–	–	0.11	3.21	–	VAR
Pyrowear 53	Carpenter	0.12	0.32	0.83	1.02	0.1	–	3.26	2.01	2.04	VIM VAR
CBS600	Latrobe	0.19	0.51	1.02	1.36	–	–	0.98	0.13	–	VIM VAR
BS1000	Latrobe	0.14	0.52	0.49	1.17	0.40	–	4.18	3.21	–	VIM VAR
Vasco X2M	Teledyne Vasco	0.14	0.37	0.90	5.12	0.44	1.35	1.38	–	–	VIM VAR
M50NiL	Latrobe	0.15	0.29	0.24	4.06	1.20	–	4.31	3.52	–	VIM VAR

The program was devised to measure the fracture toughness of the six designated steels at the following temperatures:

a. -65°F
b. Room Temperature
c. 400°F (250°F for AISI 9310)

The effect of ageing at 450°F for 1000 hours was also assessed relative to room temperature fracture toughness and Charpy impact toughness. All the materials were aged except AISI 9310; that material was not considered for ageing at 450°F because of the lower tempering temperature requirement (300°F). For this reason, elevated-temperature testing in Category C above was also limited to 250°.

Fracture toughness for all the materials was measured using the requirements of ASTM E399-83 and ASTM E813-81; consequently, all compact tension testing was carried out strictly in accordance with these two specifications. Impact toughness data were generated using the Charpy V-notch method, and all impact testing conformed to ASTM A-370 (E23). Figure A-2 details the specimen configurations and dimensions.

The compact tension specimens were machined with the crack-plane orientation transverse to the rolling direction of the bar (designated R-C in E399). Charpy impact specimens were similarly machined in the transverse direction so the crack plane orientations of all specimens were similar.

A.3.2 Method of Fracture Toughness Evaluation

The variety of materials included in the test program was such that a wide range of toughness values had to be anticipated in order to achieve satisfactory results. As a result of this consideration, test specimen size and configuration as well as the mode of testing were analyzed prior to specimen machining. Two of the materials under test, Pyrowear 53 and AISI 9310, were more ductile than the others. Calculated specimen sizes for these two materials indicated that excessively thick specimens ($>$ 2.7 inch) would be required to satisfy the validity requirements of E399 over the planned test temperature range. Therefore, it was considered impractical to test K_{Ic} specimens of the size necessary to obtain valid results for Pyrowear 53 and AISI 9310 using the E399 guidelines. In order to obtain fracture toughness data for these materials, two alternatives were considered.

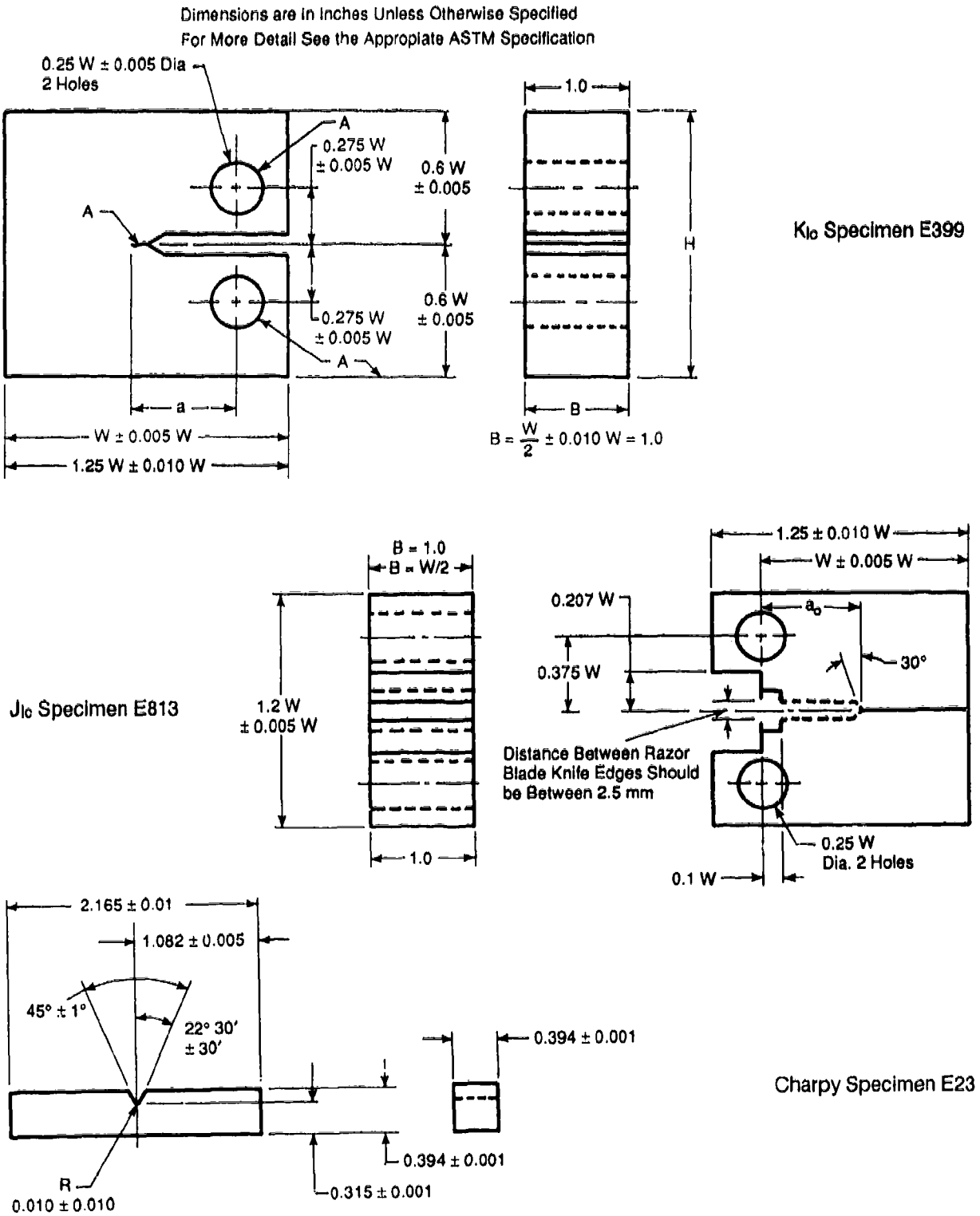

Figure A-2. Specimen Geometries.

The first involved the inevitable acceptance of invalid results by the use of smaller than required specimens for the E399 test. In this case, if the specimen size was too small, an invalid K_{Ic} result would be a certainty, and the data would be reported only as K_Q. K_Q is the conditional result in the fracture toughness test and is used to verify K_{Ic} if all other validity checks are positive. The K_Q approach has often been used in the past for establishing a guide for toughness and is probably an acceptable engineering means of comparing relative toughness as long as the service hardware is not used in thicker section size than the corresponding E399 test specimen. However, K_Q is usually only considered to be an estimate of the true value of K_{Ic}; for that reason, this particular alternative was not preferred.

The second alternative and the one finally chosen was the method of fracture toughness testing outlined by ASTM E813-81. To overcome the large-specimen-size problem, it was considered necessary to employ the use of general yielding (plastic) fracture mechanics as applied to ductile materials and as measured by the J integral technique.

The constraint of specimen thickness is not usually a consideration with the E813 test, and plane strain conditions are not a requirement. For this reason, specimen sizes can be very much smaller than corresponding K_{Ic} specimens; when positive validity checks are achieved, a value of toughness known as J_{Ic} can be directly related by the method in ASTM 813-81 to valid K_{Ic} data. For the ductile materials, a valid K_{Ic} value derived in this way was considered to be a more desirable first option than the K_Q approach.

However, since it is not generally easy or straightforward to perform a J_{Ic} test successfully, certain contingencies were planned into the E813 test schedule. Extra specimens were machined, and the configuration of the test pieces was found to be acceptable both for the requirements of E813-81 and those of E399-83. This effectively generated the option of using the J_{Ic} specimens for either the J_{Ic} test or the more standard K_{Ic} test. This was an important consideration because the result of the J_{Ic} test could not be guaranteed; consequently, at least a K_Q value could be established by the use of the first but less preferred option.

The final procedure adopted was, therefore, to use E399-83 K_{Ic} testing for CBS 600, CBS 1000, M50NiL, and Vasco X2M but to use E813-81 J_{Ic} testing for AISI 9310 and Pyrowear 53 materials.

A.3.3 Program Test Schedule

Toughness testing was scheduled over a wide temperature range in an attempt to simulate normal, prolonged, and extreme engine operating scenarios including testing of samples aged for 1000 hours at 450°F in air.

Compact tension (K_{Ic} + J_{Ic}) testing was conducted using the temperatures and conditions shown in Table A-2.

Charpy V-notch testing was conducted at room temperature and at room temperature after ageing at 450°F for 1,000 hours (6 tests per material per condition were planned so that a total of 66 tests were scheduled).

To carry out the validity checks required by E399 and E813, tensile tests at each test temperature were also incorporated into the test schedule. All tensile testing (both elevated and cryogenic) was carried out in accordance with ASTM E111. In addition, for those materials subject to the requirements of E813, Youngs modulus of elasticity at each test temperature was also determined using ASTM E111 as a guide.

A supporting metallurgical investigation involving fractography and metallography (including documentation of representative features) using a variety of accepted techniques was also set up in parallel with the test program.

A.3.4 Heat Treatment

For steels of fixed composition, the heat treatment process can often be the greatest single influence affecting both the toughness and the strength of the finished components. Considerable significance was therefore attributed to the actual heat treatment applied to each steel.

Table A-2. Test Schedule

Material	Test Type	Number of Tests -65°F	RT	RT After Age	250°F	400°F	Total Scheduled
AISI 9310	E813	6	6	–	6	–	18
	Charpy	–	6	–	–	–	6
Pyrowear 53	E399	6	6	6	–	–	18
	E813	–	6	6	–	6	18
	Charpy	–	6	6	–	–	12
CBS600	E399	6	6	6	–	6	24
	Charpy	–	6	6	–	–	12
CBS100	E399	6	6	6	–	6	24
	Charpy	–	6	6	–	–	12
Vasco X2M	E399	6	6	6	–	6	24
	Charpy	–	6	6	–	–	12
M50NiL	E399	6	6	6	–	6	24
	Charpy	–	6	6	–	–	12

It would have been preferable if each of the materials had been heat treated so that the final hardnesses were similar. However, this ideal procedure was deemed impractical for two reasons. First, not all the materials could achieve the same (core) hardness without possible degradation to other properties; second, many of the materials capable of satisfactory hardness equalization were unlikely ever to be used in that condition for service applications. Eventually, it was decided (with Air Force and other interested parties approval) that the materials would each receive the thermal processing cycle most applicable to current service requirements. This effectively dictated that M50NiL and CBS1000 would receive heat treatments appropriate for bearings while the other materials would receive heat treatments appropriate for gears.

The specific heat treatments were thus expected to generate significant differences in yield point, core hardness, and projected case hardness between the so-designated bearing and gear materials. As a result, it was anticipated that direct comparison of the toughness results between materials would probably also be inappropriate.

Table A-3 outlines the specific heat treatments applied to each material. Common to all the steels treated was a pseudocarburizing cycle and a cryogenic temper cycle. For completeness, Table A-3 also describes the hardness, grain size, and tensile yield strengths generated by each heat treatment.

To comply with the requirement that each material should receive heat treatment in line with current service application, it was necessary for a number of the materials to be processed independently. The following list details the companies who participated in the heat treatment operation and were responsible for the final condition of each assigned material.

AISI 9310	GE Aircraft Engines
Pyrowear 53	Bell Helicopter
CBS600	Sikorsky A/C
CBS1000	GE Aircraft Engines
Vasco X2M	Boeing Vertol
M50NiL	GE Aircraft Engines

Table A-3. Core Heat Treatments and Measured Mechanical Properties.

Material	Heat Treatment: Pseudocarburize	Hardening	Stress Relief	Refrigeration	Temper
AISI 9310	1700°F, 8 hr, Neutral Atmosphere	Austenitize 1500°F, Oil Quench		-110°F/1 hr	300°F 2 hr
Pyrowear 53 (Heat Treated by Bell Helicopter)	1700°F, 4 hr, Protective Atmosphere	Anneale 1150°F (4 Hours), Austenitize 1657°F		-110°F/1 hr	450°F 2 + 2 hr
CBS600 (Heat Treated by Sikorsky Aircraft)	1700°F, 5 hr, Carburizing Atmosphere, Copper Plated	Anneale 1500°F (2 Hours), Austenitelze 1625°F, Oil Quench		-110°F/2 hr	600°F 2 + 2 hr
CBS1000	1700°F, 8 hr, Neutral Atmosphere	Preheat 1500°F, Austenitize 2008°F (Salt), Oil Quench	1000°F 2 hr	-110°F/2 hr	1000°F 2 + 2 hr
Vasco X2M (Heat Treated by Boeing Vertol)	1700°F, 4 hr, Protective Atmosphere	Austenitize 1850°F, Oil Quench		-110°F/4.5 hr	600°F 2 + 2 hr
M50NiL	1750°F, 24 hr, Neutral Atmosphere	Preheat 1450°F, Austenitize 2000°F, Oil Quench	1000°F 2 hr	-110°F/2 hr	1000°F 2 + 2 hr

Material	Room Temperature Measured Properties: R_C Hardness	0.02 Yield Point, ksi	ASTM Grain Size
AISI 9310	34.8	130.9	Fine*
Pyrowear 53	33.4	134.4	As Fine as NiL*
CBS600	39.0	147.3	As Fine as NiL*
CBS1000	42.7	171.9	5 to 7
Vasco X2M	37.5	147.6	As Fine as NiL*
M50NiL	42.5	176.4	5 to 7

* Estimation of grain size based on comparison of grain boundaries for M50NiL and CBS1000 at 500 ×. (At 100 × the grain boundaries of tempered material are not accurately discernible.)

A.4 Results and Discussion

A.4.1 Data Acquisition

The photographs in Figures A-3 through A-25 illustrate the appearance of typical fracture faces of representative test specimens and record the microstructures exhibited by each material at each test condition. The fracture toughness results are tabulated in Table A-4, and a graph generated using the data from Table A-4 representing average toughness against temperature for each of the materials is presented in Figure A-26.

In general, valid K_{Ic} data were obtained, but where the K_{Ic} test was invalidated according to E399, the data are reported as K_Q in Table A-4. K_Q values so designated are distinguished from valid K_{Ic} data in Table A-4 by the inclusion of an ascribed "K_Q" marker printed adjacent to each value. No ascribed "K_Q" marker indicates that a valid data point was obtained.

In some tests, for example CBS600 at room temperature, both K_{Ic} and K_Q data were reported. It is important to note that the general trend in these cases was that K_Q was nearly always numerically very similar to K_{Ic}. For the purposes of averaging the data, therefore, it was considered acceptable to designate the average as a valid K_{Ic} value if at least two data points in the group of six tests were valid K_{Ic} points.

In Table A-4, it can be seen that 78% of the test data were valid in accordance with the strict requirements of E399. In order to appreciate the factors influencing test validity and also to explain the nature of the invalid data, a brief review of the salient features of the K_{Ic} and J_{Ic} tests and the relationship of these parameters to the test materials is given in Sections A.4.2 and A.4.3 of this appendix. Charpy data are reported only as average values for brevity in Table A-4 and are expressed in units of ft-lb. Table A-5 describes the complete range of Charpy data obtained.

A.4.2 ASTM E399-83 K_{Ic} Testing

The K_{Ic} concept is generally acknowledged to be specifically applicable to materials exhibiting a critical degree of brittleness. This is necessary in order that linear elastic fracture mechanics (LEFM) theory can apply. For materials such as Pyrowear 53 and AISI 9310 where the critical level of brittleness was judged to be insufficient for the result of the E399 test to be valid, the problems of specimen size and the level of plastic constraint become crucial. A sufficient level of plastic constraint is usually attained in the E399 test when the specimen is tested in compliance with plane strain conditions.

Crack tip stress analysis is based on two-dimensional plane models, either plane stress or plane strain. These two conditions represent extreme conditions at the crack tip that can be treated analytically in a simple manner (Reference 27).

$$\text{Plane Stress } \sigma_z = 0 \quad \varepsilon_z = -\mu(\varepsilon_x + \varepsilon_y)$$

$$\text{Plane Strain } \varepsilon_z = 0 \quad \sigma_z = \mu(\sigma_x + \sigma_y)$$

where ε = Strain
σ = Stress
x, y, z = Principal Directions
μ = Poisson's Ratio

For thin sheets and close to the surface of thicker members, the z-direction stresses are small, and plane stress conditions are approached. Near the center plane of thick members, material close to the crack tip is constrained ($\sigma_z = 0$) by the lower stressed material further away from the crack tip, and plane strain conditions are thus approached.

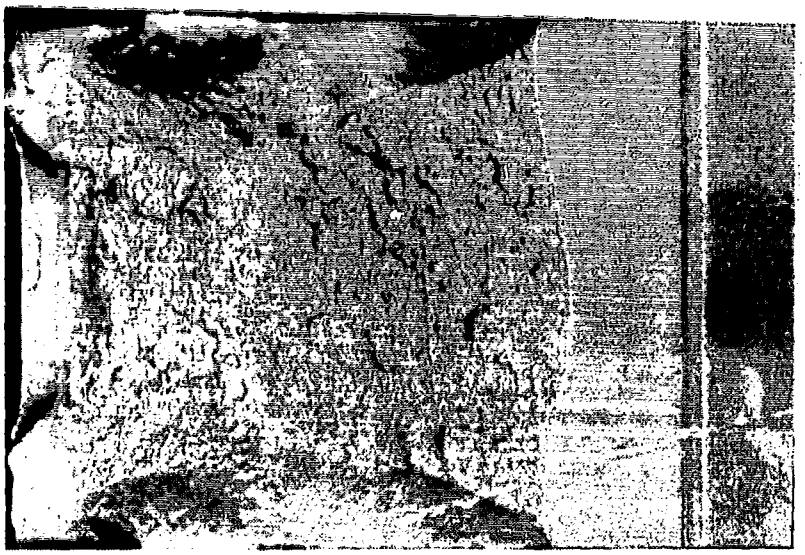

3×

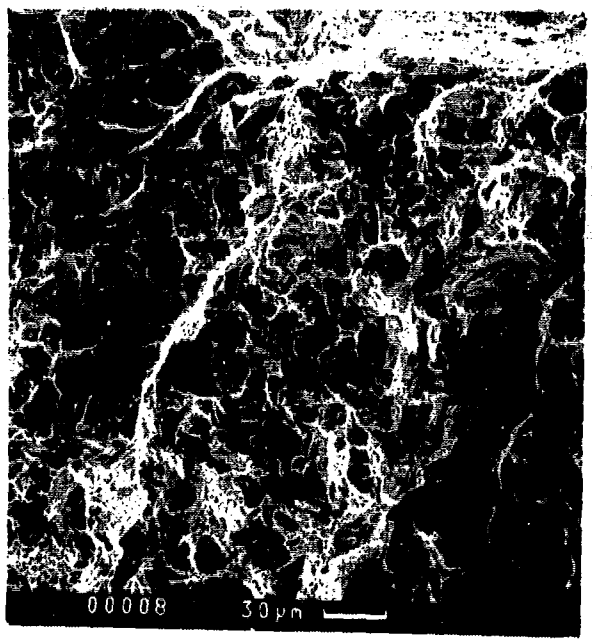

SEM Fractograph, 300 ×

Micrograph, 100 ×

Figure A-3. AISI 9310 Fracture Face (J_{Ic}), -65°F Test.

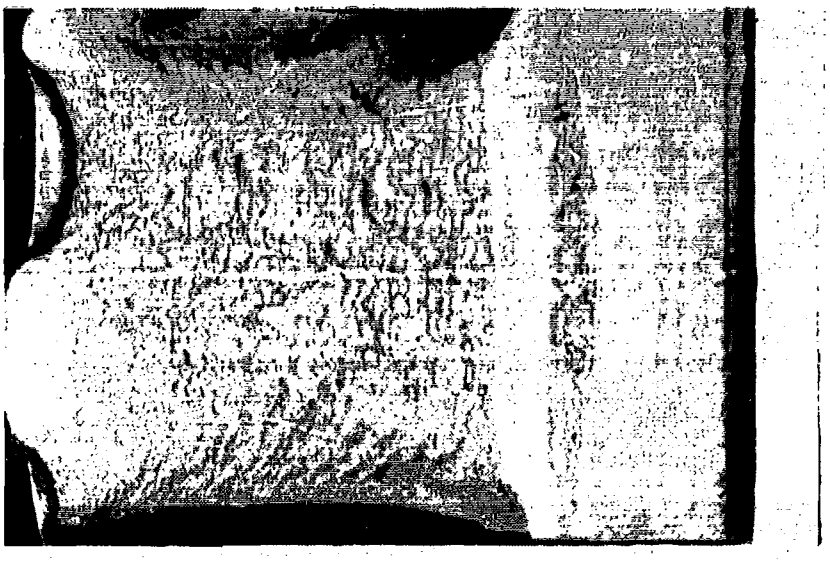

3×

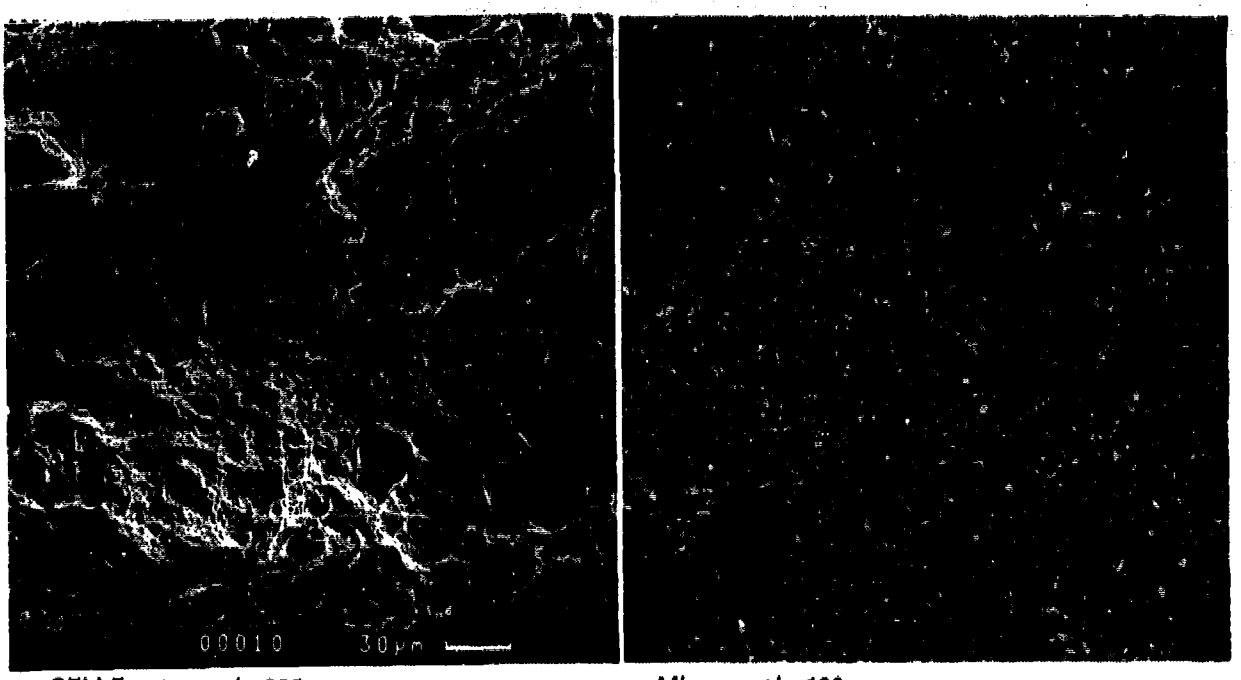

SEM Fractograph, 300×

Micrograph, 100×

Figure A-4. AISI 9310 Fracture Face (J_{Ic}), Room Temperature Test.

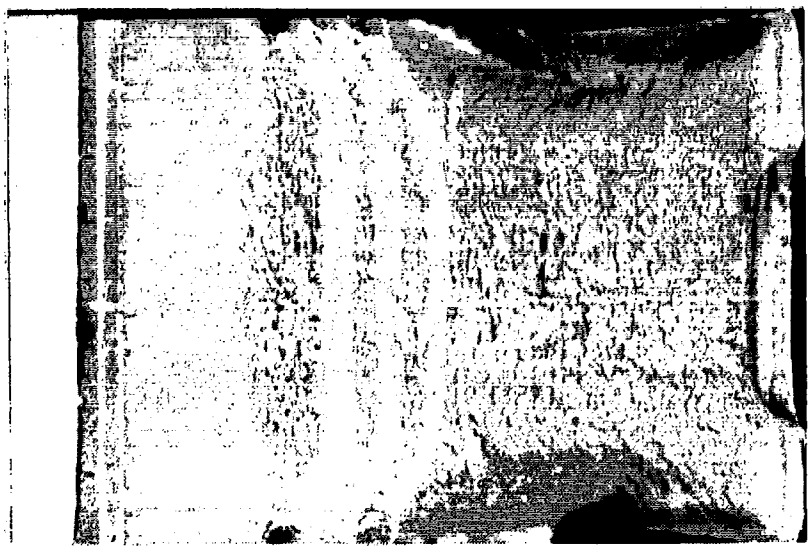

3×

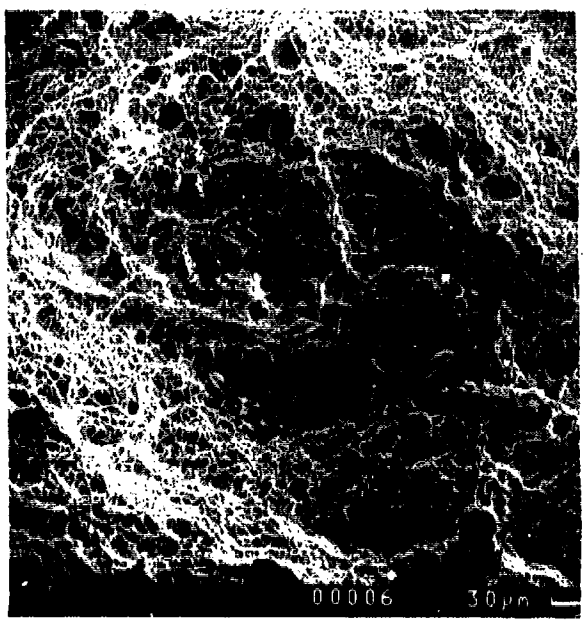

SEM Fractograph, 300×

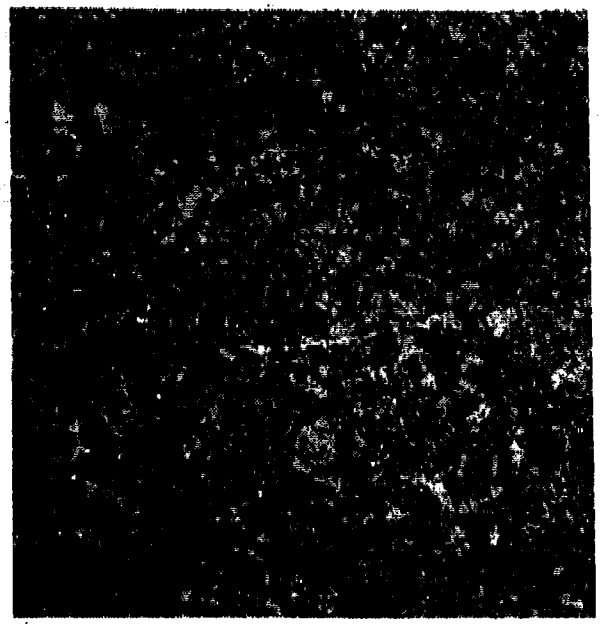

Micrograph, 100×

Figure A-5. AISI 9310 Fracture Face (J_{Ic}), 250°F Test.

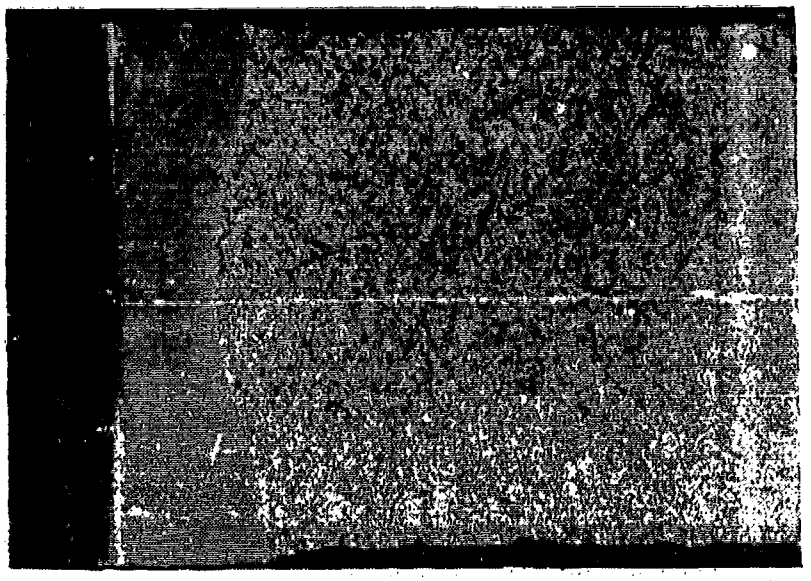

3×

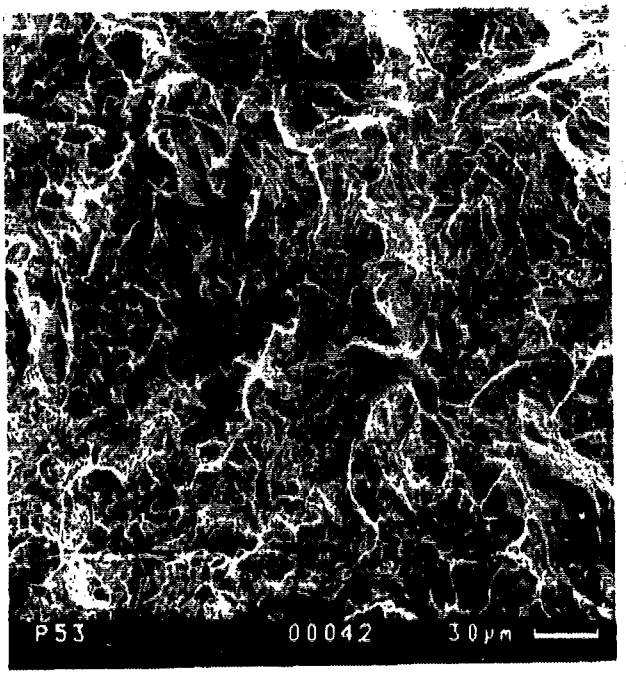

SEM Fractograph, 300×

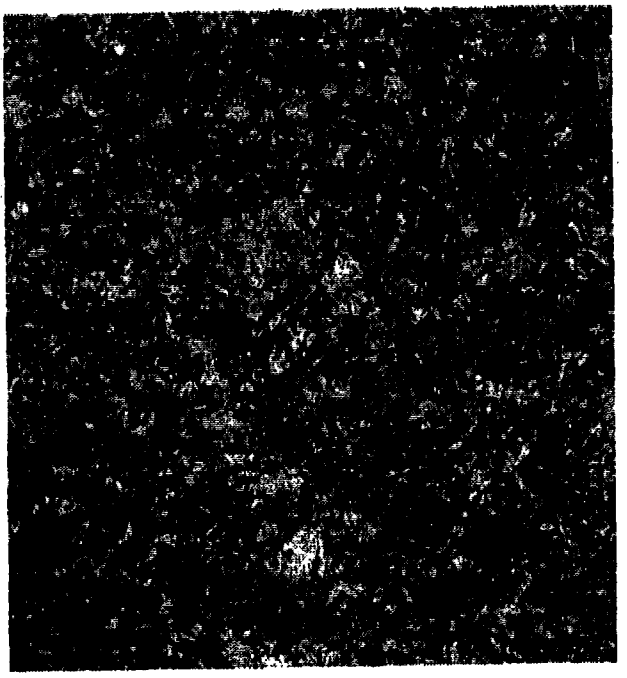

Micrograph, 100×

Figure A-6. Pyrowear 53 Fracture Face (K_{Ic}), -65°F Test.

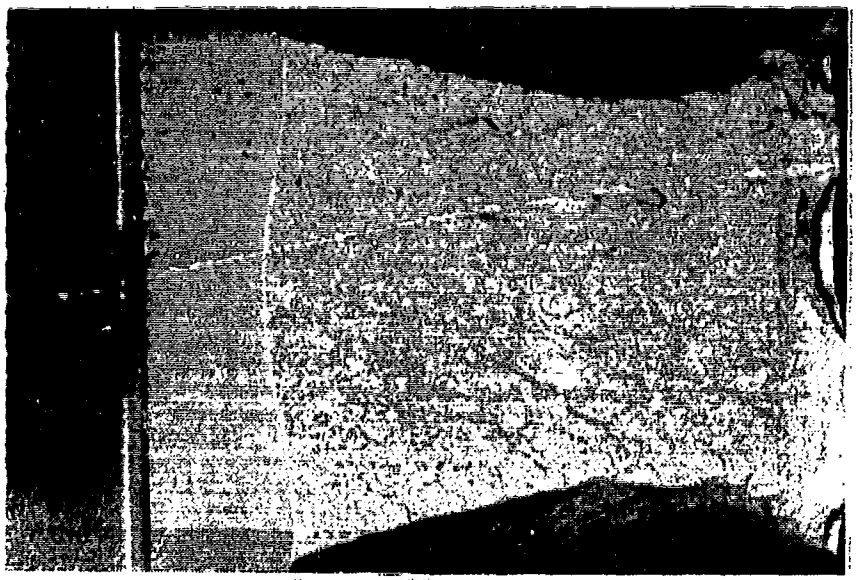

3×

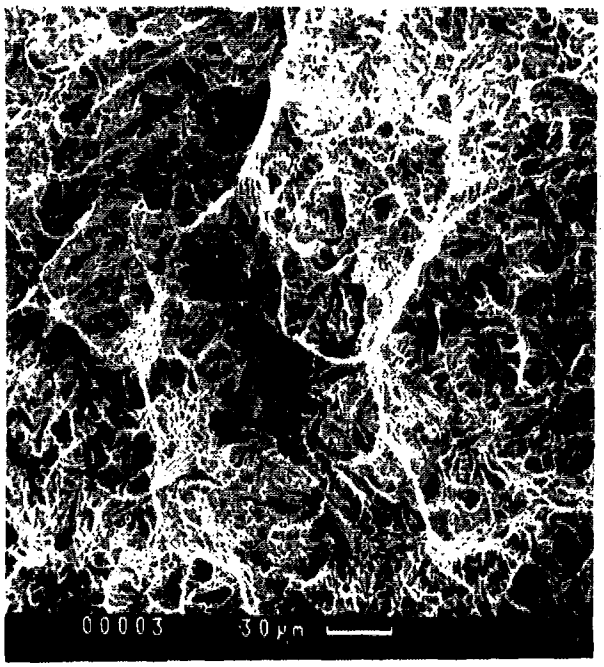

SEM Fractograph, 300 ×

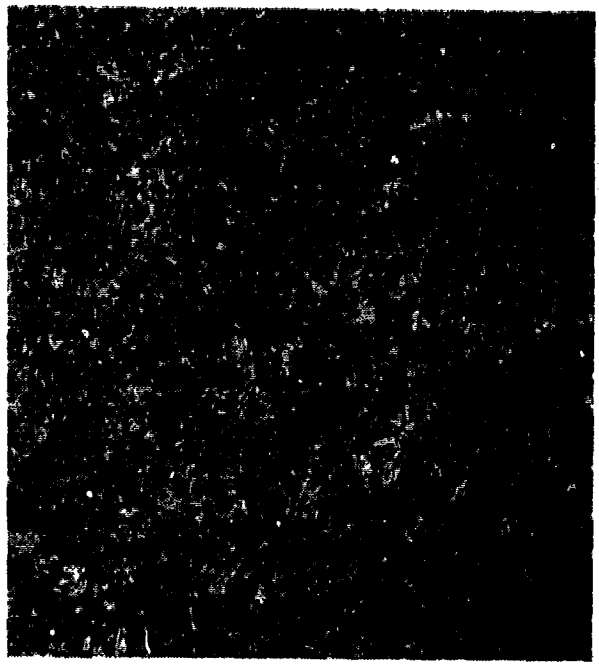

Micrograph, 100 ×

Figure A-7. Pyrowear 53 Fracture Face (K_{Ic}), Room Temperature Test.

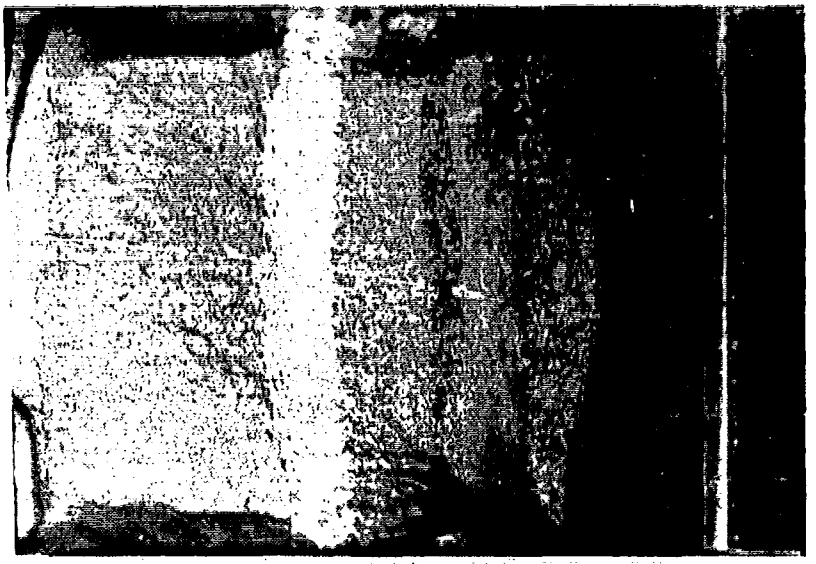

3×

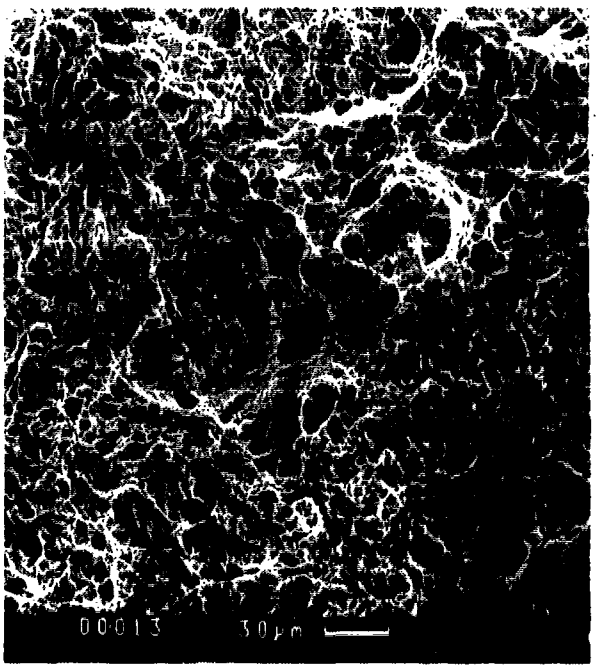

SEM Fractograph, 300×

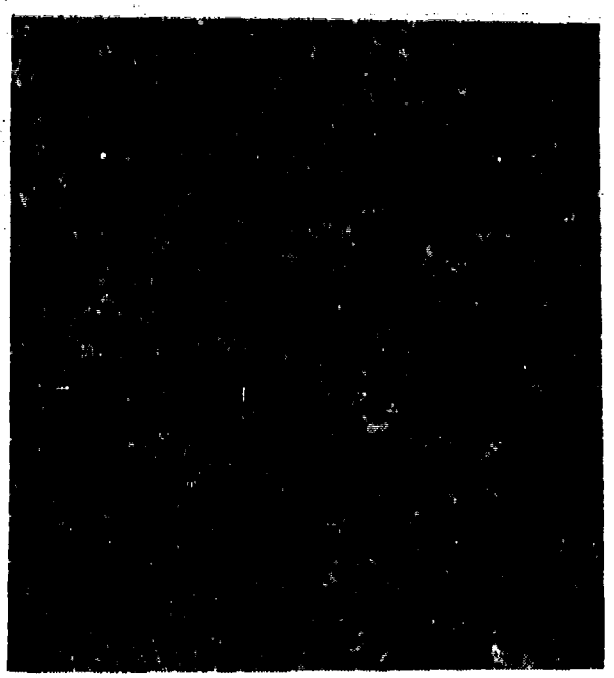

Micrograph, 100×

Figure A-8. Pyrowear 53 Fracture Face (J_{Ic}), 400°F Test.

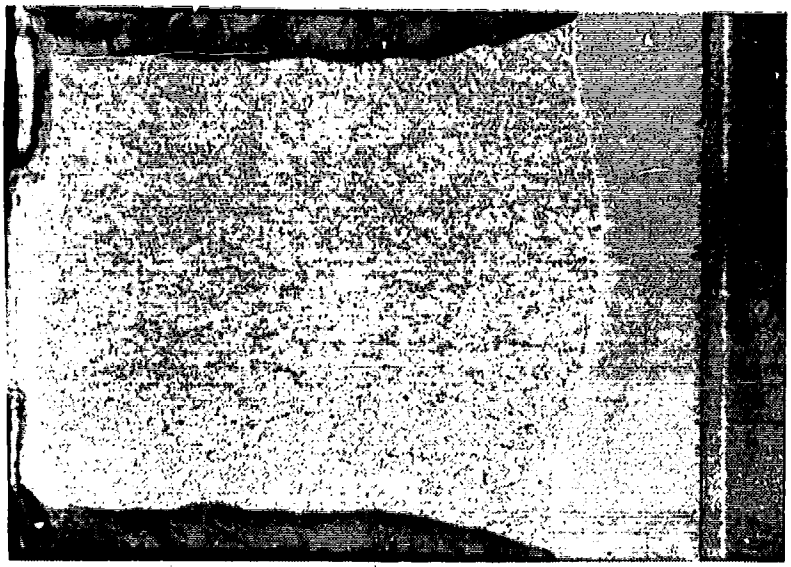

3×

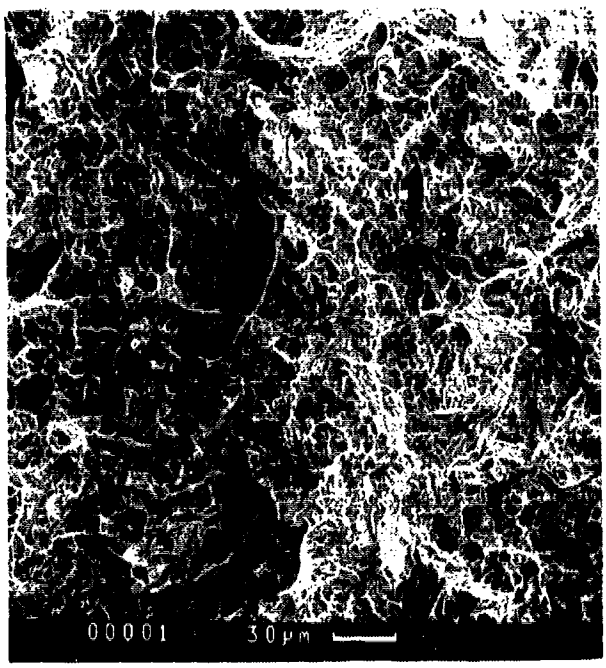

SEM Fractograph, 300×

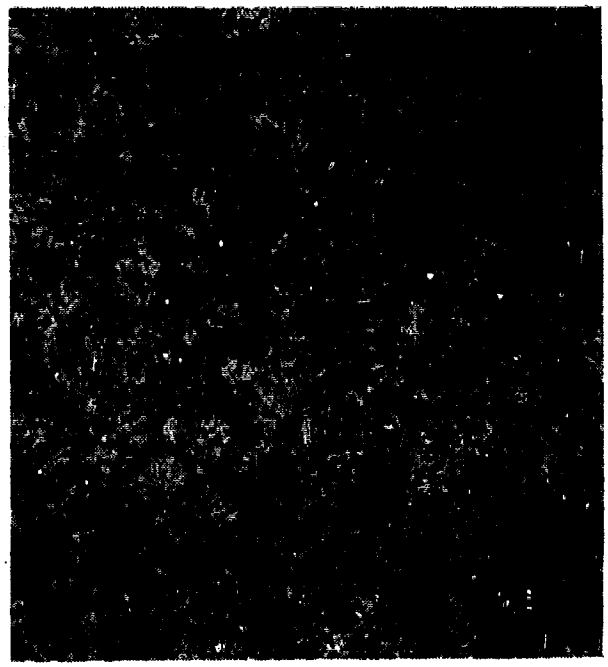

Micrograph, 100×

Figure A-9. Pyrowear 53 Fracture Face (K_{Ic}), Aged 1000 Hours at 450°F, Room Temperature Test.

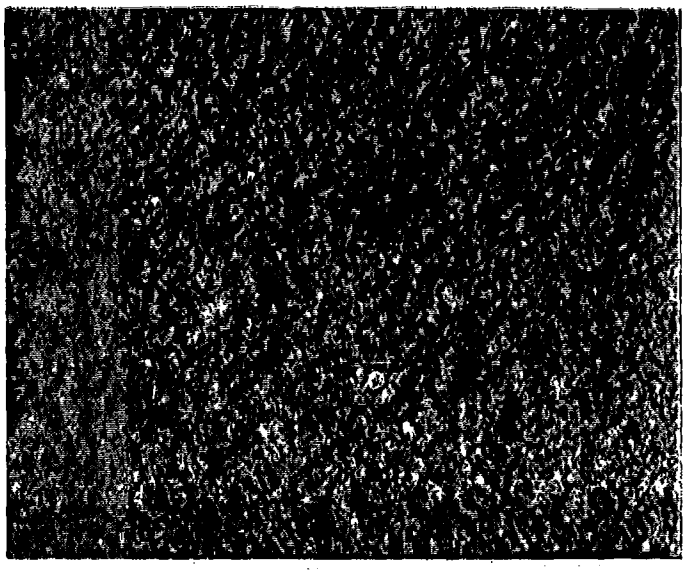

3×

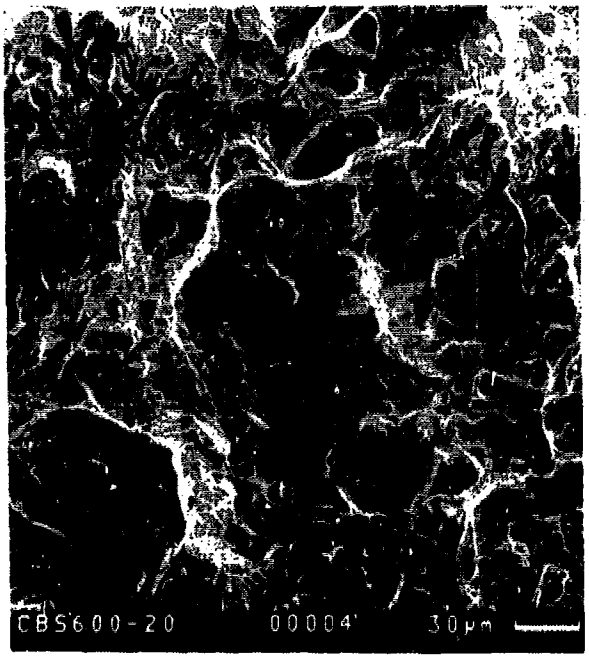

SEM Fractograph, 300×

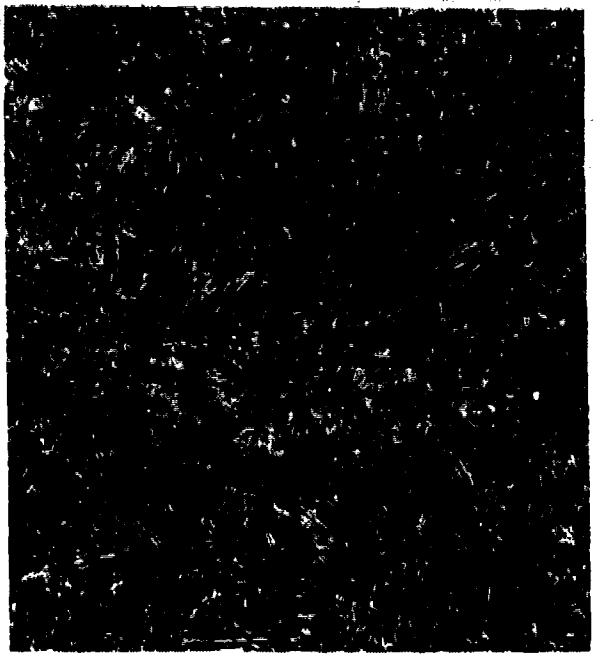

Micrograph, 100×

Figure A-10. CBS600 Fracture Face (K_{Ic}), -65°F Test.

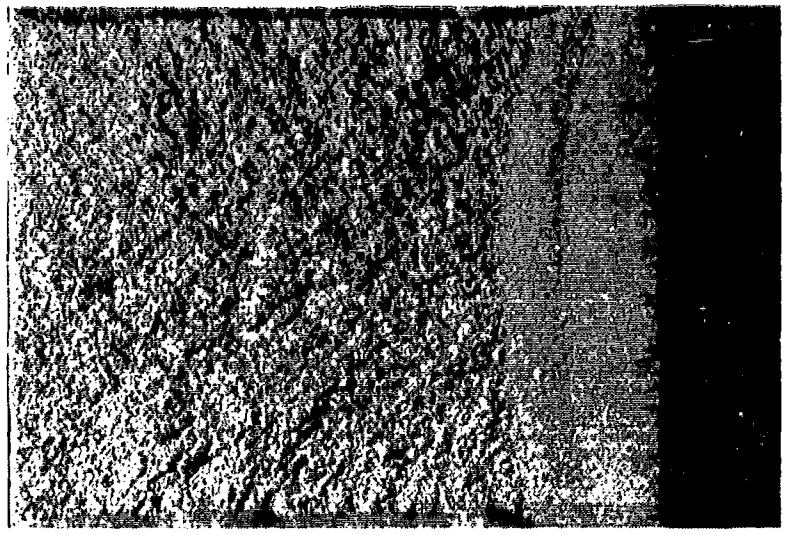

3×

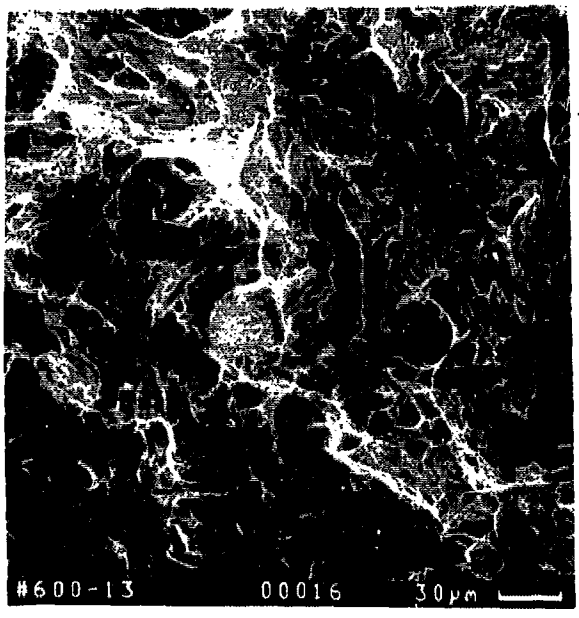

SEM Fractograph, 300 ×

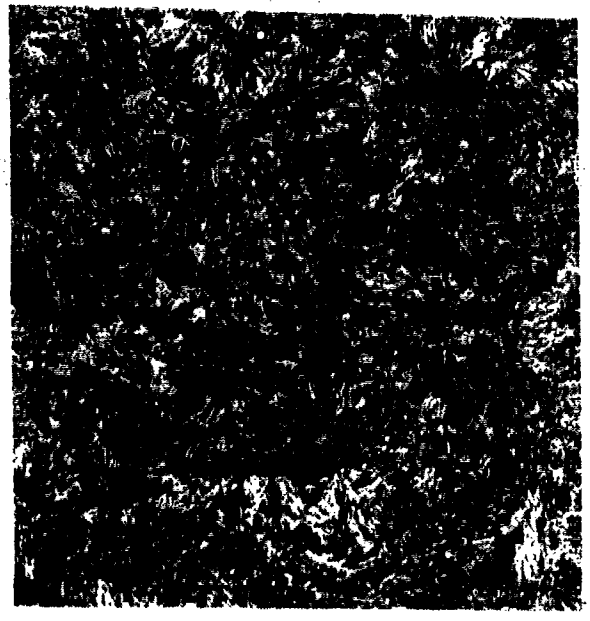

Micrograph, 100 ×

Figure A-11. CBS600 Fracture Face (K_{Ic}), Room Temperature Test.

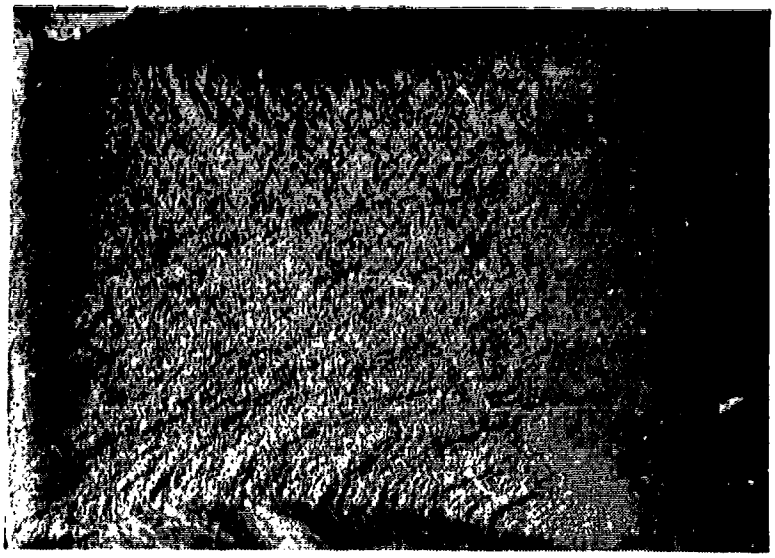

3×

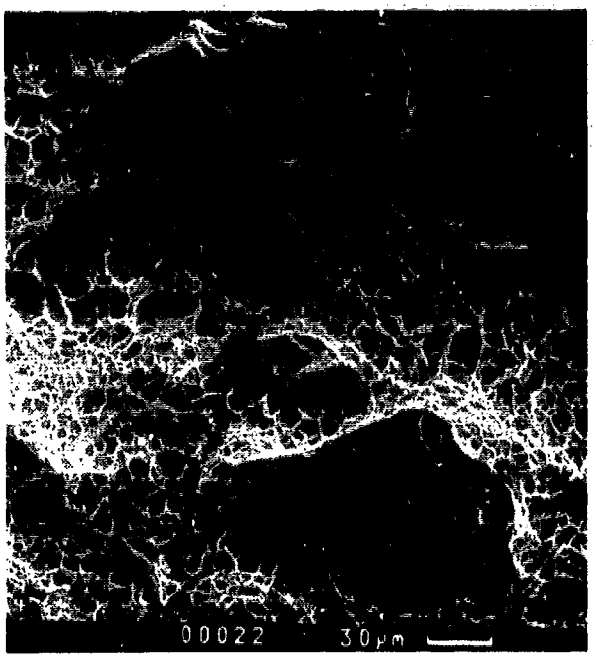

SEM Fractograph, 300×

Micrograph, 100×

Figure A-12. CBS600 Fracture Face (K_{Ic}), 400°F Test.

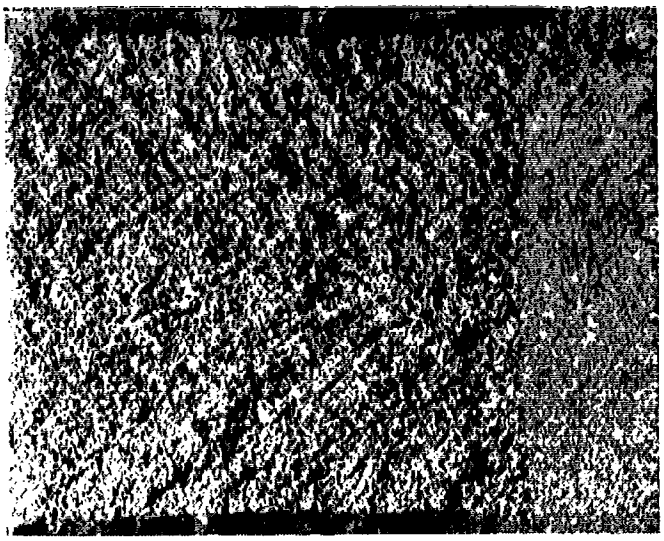

3×

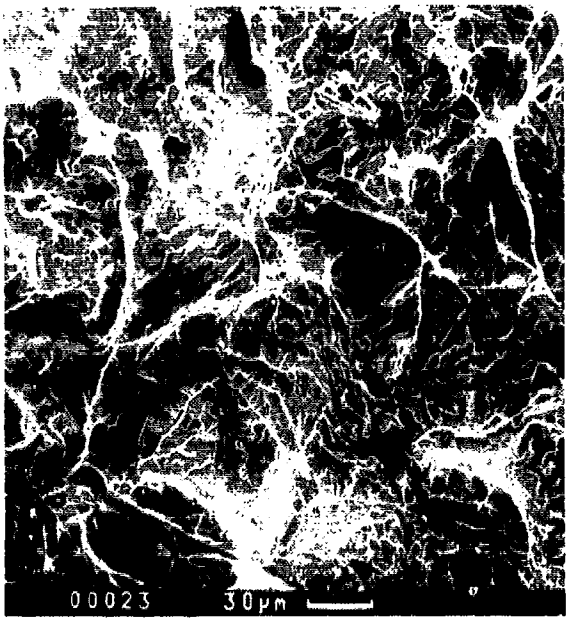

SEM Fractograph, 300×

Micrograph, 100×

Figure A-13. CBS600 Fracture Face (K_{Ic}), Aged 1000 Hours at 450°F, Room Temperature Test.

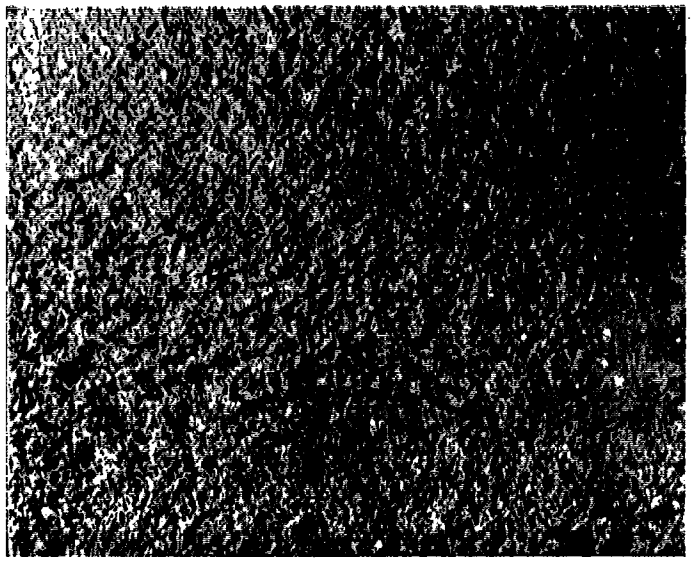

3×

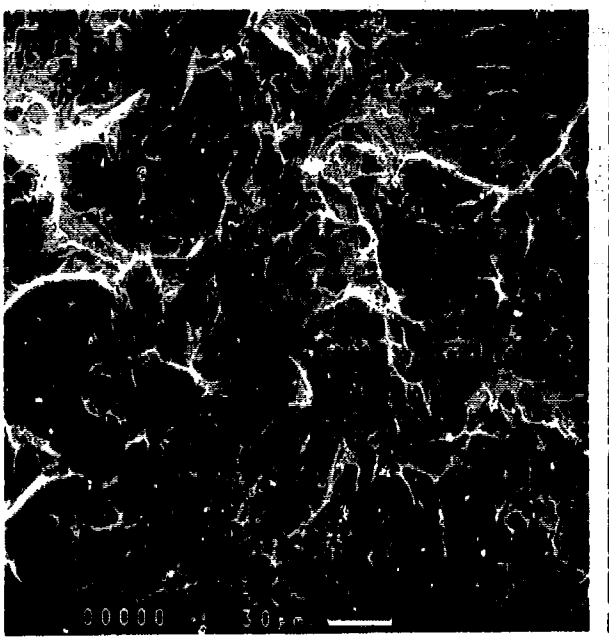

SEM Fractograph, 300×

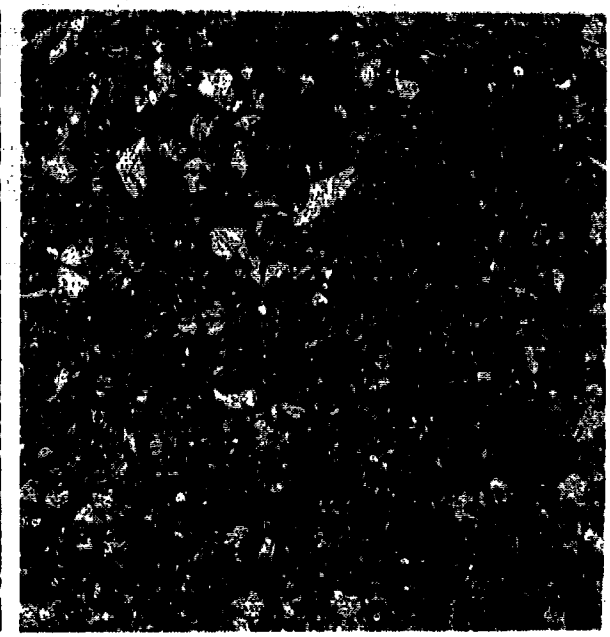

Micrograph, 100×

Figure A-14. CBS1000 Fracture Face (K_{Ic}), -65°F Test.

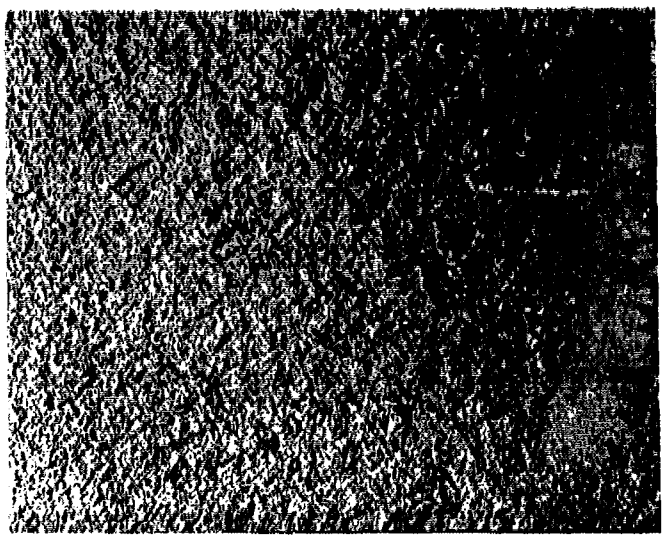

3×

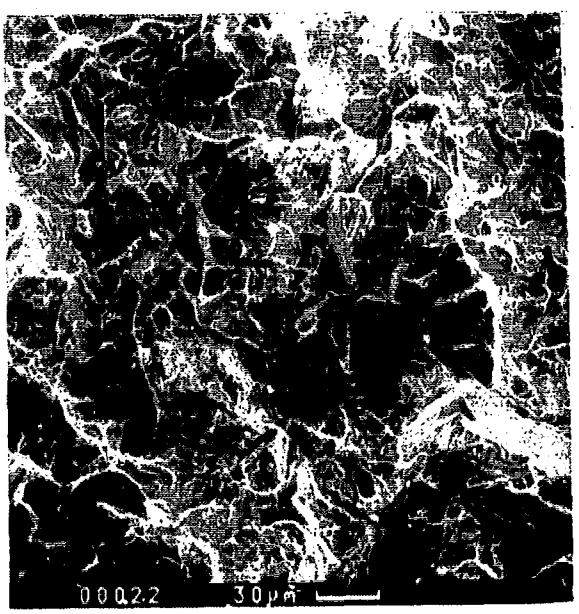

SEM Fractograph, 300×

Micrograph, 100×

Figure A-15. CBS1000 Fracture Face (K_{Ic}), Room TemperatureTest.

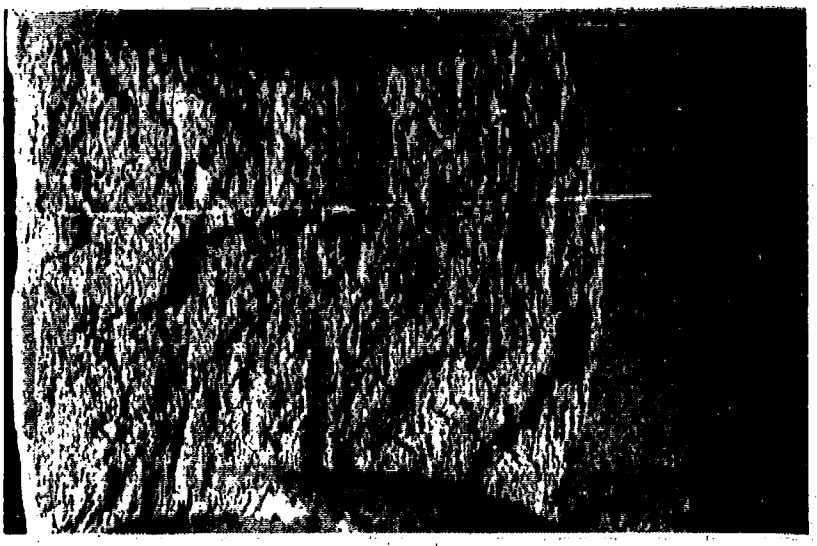

3×

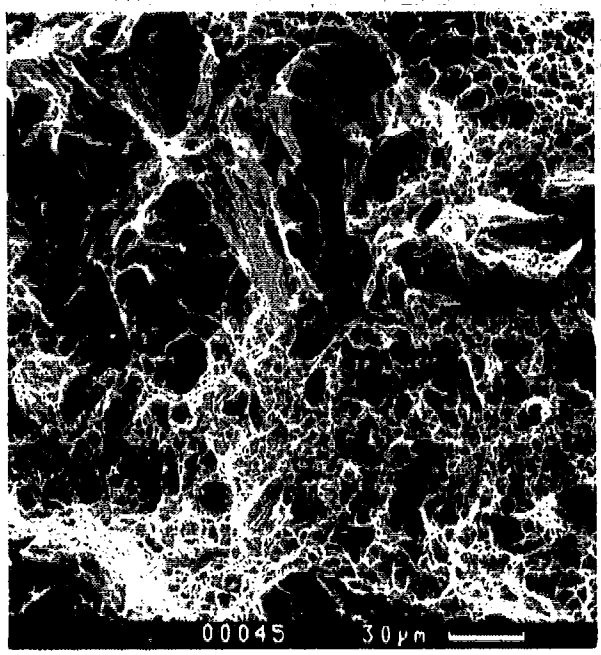

SEM Fractograph, 300 ×

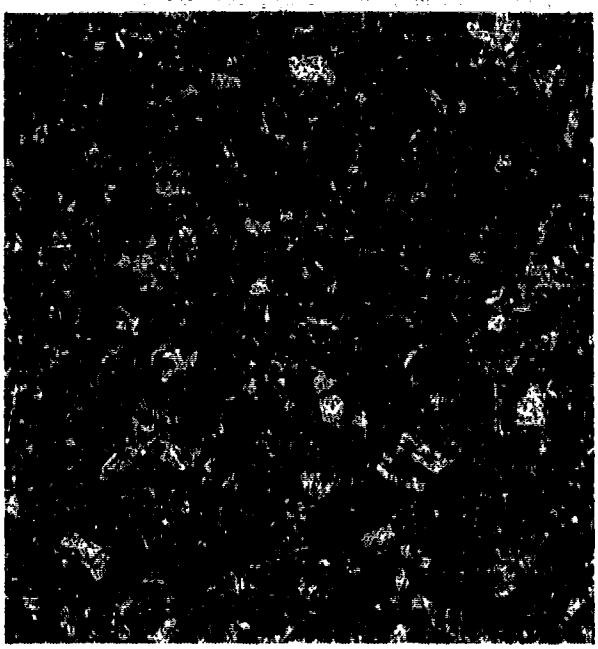

Micrograph, 100 ×

Figure A-16. CBS1000 Fracture Face (K_{Ic}), 400°F Test.

3×

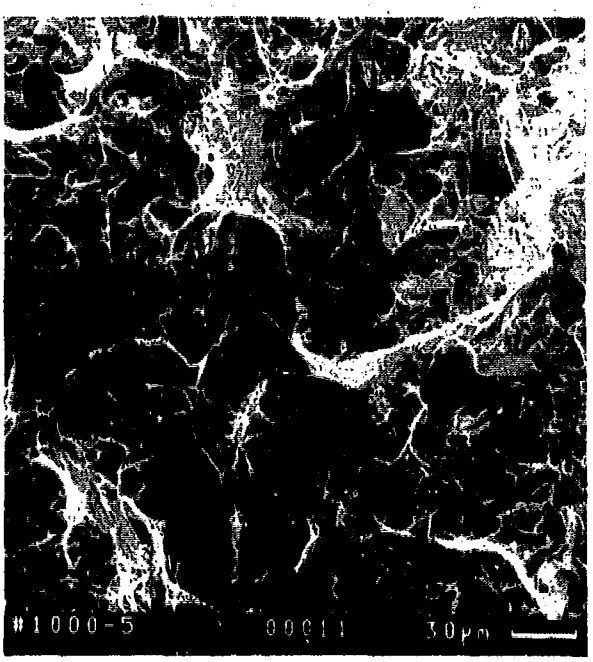

SEM Fractograph, 300 ×

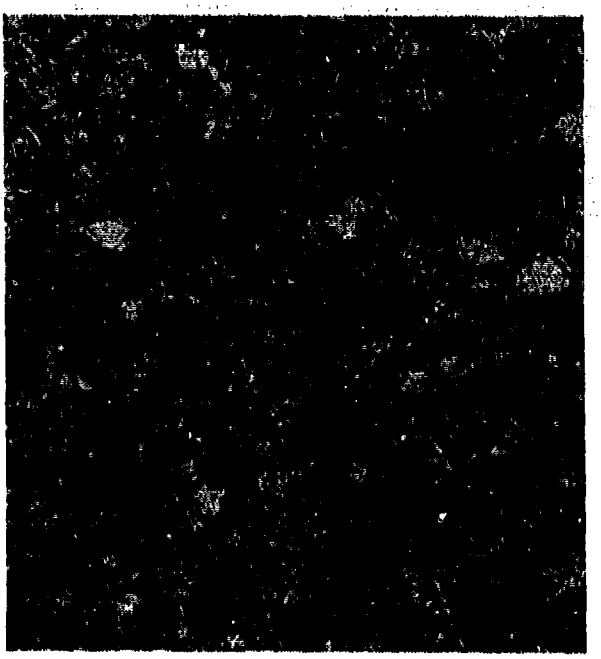

Micrograph, 100 ×

Figure A-17. CBS1000 Fracture Face (K_{Ic}), Aged 1000 Hours at 450°F, Room Temperature Test.

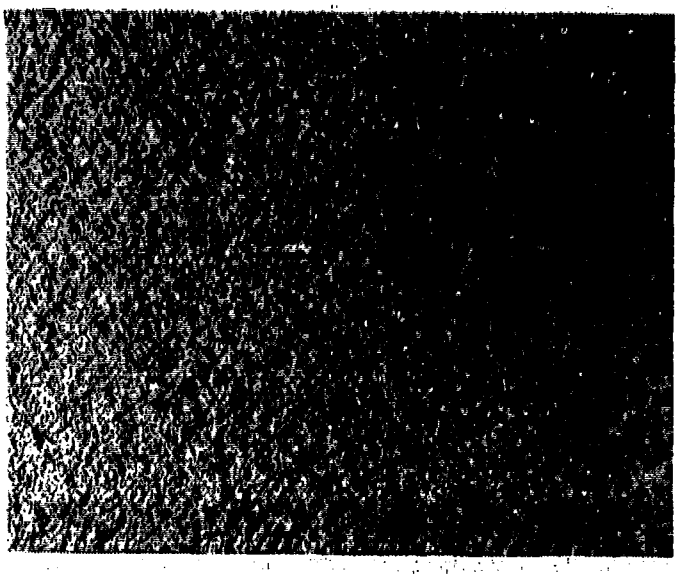

3×

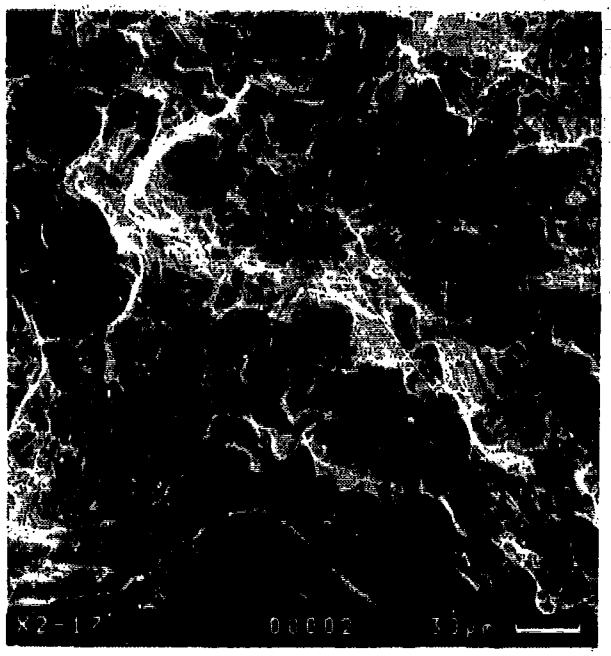

SEM Fractograph, 300×

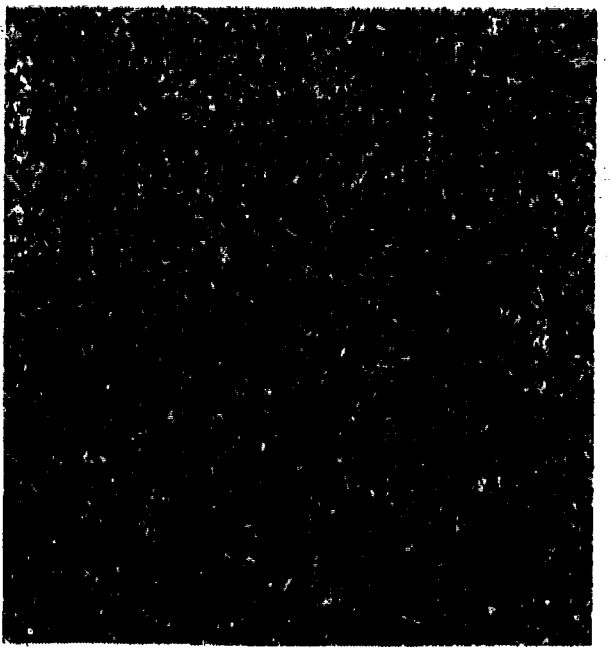

Micrograph, 100×

Figure A-18. Vasco X2M Fracture Face (K_{Ic}), -65°F Test.

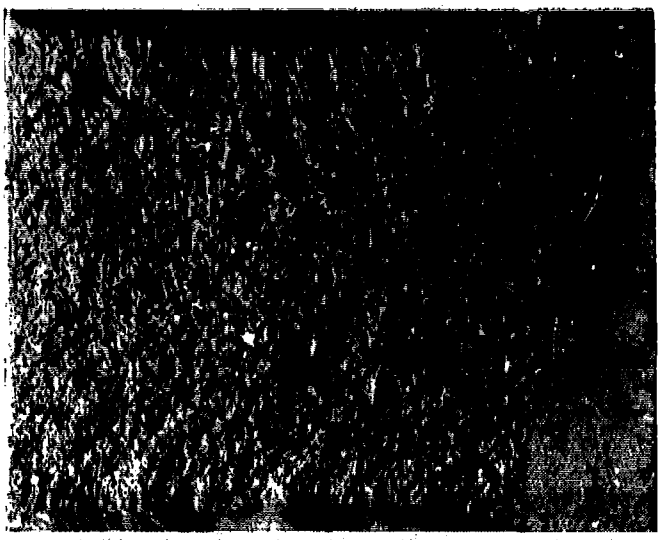

3×

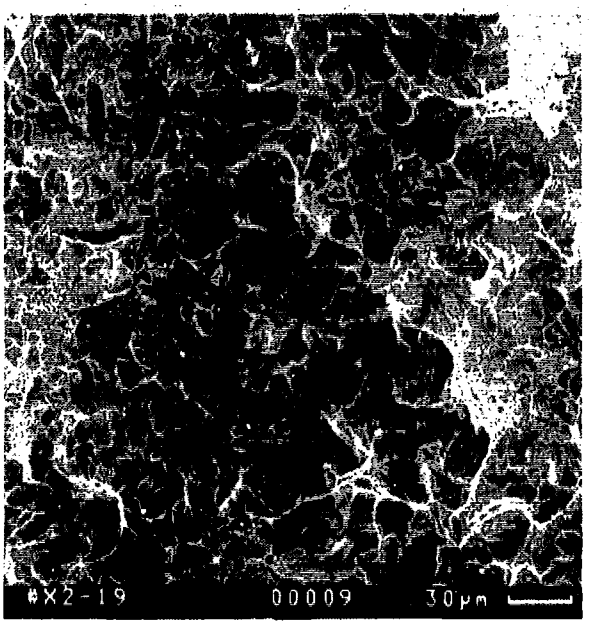

SEM Fractograph, 300×

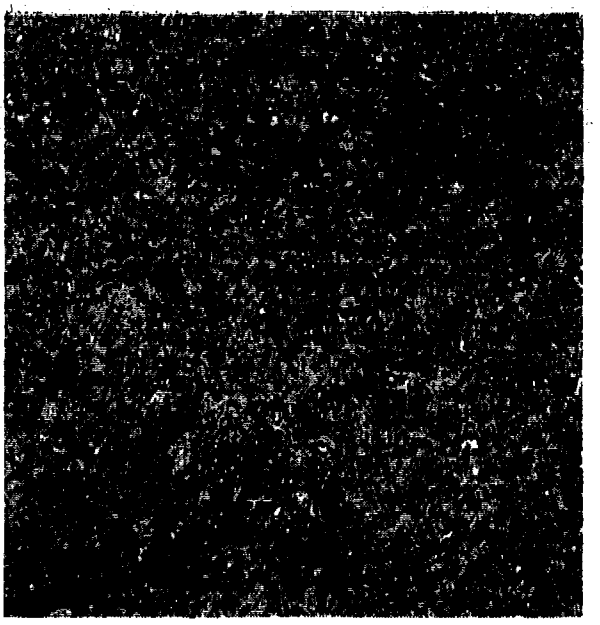

Micrograph, 100×

Figure A-19. Vasco X2M Fracture Face (K_{Ic}), Room Temperature Test.

3×

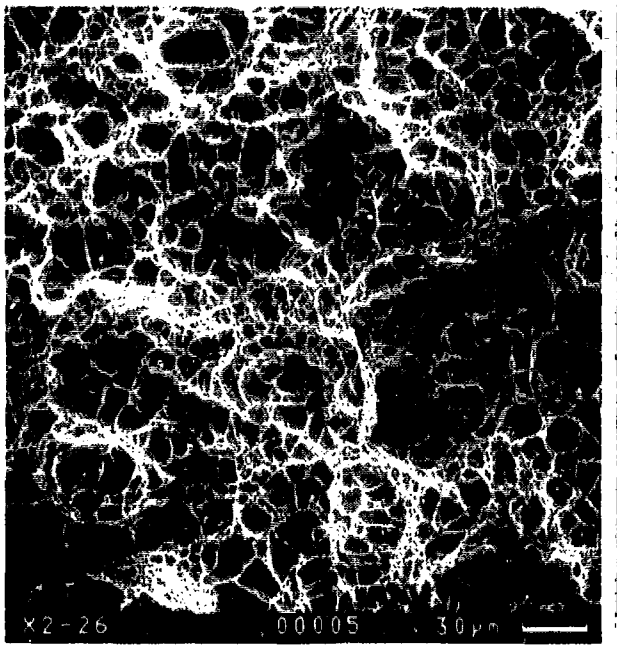

SEM Fractograph, 300 ×

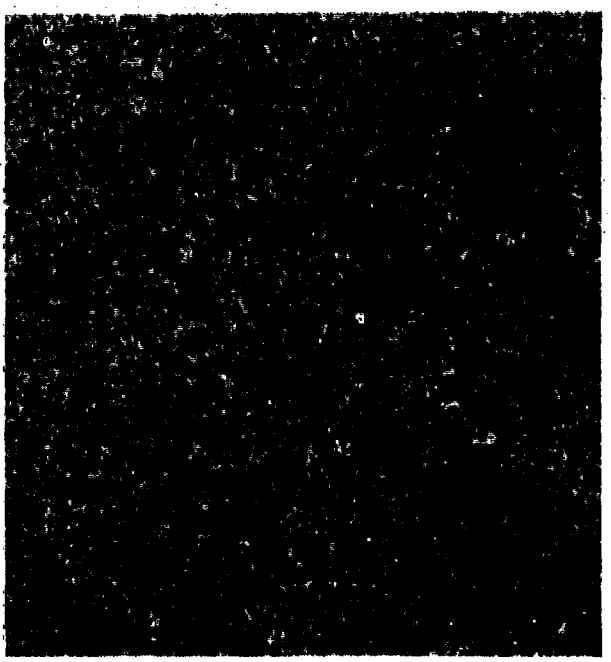

Micrograph, 100 ×

Figure A-20. Vasco X2M Fracture Face (K_{Ic}), 400°F Test.

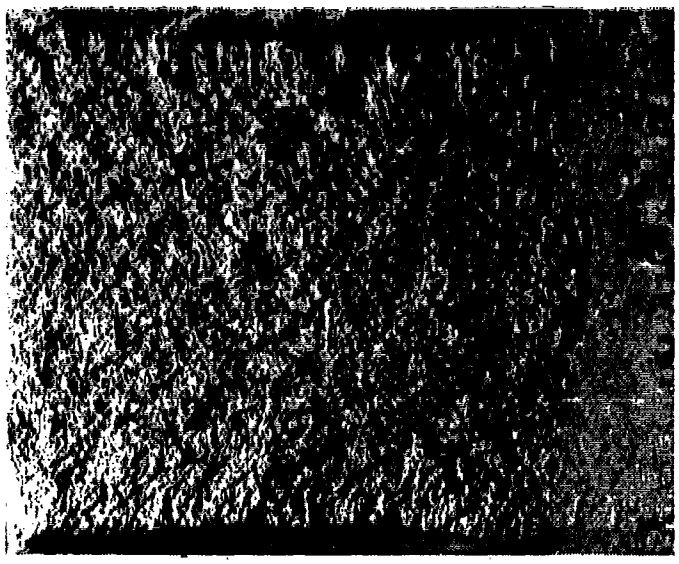

3×

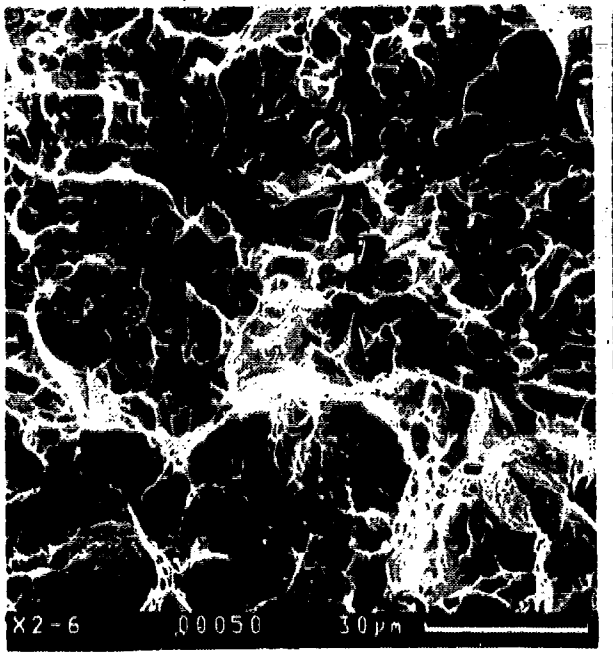

SEM Fractograph, 300 ×

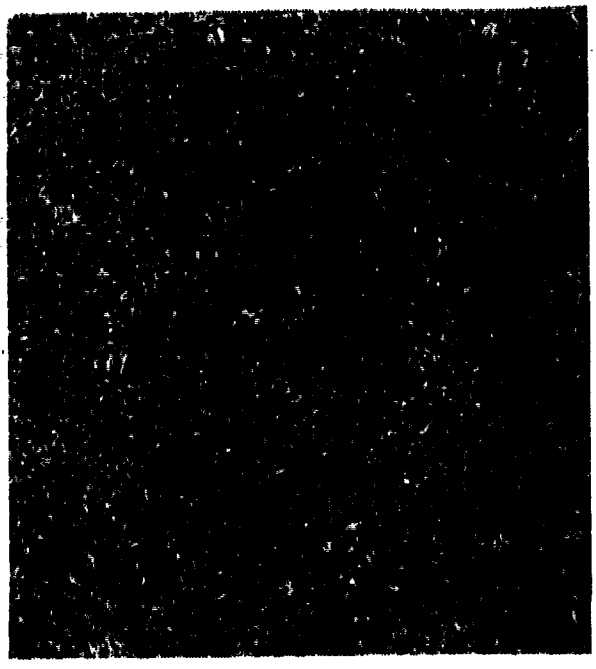

Micrograph, 100 ×

Figure A-21. Vasco X2M Fracture Face (K_{Ic}), Aged 1000 Hours at 450°F, Room Temperature Test.

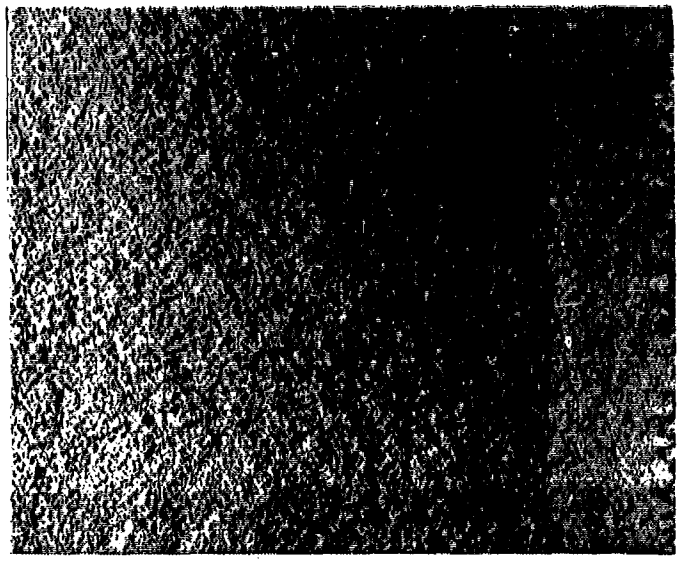

3×

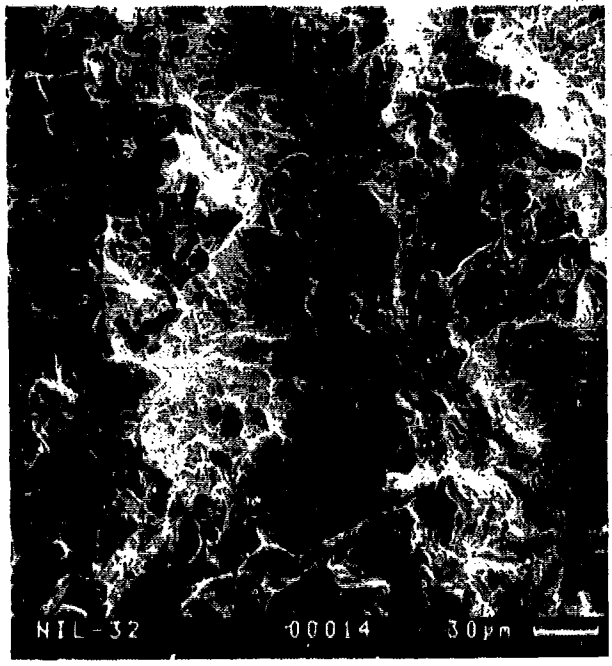

SEM Fractograph, 300×

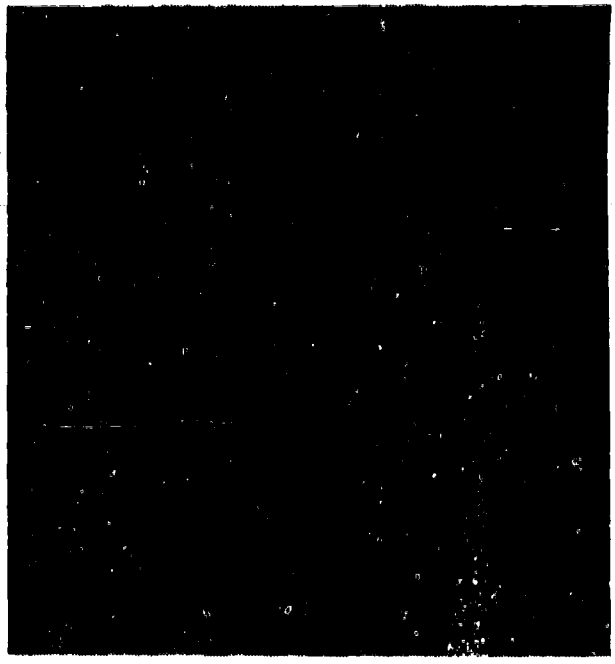

Micrograph, 100×

Figure A-22. M50NiL Fracture Face (K_{Ic}), -65°F Test.

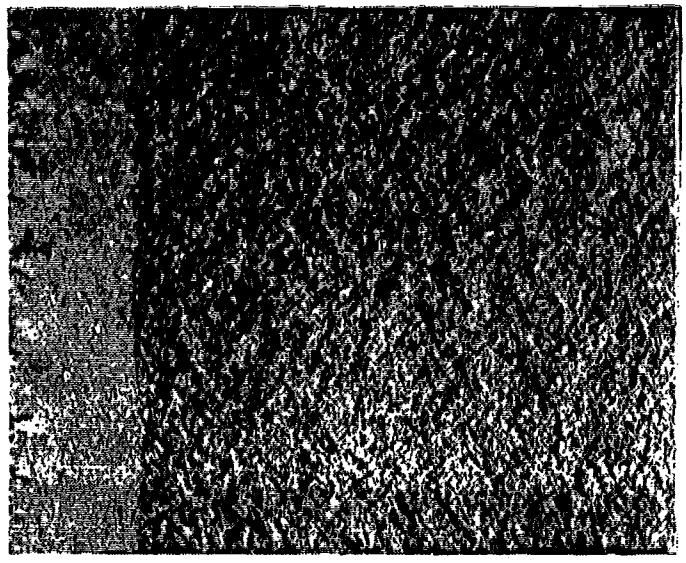

3×

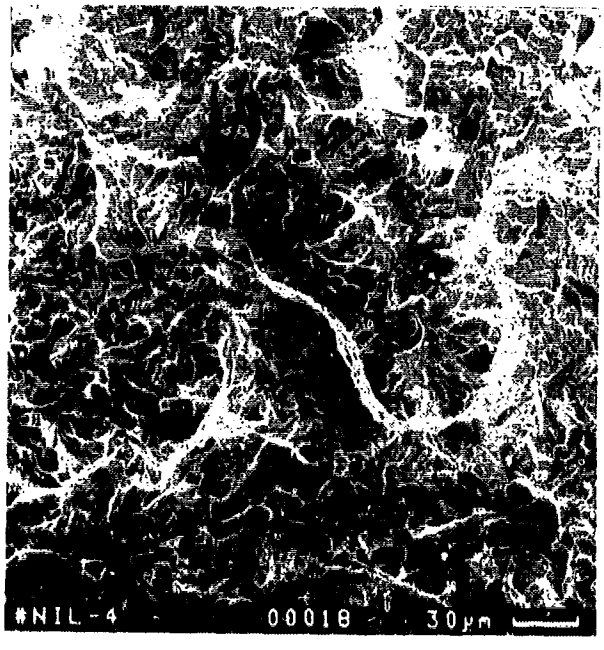

SEM Fractograph, 300 ×

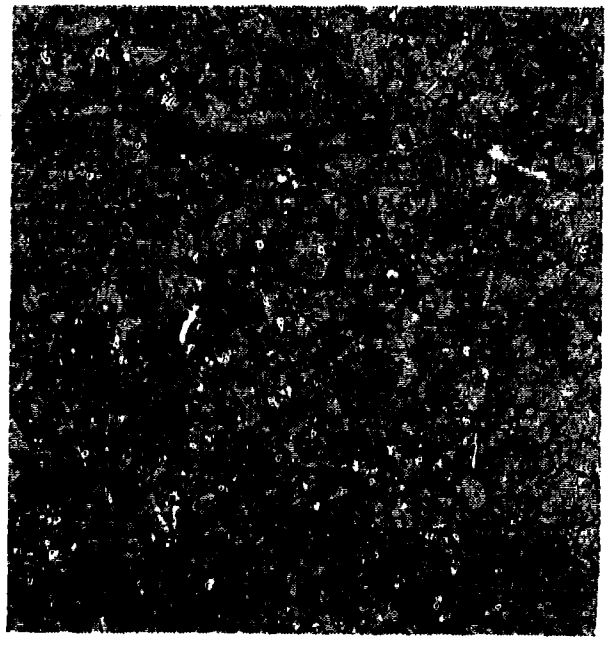

Micrograph, 100 ×

Figure A-23. M50NiL Fracture Face (K_{Ic}), Room Temperature Test.

3×

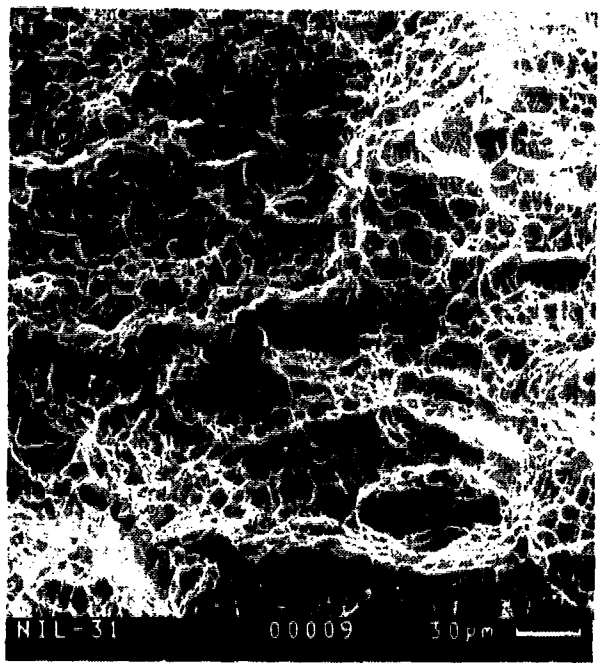

SEM Fractograph, 300×

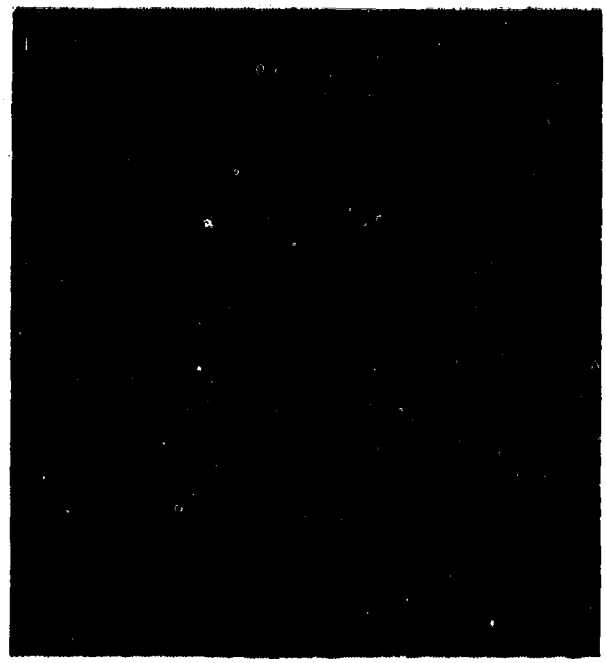

Micrograph, 100×

Figure A-24. M50NiL Fracture Face (K_{Ic}), 400°F Test.

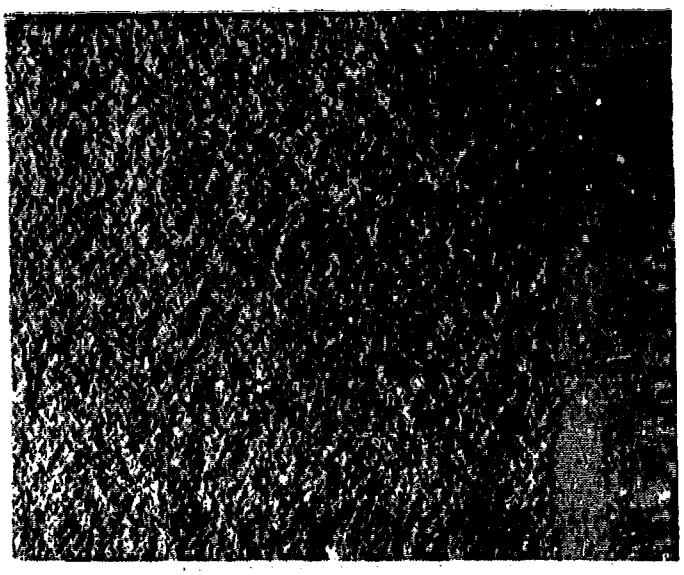

3×

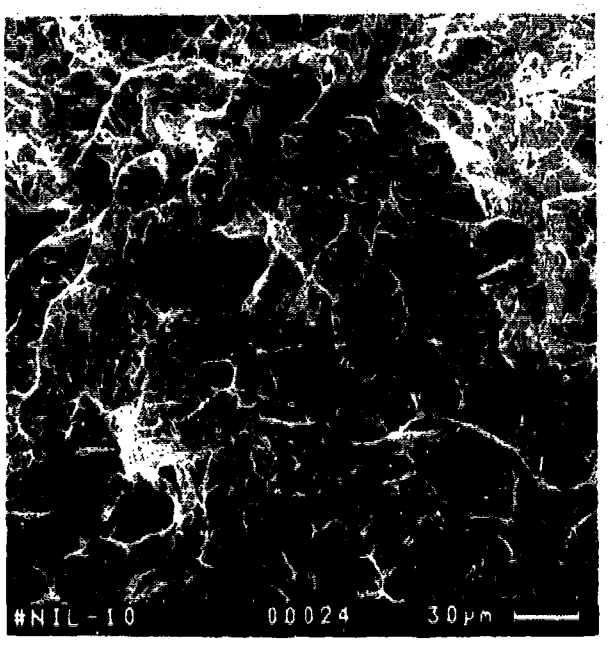

SEM Fractograph, 300×

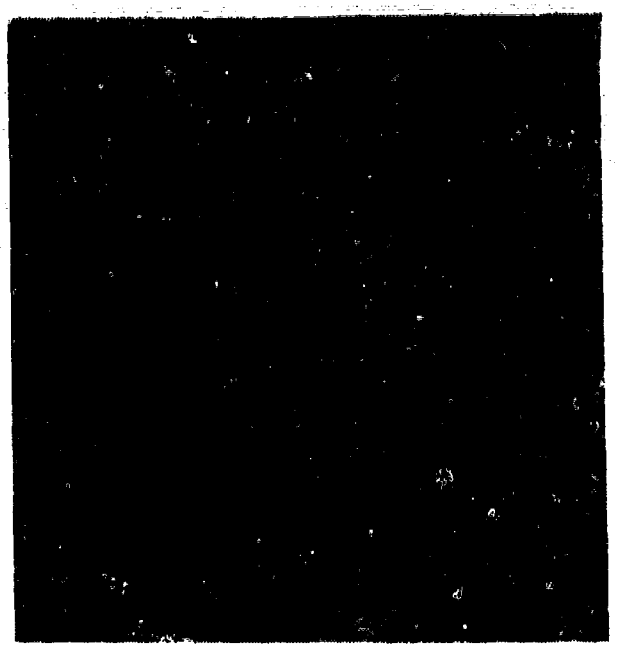

Micrograph, 100×

Figure A-25. M50NiL Fracture Face (K_{Ic}), Aged 1000 Hours at 450°F, Room Temperature Test.

Table A-4. Toughness Test Results. *All toughness values are K_{Ic} unless otherwise indicated.*

Material	Toughness, ksi · $in^{1/2}$ Room Temperature (E399 + E813)	Charpy, ft-lb Room Temperature Average of 6	Toughness, ksi · $in^{1/2}$ -65°F (E399 + E813)	Toughness, ksi · $in^{1/2}$ 400°F (250°F for AISI 9310) (E399 + E813)
AISI 9310	J_{Ic} Test ↓ K_{Ic}	75.7	J_{Ic} Test ↓ K_{Ic}	J_{Ic} Test ↓ K_{Ic}
Average	139.1		117.6	119.1
Pyrowear 53	111.5 KQ	40.3	54.0	J_{Ic}
	93.3 KQ		45.7 KQ	Test
	93.6 KQ		50.2	↓
	108.0 KQ		46.5	K_{Ic}
	123.6 KQ		47.9	
	114.8 KQ		47.7	
Average	107.1 KQ		48.7	132.4
Pyrowear 53	87.0 KQ	32.3		
Aged	78.9			
	81.4			
	83.4 KQ			
	84.6 KQ			
	86.3 KQ			
Average	83.6			
CBS600	76.3	13.0	54.3 KQ	81.0 KQ
	76.0 KQ		50.0 KQ	76.6 KQ
	78.7		49.9	78.7 KQ
	76.5 KQ		52.3	81.4 KQ
	83.0		52.6	73.1 KQ
	72.6 KQ		52.7	76.7 KQ
Average	77.0		52.0	77.91
CBC600	72.9	11.16		
Aged	76.9			
	71.0			
	77.7			
	75.4			
	73.7			
Average	74.4			
CBS1000	34.5	4.0	25.7 KQ	84.4 KQ
	35.9		24.6 KQ	91.2 KQ
	35.8		22.3 KQ	78.3 KQ
	36.3		23.7 KQ	91.8 KQ
	34.5		23.7	92.0 KQ
	35.4		25.6	93.0 KQ
Average	35.4		24.3	88.5
CBS1000	36.8	3.0		
Aged	33.8			
	34.3			
	35.6			
	34.4			
	37.0			
Average	35.3			
Vasco X2M	67.2	15.34	38.7	73.2 KQ
	68.3		36.8 KQ	70.8 KQ
	66.7		40.1	75.9 KQ
	68.7		37.7	77.8 KQ
	66.5		43.0	70.1 KQ
	69.1		39.8	72.1 KQ
Average	67.8		39.4	73.31
Vasco X2M	66.5	12.8		
Aged	64.8			
	67.3			
	66.4			
	65.1			
	67.1			
Average	66.2			
M50NiL	45.0	10.5	29.4 KQ	119.5 KQ
	50.7		29.5 KQ	111.3 KQ
	46.6		29.8 KQ	100.3 KQ
	50.9		29.2	92.3 KQ
	47.7		30.9	112.1 KQ
	47.9		38.0	113.0 KQ
Average	48.1		29.5	108.4
M50NiL	49.5	8.5		
Aged	46.8			
	46.9			
	44.4			
	49.1			
	49.0			
Average	47.6			

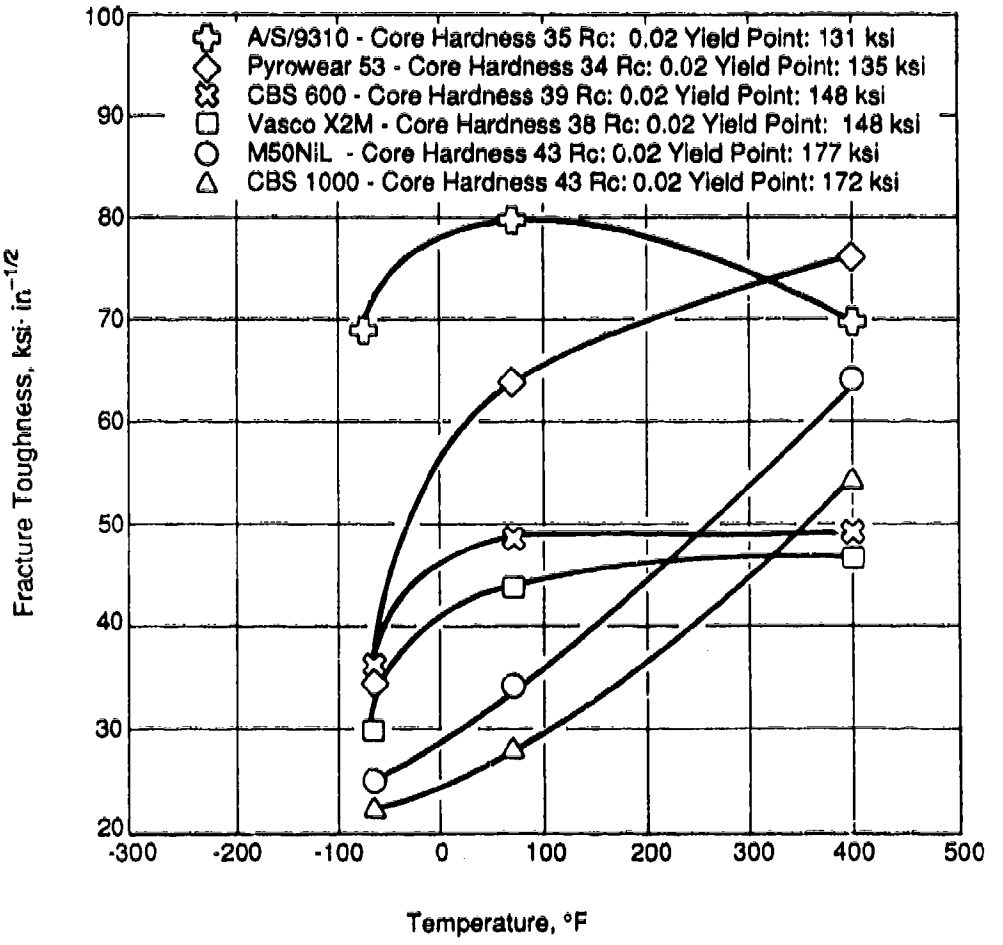

Figure A-26. Fracture Toughness as a Function of Temperature.

Table A-5. Charpy Impact Room Temperature Test Results (ft-lb).

Material	Specimen 1	2	3	4	5	6	Average
AISI 9310	76	72	58	76	84	88	75.7
Pyrowear 53	42	34	36	35	49	46	40.3
Pyrowear 53 Aged	37	44	38	24	27	24	32.3
CBS600	11	14	13	11	19	12	13.3
CBC600 Aged	10	11	9	11	8	18	11.2
CBS1000	4	4	4	4	4	4	4
CBS1000 Aged	3	3	4	2	3	3	3
Vasco X2M	13	16	17	17	14	15	15.3
Vasco X2M Aged	13	13	11	15	12	*	12.8
M50NiL	14	8	12	8	7	14	10.5
M50NiL Aged	8	7	10	9	10	7	8.5

* One specimen lost.

The condition of plane strain clearly holds the key to valid K_{Ic} data acquisition and is closely associated with the thickness of the specimen and the size of the plastically deformed zone around the tip of an advancing crack. For ductile materials, the plastic zone area can be large; correspondingly large samples are required to provide restraint adequate to prevent excessive plastic deformation. Conversely, for brittle materials, almost all the deformation at the crack tip is elastic in nature, and only small specimens are required in order for LEFM theory to hold good.

As a result of LEFM considerations, the requirements for fracture toughness testing are unusual compared to other mechanical tests because of the necessity to "compare posttest data with specimen pretest dimensions to determine if the value of fracture toughness measured (K_Q) is actually the critical value (K_{Ic}) for the material" (Reference 28). In other words, a number of validity checks are required in order to generate a valid K_{Ic} result, and there is no assurance that valid data will be confirmed. More often than not, repeat testing is necessary to obtain the true K_{Ic} value.

Table A-6 indicates the number and types of validity checks stipulated by ASTM E399. The list is comprehensive, and only one requirement, specimen size, can be predetermined or anticipated prior to testing. All the other checks depend exclusively upon the manner of each specific test and the material behavior of each particular specimen.

Validity Considerations – When tested at 400°F, Vasco X-2M, CBS 1000, CBS 600, and M50NiL all generated invalid K_{Ic} results. In every case, the very high plasticity (ductility) exhibited by these materials at this temperature caused the difficulty. At 400°F, these materials became very ductile and did not respond as elastic/brittle materials the way they do at room temperature and below. As explained previously, the E399 test is designed for elastic brittle materials; for this reason, it is doubtful if a valid K_{Ic} value based on E399 guidelines could ever be achieved at 400°F for this group of steels. Two validity requirements consistently failed to be achieved during the 400°F tests. They were E399 Section 9.1.2 - Fracture Load Ratio and Section 9.1.3 - Specimen Size. Both requirements are related to ductility and toughness; as these properties increase with increasing temperature, it becomes acutely more difficult to remain in line with the E399 guidelines. The fracture load ratio was the most significant problem since it could not be directly or externally influenced. Therefore, no matter what precautions may be taken, it appears an invalid E399 result will probably always result at 400°F for these four materials. For future reference, it may be appropriate to suggest that a valid K_{Ic} value may be derived at 400°F by the discrete use of the ASTM E813 J_{Ic} test, but even then there would be no guarantee.

Table A-6. Validity Requirements for K_{Ic} Determination: ASTM E399-83.

E399 Section	Subject
A2.3.3 A2.4.4 7.3.2.2	Fatigue Precrack
7.3.2.1	Crack Length
8.2.2	Crack Curvature
8.2.4	Crack Plane Orientation
8.3.0	Loading Rate
8.4.0	Slope of Load/Displacement Curve
9.1.2	Fracture Load Ratio
9.1.3 F.A4.1	Specimen Size

During the test program, the main areas of difficulty encountered due to validity requirements as a whole, and where special attention was required, were as follows:

1. **The Fatigue Precrack (E399 Section A.2.4.4)** - Precracking is usually carried out at room temperature (T_1) even though K_{Ic} testing may be at a different temperature (T_2). To comply, the stress intensity generated must not be greater than $[0.6(Y_1/Y_2)K_Q]$ where Y_1 and Y_2 are the yield strengths at the respective temperatures T_1 and T_2; otherwise, the test is invalid. For M50NiL and CBS 1000 at -65°F, this requirement caused considerable problems and was only overcome by painfully slow precracking rates at very low stresses.

2. **Fracture Load Ratio (E399 Section 9.1.2)** - To comply, the ratio of maximum load (P_{max}) to load at yield (P_Q) must exceed 1.10. This is a measure of the amount of plastic deformation occurring during the test and was responsible for invalidating many of the results at 400°F.

3. **Specimen Size (E399 Section 9.1.3)** - To comply, the thickness of the specimen should be greater than: $2.5[K_Q/Y_2]^2$ where Y_2 = yield strength at the test temperature. Generally, this requirement proved to be a problem only at 400°F because the size effect was anticipated successfully for all other temperatures. Specimen size is the only requirement in the E399 test that can be directly influenced prior to testing and should be estimated accurately where possible in order to avoid preventable but nevertheless potential size problems.

4. **Crack Length (Section 7.3.2.1)** - To comply, the total length of the starter notch and the fatigue precrack length should be between 0.45W and 0.55W (W is defined in Figure A-2). The crack length requirement was usually only difficult to achieve when fatigue precrack problems were also experienced.

5. **Specimen Dimensions (E399 Section A.4.1)** - To comply, the dimensions of the specimen should be such that B = 0.25W to 0.5W and 2H = 1.2W (B, W,and H are defined in Figure A-2). This requirement does not normally represent a problem if machining and inspection are carried out correctly. (Unfortunately, several CBS600 specimens were incorrectly machined and tested prior to inspection, and two invalid tests occurred before corrective action could be taken.)

To obtain valid data over the stated range of temperatures for all the materials, it was clearly necessary to contend with the combined effects of all the validity requirements (Table A-6). Consequently, many more tests were conducted (some on a trial-and-error basis) than originally anticipated; this complicated the program schedule.

A.4.3 ASTM E813-81 J_{Ic} Testing

The J_{Ic} test was adopted for use for both AISI 9310 and Pyrowear 53. It was anticipated that valid J_{Ic} data could be used to calculate a conservative estimate of K_{Ic} because both AISI 9310 and Pyrowear 53 were judged to lack sufficient brittleness to be tested for K_{Ic} according to test method E399.

ASTM E813 relates J_{Ic} to K_{Ic} using the function:

$$(K_{Ic})^2 = J_{Ic} \cdot E$$

where E is Youngs modulus of elasticity. The E813 test is subject to a number of similar validity checks in the same general manner as the E399 test but differs from E399 in that at least four separate tests are required in order to generate one J_{Ic} result.

Since the J_{Ic} concept may be used as a fracture criteria for elastic-plastic behavior in metals, the K_{Ic} test technique can also be legitimately applied using the J_{Ic} specimen configurations. For example, at -65°F, Pyrowear 53 became sufficiently brittle so as to give poor response to the J_{Ic} technique but generated valid K_{Ic} data when J_{Ic} specimens were tested according to E399. AISI 9310, on the other hand, behaved as predicted at all test temperatures; and valid J_{Ic} values were obtained as expected without undue difficulty

For both Pyrowear 53 and AISI 9310, valid K_{Ic} data were calculated from valid J_{Ic} information determined by regression analysis according to the requirements of E813.

All the AISI 9310 K_{Ic} data were derived from the J_{Ic} E813 technique, and the results indicated that the material exhibits a very low transition temperature. Upper-shelf energies were reported at all test temperatures. Although this was surprising at first, previous Charpy data for carburized AISI 9310 obtained by GE Aircraft Engines (Reference 29) also indicated that the ductile brittle transition temperature was probably below -65°F.

The K_{Ic} values reported for Pyrowear 53 at 400°F were also obtained using the J_{Ic} technique. At a temperature somewhere between 100° and -65°F, Pyrowear 53 appears to undergo the ductile brittle transition; as a result of this, E399 K_{Ic} tests as previously mentioned were directly applicable at -65°F with good effect. At room temperature, however, this material exhibited mixed ductile and brittle tendencies. Consequently, the response to room temperature J_{Ic} treatment was mediocre. No satisfactory J_{Ic} results could be obtained at room temperature for either aged or unaged Pyrowear 53 samples. Pyrowear 53 may well be one of those materials, referenced in E813 Section 5.3, which appear to be both too tough and plastic for the E399 K_{Ic} test and yet too brittle and elastic for the E813 J_{Ic} test. As a result of this behavior, E399 K_{Ic} contingency tests at room temperature were rescheduled to replace the J_{Ic} E813 tests with the knowledge that invalid results would be obtained due to load fracture (P_{max}/P_q) considerations. Consequently, K_Q values are reported for Pyrowear 53 at room temperature. Fortuitously, some K_{Ic} values for the material were obtained at room temperature after ageing due to the degradation in toughness caused by high-temperature exposure and the resulting effect on the P_{max}/P_q ratio.

A.4.4 Data Application

The interpretation of the temperature transition curve given in Figure A-26 should be considered cautiously. While the data points obtained are real, they are also specific to the individual heat treatments applied and should only be referenced in relation to the stated material condition. Toughness comparison between the materials is therefore also subject to question because of the variation in hardness and tensile properties existing between each material. A normalization treatment for yield point and projected case and core hardness differences (based on each heat treatment) was not attempted for reasons already outlined.

Care should also be employed when assessing toughness information based on K_Q values alone because it is known that K_Q can vary considerably with specimen thickness. However, considering the very high toughness shown by all the materials at elevated temperature and also based on the trends shown by the values of K_Q in relation to K_{Ic} at other temperatures, it is anticipated that the K_Q values reported here are probably adequate for design purposes with the following restriction: hardware designed using K_Q values should not be manufactured with through thicknesses greater than the specimen thickness used to generate the K_Q result. In this case, the maximum thickness for hardware should be 1.0 inch; for aircraft applications, this limit should not pose a significant barrier. (Figure A-27 illustrates the variation of K_Q with specimen thickness and highlights the danger of potential K_Q misuse). Clearly for design purposes, hardware through thicknesses should not exceed the specimen cross section thickness to be sure of correct K_Q interpretation.

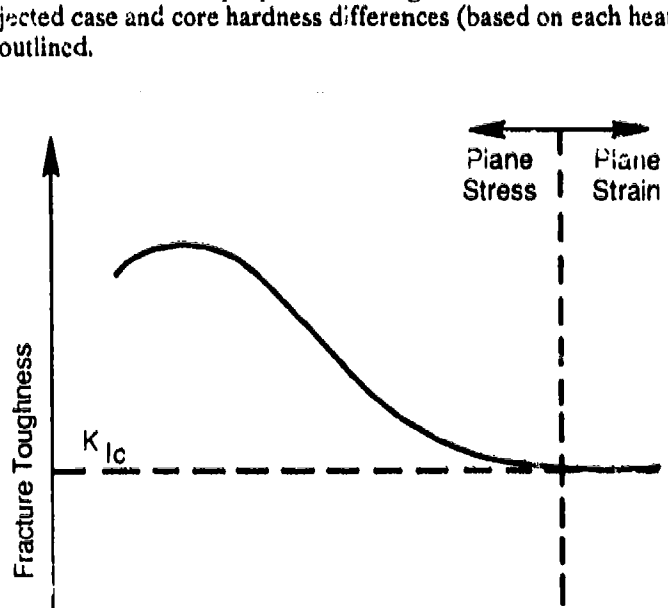

Figure A-27. Effect of Thickness on Fracture Toughness

A note of caution with respect to the K_{Ic} values derived from the J_{Ic} tests is also in order because, although under normal circumstances the J_{Ic} test often results in a conservative calculated value of K_{Ic}, under certain conditions and failure circumstances, the K_{Ic} value can be over estimated (Reference 30). In general, however, an over-estimated value is only likely at test temperatures below the ductile/brittle transition temperature; therefore, it is unlikely that the values reported here fall into this category.

A.4.5 Effect of Ageing at 450°F on Room Temperature K_{Ic}

Table A-7 lists the average fracture toughness and impact toughness values measured for all the materials before and after ageing. [Each material was exposed to 450°F in an oxidizing atmosphere (air) for 1000 hours except for AMS6265 which was not aged because the tempering temperature is below the chosen ageing temperature.] Evaluation of the data in Table A-7 provides an interesting comparison between the results of the E399 K_{Ic} and Charpy impact tests. Based on Charpy data alone, CBS1000 would appear to be the material most affected by ageing, although all the materials appeared to show significant embrittlement. However, the scatter in the Charpy data (shown in Table A-5) was much worse than the K_{Ic} data; also, small variations in absorbed Charpy energy often resulted in significant reductions in toughness. For example, a reduction from 4 to 3 ft-lb after aging results in a 25% toughness degradation for CBS 1000. For these two reasons, therefore, the K_{Ic} data were considered to be more discriminating than the concomitant Charpy data; it was therefore considered more appropriate to evaluate the effect of ageing by analysis of the K_{Ic} data only.

The analysis of the K_{Ic} data presented in Table A-7 indicated that, with the exception of Pyrowear 53, none of the materials tested suffered any significant toughness degradation after ageing. The Pyrowear 53 was substantially embrittled by the ageing treatment and suffered a reduction in room temperature toughness of about 22%.

An investigation using SEM and microprobe techniques failed to identify the cause of this loss in toughness after ageing. Analysis of the microstructure and grain boundary conditions between aged and unaged Pyrowear 53 specimens did not reveal any significant differences.

In general, toughness reductions measured by the two techniques (E399 and Charpy impact) after ageing appeared to be in direct contradiction with each other. On one hand, Charpy data suggested that the majority of the materials suffered significant toughness degradation, but the K_{Ic} data indicated the exact opposite. It is interesting to note, however, that both the Charpy and K_{Ic} test data confirmed that Pyrowear 53 was significantly embrittled by the ageing treatment and by very similar percentage toughness reductions. However, even though the Pyrowear 53 material suffered a reduction in toughness of some 22% after ageing, it still sustained a very high level of fracture toughness, equivalent to 83.6 $ksi\cdot in^{1/2}$.

Table A-7. Effect of Ageing at 450°F for 1000 Hours on Room Temperature Toughness.

		Average of Six Data Points	
Material	**Condition**	**K_{Ic}, $ksi\cdot in^{1/2}$**	**Charpy, ft-lb**
Pyrowear 53	Room Temperature	107.1 (K_Q Value)	40.30
	After Ageing	83.6	32.30
	% Reduction	21.9	19.9
CBS600	Room Temperature	77.0	13.3
	After Ageing	74.4	11.2
	% Reduction	3.4	15.8
Vasco X2M	Room Temperature	67.8	15.3
	After Ageing	66.2	12.8
	% Reduction	2.4	16.5
M50NiL	Room Temperature	48.1	10.5
	After Ageing	47.6	8.5
	% Reduction	1.0	19.0
CBS1000	Room Temperature	35.4	4.0
	After Ageing	35.3	3.0
	% Reduction	0.3	25.0

A.4.6 Correlation of K_{Ic} and Charpy (C_V) Toughness Data

Various attempts to correlate K_{Ic} and C_V have been attempted in the past; in general, the well-known published correlations (References 31 through 35) tend only to yield reasonably good results in certain toughness ranges. Based on review of the work in this field, it is apparent that no single correlation between K_{Ic} and C_V is likely to accurately take into account all the available data for every class of steel. Correlations have been devised to accommodate certain generic families of materials, particularly pressure-vessel steels, with some success; the early pioneering work in this area being done by Barson, Rolfe, and Novak (References 31 and 32). However, when these and other correlations have been more broadly applied to grades of steel other than those actually tested, the results are often anomalous, leading to a lack of confidence in the use of the correlation technique.

In considering the obvious differences between the E399 K_{Ic} and the Charpy tests, it is not surprising that some difficulty has been experienced in attempting to correlate the test data accurately. The Charpy test is a high-strain-rate technique employing a notched specimen in which the state of stress at the root of the notch in no way resembles the stress pattern which predominates in K_{Ic} specimens. In addition, the transition temperatures determined by each method are reported to be often significantly different (Reference 35), making direct comparison between K_{Ic} and C_V much more difficult. Recognizing such problems, most investigators have tried to reconcile these fundamental differences by compensating for strain rate in some way or by devising a temperature-compensation formula to narrow the transition temperatures and make them coincide with each other. In practice, most groups of materials tend to respond differently to these adjustments; consequently, certain anomalies can often occur – resulting in inconsistencies and inaccurate correlations.

With the correlation treatments devised in the past, one of the most common features has been to try to manipulate the data in order to produce the best possible linear representation of K_{Ic} and C_V. Using this procedure, values of K_{Ic} and C_V measured during this program are plotted in Figure A-28. The following relationship was calculated using the curve generated:

$$K_{Ic} = 14.72 C_V^{1/2} + 10.74 \qquad \text{(Equation A-1)}$$

Where: K_{Ic}, $ksi \cdot in^{1/2}$
C_V, ft-lb
Ambient temperature

Other correlations were attempted, but this relationship was found to give the most satisfactory result because a more accurate K_{Ic} interpretation could be achieved by expressing $C_V^{1/2}$ as the abscissa rather than C_V directly. The use of $C_V^{1/2}$ in this way served to expand the abscissa scale and increase the accuracy of inferred K_{Ic} values.

For comparison, the actual toughness data generated in this program were used to construct correlation curves using the Barson-Rolfe-Novak (References 31 and 32) and the Sailors and Corten (Reference 33) relationships for static K_{Ic} versus C_V. These curves are shown in Figure A-29 along with the correlation suggested by this work. Other correlations cannot be directly compared because many of them were either strain-rate or temperature compensated or used precracked Charpy specimens. (This program was restricted to conventional static uncompensated testing.)

The relationship defined by Equation A-1 was found to be in good agreement with the Sailors and Corten model, and together these two derivations probably describe a more reasonable estimate of K_{Ic} than does the Barson-Rolfe-Novak formula when applied to bearing and gear steels. This result was not entirely unexpected because the work conducted by Barson et al. resulted in an empirical derivation for steels exhibiting toughnesses within the upper-shelf energy ranges only. Bearing steels do not usually exhibit upper-shelf energies at room temperature but instead tend to fall between the low and transition temperatures range. The Sailors and Corten work was more representative of steels exhibiting low and transition temperature ranges, and this may explain why such good agreement is apparently shown between Equation A-1 and the model suggested by Sailors and Corten.

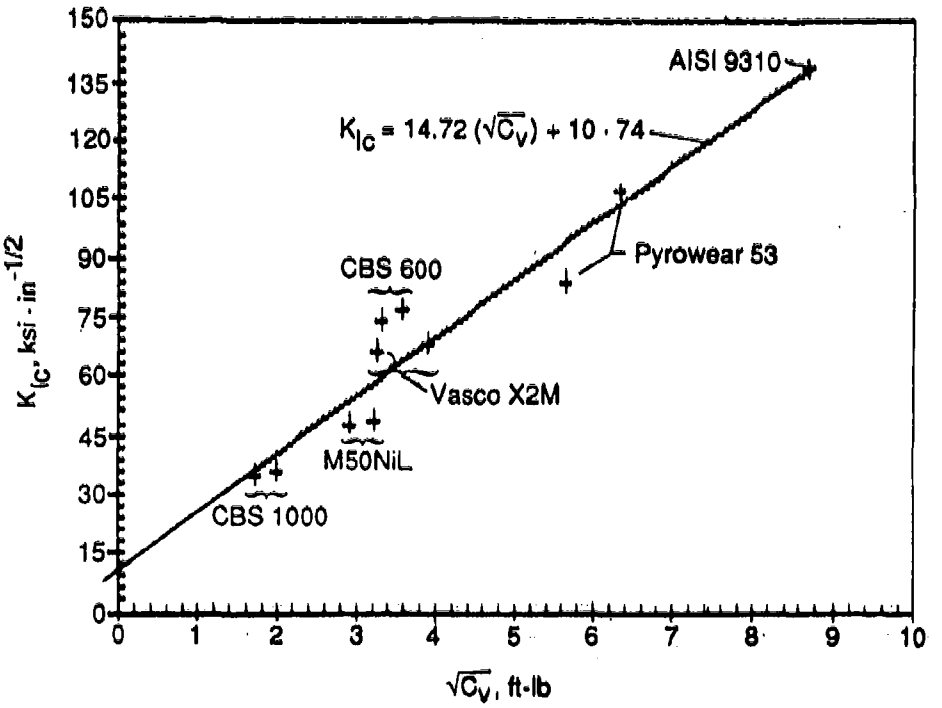

Figure A-28. K_{Ic} and Charpy Data Correlation.

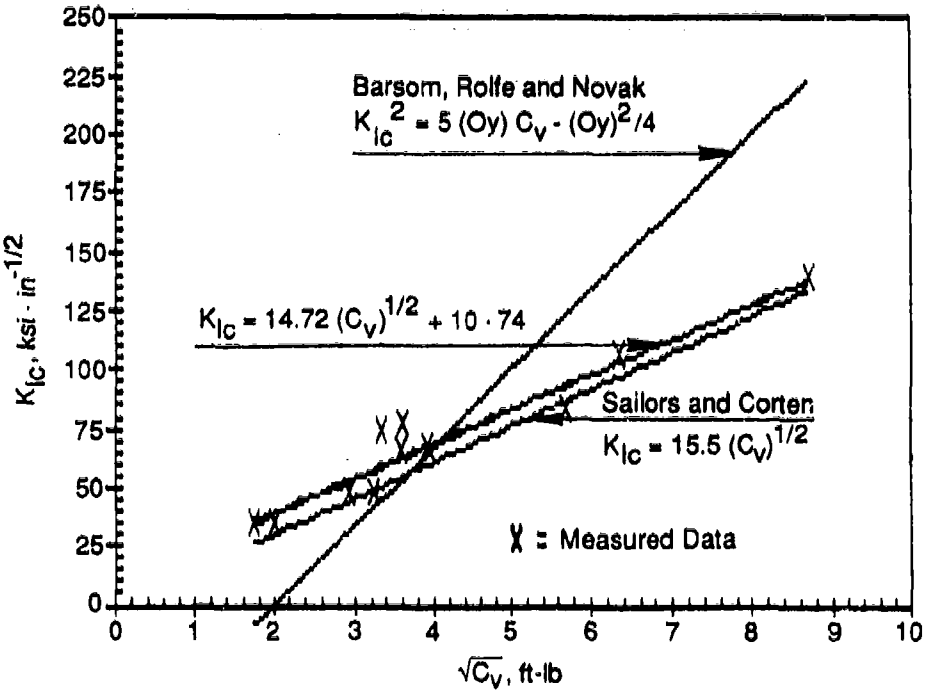

Figure A-29. Comparison of K_{Ic} Versus Charpy Data Correlations.

Close scrutiny of Figure A-28 suggests that Equation A-1 generates the greatest correlation error in the range of fracture toughness, close to 10 ksi·in$^{1/2}$. Above this level, the accuracy of fit with the measured data improves. Nevertheless, the use of Equation A-1 and all other correlations must be viewed with a great deal of consideration. For this reason, more data are needed to confirm this and other models before any type of practical use can be recommended.

However, one application that may be employed with some confidence is the use of an appropriate correlation to estimate the specimen thickness required for valid K_{Ic} determination. In order to obtain a valid K_{Ic} result, it is first paradoxically necessary to know the (approximate) value of K_{Ic} in order to estimate the correct specimen thickness (Section 9.1.3. ASTM E399-83). The curves in Figure A-29 may be useful as a guide in obtaining first estimates of K_{Ic} from preliminary tests using inexpensive Charpy specimens; in this respect, the use of Equation A-1 would have few restrictions.

A.5 Concluding Remarks and Recommendations

At elevated temperatures, the increase in ductility demonstrated by CBS1000, CBS600, M50NiL, and Vasco X2M would appear to prevent the measurement of valid K_{Ic} data by the method described in ASTM E399-83. It is recommended that, in order to overcome this difficulty, general yielding fracture mechanics using ASTM E813-81 should be considered.

Where the facture toughness data are reported as K_Q values only, it is recommended that a restriction in hardware size equivalent to the test specimen thickness should be imposed for design purposes.

The effect of long-term ageing at 450°F on the ambient ASTM E399-83 measured fracture toughness was such that only one of the materials was significantly embrittled. Pyrowear 53 appeared to be degraded in toughness by approximately 22%, but no obvious reason for this effect was established.

A preliminary correlation relating K_{Ic} and Charpy data was developed, but it is suggested that further clarification is required before any specific use of the correlation could be recommended.

Appendix B

Processing Recommendations for TDC Coating Application to M50 and M50NiL Ball and Roller Bearings

The sequence of processing should be as follows:

I. Cleaning and Degreasing
II. Preplating and Vapor Honing
III. Plating
IV. Stress Relief
V. Inspection
VI. Stripping Procedures
VII. Source Approval and Quality Assurance

I. Cleaning and Degreasing

A. Components shall have surfaces free of scale, oxide, previously coated or plated deposits, and other foreign materials. Components should be coated with rust-preventative oil and packaged in a manner to prevent damage during transport.

B. Parts should be thoroughly degreased prior to plating by soaking in room temperature solvent or by vapor degreasing with 1.1.1. trichloroethane. Parts shall be carefully inspected for oil or solvent residue after degreasing. After degreasing and prior to the liquid vapor honing operation, the parts shall be stored in a manner that will prevent oxidation from forming on the surfaces to be coated.

C. Mask all surfaces where coating is not permitted.

II. Vapor Honing – After degreasing and masking, parts should be liquid vapor honed with 1250-grit micro-crystalline novaculite media under no greater than 89-psi pressure, followed by a rinse in clean water. The grit level in the liquid hone is to be maintained at 20 to 25% by volume. After honing, the parts should be immediately submerged and held in a rust inhibitor solution until the plating process is performed.

III. Plating

A. Parts should be thoroughly rinsed with clean water, prior to immersion into the plating bath, to remove all rust inhibitor solution.

B. Rack design, setup, and maintenance should be controlled to ensure proper coating quality. Rack details should be recorded on the job record sheet for reference, to be used without change on future orders.

C. Parts Should be immersed into the plating bath which must be maintained between 1300° and 1400°F. The bath chemistry should be within limits maintained during qualification. Auxiliary anodes, if used, should be attached to the positive anode bus bar. The parts shall reach bath temperature before electrical current is applied.

D. Current density must be closely controlled to ensure proper coating quality. Proper current density settings for a particular part should be established during setup and recorded on the job record sheet for reference, to be used without change on future orders.

E. Should the plating process be interrupted (due to power failure, for example), the parts must be removed from the bath, stripped, and replated.

F. Parts removed from the plating bath will be rinsed with clean water and removed from the rack. The parts should be visually inspected for complete rinsing, stains, and general appearance before being dipped in a rust-inhibitor holding solution. Any masking materials used should then be removed from the coated parts.

IV. Stress Relief – Stress relief should be performed within an hour after plating by baking at 375 ± 10°F for four hours, followed by air cooling. Completed parts should be protected from stains and handling marks with a light oil.

V. Inspection

A. Inspect parts for complete coverage of a light-gray matte finish free of dents, nicks, scratches, pits, cracks, peeling, or other discontinuities. A slight difference where rack contact is made is acceptable.

B. Examine a surface at 500× magnification. The surface shall have complete nodularity as shown in Figure B-1 and be free of cracks and poor nodularity as shown in Figure B-2.

C. One part from each lot of work is to be inspected for proper deposit thickness using a Kocour thickness tester. It is recommended that a minimum of three reading be taken. The plate thickness measured with the Kocour instrument shall be 0.00005 to 0.0001 inch (50 to 100 μin).

VI. Stripping Procedure

A. Ferrous-based material shall be stripped in a tank containing an alkaline electrolytic stripping solution. The time that part(s) are left in the stripping tank will be dependent on the thickness and area of chrome to be removed. The plating vendor is to exercise caution during stripping to ensure that no etching of the ferrous base metal occurs.

B. Stripping will be done in a bath maintained exclusively for that purpose.

C. Parts will be rinsed with clean water immediately upon removal from the stripping tank and placed in a rust-inhibitor solution.

D. Parts with high carbide content (such as M50, M50NiL, etc.) which have been stripped **must** be returned to the appropriate manufacturing function for refinishing of the critical surfaces (raceway, journal, etc.).

Source Approval and Quality Assurance – These items are subject to the source-approval and quality-control plans of the organization using the subject coating. AMS 2438, "Chromium Coating – Thin, Hard, Dense Deposit," is recommended as a reference for appropriate quality-control measures.

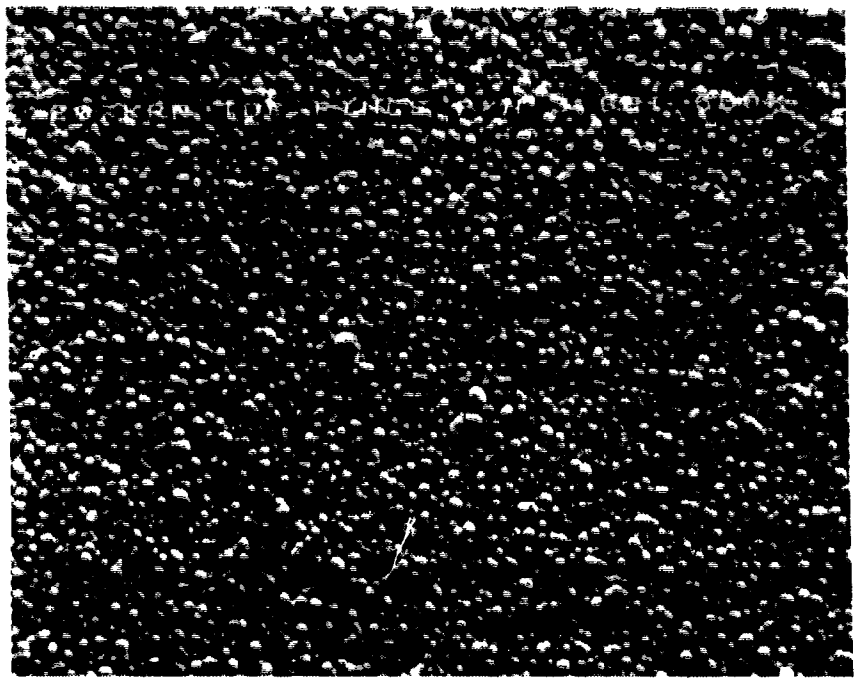

500 ×

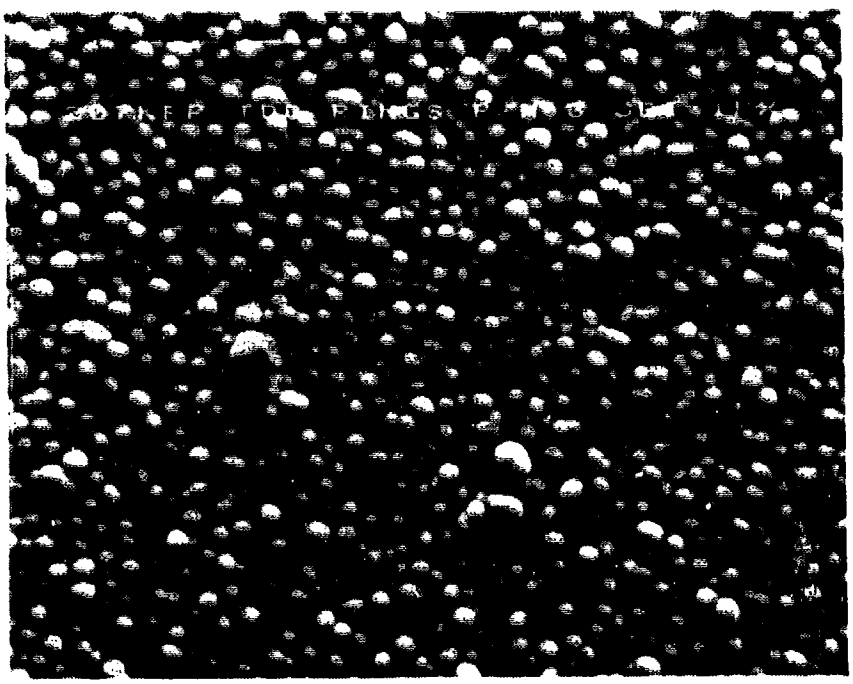

1000 ×

Figure B-1. Acceptable TDC Coating.

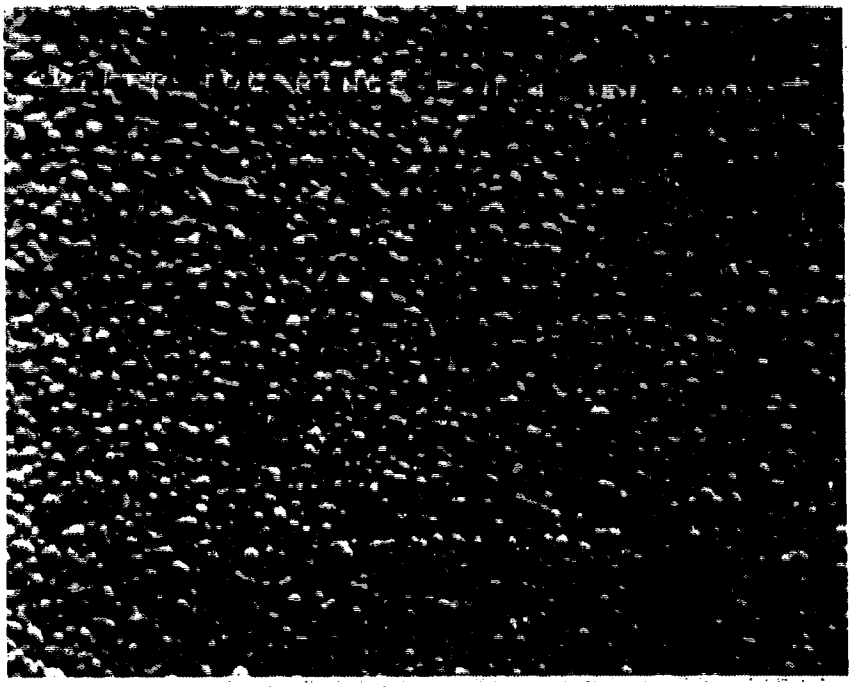

500×

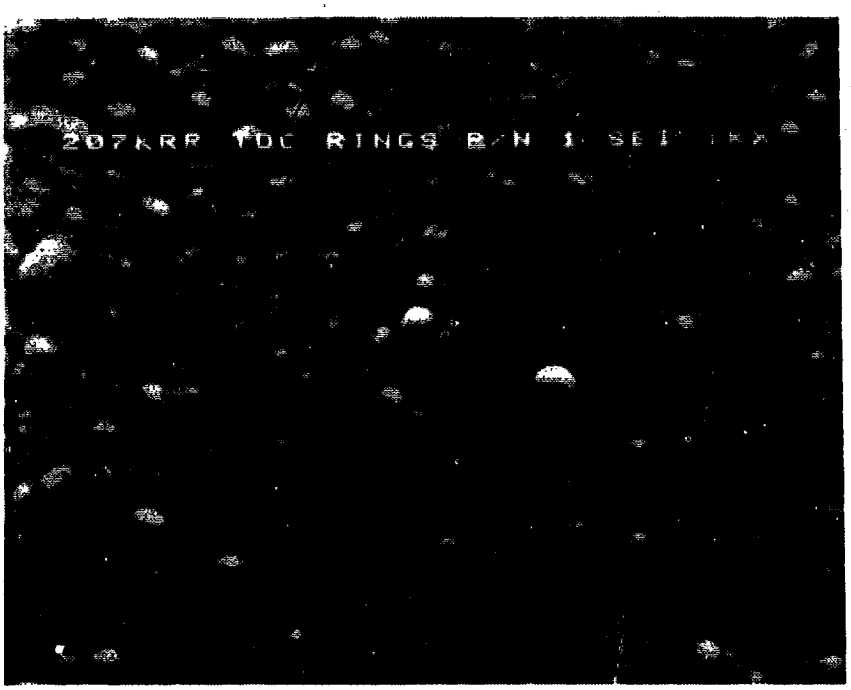

1000×

Figure B-2. Unacceptable TDC Coating.

References

1. Bamberger, E.N., Averbach, B.L., and Pearson, P.K., "Improved Fatigue Life Bearing Development," Interim Report for Period September 1984 to March 1987, AFWAL-TR-87-2059, R87AEB585, October 1987.

2. Bamberger, E.N. et al., "Life Adjustment Factors for Ball and Roller Bearings," ASME Design Guide, 1971.

3. Bamberger, E.N., Averbach, B.L., and Pearson, P.K., "Improved Fracture Toughness Bearing," Interim Report for Period 22 August 1980 to 30 September 1982, AFWAL TR-83-2022, April 1983.

4. Bamberger, E.N. and Nahm, A.H., "Improved Fracture Toughness Corrosion Resistant Material," NASA CR-174990, January 1986.

5. Bieberich, M.D., Brown, C.L., and Limpert, J.C., "Development of Corrosion Inhibited Mil-L-23699 Oils for Naval Aircraft Engines and Transmissions," D.W. Taylor Ship Research and Development Center, STNSRDC/SME 80/361, September 1980.

6. Bamberger, E.N., "Status of Understanding, Bearing Materials," *Tribology in the 80's, Vol. II,* NASA CR 2300.

7. *Mobil EHL Guidebook,* Third Edition, 1981.

8. Dreschmann, P., Lorösch, H.K., and Weigand, *Ball and Roller Bearing Engineering 1983-1,* Fag Kugelfischer, Georg Schafer, Schweinfurt, West Germany, 1983, p 34.

9. Clark, J.C., "Fracture Failure Modes in Lightweight Bearings," *AIAA Journal Aircraft,* Vol. 12, No. 4, 1975.

10. Bamberger, E.N., Averbach, B.L., and Pearson, P.K., "Improved Fracture-Tough Bearings," AFWAL-TR-83-2103, Contract F33615-80-C-2018, January 1985.

11. Averbach, B.L., Lou, B., Pearson, P.K., Fairchild, R.E., and Bamberger, E.N., "Fatigue Crack Propagation in Carburized High Alloy Bearing Steel," in Met. Trans. A, Vol. 16A, 1985, pp 1253-1265.

12. Averbach, B.L., Lou, B., Pearson, P.K., Fairchild, R.E., and Bamberger, E.N., "Fatigue Crack Propagation in Carburized X2N Steel," Met. Trans. A, Vol. 16A, 1985, pp 1267-1271.

13. Hubler, G.K., et al., "Application of Ion Implantation for the Improvement of Localized Corrosion Resistance of M50 Steel Bearings," NRL Memorandum Report 4481, Naval Research Laboratory, Washington, DC, March 1981.

14. Wang, Y.F. and Clayton, C.R., *Thin Solid Films,* Vol. 73, 1979, pp 11-18.

15. Hubler, G.K., Valori, R., and Popgoshev, D., J. Lub. Technol., Vol. 105, 1983 pp 537-543.

16. Gardos, M.N., "Physical and Chemical Stabilization of Steel Bearing Surfaces with Titanium Nitride and Titanium Carbide Hard Coatings," Paper Presented at Vanderbilt University, March 1984.

17. Hinterman, H.E., Boving, H., and Hanni, W., "Wear Resistant Coatings for Bearing Applications," *Wear,* Vol. 48, No. 2, June 1978.

18. Dill, J.F., Gardoes, M.N., and Hintermann, H., "Rolling Contact Fatigue Evaluation of Hardcoated Bearing Steels," Paper Presented at Third International Conference on Solid Lubrication, Denver, Colorado, August 1984.

19. Bamberger, E.N. and Clark, J.C., "Development and Application of Rolling Contact Fatigue Test Rig," *Rolling Contact Fatigue Testing of Bearing Steels,* ASTM STP 771, 1982.

20. Pippan, R., Berger, M., and Stuwe, H.P., "The Influence of Crack Length on Fatigue Crack Growth in Deep Sharp Notches," Met. Trans. 1987, Vol. 18A, pp 429-435.

21. Glover, D., "A Ball-Rod Contact Fatigue Tester," *Rolling Contact Fatigue Testing of Bearing Steels,* ASTM STP 771, 1982

22. Law, C.C. and Antony, M.M., "Rolling Contact Fatigue Failure of Bearings," AFWAL-TR-872079, January 1988.

23. Hills, D.A. and A. Sackfield, A., "Yield and Shakedown Stresses in the Contact of Generally Curved Bodies," Jour. Strain Analysis, 1984, Vol. 19, No. 1, pp 9-14.

24. Voskamp, A.P., "Material Response to Contact Loading," Journal of Tribology, 1985, Vol. 107, pp 359-366.

25. Ghosn, L.V., "Analysis of Crack Propagation in Roller Bearings Using the Boundary Integral Equation Method - A Mixed Mode Loading Problem," Trans. ASME, 1988, Vol. 110, pp 408-413

26. Averbach, B.L., Bingzhe Lou, Pearson, P.K., Fairchild, R.E., and Bamberger, E.N., "Fatigue Crack Propagation in Carburized High Alloy Bearing Steels," Met. Trans., 1985, Vol. 16A, pp 1253-1265.

27. Socie, D.F., Mitchel, M.R., and Caubield, E.M., "Fundamentals of Modern Fatigue Analysis," University of Illinois FCP Report No. 26, April 1977.

28. Howthorne, J.R. and Mager, T.R., ASTM STP "Fracture Toughness," (514), 1971.

29. Peterson, J.D., "Carburizing Grade Gear Steels," GE TIS84APB003, 1984.

30. Daives, M.G., "Elastic-Plastic Fracture Toughness Based on the COD and J-Contour Integral Concepts," ASTM STP668, November 1977, p 315.

31. Barson, J.M., and Rolfe, S.T., ASTM STP (466), 1970.

32. Rolfe, S.T. and Novak, S.R., ASTM STP (463), 1970.

33. Sailors, R.H. and Corten, H.T., "Fracture Toughness," ASTM STP (514), 1971.

34. Begley, J.A. and Logsdon, W.A., "Correlation of FT and Charpy Properties for Rotor Steels," in *Use of Fracture Mechanics,* by Rolfe, S.T., Review 186, International Met Reviews, Vol. 19, pp 183, 1974.

35. Marrandet, B. and Sanz, G., "Evaluation of the Toughness of Thick Medium Strength Steels by LEFM and Correlations of K_{Ic} and C_v," Institut de Recherches de la Siderurgie Francaise, 1976.

Addendum

Selected Color Photographs of Corrosion-Tested Components

The following color photos are also displayed as black and white half-tone (screened) images in Figures 50 through 53, 57, 58, 62, and 64 of this report. Discussion and comments concerning the figures are presented in Section 5.1 beginning on page 77.

An addendum of color photos is provided in the first publication of this report by GE Aircraft Engines because it is deemed efficacious to illustrate certain results of the reported investigation. However, GEAE recognizes that future reproduction or duplication of this document by WRDC, DTIC, or other qualified agencies or individuals may be required. In that event, GEAE suggests the addendum be omitted. Alternately, qualified agencies and individuals may request additional glossy prints from GEAE through EMTL (Engineering Materials Technology Laboratories) Technical Services and Communications, (513) 243-1919.

The photos have reference numbers visible in the lower right-hand area. These reference numbers should be cited if additional color prints are requested from GEAE. The numbers are listed below along with corresponding Figure numbers as discussed in the first paragraph above:

C162499	Figure 50
C162507	Figure 51
C162506	Figure 52
C162508	Figure 53
C162496	Figure 57
C162503	Figure 58
C162505	Figure 62
C162495	Figure 64

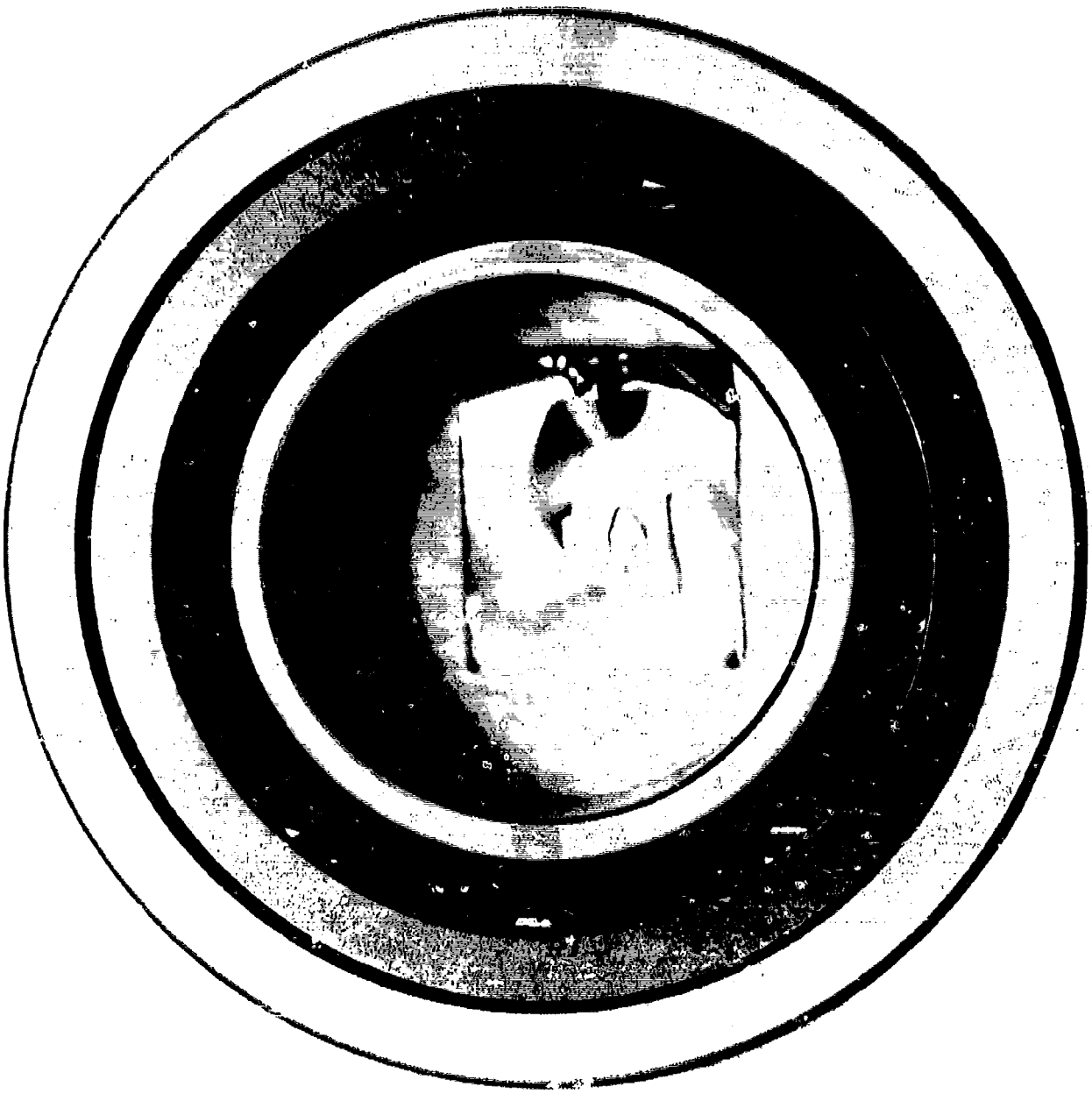

FIGURE 50

FIGURE 51
153

FIGURE 52

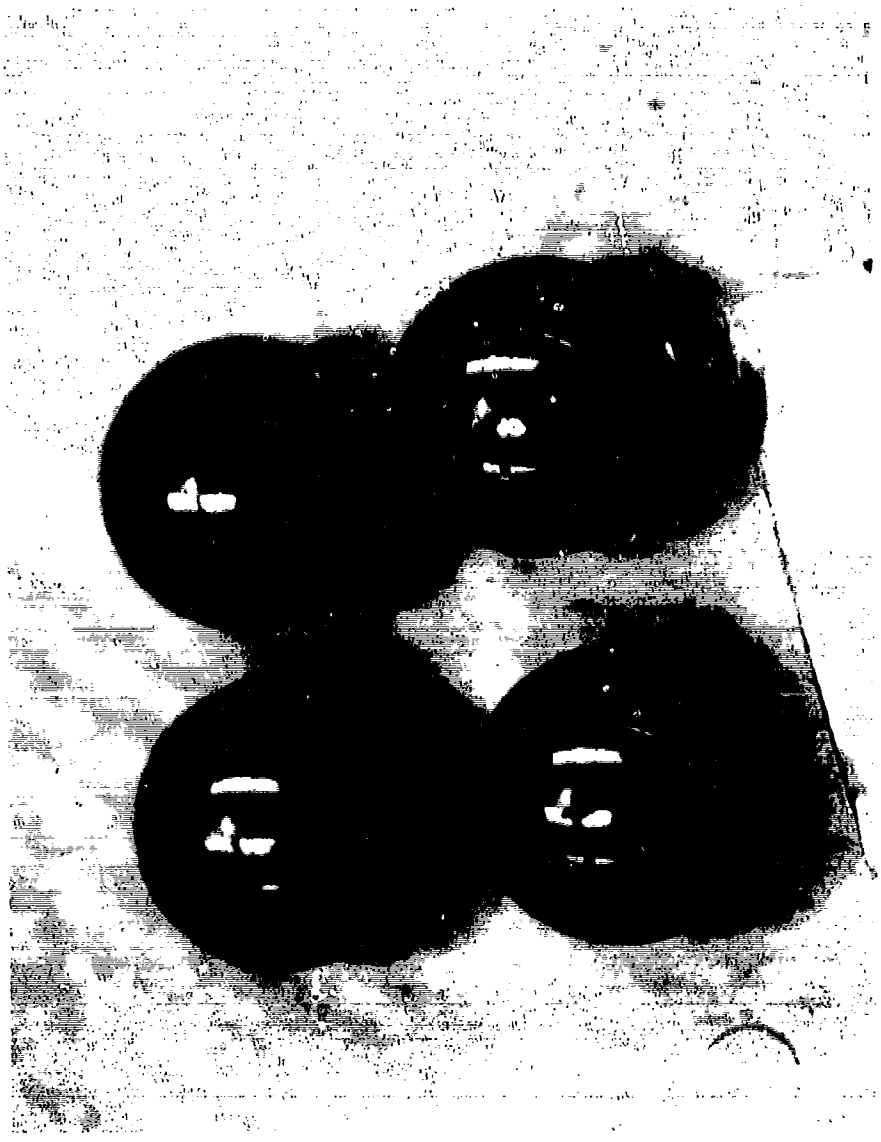

FIGURE 53

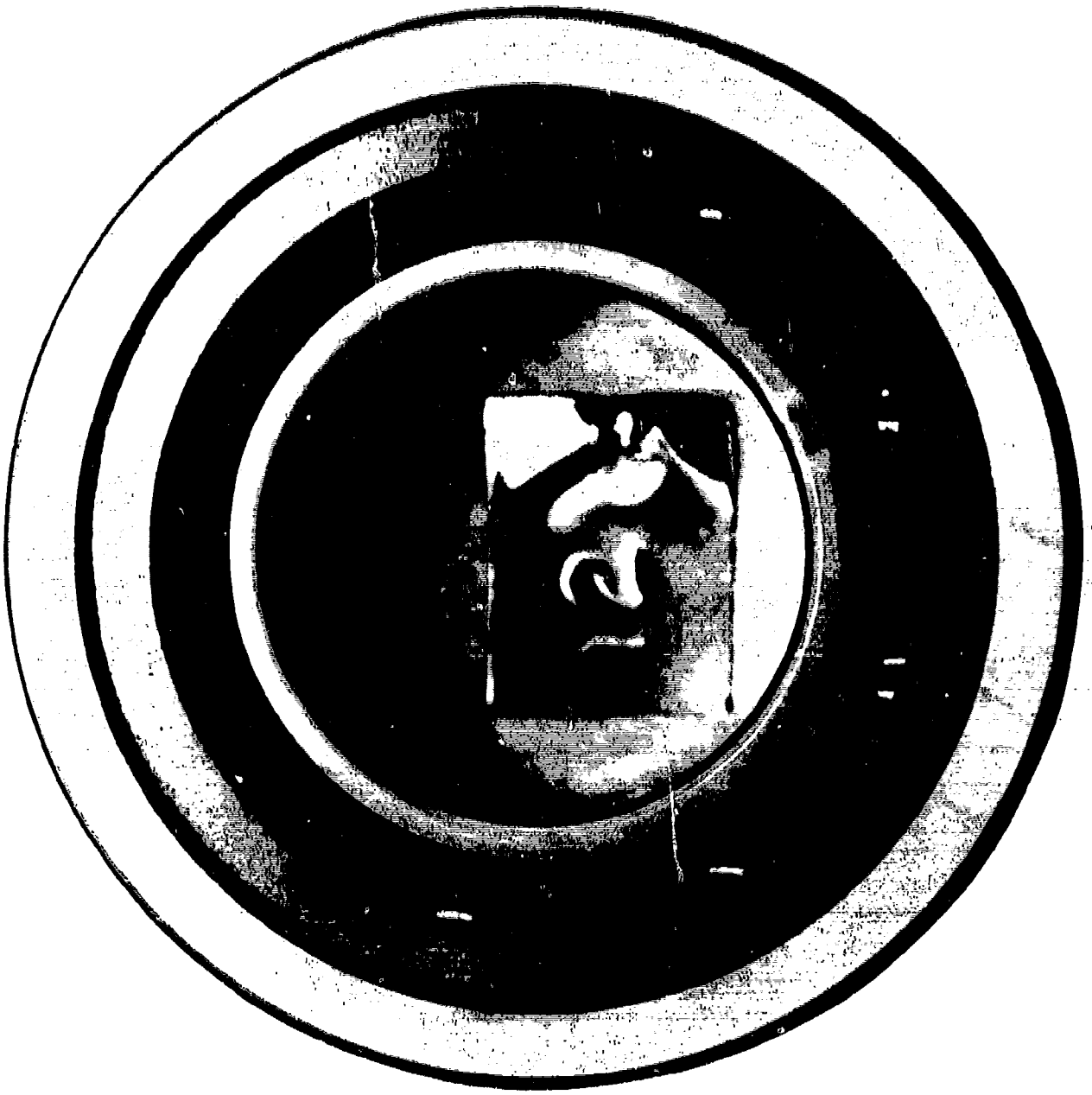

FIGURE 57

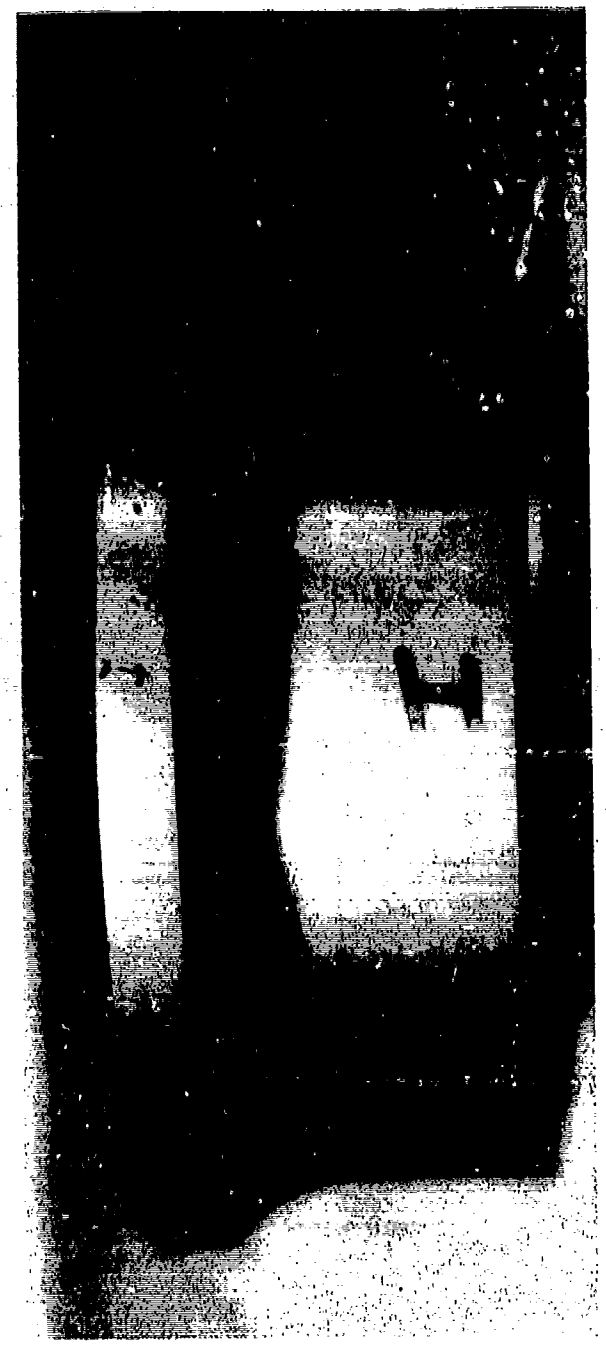

FIGURE 58

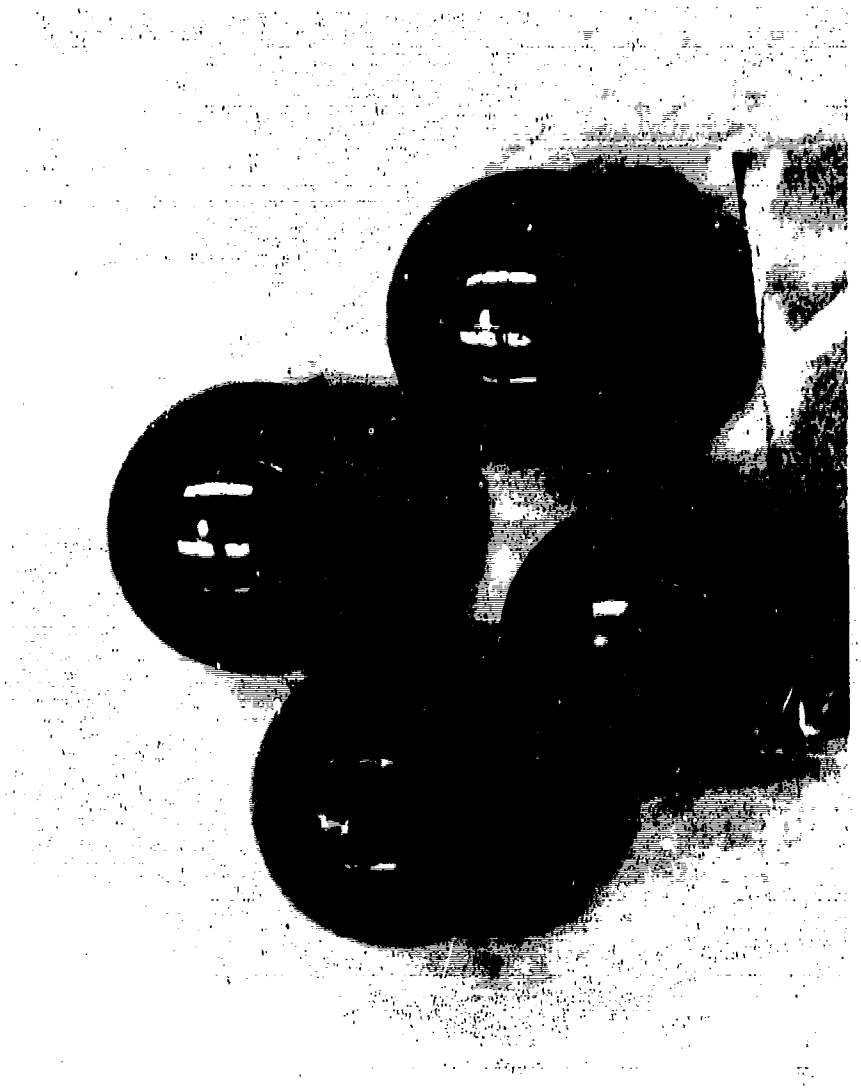

FIGURE 62

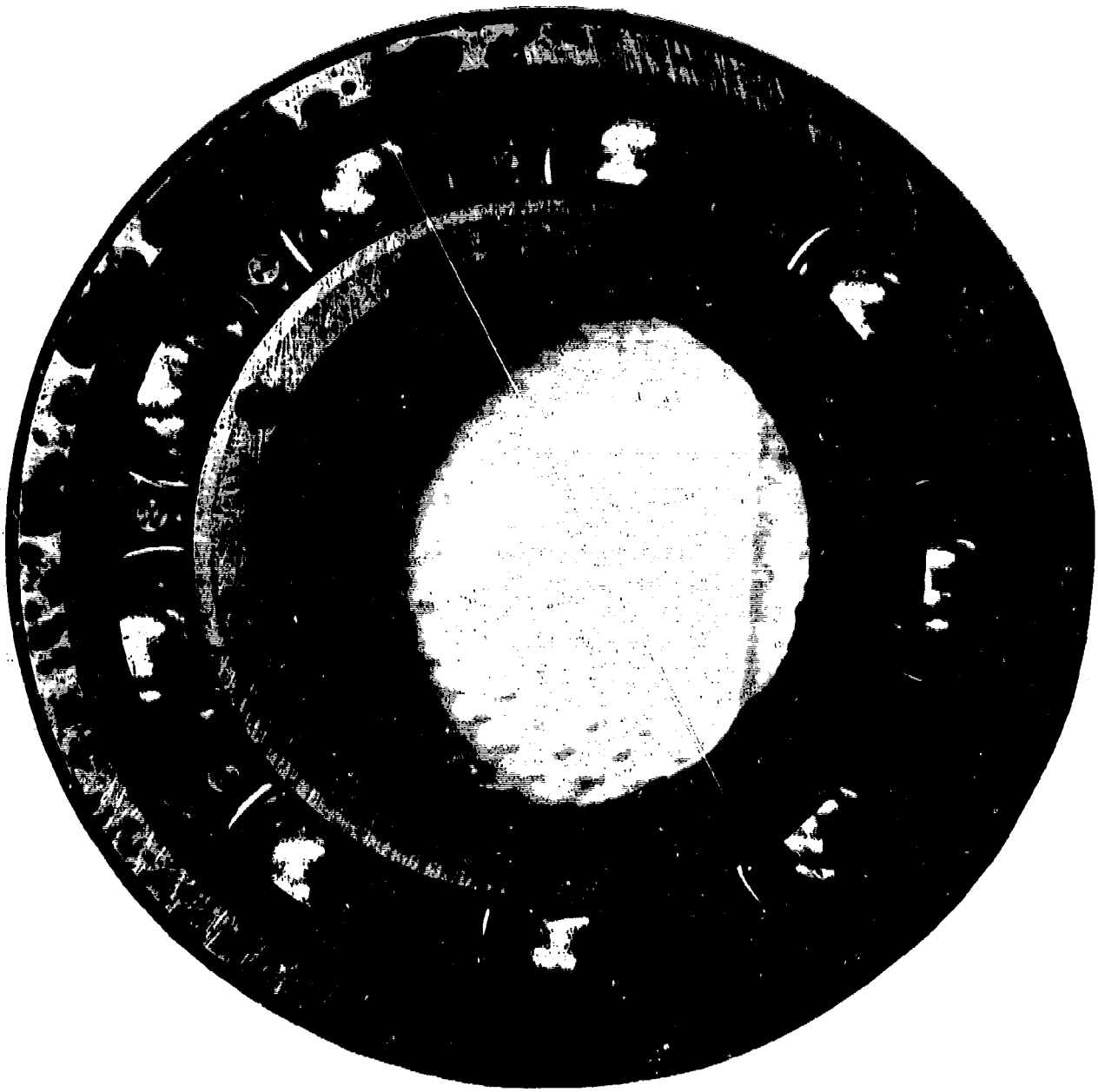

FIGURE 64

DEPARTMENT OF THE AIR FORCE
HEADQUARTERS 88TH AIR BASE WING (AFMC)
WRIGHT-PATTERSON AIR FORCE BASE OHIO

MEMORANDUM FOR: DTIC – OQ
Attn: Larry Downing
8725 John J. Kingman Rd.
Ft. Belvoir VA 22060

FROM: 88 CG/SCCM (FOIA Office)
Bldg 1455
3810 Communications Blvd
WPAFB OH 45433

SUBJECT: Freedom of Information Act (FOIA) Case, WPAFB FOIA Control # 04-382AB

1. On 17 May 2004, we received a FOIA request for document AD-B137279 "Improved Fatigue Life Bearing Development". The current distribution statement B (unclassified/limited) is no longer applicable. The document has been reviewed by The Air Force Research Propulsion Lab, and it has been determined that the distribution statement should be changed to statement A (publicly releasable).

2. I am the point of contact and I can be reached at (937) 522-3092 or DSN 672-3092.

ABBY L. BOGGS
Freedom of Information Act Analyst
Management Services Branch
Base Information Management Division

Attachment
AFMC Form 559